UNIVERSITY OF TECHNOLOGY, SYDNEY

Interactions of viral and cellular Tumour Necrosis Factor Receptor molecules

A thesis submitted in fulfilment of the requirements for the degree of Doctor of Philosophy: Science

Alexander Douglas Gale

2016

Certificate of original authorship

I certify that the work in this thesis has not previously been submitted for a degree nor has it been submitted as part of requirements for a degree except as fully acknowledged within the text.

I also certify that the thesis has been written by me. Any help that I have received in my research work and the preparation of the thesis itself has been acknowledged. In addition, I certify that all information sources and literature used are indicated in the thesis.

Signature of Student:

Date:

Presentations

Hunter Cell Biology Meeting LoveDale NSW, March 16-20th, 2015
Alexander Gale*, Michael Johnson, Michael F McDermott & Lisa M Sedger.
Abstract: Viral and cellular Tumour Necrosis Factor Receptor (TNFR) interactions and implications for inhibition of TNF and TNFR-related biology. (Poster)

8th Australasian Virology Society (AVS) Meeting. October 30th 2015
Lisa M Sedger*, Alexander D Gale, Ralph Reboblado, Khonder Rufaka Hossain, Michael S Johnson, Michael F McDermott
Abstract: Are viral Tumour Necrosis Factor-Receptors (vTNFRs) a driver for the existence of TNFR-Associated Periodic fever Syndrome (TRAPS) in humans? (Oral presentation)

EMBL – Australia Masterclass on protein analysis, October 21 -25th 2013

Garvan Institute of Medical Research, (Oral)

The 11th Hunter Meeting. March 22-25th, 2011.
Gale A*, Johnson M, Sherwood S, McDermott M, & Sedger LM.
Abstract: Visualisation of viral and cellular TNFRs with mutations in the pre-ligand assembly domain (PLAD), required for viral:cellular TNFR co-association and inhibition of TNFR signalling. (Poster)

Acknowledgements

As I begin to look back at the journey this project has lead me down, both within this project and also the events that have occurred outside of this project over the last few years have been the hardest challenges I've had to face, and without all the help and support of my friends, family and mentors along the way, this all would not have been possible. This has been one of my greatest achievements and can't thank all who have enough, so I dedicate this to you all.

To my supervisor Lisa Sedger, thank you for being accepting me on this project. From my naive beginnings, I have taken with me not only the skills to be more analytical of myself as well as others, but to also further myself in many ways to become a much stronger person. Despite all the challenges we have both faced I thank you for all your support as well as help in the development of the FRET methodology.

To Michael Johnson, I thank you for support and guidance both practical and morally. Your perception and inclusion of all thing technical on the project has inspired my interest in the work you do, and is reflected by the many paths taken in this in this project. I'd also like to acknowledge your input and training with all the microscopy experiments

To Michael Wallach, you undertook me as your student when times proved difficult and have continued to support me until the end. I am in debt for all your generosity and many avenues made possible. To Sonja Frolich, I also want to thank you for welcoming me into your lab and making my stay at UTS much more enjoyable.

Sarah Sherwood, you have taught me and mentored me in the lab to enable me with many of the skills to take on this project. As well as that you have always taken the time to ensure my time in the lab was always enjoyable, for this I am extremely lucky and grateful. Joyce Tran you have been my saviour in the lab and I cannot express how much you have helped me along the way. Your continuing support and guidance has pushed me through some of the hardest times that have challenged me. To all my friends and fellow PhD students I have made along the way; Rita (Monahan), Sam Burns, Raquel Alvarado, Amelia Hynan, Maria Lund, Mike Strauss, Charmain Castel, Erin Gloag, Padraig Winter and Akane Tanaka, your patience, reassurance, guidance, and mental distractions have kept me sane to continue on a path to complete my journey. Your friendships are all unique and is something I am extremely lucky to have gained during my time as a student. For the house of Jumbunna I only wish I could provide the care and welcome that you have provided me. You make me proud to represent the indigenous community in the field of science and I hope that I can inspire more to follow in my path.

My parents, although you may not understand what I have embarked on, you have unconditionally supported my decisions. Lastly to my endearing Wife Kylie. I know that you wish only the best of me and have unconditionally loved and supported me through the most difficult times in my lifetime. However through this we have become so much stronger together and I am now proud to call you my wife. I am excited to begin the next chapter in our lives together.

I would also like to acknowledge the financial assistance of the Faculty of Science as well as the house of Jumbunna, for who this project would not be possible.

Table of contents

List of figures

List of tables

Abbreviations

CFP – Cyan Fluorescent protein

CMV- Cytomegalovirus

CRD – Cysteine Rich Domain

CRM- – Cytokine Response Modifying Protein

DD – Death Domain

DED – Death Effector Domain

FADD – Fas-associated Death Domain Protein

FHF - Familial Hibernian Fever

IKK – Inhibitor of Nuclear Factor Kappa B Kinase

IκB – Inhibitor of Nuclear Factor Kappa B

JNK – c-Jun N Terminal Kinase

LTα - Lymphotoxin alpha

MPV – Monkeypox virus

MPVJ2R – Monkeypox virus J2R

MYXV – Myxoma virus

MYXT2 – Myxoma virus T2

NFκB – Nuclear Factor Kappa B

PLAD – Pre-Ligand Assembly Domain

RIP – Receptor Interacting Protein

SECRET – Smallpox virus-Encoded Chemokine REcepTor domain

SODD – Silencer of Death Domain

TACE - Tumour necrosis Factor Alpha Converting Enzyme

TNF - Tumour Necrosis Factor Alpha

TNFR – Tumour Necrosis Factor Receptor

TNFRSF – Tumour Necrosis Factor Receptor Super Family

TNFSF - Tumour Necrosis Factor Super Family

TRADD - Tumour Necrosis Factor Receptor Associated Death Domain Protein

TRAF - Tumour Necrosis Factor Associated Factor

TRAPS - Tumour Necrosis Factor Receptor Associated Periodic Syndrome

VARV – Variola virus

VARG4R – Variola virus G4R

vTNFR – viral TNFR

YFP – Yellow fluorescent protein

Abstract

Tumour necrosis factor (TNF) is potent pro-inflammatory and anti-viral cytokine, acting via two cellular receptors, TNFR1 and TNFR2 that induces apoptosis and inflammation. Poxviruses encode homologues of TNF-receptors (viral TNFRs) that independently interact with both TNF, and simultaneously with cellular TNFRs, to subvert TNF-induced anti-viral apoptosis. The vTNFRs are expressed during poxvirus infection and are considered as bona fide virulence factors. The recently discovery of a "Pre-ligand Assembly Domain (PLAD)" within the N-terminus of the cellular TNFRs is shown to be required for receptor trimerisation and efficient cell death signalling. Whilst it has previously shown that the rabbit-trophic Myxoma (MYX) viral TNFR also contains a PLAD required for viral TNFR:cellular TNFR interactions, little is known about the human-trophic poxvirus TNFRs, nor physical characteristics of the interactions of vTNFRs and cellular TNFRs.

To assess the importance of the PLAD domain in TNFR structure, function and viral subversion of TNFRs, this study focused on naturally occurring mutations in the TNFR PLAD domain, that occur in transient periodic fevers (TRAPS) – a clinical syndrome of febrile attacks of inflammation. TRAPS PLAD domain mutations were generated in a TNFR1-YFP in plasmids by site-directed mutagenesis and cloning. WT and TRAPS mutant TNFR1 constructs were transfected into U20S cells and TNFR1 location was determined by confocal microscopy. Neither WT TNFR1 nor TRAPS TNFRs were unable to be detected at the cell surface by both widefield and confocal microscopy despite published data on surface expression of WT TNFR1. WT TNFR1-YFP fusion proteins were found to be expressed within endocytic vesicles known as receptosomes and also as aggregates

in a membranous structure resembling Golgi/ER. In addition it was found that TRAPS mutations in particular those affecting critical amino acids such as cysteines in disulphide bonds, display reduced TNFR-induced cell death as determined by flow cytometry.

To better understand the biology of the vTNFR association with cellular TNFRs, and with WHO Smallpox committee approval, the human tropic poxviral TNFRs from Variola (Smallpox) (VAR) and Monkeypox (MPV) were synthesised and cloned as CFP/YFP and MycHis expression plasmids. Using multi-colour flow cytometry we have shown that, like the MYXT2 vTNFR, VARG4R and MPVJ2R TNFRs are potent intracellular inhibitors of TNFR1-induced cell death. As each vTNFR was able to inhibit TNFR-induced cell death, an assay was developed by flow cytometry to measure the intracellular abundance of the vTNFRs in the presence of cellular TNFR overexpression. MYXT2 was found to increase in intracellular abundance however for unknown reasons VARG4R and MPVJ2R did not convincingly increase in abundance. A structure for each of the vTNFRs was then attempted to be determined by X-ray crystallography, however bacterial expression of the both the cellular TNFRs and viral TNFRs proteins were unable to be obtained.

Lastly to determine the structural orientations and conformations of cellular vTNFR interactions, a method of fluorescence resonance energy transfer (FRET) was established by flow cytometry. Using the generated C-terminal fusion -CFP and -YFP TNFRs, interactions were assessed between each of the cellular and vTNFRs. It was found that in addition to the reduced cell death TRAPS TNFRs when expressed with WT TNFR1, TRAPS mutations also cause reduced FRET possibly due to altered conformations

in the receptor. Again mutations affecting more critical structural amino acids were found to have a more dramatic effect. Moreover differences were observed between mutations in distribution of FRET histograms further indicating altered network formations of higher order complexes. Next the FRET method was used to assess interactions between each of the vTNFRs with WT human TNFRs as well as with themselves and other vTNFRs. However no FRET was detectable between each of the molecules despite evidence of MYXT2 associating with human TNFR1 and TNFR2. Thus Comparative homology modelling and automated docking simulations were performed to explain possible orientations of the interactions tested in FRET. These data suggest that the interactions of vTNFRs with cellular TNFRs may possibly occur in a C-N anti-parallel orientation and not the previously predicted PLAD-PLAD interactions.

Taken together, these data further our understanding of basic TNFR biology as well as for the first time characterise an entire panel of PLAD TRAPS mutations. It also furthers the characterisation of the very limited evidence of vTNFR subversion of TNFRs for the human trophic viral proteins VARG4R and MPVJ2R. Overall these results show the importance of PLAD interactions to TNFR biology and a possible new avenue in which TNFR signalling may be exploited in the development of new therapeutics.

Chapter One - Introduction

1.1 The human cytokine, tumour necrosis factor alpha (TNF)

In 1975 a serum factor capable of inducing necrosis of tumour cell lines was discovered in the serum of experimentally infected mice (Carswell et al. 1975). Its effects, since then, discovered *in vivo* and *in vitro,* have proven both beneficial and detrimental in biological processes. TNF is the most pleiotrophic cytokine known, with implications in lipolysis (Rydén et al. 2004) organogenesis (Heinrich et al. 1997), chemotaxis (Vaday et al. 2000), apoptosis (Grell et al. 1994) and cell proliferation (Baseta & Stutman 2000). TNF is secreted by a wide array of cell types including activated T-cells, mast cells, granulocytes, natural killer cells and most epithelial tissue (Bonavida 1991; Strieter, Kunkel & Bone 1993). Monocytes and macrophages however, are the major source of TNF (Belge et al. 2002).

The cDNA of TNF was cloned (Gray et al. 1990) and the protein has been characterised (Eck & Sprang 1989). TNF exists as a 26 kDa transmembrane protein, also known as “pro- TNF" or membrane TNF expressed on the plasma membrane (Tang, Hung & Klostergaard 1996) It is then proteolytically cleaved by a metalloprotease: TNF-converting enzyme (TACE) (Black 2002), to release a soluble 17 kDa TNF (Kriegler et al. 1988)(Figure 1.1). Both the membrane bound and soluble TNF are biologically active as homotrimers (Pfeffer 2003).

TNF belongs to a family of structurally related cytokines called the TNF superfamily. This family contains more than 20 members including: lymphotoxin-α, lymphotoxin-β, CD40L, Fas ligand (FasL), CD27L, CD30L, TNF-related apoptosis-inducing ligand (TRAIL),

osteoprotegerin-L, TNF-related weak inducer of apoptosis (TWEAK), a proliferation-inducing ligand (APRIL), B cell activating factor (BAFF), herpes virus entry mediator (HVEM) ligand, OX-40 ligand, vascular endothelial cell-growth inhibitor (VEGI), and glucocorticoid-induced TNF-receptor related protein ligand (GITR) (for review on complete family see (Bodmer, Schneider & Tschopp 2002).

1.2 TNF Receptors (TNFR) -1 and -2

The effects of TNF are initiated by the binding to two receptors, TNFR1 (p55/p60/CD120a), and TNFR2 (p75/p80/CD120b) (Loetscher et al. 1991; Loetscher, Pan, et al. 1990; Loetscher, Schlaeger, et al. 1990) (Figure 1.1). These two receptors form the prototype of a large family of structurally-related molecules, termed the TNFR-Superfamily (TNFRSF). These molecules are characterised by their homologous extracellular cysteine rich domains (CRDs) (Smith et al. 1990). Interestingly, TNFRSF proteins include a number of viral homologues, some of which were discovered before their cellular counterparts. For example, the Myxoma T2 protein (MYXT2) which was cloned before TNFR2 (Upton et al. 1991) (for review see (Sedger 2005).

As stated above, both TNFR1 and TNFR2 are type I trans-membrane proteins which contain 4 cysteine rich repeat domains (CRDs) consisting of six cysteines, forming intra-molecular disulphide bridges (Loetscher et al., 1990b) (Figure 1.1). TNFR1 and TNFR2 form non-covalent homo-trimers and bind to TNF, which induce clustering of neighbouring trimers. The C-terminal regions of TNFR1 and TNFR2 share no sequence homology but contain amino acid motifs related to receptor function. TNFR1 contains a so-called “death domain” (DD) in its C-terminal region (Sukits et al. 2001) whereas

TNFR2 contains a TNF Receptor Associated Factor (TRAF) binding domain (Boldin et al. 1995; Feinstein et al. 1995; Rothe et al. 1995)(Figure 1.1).

Neither TNFR1 or TNFR2 have enzymatic activity, but rather these molecules initiate signalling through the recruitment of intracellular adaptor proteins, including TNFR associated death domain protein (TRADD) (Hsu, Xiong & Goeddel 1995), Fas associated death domain protein (FADD) (Chinnaiyan et al. 1996), receptor interacting protein kinase (RIP) (Hsu, Huang, et al. 1996) and TNFR-associated factor (TRAF)-2 (Rothe et al. 1995) (Figure 1.2). The clustering or TNFR trimers allows oligomerisation of adaptor proteins, and further recruitment of additional adaptor proteins (Dempsey et al. 2003). *In vitro*, the initiation of a receptor signalling complex can also occur in the absence of TNF (Haridas et al. 1998) The over-expression of either TNFR1 or TNFR2 is thought to induce clustering of intracellular regions of the receptor, such as the death domain, and initiate signalling pathways (Boldin et al., 1995; Haridas et al., 1998). Thus it is easy to induce *in vitro* experimentally e.g. by transfection–based expression, but it remains controversial as to whether an up-regulation of TNFRs is sufficient to induce TNFR signalling *in vivo,* independent of ligand.

1.3 The TNFR Pre-ligand Assembly Domain (PLAD).

The ability of the TNFRs to oligomerise and form signalling complexes is dependent on a N-terminal domain called the pre-ligand assembly domain (PLAD) (Chan 2000). The PLAD is a highly conserved domain that is located within the first CRD of both TNFR1 and TNFR2. The highly conserved sequence and structure allows the oligomers to form stable non-covalent interactions in the absence of TNF (Chan et al. 2000a). Experimental

deletion of the PLAD renders TNFRs unable to self-associate and renders TNF unable to competently bind and induce receptor signalling (Chan et al. 2000a). Thus a fully functional PLAD is required for competent TNFR signalling.

Although much is known about TNFRs themselves and subsequent signalling pathways, little is known about the ligand induced activation of the receptors. An early model suggested that the receptors are required to form trimers before ligand binding, however recent evidence has raised doubts about the stoichiometry of ligand:receptor complexes (Banner et al. 1993; Eck & Sprang 1989; Mukai et al. 2010). From early crystallography studies, two structures of TNFR1 have been described, one a parallel N-N dimer and the other an anti-parallel C-N dimer, in the absence of ligand (Naismith et al. 1996). The parallel dimer allows TNF binding whereas the anti-parallel conformation is thought to occlude the TNF binding site (Naismith et al. 1996). These two structures of TNFR1 may indicate different active conformational changes in TNFR1 under different biological conditions. However because the binding sites of TNF are occluded in the anti-parallel conformation, it is questionable whether this is biologically relevant. It may represent a “closed state” of TNFR1, to prevent TNF from further activating signalling pathways, i.e. by occluding the TNF-binding site.

A recent model of TNFR receptor activation has been suggested that gives evidence for the receptors transitioning between various stoichiometries. It has been shown that the PLAD or CRD1 is required for TNFRs to preassemble as well as stabilising CRD2 for ligand binding (Branschädel et al. 2010; Chan 2000). These dimers or trimers arrange into clusters or aggregates once ligand is bound for efficient activation of signalling pathways at the cell surface (Ranzinger et al. 2009). In support of this model, deletion of the PLAD

domain results in a decrease in the amount of TNF able to bind at the cell surface (Chan 2000). A contradiction to this however, is that all crystal structures of TNF-TNFR super family complexes such as TNFR1, DR5 and OX40 are found with PLAD domains dissociated. PLAD mutations in Fas receptors render them unable to bind Fas ligand (FasL) and they form “dominant negative” complexes with wild type Fas molecules that are unable to trigger apoptosis (Siegel et al. 2000). In both cases, the mutated proteins are expressed and confer pathological symptoms. Hence PLAD domain mutations of TNFRSF molecules confer altered TNFR function. The impact of the PLAD mutations to normal TNFR biology, and the fact that poxvirus pathogens, have specifically targeted TNFR biology through encoding a TNFR of their own, likely reflects the PLAD’s importance in TNFR biology.

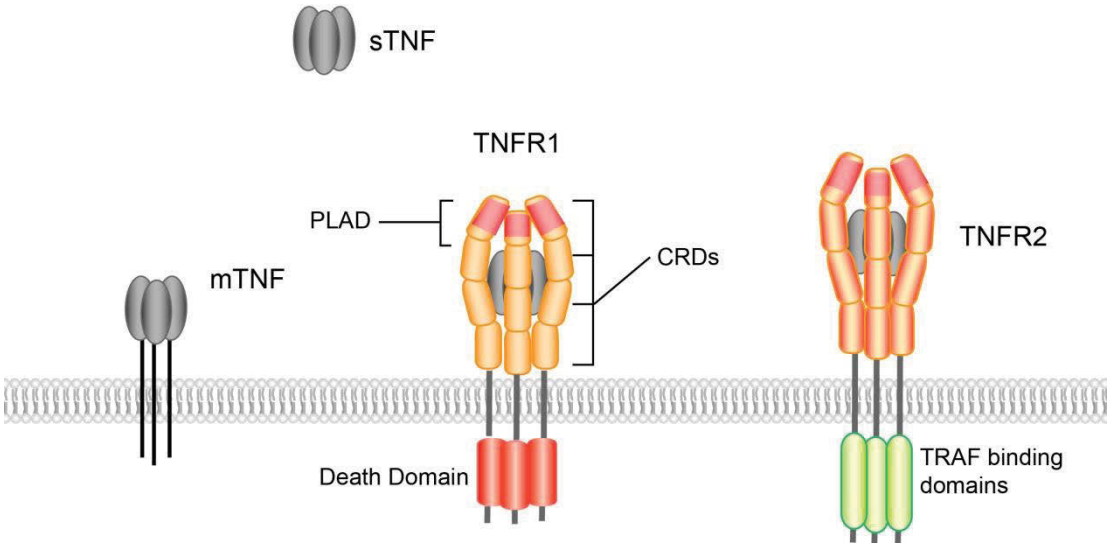

Figure 1.1 Model of TNF and cognate receptors, TNFR1 and TNFR2.
TNF depicted in its trimeric soluble and membrane pro-forms at the cell surface. Trimerised TNFR1 and TNFR2 shown bound to soluble TNF with functional domains depicted: CRDs and PLAD.

1.4 Signalling pathways of TNFRs

As stated above, TNF is a highly pleiotrophic cytokine. This is reflected by the numerous and complex pathways which can be initiated from TNFRs upon TNF binding. Although its name suggests it is involved in the activation of cell death, this usually only occurs in times of cellular stress (Warzocha 1998). In most cases, however, TNFRs signalling activates two major transcription factors: AP-1 and NFκB – both of which are involved in creating an inflammatory state within cells (Barnes & Karin 1997; Karin, Liu & Zandi 1997).

TNF binding to the TNFRs triggers the recruitment of intracellular adaptor proteins to trigger signalling cascades (Figure 1.2). These adaptor proteins include TNF-receptor associated death domain protein (TRADD) (Hsu, Xiong & Goeddel 1995), receptor interacting protein kinase (RIP) (Hsu, Huang, et al. 1996), TNFR associated factor 2 (TRAF2) (Hsu, Shu, et al. 1996), and Fas associated death domain (FADD) (Chinnaiyan et al. 1996). The recruitment of adaptor proteins to TNFRs can activate pathways such as (i) the caspase (a family of cysteine proteases) cascade leading to cell apoptosis, (ii) the c-Jun N-terminal kinase (JNK) and nuclear factor kappa B (NF-κB) pathways involved in cell proliferation, and (iii) the acid and (iv) neutral sphingomyelinase pathways - involved in the production of ceramides (MacEwan, 2002) (Figure 1.2).

The binding of TNF to the trimerized receptors is proposed to induce a conformational change in the receptor structure which modifies the position of the intracellular domains of the TNFRs (Miki & Eddy 2002). This change in conformation is also proposed to release the adaptor protein silencer of death domain (SODD) which is thought to prevent

constitutive TNFR1-death signalling prior to ligand binding (Takada et al. 2003). TNFR-adaptor proteins can only be recruited into a TNFR signalling complex once SODD is released from the receptor (Eichholtz-Wirth, Fritz & Wolz 2003).

The "activation" of TNFRs is known to permit the receptors to be recruited into specialised lipid-rich micro domains (lipid rafts) on the cell surface plasma membrane (Legler et al., 2003; Muppidi et al., 2004). The localisation of TNFR1 to lipid rafts facilitates the recruitment of TNFR1 adaptor molecules at the cell surface, which then become modified by phosphorylation and or processed by mechanisms such as ubiquitylation (Legler et al., 2003). These modified adaptor molecules then activate signalling pathways essential to processes such as the activation of the (NF-κB) (Figure 1.2). In fact, disruption of lipid rafts with methyl-cyclodextrin, an agent which removes cholesterol, inhibits TNFR1-induced NF-κB activation (Legler et al., 2003)

1.4.1 TNFR-induced activation of NF-κB

TNFR1 signalling leading to NF-κB activation occurs through the degradation of the inhibitor of NF-κB complex (IKK) - also referred to as the "classical" NF-κB pathway (Figure 1.3). NF-κB activation by TNFR1 involves the recruitment of TRADD and RIP through death effector domains contained in the C-terminus of these proteins, followed by recruitment of TRAF2 via a TRAF-interacting domain (Micheau & Tschopp 2003). TRAF2 subsequently binds the cellular inhibitors of apoptosis proteins (cIAPs) to form the TNFR1 signalling complex I (Figure 1.2). This is further processed through ubiquitination by proteins such as E3 ligases including HOIL-1 and HOIP (Haas et al. 2009; Shambharkar et al. 2007).

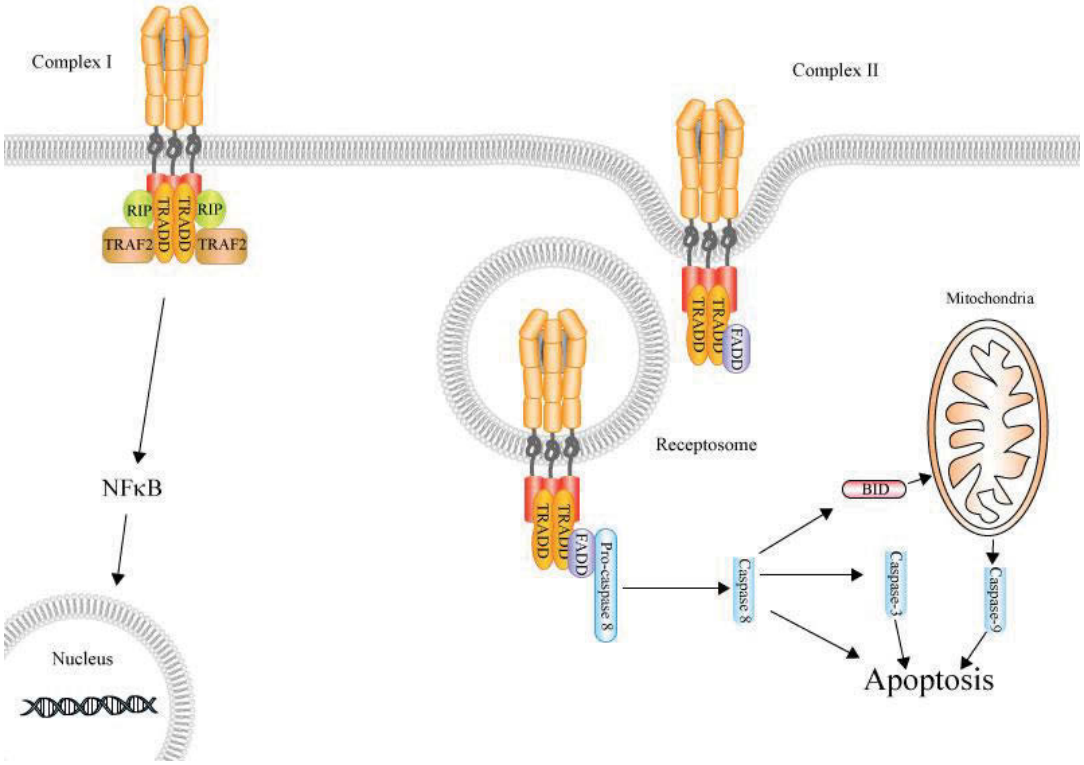

Figure 1.2 Proposed model of TNFR1 signalling complexes.
TNF binding to trimerized receptors induces conformational changes and allows the recruitment of adaptor molecules. The formation of complex 1and recruitment of TRADD, RIP and TRAF2 leads to NFκB activation. In the absence of proliferative signals complex 2 is formed and internalised, recruiting TRADD and FAD leading to caspase activation and apoptosis.

The formation of TNFR1 signalling complexes within lipid rafts facilitates ubiquitination of RIP and TRADD, and indeed, lipid raft disruption prevents NF-κB activation of TNFR1 (Legler et al. 2003). Eventually a number of intermediate kinases and ubiquitinases are activated and this leads to phosphorylation of the IKK complex and the proteasomal degradation of IKK (Delhase & Yi 1999; Ea et al. 2006; Tang et al. 2003) (Figure 1.3). The cytoplasmic NF-κB subunits are then released and free to translocate into the nucleus that then in turn acts as a DNA-binding transcription factor to up-regulate NF-κB response genes and inflammation.

A key difference between TNFR1 and TNFR2 is the absence of a C-terminal death domain (in TNFR1) and the inability to recruit TRADD and RIP directly. Instead, TNFR2 utilises TAF-binding motifs (Rodríguez et al. 2011). Although, as described above, TRAF2 is required for NF-κB signalling in the classical pathway, TRAF2 also activates NF-κB through the alternative pathway (Rauert et al. 2010) (Figure 1.3). The stimulation of TNFR2, such as by membrane TNF, induces degradation of TRAF2 (Ka-Ming Chan & Lenardo 2000). This causes the accumulation of NF-κB-inducing kinase (NIK), and activates IKK1 to process the p100 NF-κB for proteosomal degradation, thus releasing the active NF-κB (Rauert et al. 2010; Rodríguez et al. 2011; Xiao, Harhaj & Sun 2001). The accumulation of NIK in the cytoplasm is highly regulated by the levels cellular IAPs: cIAP1 and cIAP2, and TRAF3, which also influences TNFR1 signalling cross-talk between the two receptors (Sun & Ley 2008).

1.4.2 TNFR activation of cell death

TNF, as its name indicates, is perhaps most notably renowned for its ability to induce cell death. Although TNFR1 contains an intracellular death domain motif, TNFR1 does not strongly activate apoptosis in most cell types (Deng et al. 2003; Fotin-Mleczek et al. 2002).

TNFR1-induced cell death occurs through the formation and the recruitment of the "death inducing signalling complex" or DISC, comprising TRAD, FADD and pro-caspse-8 (Feinstein et al. 1995; Micheau & Tschopp 2003; Schneider-Brachert et al. 2004).

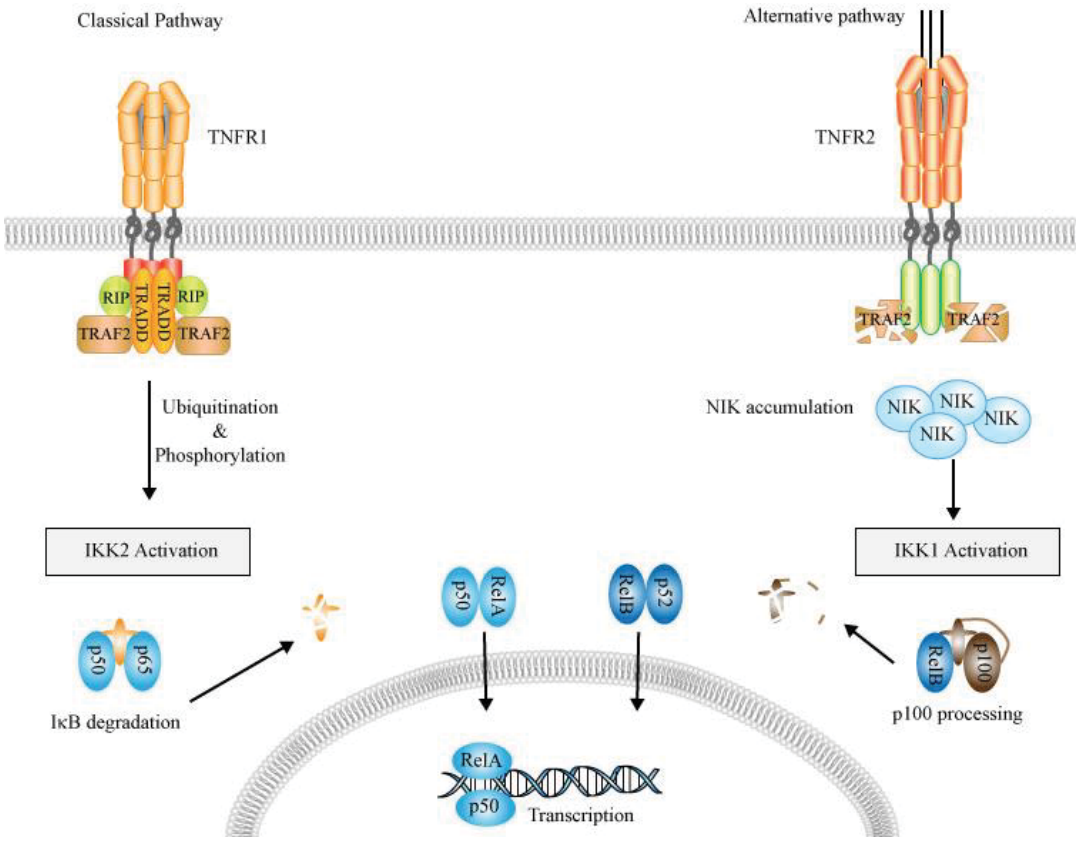

Figure 1.3 Activation of NFκB by TNF via TNFR1 and TNFR2.
Activation of TNFR1 leads to the recruitment of TRADD RIP and TRAF adaptor molecules. This complex is ubiquinated which leads to the phosphorylation of the IKK2 complex and subsequent activation and translocation of p50 and RelA NFκB subunits. The activation of TNFR2 causes the degradation of TRAF2 adaptor molecules and accumulation of NIK intracellularly. NIK activates the IKK1 complex leading to proteolytic processing of p100 and RelB NFκB subunits. Translocation of NFκB subunits into nucleus leads to upregulation of various proliferative and inflammatory genes.

The Death inducing complex firstly requires the down regulation of anti-apoptotic signals such as NF-κB. TRADD is firstly recruited to the death domain of TNFR1, and in the absence or down regulation of TRAF2 and RIP, this complex is then internalised into endosomes (otherwise called “receptosomes”) (Hsu, Xiong & Goeddel 1995; Micheau & Tschopp 2003). The internalised complex then recruits FADD and pro-caspase-8 to form the TNFR1-associatated DISC, where pro-caspase-8 is auto-catalytically processed into active caspase-8 (Salvesen & Dixit 1999) (Figure 1.4). Active caspase-8 then cleaves and activates effector caspases, such as caspase-3 and caspase-7, that results in the cleavage

of diverse substrate proteins including the inhibitor of caspase-3-activated DNase (ICAD), releasing CAD to translocate into the nucleus and cleave genomic DNA (Enari et al. 1998) (Figure 1.4). Active caspase-3 also acts on BH3 Interacting Death domain agonist (BID), resulting in cytochrome c release and thereby amplifying the TNFR1 apoptosis pathway (Rath & Aggarwal 1999).

The internalised TNFR1 death complex has also been shown to fuse with trans-Golgi vesicles containing pro-sphingomyelinase (SMase) and pre-pro-cathepsin D (Schneider-Brachert et al. 2004). Fused Golgi-receptorsome vesicles containing active caspase-8 and activated Acid-SMase, which produces ceramide, and subsequently activates cathepsin D (Heinrich et al., 2004). Cathepsin D migrates into the cytoplasm and proteolyticaly cleaves BID (a BH3 domain-only death agonist protein) to generate truncated BID (tBid). This subsequently results in cytochrome c release from mitochondria and hence the down-stream activation of pro-caspase-9 and also pro-caspase-3, thereby leading to apoptotic cell death (Heinrich et al. 2004; Schneider-Brachert et al. 2004).

1.5 TNF and TNFR pathology

The regulation of TNF and TNFRs is strictly regulated and abnormalities or aberrant activation of the TNFR signalling cascade can be detrimental to host cells and tissue.

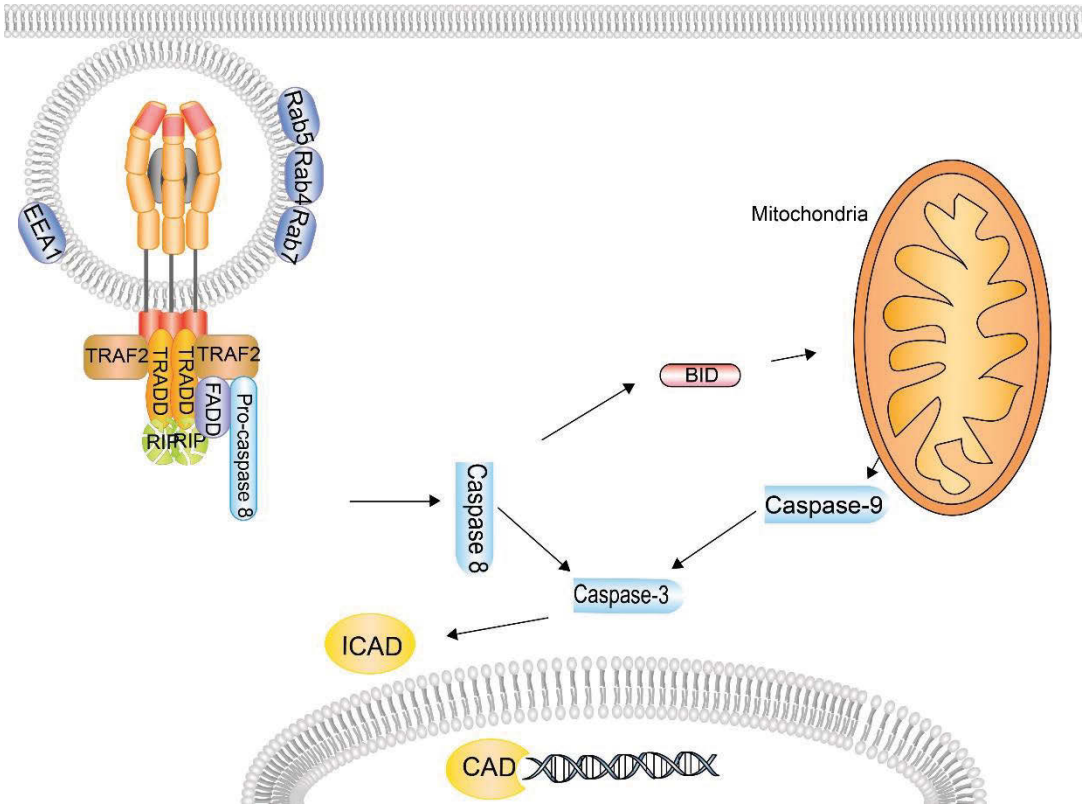

Figure 1.4 TNFR1 activated cell death.
Degradation or downregulation of RIP and TRAF2 of TNFR1 leads to the internalisation of TNFR1 complexes into Rab5 positive endosomes or "receptosomes". FAD and procaspase 8 is then recruited to the complex where procaspase 8 is autocatalytically processed to activate the caspase cascade. This leads to the activation of CAD, DNA degradation and apoptosis.

TNF has been implicated in numerous non-infectious inflammatory diseases such as rheumatoid arthritis (RhA) (Brenner et al. 1989; Buchan et al. 1988), Crohn's disease, ulcerative colitis (Macdonald et al. 1990; Reimund et al. 1996), psoriasis (Kristensen et al. 1993), multiple sclerosis (Selmaj et al. 1991), systemic lupus erythematosus (Maury & Teppo 1989) and both types 1 and 2 diabetes (Dandona, Aljada & Bandyopadhyay 2004; Kroeger, Carville & Abraham 1997). In the majority of these disease states there is an excess of TNF due to constant activation of inflammation which creates a harmful pro-inflammatory state within host tissues. Because of the implication of TNF in these diseases states and its central role in the immune system, it has become an attractive target for drug design which aims to modulate TNF and TNFR signalling.

1.5.1 TNF Receptor-Associated Periodic Syndrome (TRAPS)

One particular pathology found to be associated with TNFR1 (the primary mediator of cell death) has been discovered in patients suffering from bouts of periodic inflammation known as TNFR-associated periodic fever syndrome (TRAPS). TRAPS is an autosomal dominant inherited disease syndrome conferred by mutations in the TNFR1 gene (McDermott et al. 1999). TRAPS was first described in a large family with Scottish/Irish ancestry and hence was previously referred to as Familial Hibernian Fever (Williamson et al. 1982). It was not until the discovery of the TNFR1 loci and genome screening of several TRAPS families that the TRAPS pathology was associated with mutations in the TNFR1 loci, located on chromosome 12p (McDermott et al. 1998). The discovery of mutations in the TNFR1 gene provided a link to the recurrent inflammatory symptoms observed in TRAPS patients, as TNF is a potently pro-inflammatory cytokine.

The TRAPS mutations in TNFR1, although rare, are clinically associated with irregular recurrent long fevers lasting more than a week and a multitude of other inflammatory symptoms that vary depending on the severity of each case. In 80% of patients the fevers are accompanied by myalgia, arthritis, fasciitis, abdominal pain, skin patches, skin lesions, conjunctivitis, periorbital oedema and in severe cases amyloidosis (Lachmann et al. 2013; Lahaxe et al. 2010; McDermott, Smillie & Powell 1997; Quillinan et al. 2010; Rösen-Wolff et al. 2001; Williamson et al. 1982). A small percentage (15%) of patients also develop inflammatory associated amyloidosis, which is an accumulation of misfolded proteins that deposit throughout organs and tissues (Jacobs & Ciaccio 2010). Some studies also suggest that TRAPS patients suffer persistent subclinical features

between febrile attacks, and this is thought to be due to a chronic acute inflammatory response (Quillinan et al. 2010).

The onset of TRAPS clinical symptoms can vary widely, ranging from 2 weeks to 53 years of age, with periodicity between attacks ranging from a few weeks to years (Hull et al. 2002; Nedjai et al. 2009). The disease is more common in Caucasians, Arabic and Mediterranean populations but has been reported in populations and ethnicities across the world (Aksentijevich 2014; Ravet et al. 2006). The disease is usually diagnosed on suspicion of recurrent fever episodes and hospitalisations followed up by genetic testing. The combination of a broad clinical inflammatory presentation shared by many other periodic fever syndromes and a lack of accessible means of testing leaves the epidemiology and incidence of TRAPS largely unknown (Lachmann et al. 2013). One large study estimated the incidence as 5.6 cases per 10^7 person-years for the period of 2003-2006, or approximately 6-10 new cases each year in Germany (Lainka et al. 2009). Worldwide it is estimated to be present in about 1 in every 1 million people (Hull et al. 2002; Lachmann et al. 2013). Although TRAPS is defined as an autosomal dominant inherited syndrome it is important to note that less than two thirds of diagnosed patients report not having a family history, possibly due to a lack of sufficient genetic screening measures and/or the low penetrance of some mutations. Therefore many TRAPS cases are not reported or misdiagnosed.

1.5.2 TRAPS mutations

There are currently 141 sequence variants of TNFR1 said to be associated with the TRAPS phenotype, documented in the extensive online periodic fever database ‘Infevers”

(Aksentijevich 2014) . The majority of all TRAPS mutations are single point mutations resulting in a single amino acid substitution, and interestingly, the vast majority reside within the first two CRDs of TNFR1 (Figure 1.5). This region of TNFR1 includes the TNF binding domain (CRD2 and CRD3) and the PLAD domain (CRD1) which is essential for receptor trimerisation and ligand-induced signalling (Branschädel et al. 2010). A number of rare mutations such as single in frame deletion variants also exist as well as an interstitial deletion of 9 amino acids in exon 4 (D'Osualdo et al. 2006), and a splice variant that introduces 4 amino acids (Aksentijevich et al. 2001). Currently there are no mutations that have been described in the transmembrane or intracellular domains of TNFR1 (Figure 1.5). There are also no mutations described which disrupt the expression of the protein such as large truncations.

Many of the TRAPS mutations affect amino acids important to the folding or stability of the TNFR1, such as cysteines residues involved in intramolecular disulphide bridges (Todd, Tighe & Powell 2005). Other mutations affect amino acid residues such as proline, which are important in structural loops and hydrogen bonding (Rebelo et al. 2006). The type of amino acid mutation appears to correlate with the severity of TRAPS symptoms. Cysteine mutations such as C33Y and C29Y, particularly those involved in disulphide bridges in CRD1 and CRD2 tend to show a higher penetrance, more severe phenotype, and higher risk of amyloidosis, compared to other TNFR1 mutations (Hull et al. 2002; Lachmann et al. 2013). Structural modelling of TRAPS mutant proteins indicate that changes in amino acid residues place strain on the structure of the protein and it has been suggested that this may alter TNF binding (Rebelo et al. 2006). The R92Q and P46L mutations are associated with a lower penetrance, fewer rash and eye clinical presentations and no cases of amyloidosis have been reported with this mutation

(Aksentijevich et al. 2001). The R92Q mutation, in particular, is said to be the most common variant, and it presents as mildly symptomatic or asymptomatic, with patients occurring with an allele frequency of 1-3% in Irish North American and German control populations (Hoffmann et al. 2005; Lainka et al. 2009).

The severity or penetrance of clinical TRAPS however does not directly correlate with the predicted major structural changes caused by mutations. Many studies have found a wide variation among patients of clinical presentations, and even between patients with similar or even the same mutations (Siebert, Amos, et al. 2005; Siebert, Fielding, et al. 2005; Todd et al. 2004; Yousaf et al. 2005) (Table 1-1). This may possibly be due to the fact that TRAPS patients are heterozygous for wild type TNFR1 and mutant TNFR1 alleles, and the underlying pathology is not only dependant on the aberrant function but also due to more complex protein interactions such as up- or down- regulation of alleles or interactions of mutant TNFR1 with other TNFR1 associated proteins (Yousaf et al. 2005). The exact mechanism or trigger or TRAPS symptoms is still unknown but studies have found that many TRAPS mutations show aberrant NF- κB activation (Churchman et al. 2008), an inability to bind TNF (Siebert, Fielding, et al. 2005), reduced surface expression (Lobito et al. 2006), reduced receptor shedding (Hull et al. 2002), reduced apoptosis (Hull et al. 2002) and elevated cytokine profiles such as TNF, IL6 and Il-1 (Rebelo et al. 2006; Todd et al. 2004) all of which are characteristic of the inflammatory clinical picture see in TRAPS patients (D'Osualdo et al. 2006; Huggins et al. 2004; Nedjai, Hitman, et al. 2011; Nedjai et al. 2008; Siebert, Fielding, et al. 2005; Todd, Radford, Ziegler-Heitbrock, et al. 2007). There is also reports suggesting that incorrect TNFR1 folding leads to its accumulation in the endoplasmic reticulum and thus an induction of an “unfolded protein response”. This most likely activates the inflammasome that leads

to production of mitochondrial reactive oxygen species (ROS) and cytokines, as seen in some TRAPS patients (Bulua et al. 2011; Menu et al. 2012).

The triggers of these periodic fever episodes is still yet to be defined, and throughout the literature there is a gap in the understanding of how these proteins interact, or complex with, wild type TNFR1. It is also unclear how wild type TNFR1 itself interacts to form an initial signal complex in the presence of TRAP mutant TNFRs. For example, the stoichiometry of wild type TNFR1 complex is still unknown (considering that TNFRs form trimmers), and the full length TNFR1 protein is still yet to be crystallised. It is still unclear whether TRAPS proteins have an ability to form larger signalling complexes and whether completely differential signalling pathways are activated.

There is also much controversy and many inconsistencies surrounding studies investigating the effect of mutations on TRAPS biology. This might in part be due to variations between different experimental methods, or differences in the cells used in different laboratories, or differences emanating from patients themselves, etc. For example, mutant TRAPS cell lines display reduced activation, whereas isolated peripheral blood monocytes of TRAPS patients show increased NF-κB activation (Lobito et al. 2006; Todd et al. 2004). In addition to these complications, the mutations themselves and the presence of endogenous TNFR1 within cells, makes interpretation of results deceptive and not necessarily straight forward. A summary list of mutations and their effects can be found in (Table 1-1).

Table 1-1 Known mutations in the PLAD domain and effects on receptor biology.

Mutation	Substitution	Amino acid change	Receptor/Cell Abnormalities	Reference
Y20D	TAT>GAT	Tyr>Asp	N/A[#]	
Y20H	TAT>CAT	Tyr>His	N/A[#]	
H22R	CAC>CGC	His>Arg	N/A[#]	
H22Y	CAC>TAC	His>Tyr	Reduced Fret with WT receptor, Reduced NF-κB levels, defective shedding, Surface expression not detectable, reduced apoptosis	(Hull et al. 2002) (Lobito et al. 2006)
C29F	TGC>TTC	Cys>Phe	N/A[#]	
C29Y	TGC>TAC	Cys>Tyr	N/A[#]	
C30F	TGT>TTT	Cys>Phe	N/A[#]	
C30R	TGT>CGT	Cys>Arg	Reduced shedding/ not secreted, Reduced FRET with WT, Reduced NF-κB, Surface expression not detectable	(Hull et al. 2002) (Lobito et al. 2006) (Siebert, Fielding, et al. 2005)
C30S	TGT>TCT	Cys> Ser	defective shedding	(Hull et al. 2002)
C30Y	TGT>TAT	Cys>Tyr	N/A[#]	

C33G	TGC>GGC	Cys>Gly	Reduced NF-κB, defective shedding, Surface expression not detectable, Reduced apoptosis	(Hull et al. 2002) (Lobito et al. 2006)
C33Y	TGC>TAC	Cys>Tyr	Elevated CD16 in CD14+CD16 PBM, formation of inclusion bodies, Full length receptor Not detectable at surface, truncated c-terminal receptor show surface expression, unable to bind TNF at surface, Reduced apoptosis, reduced IL8, elevated IL6, Elevated Il-8	(Nowlan et al. 2006) (Todd, Radford, Ziegler-Heitbrock, et al. 2007) (Todd et al. 2004) (Rebelo et al. 2006) (Hull et al. 2002)
T37I	ACC>ATC	Thr>Ile	N/A[#]	
Y38S	TAC>TCC	Tyr>Ser	N/A[#]	
L39F	TTG>TTC	Leu>Phe	N/A[#]	
C43R	TGT>CGT	Cys>Arg	N/A[#]	
P46L	CCG>CTG	Pro>Leu	overexpression of mutant caused less downregulation of WT, defective shedding	(Hull et al. 2002) (Yousaf et al. 2005)

[#]N/A – data not available for mutation

1.5.3 Significance of TRAPS mutation

The presence of TRAPS mutations is effectively a unique natural example of an extensive structure/function mutational analysis *in vivo*. TRAPS was the first syndrome to define a new class of hereditary disorders that classically were not defined by autoimmune diseases (Aksentijevich et al. 2001). These auto-inflammatory diseases do not display characteristics of adaptive immunity but rather a dysfunction of the innate immunity (Masters et al. 2009). TRAPS mutations are not embryonic lethal but are severe enough to cause clinical disease, and although rare, it is intriguing to speculate whether these mutations have some selective biological advantage or whether they are always biologically expensive and disadvantageous. The exclusive presence of TRAPS mutations in the extracellular domain of TNFR1, along with a higher proportion of mutations appearing in people of Caucasian Mediterranean decent, might arguably suggest that these mutations may have once, or still serve as a protective measure against infection or diseases present within this same area. Familial Mediterranean fever (FMF) is an autosomal recessive disease that is clinically almost identical to TRAPS but which is caused by mutations in a gene encoding the protein pyrin - a protein involved in down regulating the inflammatory response (Chen et al. 1998). FMF is typically seen in Mediterranean populations (hence the name) of Jewish, Turkish, Armenian and Arabic ethnicity (Belmahi et al. 2006; El-Shanti, Majeed & El-Khateeb 2006; Shinawi et al. 2000).

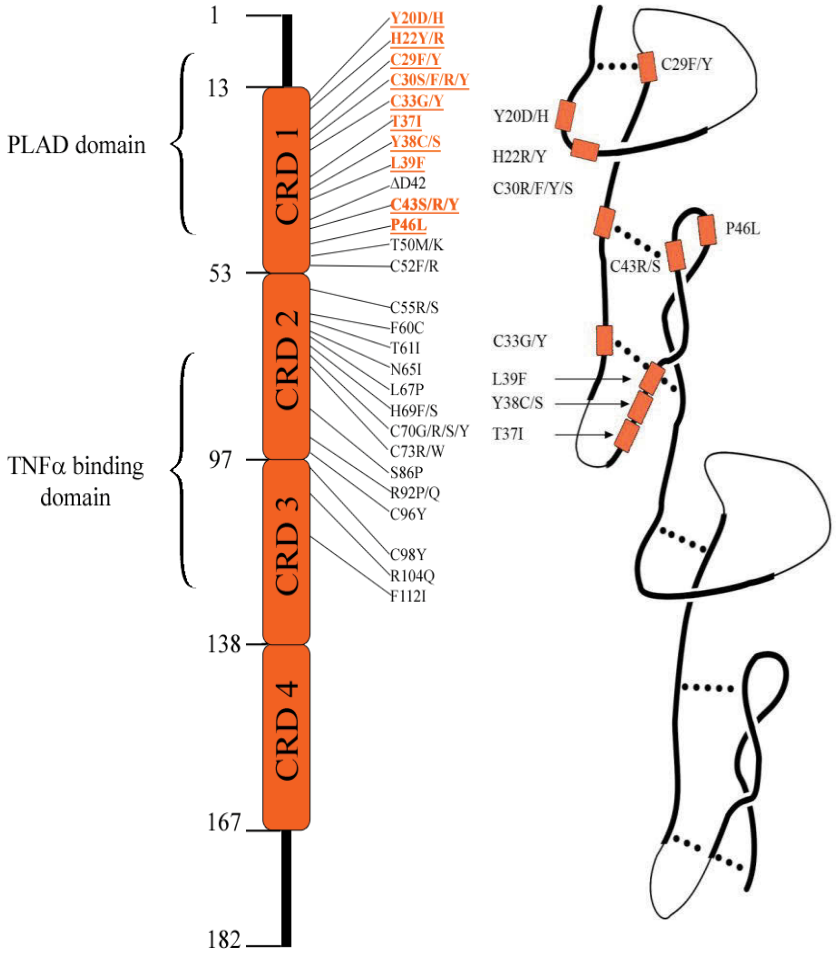

Figure 1.5 TRAPS mutations in TNFR1 extracellular domain.
(A) Linear representation of TNFR1protein extracellular domain and location of known TRAPS mutations. **(**B) Corresponding ribbon diagram of TNFR1 extracellular domain and associated TRAPs mutations. Cysteine disulphide bonds are represented as dotted lines. [Adapted from (Kimberley et al. 2007)].

Although, like TRAPS, people carrying these mutations suffer severe bouts of fever and inflammatory symptoms (including the development of amyloidosis) there is evidence that FMF mutations may protect against infection. For example mice expressing a truncated form of pyrin exhibit increased IL-1 production and increased sensitivity to endotoxin, but this may simultaneously protect them against bacterial infection (Chae et al. 2003). Additionally, it is speculated that brucellosis, a disease endemic to the

Mediterranean region and more prevalent in ancient times, provided a selective pressure on the population, especially those bearing low penetrance heterozygous mutations (Ross 2007). Likewise, TRAPS mutations affecting TNFR1, important component of antiviral apoptosis, may have provided protection against certain viral infections. One could envisage that this would include virulent virus infections such as smallpox. In particular, the low penetrance TRAPS mutation P46L, which is common in more than 1% of African American populations, were likely subject to severe epidemics of smallpox in Africa (Lainka et al. 2009; Ravet et al. 2006).

1.6 Anti-TNF Therapeutics.

The initial discovery of TNF led to its potential use as a therapeutic to selectively target tumour cells. Used first in mice, this was the first instance in which TNF was used or targeted to treat disease (Ziegler-Heitbrock et al. 1986). The development of a recombinant form of TNF and its apparent safety in mice, then led to a series of extensive human clinical trials, such as for its use as a broad spectrum anti-cancer agent (Abbruzzese et al. 1990; Creaven et al. 1987; Feinberg et al. 1988; Whitehead et al. 1990). It quickly became apparent, however, that there was no objective benefit evident in any of the patients. Moreover, many trial participants developed acute toxicities which were more severe with increasing doses of TNF. These toxicities included fever, chills, nausea, vomiting, myalgia, arthralgia, loss of appetite, leukopenia and hepatoxicity (Heim et al. 1990; Whitehead et al. 1990). The trials of recombinant TNF were also tested in combination with recombinant interferon, and/or with various interleukins, such as IL-2. These combinations all appeared to exacerbate the above adverse side effects (Abbruzzese et al. 1990; Negrier et al. 1992). It soon became

apparent from the trials that the range of side effects were being mediated from the administration of TNF and that TNF was responsible for a broad host of biological functions than were not anticipated.

The next wave of trials of TNF therapy came from the development of antibodies to TNF i.e. agents trialled to block TNF's pro-inflammatory actions. Thus the many trials using recombinant TNF to treat various cancers directly lead to the discovery of TNF as a highly potent inflammatory molecule. By using antibodies to block TNF, benefits could be seen in various inflammatory conditions such as rheumatoid arthritis (RhA) (Beutler, Milsark & Cerami 1985; Elliott et al. 1993; Williams, Feldmann & Maini 1992; Williams et al. 1995). The success of anti- TNF antibodies in animal models, initially in sepsis models, ultimately led to the development of the anti- TNF therapeutics in humans (Boillot et al. 1995; Elliott et al. 1994; Giroir 1993) (Table 1-2).

Infliximab was the first anti- TNF monoclonal antibody approved for therapeutic use in humans (Maini et al. 1999). Infliximab, also known by its trade name Remicade, is a chimeric mouse/human anti- TNF monoclonal antibody (Maini et al. 1999). The antibody binds to soluble and membrane TNF blocking it from binding to the TNFRs, thereby preventing TNF-induced inflammation (Maini et al. 1999; Scallon et al. 1995). Infliximab is a successful inhibitor of TNF in a number of human inflammatory diseases; it us currently FDA-approved for use in Crohn's disease, ulcerative colitis, rheumatoid arthritis, ankylosing spondylitis and plaque psoriasis (Janssen Biotech Inc 2014). A number of variants of infliximab have also now been developed and approved for use inhuman inflammatory diseases. Infliximab variants include; Adalimumab, Golimumab, Humicade and Certolizulmab and with a range of biosimilars still in the pipeline a

number of generic therapeutics are soon to be released. These agents are all antibodies specific to TNF but most are fully human immunoglobulins. A complete list of anti-TNF biologics is provided in table (Table 1-2). An exception to this range of anti TNF monoclonal antibodies is Etantercept (commercially known as Enbrel). Etanercept is a chimeric fusion protein comprising a recombinant form of the human TNFR2 extracellular region expressed in frame with the constant region a human IgG1-Fc. Because Etanercept contains the TNFR2 protein it not only binds to TNF but also to lymphotoxin-a (Scallon et al. 2002). Consistent with this it has been demonstrated that the binding characteristics of Etanercept mimic that of soluble TNFR2 (Tsimberidou et al. 2003) and its efficacy differs to that of the many antibodies against TNF in treating inflammatory diseases (Agnholt, Dahlerup & Kaltoft 2003; Mitoma et al. 2005; Scallon et al. 2002). Although Anti- TNF biologics have proven successful in treating many inflammatory diseases their mode of action is still poorly understood and one agent which may prove successful in one disease may be unsuccessful or yet worsen the symptoms in another similar disease such as TRAPS, Crohn's, colitis and RhA (Breda et al. 2011; Choy et al. 2002; Poddubnyy & Rudwaleit 2011).

Table 1-2 Current Anti-TNF biologics

Biologic Name	Trade name	Description	Therapy protocol	Reference
Infliximab	Remicade	Chimeric mouse-human anti- TNF Ab[#]	2 hour IV[*] infusion, 5mg/kg every 8 weeks after induction period	www.remicade.com (Maini et al. 1999)
Etanercept	Enbrel	TNFR2-IgG Fc region fusion protein	50mg/week S.C.[≠] Injection every 1-2 weeks	www.enbrel.com (Tsimberidou et al. 2003)
Adalimumab	Humira	Humanised anti-TNF Ab	40mg S.C. injection every two weeks	www.humira.com (Weinblatt et al. 2003)
Golimumab	Simponi	Human monoclonal Anti - TNF Ab	50mg/month S.C injection	www.simponi.com (Zhou et al. 2007)
Certolizumab pegol	Cimzia	PEGylated Fab fragment	200mg S.C. Injection every 4 weeks after induction period	www.cimzia.com (Schreiber et al. 2005)
Developmental anti-TNF biologics				
Pegsunercept	Terminated 2009	PEG-TNFR1	N/A	www.pegsunercept.com (Bendele et al. 1999)
Lenercept	Terminated 2009	TNF-R1-IgG1 fusion protein	0.125mg/kg IV infusion	(Abraham et al. 2001)
Avx 470		Polyclonal Anti-TNF Ab	Oral, dosing N/A	(Bhol et al. 2013)

Adapted from (Sedger & McDermott 2014)

1.6.1 Limitations of TNF therapeutics

Although the new range of biologic therapeutics has proven a great success to diseases like rheumatoid arthritis and Crohn's disease, they have not been found to be without limitations. Due to the nature of TNF's potent inflammatory action in immune regulation it is perhaps expected to see that one of the major side effects of using these therapeutics is an increased risk of infection, especially chronic and latent viral infections such as tuberculosis (Cagatay et al. 2010), herpes zoster and varicella-zoster (Lawrance et al. 2010). Patients receiving TNF-neutralising biologics become immunosuppressed, but, in general, most patients do not experience serious complications. The most serve complications reported with the use of these agents are frequently in the elderly, pregnant or patients receiving multiple co-therapies i.e. causing further immunosuppression (Salvana & Salata 2009). Furthermore, because most patients are immunosuppressed, vaccinations must be taken with caution. Of note, vaccines containing live or attenuated pathogens are contra-indicated with the use of anti-TNF therapies due to the risk of vaccination induced disease.

From the numerous clinical trials of the anti- TNF agents other adverse side effects were observed in the treatment groups including malignancies, neurological complications, allergic reactions, liver disease and exacerbation of the condition being treated. In clinical trials treatment groups had a higher percentage of patients that developed malignancies compared to the placebo groups (Lopez-Olivo et al. 2012), including solid tumours, skin cancers, lymphomas and blood cancers such as multiple myeloma leukaemia (Askling 2010; Lopez-Olivo et al. 2012). On the other hand a comprehensive study comparing treatment and placebo groups found that although there was a slight

increase in the treatment groups of developing malignancies, this was not statistically significant 0.72% vs 0.66% respectively (Lopez-Olivo et al. 2012). Hence with most conditions involving chronic inflammation, there is already a higher risk of developing malignancies, and the addition of long term co-therapies such as corticosteroids and anti-metabolites may also contribute to a heightened risk (Askling 2010; Kandiel et al. 2005). Therefore it is generally seen that malignancies are not a direct result of anti- TNF biologics per se, but may, instead, be due to other unrelated risk factors such as family history risks or environmental factors such as sun exposure, diet and tobacco use (Askling 2010; Lopez-Olivo et al. 2012).

There have also been reports of cases of neurological diseases/disorders, during clinical trials administering anti- TNF biologics. These include demyelinating events, such as multiple sclerosis-like symptoms, and encephalopathy (Singh et al. 2013; Toussirot & Bereau 2014), however, as with malignancy, it is generally thought that a rare risk may be implicated with use of these agents and no significant statistical differences is found against controls populations. Thus, the incidence of demyelinating disease may also be associated with other factors but not necessarily with the anti-TNF agents themselves.

By far one of the biggest complications with the use of biologics is the development of neutralising antibodies to the TNF-specific antibody-based drugs (van Schouwenburg, Rispens & Wolbink 2013a). Given that Infliximab contains a mouse gene antibody FV segment, it is arguably more immunogenic than the fully human (or humanized) other anti-TNF antibodies like Adalimumab and Humicade. The presence of anti-drug antibodies can neutralise the drug making them ineffective (van Schouwenburg, Rispens & Wolbink 2013b). They may also contribute to immune complex formation. Of note,

even fully humanised Ig molecules such as Adalimumab are still capable of eliciting anti-drug antibodies (van Schouwenburg, Rispens & Wolbink 2013b). It has been found that co-therapy of corticosteroids and anti-metabolites such as methotrexate may reduce the rate of anti-drug antibodies from developing (van Schouwenburg, Rispens & Wolbink 2013a). Nevertheless, once anti-drug antibodies have developed in a patient it quickly becomes ineffective and unusable in the future.

1.7 Viral inhibitors of TNF and TNFRs

The success of viral replication and production of viral progeny is dependent on a number of factors such as virulence and host range, and the interaction with host immune defences. The success of a virus completing its life cycle and maximally producing viral progeny is dependent on viral subversion of host defences, aimed at maximising viral dissemination in the host (Herbein & O'Brien 2000).

TNF interferes with viral replication in several ways. The binding of TNF to the TNFRs can activate, differentiate, or kill infected cells interrupting the viral lifecycle. For example many of signalling pathways described earlier such as the NFκB pathway upregulate multiple proinflammatory and immunomodulatory genes i.e. IFNs (Raitano, Scuderi & Korc 1991). Not surprising, viruses have developed strategies to inhibit basically all components of TNF signalling (For review see (Benedict, Banks & Ware 2003; Rahman, Lucas & McFadden 2009a; Sedger 2005)). In fact all steps within the TNF signalling pathway are targeted by various viruses to subvert TNF signalling or production of TNF (Sedger 2005). Some viruses have developed mechanisms of down-regulating cell surface TNFRs as well as TNF such as the Epstein Bar virus which can transcriptionally

down regulate TNF and TNFR1 (Gosselin et al. 1991; Morrison et al. 2004). For review on viral inhibitors of TNF and TNFRs see (Sedger 2005).

Poxviruses have the capacity to produce viral proteins that bind and sequester TNF through virally encoded TNFR-like proteins (Reading, Khanna & Smith 2002; Saraiva & Alcami 2001; Smith et al. 1996b). By preventing TNF from binding to its complement receptors it can no longer trigger downstream pathways (Reading, Khanna & Smith 2002; Smith et al. 1991b; Smith et al. 1996b).

1.8 Viral TNFR homologues and the CRM- family

Members of the Orthopoxviruses (Alcami et al. 1999; Hu, Smith & Pickup 1994; Saraiva & Alcami 2001), Leporipoxviruses (Smith et al. 1991a; Upton et al. 1991) and Yatapoxviruses (Brunetti et al. 2003; Rahman et al. 2006) have all been found to express TNF binding proteins (Table 1-3). More recently evidence for other TNF binding proteins from other poxvirus genus's such as the Avipoxviruses have also been found to contain sequences homologous to the TNFRs (Offerman et al. 2014; Tulman et al. 2004). TNFR homologues have been identified outside of poxviridae such as in members of the Iridoviridae family but are still yet to be characterised (Offerman et al. 2014). For the purpose of this thesis, only TNFR homologues found within Poxviridae will be discussed.

vTNFRs can be classified into two groups of TNF proteins, those which are homologues to the extracellular domain of host TNFRs and those which bind TNF but have no known amino acid similarity to cellular proteins. vTNFRs which are homologous to host extracellular TNFRs contain cysteine rich domains of varying numbers. These include the

T2 proteins from the Leporipoxviruses Myxoma virus (Upton et al. 1991) and Shope fibroma virus (Smith et al. 1991b), and four vTNFRs termed cytokine response modifying proteins (CRM-s); CRM-B (Hu, Smith & Pickup 1994), CRM-C , CRM-D (Loparev et al. 1998) and CRM-E (Saraiva & Alcami 2001) which are differentially expressed by members of the Orthopoxviruses. Each of these proteins bind soluble TNF with high affinity and in some cases LTα (Epperson, Lee & Fremont 2012; Gileva et al. 2006).

CRM-C and CRM-E contain 3 CRDs most homologous to the extracellular domain of TNFR2 and bind TNF but not LTα (Saraiva & Alcami 2001; Smith et al. 1996a). CRM-E is the only vTNFR as yet to be structurally determined and adopts the same tertiary structure as TNFR2 (Graham et al. 2007). Although the overall structure of CRM-E is similar to TNFR2, the modelling of TNF with CRM-E has not been accurately modelled due to the flexibility of the CRDs (Graham et al. 2007). It is predicted that CRM-E like TNFR2 binds TNF through the 50s and 90s loop in CRD2 and CRD3 and may undergo a conformational change upon ligand binding (Graham et al. 2007). Interestingly CRM-E has been shown to be expressed at the cell surface and cell surface CRM-E is sufficient to inhibit TNF-mediated apoptosis of infected cells (Reading, Khanna & Smith 2002).

CRM-B and CRM-D are structurally related to T2 proteins with 4 CRDs as well as a C-terminal domain with no known homology to cellular proteins (Hu, Smith & Pickup 1994; Smith et al. 1996a; Xue et al. 2011). Both CRM-B and CRM-D are secreted from infected cells and bind with TNF and LTα with high affinity. CRM-B and CRM-D proteins are also known to bind a limited number of chemokines by virtue of their C-terminal domains or "SECRET" (Smallpox virus-Encoded Chemokine RECepTor) domains. (Alejo et al. 2006; Antonets, Nepomnyashchikh & Shchelkunov 2010; Xue et al. 2011). These include

CCL25, CCL27, CCL28, CXCL12β, CXCL13 and CXCL14 all largely involved in mediating T and B cell recruitment (Alejo et al. 2006). CRM-B and CRM-D proteins have the ability to bind both TNF and chemokines simultaneously as both domains act independently of each other (Alejo et al. 2006). Although the SECRET domain has been found in T2 molecules chemokine activity has yet to be examined. Yatapoxviruses also encode TNF binding proteins however these proteins have no homology to cellular TNFRs (Brunetti et al. 2003). These include the 2L proteins from Tanapox (TPV) and Yaba monkey tumour virus (YMTV) (Brunetti et al. 2003; Rahman et al. 2006) as well as orthologues in Swinepox (SP003/SP148) (Rahman et al. 2006) and Deerpox (Afonso et al. 2005). The 2L class of proteins have no structural resemblance to TNFR family molecules and are structurally more closely related to MHC class 1 heavy chains (Brunetti et al. 2003). Interestingly TPV 2L has an extremely slow rate of dissociation with TNF and is the strongest reported interaction with TNF. TPV 2L has a dissociation rate of 43pM vs cellular TNFRs of 500pM (Brunetti et al. 2003; Schall et al. 1990). The high affinity and slow dissociation rate of 2L proteins provides evidence that these proteins have evolved to sequester and neutralise TNF in favour of viral replication. See Table 1-3 for a summarised description on the properties of vTNFRs and TNF-binding proteins.

Table 1-3 Known poxviral TNF binding proteins

TNF-BP classification	Organism/Species	Size	Domains	Ligand specificity	Reference
T2	Myxoma Virus Shope Fibroma Virus	326AA	4 N-terminal CRDs, SECRET domain	TNF, LTα,	(Schreiber & McFadden 1996; Smith et al. 1991b; Upton et al. 1991)
CRM-B	Variola Virus Cowpox Virus Monkeypox Virus Feline pox Camel pox Cotia Virus Taterapox Virus	~349AA	4 CRDs, SECRET domain	TNF, LTα, CCL25, CCL27, CCL28, CXCL11, CXCL12, CXCL13, CXCL14	(Alcami et al. 1999; Antonets, Nepomnyashchikh & Shchelkunov 2010; Gileva et al. 2006; Hu, Smith & Pickup 1994)
CRM-C	Vaccinia Virus Cowpox Virus	186AA	3 CRDs	TNF	(Loparev et al. 1998; Smith et al. 1996a)
CRM-D	Cowpox Virus Ectromelia Virus	320AA	4 CRDs, SECRET domain	TNF, LTα, CCL28, CCL25, CXCL12, CXCL13, CXCL14, XCL1, CCL20	(Chen et al. 2000; Loparev et al. 1998; Xue et al. 2011)
CRM-E	Ectromelia virus Vaccinia Virus Cowpox Virus Cotia Virus	167AA	3 CRDs	TNF	(Graham et al. 2007; Reading, Khanna & Smith 2002; Saraiva & Alcami 2001)
2L	Yaba Monkey Tumour Virus Yaba-like disease Virus Tanapox Deerpox Swinepox	~341AA	Resembles MHC-1	TNF	(Brunetti et al. 2003; Rahman et al. 2006; Yang, West & Bjorkman 2009)
Not classified	Canary pox virus Racoon pox Virus Penguin pox Virus		Contains Variable CRD regions (termed TNFR like regions)	TNF	(Offerman et al. 2014; Oie & Pickup 2001; Tulman et al. 2004)

1.9 Myxoma virus

Myxoma virus (MYXV) belongs to the Leporipoxviruses which largely infect rabbits, hares, squirrels and other leporids (Fields, Knipe & Howley 2007). Myxoma virus is the causative agent of myxomatosis (Fenner 1959) which is characterised by a fibroma and a self-limiting disease in its natural host (genus: *Sylvilagus*) of wild brush rabbits, jungle rabbits and tapeti (Meredith 2013). However in European rabbits (*Oryctolagus cuniculus*) the disease is much more severe and even lethal, causing systemic inflammation and systemic viremia, swelling of the head frequently leading to death in 10-12 days (Rivers 1930). The high lethality of MYXV lead to its use as a biological control agent in countries such as Australia however rapid mutation of the virus led to resistance and co-evolution in pest rabbits with lower fatality rates and higher transmission rates (Marshall & Fenner 1960).

1.9.1 Myxoma virus MYXT2

MYXT2 was first discovered from supernatants of virus infected cells and found to bind TNF with high affinity and specificity (Schreiber & McFadden 1994). Myxoma virus contains within its genome two copies of the vTNFR ORF known as T2, as it is the second ORF within the terminal inverted repeats of the viral genome (Upton et al. 1991). T2 molecules were first discovered in the Shope fibroma virus (SPV), a related virus from the Leporipoxviruses, however T2 from MYXV (MYXT2), has been the most comprehensively studied member of the family (Upton, DeLange & McFadden 1987).

MYXT2 contains 4 CRDs with high homology to TNFR2 and a C-terminal region with no known similarities except to other vTNFRs (Upton et al. 1991). From amino acid sequence MYXT2 has a predicted molecular mass of 33.4 kDa however MYXT2 is found to be heavily N-linked glycosylated, therefore the observed mass of the protein in SDS-PAGE is between 55-65 kDa. MYXT2 proteins are present in the supernatants of virus infected cells, and is found as either a dimer or monomer, with the dimer being a more potent inhibitor of TNF (Schreiber, Rajarathnam & McFadden 1996).

Due to the high sequence similarity to TNFR2 it is predicted that MYXT2 conforms to a similar structure of the mammalian receptor and is predicted to bind TNF within the second and third CRDs (Schreiber & McFadden 1996). Experimentally created mutations, or deletions, within CRD-1 and CRD-2 of MYXT2 abolishes its ability to bind rabbit TNF; these mutant vTNFR proteins are also unable to prevent cells from dying due to TNF (Schreiber & McFadden 1996; Schreiber, Sedger & McFadden 1997). Truncations of the C-terminal domain in MYXT2 led to retention of these proteins in the endoplasmic reticulum, yet are still able to bind and neutralise rabbit TNF (Schreiber & McFadden 1996). This suggests that the C-terminal domain of MYXT2 is required for MYXT2 secretion, which is dependent on a N-terminal 17 amino acid signal sequence (Schreiber & McFadden 1996).

MYXT2 will only bind and neutralise rabbit soluble TNF unlike (Shope Fibroma virus T2) S-T2 which has the ability to bind to rabbit as well as human TNF and LTα. Immunocompetent rabbits infected with an MYXT2 knockout virus develop an attenuated form of myxomatosis and the majority of infected rabbits recover and

develop immunity to secondary challenge (Upton et al. 1991). This clearly demonstrates that MYXT2 is a virulence factor for *in vivo* MYXV infection.

1.10 Variola Virus

Variola virus (VARV) belongs to the family of viruses Chordopovirinae and the genus Orthopoxvirus (Fields, Knipe & Howley 2007). VARV is the causative agent of smallpox and the major strain involved in most pandemics was VARV major which had overall 30% mortality rates (Fenner 1993). Smallpox infection is associated with extensive lesions covering the body, high fevers (>40°C), a characteristic papular rash, severe back pain and vomiting (Lofquist, Weimert & Hayney 2003). A less severe form of smallpox is caused by VARV minor which was first recognised as a disease of North America (Dumbell, Bedson & Rossier 1961). VARV minor is also referred to as Variola alastrim (Dumbell, Bedson & Rossier 1961); it is characterised by its low fatality rates (<1%) and much milder symptoms which were often mistaken for impetigo and similar diseases (Dumbell & Huq 1986; Ribas 1911).

VARV has a very strict host range and has no known reservoir outside of humans (Baxby 1977). Under experimental conditions, however, it has been found that many species of monkeys are susceptible to VARV infection and there have been 7 known cases of smallpox transmitting to primates in the wild (Arita & Henderson 1968; Herrlich et al. 1963). One case was reported in Jakarta zoo where orang-utans had contracted a smallpox-like disease during a human smallpox epidemic at the same time; this is the only known case where virus was isolated and characterised which was found to resemble VARV in its infectivity (Arita & Henderson 1968; Herrlich et al. 1963). However

this was before the discovery of Monkeypox virus (MPV) which may have been easily mistaken for VARV. Continual passage of VARV in animals has been unsuccessful (Herrlich et al. 1963). Therefore true virulence factors in VARV have been difficult to determine for obvious ethical reasons - and as humans are the only known natural hosts of this virus.

The only virulence factors identified in VARV to date are predicted based on the activity of other poxvirus protein homologues and infection in their natural hosts, e.g. as for MYXT2 infection in rabbits (Upton et al. 1991). All poxvirus genomes contain a core region of highly conserved DNA, this DNA encodes ORFs/molecules that are essential for viral replication and growth, such as viral DNA polymerases. ORFs located in the terminal regions have been sequenced and largely contain virulence factors (Johnston & McFadden 2003; Macaulay, Upton & McFadden 1987; Upton, DeLange & McFadden 1987). Many of these proteins are found to be inhibitors of chemokines and cytokines involved in viral surveillance and regulation such as type I interferons (Fernández de Marco et al. 2010; Shchelkunov 2003), TNF (Gileva et al. 2006; Gileva et al. 2005), complement binding proteins (Liszewski et al. 2009), chemokine binding proteins (Alejo et al. 2006; Antonets, Nepomnyashchikh & Shchelkunov 2010), interleukin binding proteins (Massung et al. 1993), as well as a number of signalling molecules involved in apoptosis and TNF signalling (Bratke, McLysaght & Rothenburg 2013; Esposito et al. 2006).

1.10.1 History of smallpox

The origins of VARV are still somewhat unclear but are thought to have disseminated from either India or Africa (Li et al. 2007; Shchelkunov 2011). The first clear accounts of smallpox are from ancient records in China, dating back to the 4th century AD and the 7th century AD in India and the Mediterranean (Fenner 1988). By this time the accounts clearly describe symptoms of smallpox which was by then a well-known human disease (Fenner 1988). One of the earliest accounts is that of mummified royals found in Egypt which contained pox-like lesions dating back to 1200-1100 BC, one of which was King Ramses V (Fenner 1988; Ruffer & Ferguson 1911). As such, Smallpox was first believed to be endemic in the populated Nile valley approximately 1570-1085 B.C. with the discovery of three mummified bodies containing pox-like lesions (Fenner 1988; Ruffer & Ferguson 1911). Supporting evidence is documented by an outbreak of a plague amongst the Hittites due to war between the Egyptians which described a severe illness involving a rash which decimated the numbers of Ethiopian soldiers (Ellner 1998). From there it is thought that trade caravans or ships may then have introduced the disease into India, with ancient writings mentioning smallpox in 100 B.C. (Fenner 1988). Smallpox, through trade and travel eventually disseminated globally with horrific epidemics occurring and reoccurring over the centuries and becoming endemic to most places in the 18th century. The many countries that were still free of smallpox until this point provided naive susceptible populaces which allowed devastating pandemics to sweep across Europe in the 17th and 18th centuries (Fenner 1988).

Historically it was observed that individuals that had contracted smallpox and survived were immune to future infections (Eyler 2003). This observation led to attempts to

induce this immunity through purposely infecting healthy individuals with contagious secretions or lesion (Lofquist, Weimert & Hayney 2003). This practice was latter termed "variolation" which distinguished it from the practice of "vaccination", which is the practice of inoculating with a non-virulent agent/pathogen. The early success of variolation led to it being a popular practice in areas endemic to smallpox especially in 17th and 18th century Europe (Fenner 1993). Although variolation was mostly successful, the method involved infecting people with live VARV, meaning that artificially infected persons could potentially transmit and spread the naturally occurring form of the disease as well as fall to the disease themselves (Ellner 1998; Fenner 1988). Variolation proved to be effective in reducing the severity of epidemics and was practiced until the introduction of vaccination in 1800. An observation that milkmaids infected with a disease from cow rarely suffered from smallpox (Fenner 1993). Jenner took this observation further by infecting a child, James Phipps, with cowpox lesions from the hand of a milkmaid in 1776 (Fenner 1993). He then challenged the child again several months after with live smallpox to which he remained immune (Fenner 1993). The success of vaccination became apparent with the subsequent decline in numbers of smallpox deaths, and on this basis a number of governments introduced legislation to make vaccination compulsory. Soon after, a World Health Organisation campaign was initiated in 1959, to eradicate smallpox. This was revised and intensified in 1967 with the aim of eliminating smallpox within the next 10 years (Henderson 2011). The program proved successful and the last naturally documented case occurring in Somalia in 1978 (Deria et al. 1980). The remaining strains of VARV now reside within two laboratories, one in the United States at the Centre for Disease Control and Prevention (CDC) in Atlanta, Georgia; and the other in the former Soviet Union at the State Centre for Research of Virology and Biotechnology (VECTOR) in Novosibirsk (Shchelkunov 2011).

1.10.2 Variola G4R (VARG4R) or CRM-B

Sequence analysis of VARV genome has permitted the identification of a single vTNFR ORF known as VARG4R (a CRM-B protein) (Massung et al. 1993; Massung et al. 1994). VARV G4R was identified from one of the most virulent strains of VARV and has since been synthesised and expressed in a baclovirus expression system (Alejo et al. 2006; Gileva et al. 2006). The purified VARG4R protein is primarily a dimer, and it binds human mouse and rat TNF with high affinity (K_d 278pM, <20pM, <20pM respectively) and inhibits TNF-mediated L929 cell cytotoxicity (Alejo et al. 2006; Gileva et al. 2006). It is also found to bind human LTα, although with a much lower affinity K_d 7.55nM (Alejo et al. 2006). However, another study found that VARV CRM-B was more efficient at inhibiting rat and mouse TNF compared to human TNF, (Alejo et al. 2006). These differences may be due to small discrepancies between the two methods in assaying cell death or due to differences in cell passages of the L929 cells.

The C-terminal domain of VARV CRM-B is homologous to other vTNFRs containing a CRM-B orthologue. Recently a screen of various human immunomodulatory molecules led to the discovery that VARV CRM-B also contains chemokine binding activity (Alejo et al. 2006). The region of VARV CRM-B responsible for this activity is the C-terminal (non-TNFR-homologous) domain. Given that there are no chemokine-receptor homologous sequence motifs this domain has been referred to as the SECRET domain (Alejo et al. 2006). The VAR CRM-B SECRET domain is capable of binding and inhibiting chemokines CCL28, CCL25, CXCL12β, CXCL13, CXCL14 (Alejo et al. 2006). Using surface Plasmon resonance assays it has been shown that the SECRET domain and TNF-binding domains

are separate domains in CRM-B, as saturation of one site does not inhibit further binding of the other (Alejo et al. 2006). Hence, the N-terminal region of CRM-B is responsible for binding TNF, and the C-terminal SECRET domain is responsible for binding chemokines. To avoid confusion within this thesis VARV CRM-B will be referred to as VARG4R with respect to the open reading frame from which it was synthesised, and to differentiate it from Monkeypox virus (MPV) CRM-B, ORF J2R (Chen et al. 2005; Shchelkunov et al. 2001).

1.11 Monkeypox virus

MPV is a member of the Orthopoxviruses, and the virion morphology is identical to other orthopoxvirus members (Fenner, Wittek & Dumbell 1989). MPV has a much broader host range, being capable of productively infecting rodents, primates, and small mammals (Arita & Henderson 1968; Marennikova 1979; Marennikova, Shelukhina & Efremova 1984; Shchelkunov, Marennikova & Moyer 2006). MPV is also the cause of human Monkeypox, and clinically the symptoms resemble that of VARV or smallpox - but milder. One differentiating feature being lymphadenopathy in MPV infection, which is generally not seen in human Smallpox infection. Human MPV infection can be contracted from infected animal bites, or direct contact with bodily fluids of infected animals. It can be spread from person to person, but with a much lower transmission rate compared to Smallpox (Fenner 1993; Jezek et al. 1988). Human transmission is thought to occur through aerosolised respiratory droplets but also through direct contact of bodily fluids and fomites (Lofquist, Weimert & Hayney 2003).

Strains of MPV are usually classified into two clades: those that originate from West Africa and those from the Congo Basin (Chen et al. 2005). Strains belonging to the Congo Basin usually cause a much more severe human injection, with viremia, sometimes even resulting in death (Chen et al. 2005). There is also a higher secondary transmission rate, which appears to be irrespective of age or vaccination status (Likos et al. 2005b). On the other hand, West African Strains, such as MPXV-USA-2003-044 that which was involved in the 2003 US outbreak (Likos et al. 2005a), have not been associated with human deaths and not shown evidence of human-to-human transmission (Jezek et al. 1988). Moreover, human MPV infection is usually a much milder than Smallpox, and produces a more localised rash (Likos et al. 2005b). The Congo Basin and West African strains sequences share 95% identity with the greatest difference in the terminal genomic regions that largely containing virulence and host range factors (Chen et al. 2005; Likos et al. 2005a).

Research on MPV is restricted and closely monitored due to its status as a serious human pathogenic organism. It is also considered a potential bioterrorism agent. Therefore little data exists on virulence factors of MPV. The complete genome of MPV has been sequenced and a number of predicted immuno-modulatory ORFs are present - usually within the terminal inverted repeats of the virus genome. The terminal genomic regions of MPV are somewhat similar to VARV with 83.5-93.6% identity; it also shares many orthologous known poxvirus virulence factors including IFN-γ and IFN-α/β binding proteins (ORFS, B9R, B16R) complement binding protein (ORF D15L), TNF binding proteins (ORF J2R) and IL-18 binding protein (D6L). For full comparison see (Shchelkunov et al. 2001).

1.11.1 Monkeypox J2R (MPVJ2R) or CRM-B

Sequencing of the Monkeypox (MPV) genome indicates the presence of a single vTNFR ORF, J2R, with a very high (85.1%) sequence similarity to VARVG4R (Gileva et al. 2005; Shchelkunov et al. 2001). MPVJ2R is a CRM-B molecule, and similarly contains 4 N-terminal CRDs and a C-terminal SECRET domain (Gileva et al. 2006). However, sequence analysis of MPVJ2R against VARG4R reveals amino acid differences between these molecules within their SECRET domains, which is thought to contribute to differing specificity of chemokines and TNF (Gileva et al. 2006). In TNF binding assays MPVJ2R is a weak inhibitor against the cytotoxic effects of human, mouse, and rabbit TNF , on TNF-sensitive L929 cells (Gileva et al. 2006). Interestingly, this is despite the broad host range of MPV compared to VARG4R who's only known reservoir is humans, therefore another function of MPVJ2R may exist – but not yet described. MPV has the ability to infect humans (Lourie et al. 1972) and thus it is regarded as a potential "high risk" biohazard (Parker et al. 2007; van Aken & Hammond 2003). As a result, research on MPV is very closely monitored and restricted to approved laboratories, therefore little data exists on the structure and biological functions of MPVJ2R.

1.12 Viral PLAD

Sequence alignment of vTNFRs against human TNFRs has revealed a high sequence similarity between the N-terminus amino acids (Sedger et al 2006). This high sequence identity led to the hypothesis that the vTNFRs may also be able to associate with cellular TNFRs. Evidence supporting this idea came from studies which expressed MYXT2 from within human Jurkat T cells (Sedger 2006). Here, constitutive MYXT2 expression

protected the stably- transfected lines against human TNF / human TNFR1-induced cell death without altering the cell surface expression of the cellular TNFRs (Sedger et al. 2006). This is a surprise as MYXT2 only specifically binds and inhibits rabbit TNF not human (Schreiber & McFadden 1994). Thus intracellular (or cell associated) MYXT2 protected cells from TNFR1-induced apoptosis. Moreover, deletion of the PLAD domain within MYXT2 abolishes the protective effects (Sedger et al. 2006). Subsequent immunoprecipitation – Western immunoblotting demonstrated that MYXT2 physically associated with cellular TNFR1 and TNFR2, and that the viral PLAD domain was required for this interaction. Thus MYXT2 not only binds to rabbit TNF, but functions as a dominant negative inhibitor of human TNFRs (Sedger et al. 2006) (Figure 1.6). Given that this viral PLAD domain is highly conserved within all poxviral vTNFRs, it is thought that by associating and inhibiting TNFR all poxviral vTNFR/CRM- proteins likely act to inhibit the host TNFRs (Figure 1.6). Indeed the non-species specificity of this interaction may indicate that this is more importantly activity of vTNFRs, indeed such a mechanism would permit the vTNFRs to be functional for broad-specific trophic poxviruses such as MPV. It should be noted that although MYXT2 has been shown to interact with human TNFRs *in vitro*, this expression system is artificial and not the normal biological conditions under which MYXV would infect its host. However the implications of how MYXT2 interacts with TNFRS still has importance and could lead to future clinical implications.

The mechanisms by which MYXT2 inhibits TNFRs is still under investigation in our laboratory. It is clear that secreted MYXT2 exists as both a monomer and disulphide-linked homo-dimer (Schreiber, Rajarathnam & McFadden 1996). Although both the monomer and dimer were found to bind TNF with the same affinity, only the dimeric

form is an effective inhibitor of TNF cytotoxicity (cell death) (Schreiber, Rajarathnam & McFadden 1996). Interestingly, VARV CRM-B is primarily found as a dimer whereas MPV and CPV CRM-B proteins both are monomeric (Gileva et al. 2006). The differences observed between the different poxvirus species may suggest that one mechanism of inhibiting the TNF/TNFR axis may be preferred due to its host range. For example VARV has a strict host range only infecting humans (Buller & Palumbo 1991; McFadden 2005) and is primarily found as a dimer (Gileva et al. 2006). This may suggest that VARVG4R can only bind and neutralise TNF in a species- specific manner, consistent with the strict host range (in humans). MPV, conversely, is primarily found as a monomer (Gileva et al. 2006) but has a very broad host range (Essbauer, Pfeffer & Meyer 2010; Weaver & Isaacs 2008). It may therefore require the capacity to inhibit TNFRs by intracellularly associating with the cells TNFRs - in a non-species-specific manner. Therefore the intracellular mechanism of vTNFRs inhibiting TNFRs may be the more important TNF neutralising mechanism for poxviruses with a broad host range.

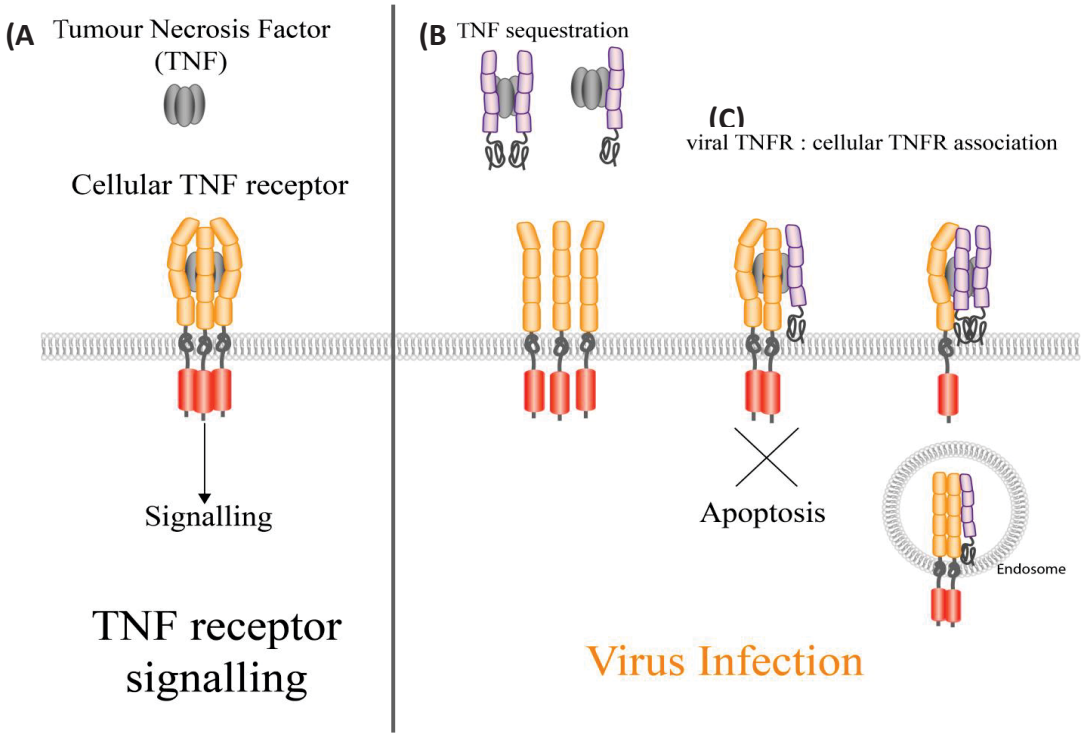

Figure 1.6 Proposed mechanisms of viral TNFα and TNFR inhibition.
(A) Normal TNFα binding to TNFR, and subsequent TNFR-mediated signalling. (B) In poxvirus infected cells, vTNFRs are both secreted from the cell to bind and sequester soluble host TNFα and prevent soluble TNF from binding to cellular TNFRs. (C) Proposed mechanism of intracellular inhibition of cellular TNFRs: vTNFRs associate with cellular TNFRs to inhibit TNFR-induced apoptosis ,even in the presence of TNFα.

1.13 Thesis aims and scope

The importance of TNFRs to normal biology is obvious through its many pleiotrophic effects as outlined above, especially in the inflammation process as well as an important antiviral host defence. Although the effects of and structures of human TNFR1 and TNFR2 are well characterised, there is still a lack of understanding as to how TNFRs initiate many of their effects and their interactions in cellular biology. This is especially evident with the aberrant effects of mutations found in naturally occurring TNFR1 mutations known as TRAPS and how these mutations result in the underlying pathology. In addition to this, many of the current therapeutics based on blockade of the TNF pathways, although have proven effective, are also associated with severe side effects such as comprised immunity and development of lymphomas. In the development of the possible next generation of anti-inflammatory agents, vTNFRs may serve as possible avenue in to which new agents may be based upon. By developing a better understanding of how vTNFRs are able to interact and subvert cellular TNFRs it is hoped that a more specific mechanism of TNFR subversion is possible. Therefore the aims of this Thesis is to:

1) To characterise the intracellular interaction of cellular TNFRs with PLAD mutant TRAPS TNFRs.

2) To characterise MYXT2, VARG4R and MPVJ2R proteins and further the understanding of vTNFR subversion of TNFR-induced cell death

3) To structurally analyse PLAD TRAPS mutant TNFRs and viral TNFRs either alone, or in association with WT TNFRs.

Chapter 2
Methods

Chapter 2 – Methods

2.1 Molecular methods

2.2 TNFR plasmids

pcDNA3.TNFR1-YFP, pcDNA3.TNFR1-CFP, pcDNA3.TNFR2-YFP and pcDNA3.TNFR2-CFP were all kindly donated by Dr Francis Chan (Chan et al. 2000b). All expression plasmids are under the control of a cytomegalovirus early/intermediate promoter and were cloned into the multi-cloning sites *Hind*III and *Xho*I 5' to 3' respectively with the ORF of Cyan fluorescent protein (CFP) or Yellow fluorescent protein (YFP) cloned downstream into *Xho*I and *Xba*I as fusion tags. The pcDNA3 vector contains a downstream bovine hormone growth polyadenylation signal for mammalian expression, ampicillin and neomycin resistance genes for selection in both bacteria and mammalian cells respectively.

2.2.1 Viral TNFR plasmids for mammalian expression

pcDNA3.1B.MYXT2-MycHis was created previously through PCR of the Myxoma virus (MYX) T2 ORF (NCBI accession: AAA46632) which was then cloned into pcDNA3.1B-MycHis (Sedger et al. 2006). MYXT2 expression is under control of a CMV early/late promoter and also contains neomycin resistance and a downstream polyadenylation signal.

pUC19.VARG4R-MycHis and pUC19.MPVJ2R-MycHis were designed and codon optimised for *Homo sapiens* and *Mus musculus* expression by a previous PhD student

Sarah Sherwood. The sequence for Variola G4R was codon optimised from the Variola India 1967 strain sequence (NCBI accession: NP_042240.1). The sequence for MPVJ2R was codon optimised from the Monkeypox 1996 Zaire strain sequence (NCBI accession: AF380138.1). The sequences were synthesised by Codon devices Inc. USA into pUC19 between the *Kpn*I and *Xho*I restriction sites 5'-3' respectively. Due to biohazard restrictions on handling Variola virus (VAR) and Monkeypox virus (MPV) and The ORFs of G4R and J2R were synthetically synthesised with WHO and smallpox committee approval.

pcDNA3.A.VARG4R-MycHis and pcDNA3.A.MPVJ2R-MycHis were created by previous PhD student Sarah Sherwood. The ORF of VARG4R and MPVJ2R from pUC19.VARG4R-mycHis and pUC19.MPVJ2R-mycHis were digested with *Kpn*I and *Xho*I to remove the cDNA and subcloned into corresponding restriction sites in the multiple cloning site of pcDNA3.A.MycHis. This created the VARG4R and MPVJ2R ORFs in frame with a 3' MycHis fusion tag in pcDNA3.A.MycHis.

2.2.2 Generation of pcDNA3.VARG4RCFP and pcDNA3.MPVJ2R.CFP

pcDNA3.VARG4R.CFP, pcDNA3.MPVJ2R.CFP were generated by digesting pUC19.VARG4R-mycHis and pUC19.MPVJ2R-mycHis with *Kpn*I and *Xho*I to remove the viral TNFR ORFs. The VARG4R and MPVJ2R ORFs were then subcloned into the subsequent restriction sites in pcDNA3.TNFR2-CFP replacing the TNFR2 cDNA with VARG4R and MPVJ2R ORFs. This produced VARG4R and MPVJ2R in frame with the sequence of CFP as a fusion sequence.

pcDNA3.VARG4R.YFP, pcDNA3.MPVJ2R.YFP and pcDNA3.MYXT2-YFP were designed and cloned by Sarah Sherwood in her PhD. pUC19.VARG4R-MycHis and pUC19.MPVJ2R-MycHis were digested with *Kpn*I and *Xho*I removing the ORFs, which were then subcloned into pcDNA3.TNFR2-YFP (replacing the TNFR2 ORF). This created VARG4R and MPVJ2R as fusion constructs with YFP. pcDNA3.MYXT2-YFP was subcloned by digesting pcDNA3.1B.MYXT2-mycHis with *Bam*HI and *Xho*I instead as the MYXT2 ORF contains an internal *Kpn*I restriction site. This was then ligated into pcDNA3.TNFR2-YFP with the respective restriction sites (replacing the TNFR2 ORF).

2.2.3 DNA quantification

Plasmid DNA was quantified using the Nanodrop ND-1000 (Nanodrop technologies, Montchanin, USA). Briefly, 2µl of water or Tris EDTA (TE) was used as a blank standard and absorbance was read at 260nm. A DNA sample of 2µl was then loaded and the concentration was determined by absorbance at 260nm. Purity of samples was determined from absorbance ratios of A260/280nm and also at A260/230nm.

2.2.4 Sequencing

DNA Sanger sequencing reactions were carried out by Macrogen, Seoul, Korea and were performed using an AbI3730XL capillary sequencer. Samples were also sequenced at the Australian Cancer Research Foundation Biomolecular Resource Facility, Canberra, using an ABI3730 capillary sequencer. DNA samples were diluted to a concentration of 100ng/µl and primers diluted to 1.6pM for both companies and delivered via post. DNA sequencing reactions were then carried out by the facility staff.

2.2.5 Sequencing analysis

Sequencing chromatogram files were analysed using the Chromas Lite software (Technelysium, http://technelysium.com.au/) (Version 2.1.1). Sequences were aligned using the Basic local alignment search tool (BLAST) from the National Center for Biotechnology Information (NCBI) (http://blast.ncbi.nlm.nih.gov/Blast.cgi) and ClustalW2 (http://www.ebi.ac.uk/Tools/msa/clustalw2/) using default parameters.

2.2.6 DNA electrophoresis

Tris-borate-EDTA (TBE) agarose gels 1% (W/V) were cast by dissolving 0.5g or 1g of agarose (Biochemicals, Gymea, NSW) in 50ml or 100ml of TBE respectively while heating till molten. Once cool, Gel Red (Biotium) was added at recommended concentrations and set in a casting mould (Bio-Rad) until set. DNA samples and molecular ladders were mixed with 6x Blue orange loading dye (Promega, USA) and loaded into appropriate wells and electrophoresed in TBE electrophoresis buffer at 90V for 1-1.5 hours. DNA was visualised using a UV trans illuminator (Ultralum, Inc., USA) and images were acquired using a Kodak EDAS 290 camera and Carestream software imaging package (Version 5.0.2.3).

2.2.7 DNA restriction digest

A restriction digest master mix was made to contain 1x optimal enzyme buffer (New England Biolabs, USA), 0.1mg/ml BSA (New England Biolabs, USA), 1 unit of restriction enzyme (New England Biolabs, USA), approximately 100ng of plasmid DNA and sterile

H_2O to a final volume of 10µL. Plasmid DNA templates used for cloning contained 1ug of DNA instead. Reactions were incubated at 37°C for 1 hour and visualised by agarose gel electrophoresis.

2.2.8 DNA gel extractions

Plasmid DNA was loaded on a TBE 1% agarose gel (W/V) containing gel red (Biotium). Samples were run in duplicate wells and half of the gel was visualised and used as a guide to excise gel fragments to avoid UV illumination of excised DNA to be ligated. The DNA was then extracted and purified using the Pure link HiYield gel extraction kit (Life Technologies). Agarose gel pieces containing DNA were weighed and 3 Gel volumes of solubilisation buffer (L7) was added (Life Technologies) before melting the gel pieces at 55°C. After the gel pieces had melted, 1 gel volume of isopropanol (Sigma) was added, and then transferred to a gel extraction column. DNA was passed through the column by centrifugation 14000rpm for 1 min (Eppendorf 5415C), then washed with wash buffer (W8) by centrifugation at 14000 rpm 1min. Gel extraction columns were then centrifuged for a further 2 minutes to remove residual buffer and the DNA was eluted in 20µl of TE (pH8) by centrifugation at 14000rpm for 30 seconds (Eppendorf 5415C). All reagents were provided in the kit by Life Technologies unless otherwise stated.

2.2.9 DNA mini prep

Quick isolation of plasmid DNA was achieved using the Lab "Dirt miniprep" method. Transformed overnight bacterial cultures (1.5ml) containing the plasmid were centrifuged at 14000rpm (Eppendorf 5415C) for 10min and the supernatant was

discarded. The bacterial pellet was resuspended in 200µl of resuspension solution (50mM Tris HCl, pH 7.5, 10mM EDTA) then lysed in 200µl of cell lysis buffer (0.2M NaOH, 1% SDS) for 5 minutes and mixed repeatedly by inversion. Cell protein and debris was then precipitated in 200µl of Cell neutralisation solution (0.75M KOAc, pH 4.8) and centrifuged at 14000rpm (Eppendorf 5415C). The lysate was mixed with immunoresin (473 g/l Guanidine Thiocyanate Salt, 20mM EDTA, 50mM Tris HCl, pH 7.5) then transferred to a Wizard minicolumn (Promega) attached to a vacuum manifold (Promega) and drawn through under vacuum. The column was washed with 2ml of wash solution (100mM NaCl, 2.5mM EDTA, 10mM Tris HCl, pH 7.5, in 50% ethanol). Excess wash solution was removed by centrifugation 14000rpm of the column for 2 minutes (Eppendorf 5415C). Plasmid DNA was eluted by adding 50µl of TE (pH8) to the column then centrifuging into a sterile microfuge tube at 14000rpm for 1min (Eppendorf 5415C).

2.2.10 DNA maxi-prep purification

Plasmid DNA was amplified in DH5α *E.coli* then purified using the Pure link HiPure plasmid filter maxi kit (Life Technologies). Briefly 5ml of sterile Luria Bertani (LB) broth containing 100µg/ml ampicillin was inoculated with transformed DH5α *E.coli* containing the plasmid DNA of interest and incubated for 8 hours at 37°C with shaking at 260 rpm. The *E.coli* was subcultured 1/1000 into 200ml of sterile LB broth containing 100 µg/ml ampicillin and incubated for 16hours at 37°C with shaking at 260rpm. Bacterial cultures were then pelleted by centrifugation at 6000g for 10 minutes in a Super T21 centrifuge (SL-250T rotor)(Sorvall, USA). Bacterial pellets were then aspirated and resuspended in 10ml of R3 buffer, lysed in 10ml of L7 buffer then immediately mixed by inversion and allowed to stand for 5 minutes. Lysates were precipitated with 10ml of N3 buffer and

mixed immediately by inversion. Precipitates were centrifuged at 16000g for 10 minutes (SL-50T rotor) (Sorvall, USA) and the clear supernatant was transferred to an equilibrated DNA filter column and allowed to empty by gravity. The column was then washed with 60ml of wash buffer (W8) and the plasmid DNA was eluted in 15ml of elution buffer. The plasmid DNA was then precipitated with 10.5ml of isopropanol (Sigma) and pelleted by centrifugation at 17000g (SL-50T) (Sorvall). The DNA pellet was washed with 5ml of 70% ethanol (Sigma) then aspirated and allowed to air dry for 10 minutes. DNA pellets were then resuspended in 1ml of TE buffer pH8 (Life Technologies). All buffers and solution were provided in the kit by Life Technologies unless otherwise stated.

2.2.11 Plasmid DNA ligation

Ligation DNA was performed by adding restriction enzyme digested plasmid DNA and plasmid DNA vectors in approximately a 1:3 molar ratio into a mixture containing 1x ligase buffer (New England Biolabs), T4 DNA ligase (New England Biolabs) and autoclaved dH_2O to a final volume of 10µL. Reactions were incubated at 16°C overnight then transformed into chemically competent *E.coli* (section 2.3.3).

2.2.12 Site-directed mutagenesis

The TNFR1-YFP TRAPS mutants were created through site-directed mutagenesis of the pcDNA3.1-TNFR1-YFP plasmid. pcDNA3.1-TNFR1-YFP was first methylated by adding 100ng of plasmid DNA to a mixture containing 4 units of CpG methyltransferase (New England Biolabs, USA), 1x S-adenosylmethionine (SAM) (New England Biolabs, USA), 1x

methylation buffer (New England Biolabs, USA), and the final volume was adjusted using sterile dH_2O. The reaction was incubated for one hour at 37°C. A mutagenesis PCR was then performed on the methylated plasmid DNA template to introduce the desired point mutations (T-gradient thermocycler) (Biometra, Germany). Mutations were introduced using two primers containing an overlapping region and the desired mutation upstream of the complementary region on the sense primer Table 2-1. Each PCR mix contained 1x PCR buffer (Aliment Technologies), 0.2mM of each dNTP (Bioline), 6% DMSO (final concentration) (Sigma), 12pM of each primer, 2.5U Pfu turbo DNA polymerase (Aligent Technologies), 12-30ng of methylated plasmid DNA and sterile dH_2O to a final volume of 50µl. The PCR mix was then denatured at 94°C for 2 minutes then followed by 20 cycles of denaturing at 94°C for 30 seconds, re-annealing at 1-2°C below the Tm of the lowest primer for 30seconds and an extension of 2 min/Kb DNA at 68°C. A final extension at 68°C was performed, and then PCR reactions were held at 4°C. Amplified products were analysed by a 1% agarose gel electrophoresis.

The PCR products were purified by simple dialysis on a 2mm 0.05µm membrane filter (Merck Millipore) in sterile dH2O for 5 minutes. The purified plasmid DNA was then transformed into chemically competent DH5α *E.coli* (Life Technologies) (See section 2.3.3). Positive colonies for each mutant were selected and plasmid DNA was purified by mini prep (section 2.1.9). The isolated plasmid DNA was then sent for sequencing to confirm mutations and glycerol stocks were made for each mutant bacterial clone.

Table 2-1 Table of Primers

Primer Name	Primer Sequence 5'-3'	Sense	Tm (°C)
pcDNA3.1 Sequencing Primers			
T7-FWD	TAATACGACTCACTATAGGGAGACCC	Sense	58
T7-REV	GCAACTAGAAGGCACAGTCGAG	Antisense	57
pcDNA3.1 TNFR Primers			
HuTNFR1-FWD2	ACTCAGGCACCACAGTGCTGTT	Sense	57
HuTNFR1-REV2	AACAGCACTGTGGTGCCTGAGT	Antisense	57
YFP-FWD2	CCACATGAAGCAGCACGACTTC	Sense	57
YFP-REV2	GAAGTCGTGCTGCTTCATGTGG	Antisense	57
CFP-FWD2	AGGACGACGGCAACTACAAGACC	Sense	59
CFP-REV2	GGTCTTGTAGTTGCCGTCGTCCT	Antisense	59
vTNFR Primers			
VARG4R_FWD1	AGTCGGTACCATGAAGAGCGTCCTC	Sense	61
VARG4R-FWD2	GACCAGCGAGCTGACTATCACA	Sense	57
VARG4R-REV2	TGTGATAGTCAGCTCGCTGGTC	Antisense	57
MPVJ2R_FWD1	AGTAGGTACCATGCGATCTGTTCTG	Sense	58
MPVJ2R-FWD2	TCAATCTCTACTAGCGAGCTGACA	Sense	56
MPVJ2R-REV2	TGTCAGCTCGCTAGTAGAGATTGA	Antisense	56
MyxT2-A	TAACGCTACTACTCGCGTACGTCG	Sense	59
MyxT2-G	ATGTCCTCGGTACACGTATTCCG	Sense	57
MyxT2-G2	CGGAATACGTGTACCGAGGACAT	Antisense	57
Mutagenesis Primers			
Y20D_F	TGTGTCCCCAAGGAAAAGATATCCACCCTC	Sense	63
Y20H_F	TGTGTCCCCAAGGAAAACATATCCACCCTC	Sense	63
H22R_F	TGTCCCCAAGGAAAATATATCCGCCCTCAAAATA	Sense	62
H22Y_F	TGTCCCCAAGGAAAATATATCTACCCTCAAAATA	Sense	60
TNFR1-22_R	TTTTCCTTGGGGACACACACTATCTCT	Antisense	58
C29Y_F	TCAAAATAATTCGATTTACTGTACCAAGTG	Sense	55
C29F_F	TCAAAATAATTCGATTTTCTGTACCAAGTG	Sense	55
C30R_F	CAAAATAATTCGATTTGCCGTACCAAGTGCCA	Sense	60
C30F_F	CAAAATAATTCGATTTGCTTTACCAAGTGCCA	Sense	58
C30Y_F	CAAAATAATTCGATTTGCTATACCAAGTGCCA	Sense	58
C30S_F	CAAAATAATTCGATTTGCTCTACCAAGTGCCA	Sense	59
TNFR1-30_R	AAATCGAATTATTTTGAGGGTGGATATATT	Antisense	53
C33G_F	CGATTTGCTGTACCAAGGGCCACAAAGGAA	Sense	63
C33Y_F	CGATTTGCTGTACCAAGTACCACAAAGGAA	Sense	60
TNFR1-33_R	CTTGGTACAGCAAATCGAATTATTTTG	Antisense	54
T37I_F	CAAGTGCCACAAAGGAATCTACTTGTACAA	Sense	59
TNFR1-37_R	TTCCTTTGTGGCACTTGGTACAGCAAATCGA	Antisense	62

Y38S_F	CAAGTGCCACAAAGGAACCTCCTTGTACAA	Sense	62
Y38C_F	CAAGTGCCACAAAGGAACCTGCTTGTACAA	Sense	62
L39F_F	CACAAAGGAACCTACTTCTACAATGACTGT	Sense	59
TNFR1-39_R	AAGTAGGTTCCTTTGTGGCACTTGGTA	Antisense	58
C43R_F	CCTACTTGTACAATGACCGTCCAGGCCCGG	Sense	67
C43S_F	CCTACTTGTACAATGACCCTCCAGGCCCGG	Sense	67
TNFR1-43_R	GTCATTGTACAAGTAGGTTCCTTTGTG	Antisense	57
P46L_F	CAATGACTGTCCAGGCCTGGGGCAGGATA	Sense	66
TNFR1-46_R	GGCCTGGACAGTCATTGTACAAGTAGG	Antisense	61
MT2-AlaMt-FWD	ACGATGTAGACTCGTTTCAGCGCTCGAGATGG	Sense	66
MT2-Xho-FWD	ACGATGTAGACTCGTTTCA__CTCGAGATGGTG	Sense	63
Mt2-Mut-REV	TGAAACGAGTCTACATCGTTTGGGTGAGGGA	Antisense	63
pETDuet -1 Primers			
pET-UP1-FWD	ATGCGTCCGGCGTAG	Sense	55
pET-UP2-FWD	TTGTACACGGCCGCATAATC	Sense	52
pET-Down1-REV	GATTATGCGGCCGTGTACAA	Antisense	52
pET-Down2-REV	GCTAGTTATTGCTCAGCGGT	Antisense	52
pProEx-1 Primers			
FWDpProHis	AGCATCTCATGAATGTCGTACTACCATCACCAT	Sense	62
T2REVpPRO	TTGATCAAGCTTTTATGAAACGAGTCTACATCGTTTGG	Antisense	62
G4RREVpPRO	TGCTTAAAGCTTTTACAGGAATCTAGTGGGCTTAGA	Antisense	62
J2RREVpPRO	TGCTTAAAGCTTTTACAGGTGTGTAGGGTT	Antisense	63
CD27 Primers			
huCD27FWD	AGCAGGTACCATGGCACGGCCACATCCCTGGTGG	Sense	71
huCD27REV	TACTAACTCGAGGGGGGAGCAGGCAGGCTCCGGTT	Sense	71

2.2.13 PCR bacteria colony screening

PCR master mixes were made to contain 0.04mM of each dNTP (Bioline), PCR buffer containing 0.6mM $MgCl_2$ (QIAGEN), 10pM of both sense and antisense primer and 1 unit of Hotstar Taq DNA polymerase (QIAGEN) to a final volume of 25µL in ddH_2O for each reaction. A small amount of a transformed *E.coli* colony was picked with a sterile plastic tip and inoculated onto a master LB agar plate containing 100 µg/ml ampicillin (Amresco) then inoculated into the PCR master mix. Reactions were heated at 95°C for 15 minutes to activate the DNA polymerase then cycled at 95°C for 1 minute, annealed

at Tm-5°C of lowest primer pair for 1 minute, 72° C for 1minute/Kb of DNA for 30 cycles. A 10 minute 72°C extension followed the final cycle before being held at 4°C. Reactions were carried out in an Eppendorf gradient master cycler.

2.3 Bacterial methods

2.3.1 Preparation of agar plates

Agar plates were made by dissolving 12.5g of Lennox Broth powder (Oxoid) with 7.5g Agar (Oxoid) into dH_2O. The Agar mixture was then autoclaved (121°C, 15 minutes) and allowed to cool before pouring into 10cm plastic dishes (Starstedt) to set. For ampicillin selection plates, agar was allowed to cool to 55°C before the addition of ampicillin (100 μg/ml) (Amresco).

2.3.2 Preparing chemically competent *E.coli*

Chemically competent *E.coli* cells (Dam^-Dcm^- (New England Biolabs), DH5α (Life Technologies), Bl21 De3 (Life technologies) Jm109 (Promega) were prepared by streaking single colonies on a LB agar plate then transferring a single colony into 5ml LB broth overnight at 37°C with shaking 260 rpm. The following day the *E.coli* broth was subcultured into 10ml of fresh LB broth and grown into log phase. *E.coli* broths were pelleted at 4000g (Hereaus Multifuge 3s-R) and resuspended in 0.1M $MgCl_2$ (Sigma) then pelleted again and the supernatant aspirated. The cell pellet was resuspended in 0.1M $CaCl_2$ (Sigma) and incubated on ice for 1 hour. The cells were then pelleted at 4000g and

resuspended in 0.1M $CaCl_2$ containing 15% glycerol (Sigma) and aliquoted in 1.5ml microfuge tubes and stored at -80°C.

2.3.3 Bacteria transformations

Chemically competent *E.coli* were thawed on ice and mixed with (100pg-1ng) plasmid DNA for 10 minutes on ice. The mixture was then heat shocked by placing the chemically competent *E.coli* in a 42°C heating block for 30 seconds then returning cells to ice for a further minute. Sterile LB media was added to the *E.coli* and incubated at 37°C for 1 hour in a shaking incubator. Cells were then centrifuged at 3000rpm (Eppendorf 5415C centrifuge) for 3 minutes and resuspended in 100µl of sterile LB media. *E.coli* mixtures were then spread onto LB agar plates containing 100 µg/ml ampicillin and incubated at 37°C overnight.

2.3.4 Bacterial glycerol stocks

Single colonies off selective LB agar plates containing ampicillin (100 µg/ml) were used to inoculate a LB broth containing 100 µg/ml ampicillin. Overnight bacterial broths were then transferred into a cryovial (Sarstedt) and combined with glycerol (20% final concentration) (Sigma). Bacterial glycerols were vortexed thoroughly and stored immediately at -80 °C.

2.4 Protein methods

2.4.1 Protein precipitation of cell supernatants

Expression of viral secreted protein from HEK 293 cells was concentrated for western blot detection by solvent precipitation. Cell supernatants were collected and centrifuged 4000rpm at 4°C for 5 minutes (Hereaus Multifuge 3s-R) to remove dead cells. The supernatants were transferred to a clean centrifuge tube and 5 volumes of acetone and methanol (1vol: 1vol) was added and incubated at -20°C for 1 hour. The precipitated proteins were collected by centrifugation at 4000g (Hereaus Multifuge 3s-R) for 10 minutes at 4°C and the acetone/methanol was aspirated. The pellet was left to air dry to remove residual acetone/methanol for 10 minutes and then resuspended in 1x loading SDS-PAGE loading buffer and stored at -20°C until use.

2.4.2 Total cell lysates

For the detection of intracellular or surface expression of proteins, total cell lysates were prepared and detected by SDS-PAGE electrophoresis and Western blotting. Adherent cell monolayers of HEK 293 cells were washed twice in ice cold saline (0.9% w/v NaCl) (Baxter) and lysed with 50-200µl of radio immunoprecipitation assay buffer (RIPA) buffer (150mM NaCl, 1% v/v nonidet P40 (NP-40), 0.5% w/v Na, deoxycholate (DOC), 0.1% w/v SDS, 50 mM Tris, pH 8.0) containing 1 times complete protease inhibitors (Roche). The cells were incubated on ice for 30 minutes then centrifuged at 14000rpm (Eppendorf 5415C) for 5 minutes to remove cell DNA. Lysates were then stored at -20°C.

2.4.3 Denaturing SDS-PAGE electrophoresis

Sodium dodecyl sulphate polyacrylamide gel electrophoresis (SDS-PAGE) was performed as described in (Laemmli 1970). Briefly, protein samples were mixed or resuspended in 1x SDS-PAGE sample loading buffer (200 mM Tris-HCl (pH 6.8), 400 mM DTT, 8% SDS, 0.4% bromophenol blue, 40% glycerol) then boiled for 10 minutes. Samples were then quickly loaded into a cast 12% (w/v) SDS-PAGE gel with a 4% w/v stacking gel. The 12% stacking Gel contained 30% acrylamide and bis-acrylamide solution, 37.5:1 (12% total) (Bio-Rad), 380mM Tris Ph8, 0.1% SDS (Sigma), 0.1% ammonium persulfate (Sigma) and 0.04% N,N,N',N'-Tetramethylethylenediamine (TEMED) (Sigma) to a final volume in ddH_2O. The Stacking gel contained 30% acrylamide and bis-acrylamide solution, 37.5:1 (4% w/v total) (Bio-Rad), 380mM Tris pH 6.8, 0.1% SDS (Sigma), 0.1% ammonium persulfate (Sigma) and 0.04% N,N,N',N'-Tetramethylethylenediamine (TEMED) (Sigma) to a final volume in ddH_2O. Proteins were electrophoresed in SDS-PAGE running buffer (24mM Tris, 38.4mM glycine, 0.1% SDS w/v, pH8) at 80V until dye front entered the separating gel then increased to 180V for 1.5 hours. Large casted SDS-PAGE gels were run for approximately 3-4 hours at 180V.

2.4.4 Western blotting

SDS-PAGE gels after electrophoresis were fastened in a blotting module (Bio-Rad) with a polyvinylidene difluoride (PVDF) membrane (Merck Millipore). The proteins were transferred in 25mM Tris, 192mM glycine and 20% methanol in dH_2O at 400mA for 1 hour for mini gels or 150mA overnight at 4°C for large gels. The blot was then rinsed in dH_2O and blocked for 1 hour in 5% skim milk powder in phosphate buffered saline (PBS).

The blot was then stained with the appropriate antibodies with 3, 1 minute washes in PBS containing tween 20 (0.05%) (Bio-Rad) (PBST) in between. The blot was then developed in BCIP/NBT (Bio-Rad) in alkaline phosphatase buffer (100mM NaCl, 5mM $MgCl_2$, 100mM Tris). All reagents were purchased from Sigma unless stated.

2.4.5 Bacterial expression of vTNFRs

To bacterially express vTNFRs, transformed Bl21 (DE3) *E.coli* containing pETDuet expression vectors were inoculated onto LB agar containing ampicillin (100µg/µl). Single colonies were then inoculated into 10mls of LB broth containing ampicillin (100µg/µl) overnight at 37°C with shaking. The following day cultures were subcultured into 1L of LB containing ampicillin (100 µg/µl) and cultured to log growth (OD 0.8). Cultures were then inoculated with 1mM isopropyl β-D-1-thiogalactopyranoside (IPTG) (Sigma) and cultured for a further 5 hours. Pellets were obtained by centrifugation at 10000g and resuspended in Lysis buffer (50mM NaH_2PO_4, 300mM NaCl, 10mM Imidazole).

2.4.6 Bacterial protein and Inclusion body purification

Bacterial *E.coli* pellets in lysis buffer were sonicated on ice for 20 seconds on full power for 10 repetitions. Lysates were then pelleted at 20000g for 10 minutes and transferred to a new tube to be analysed. Pellets containing inclusion bodies were washed in 50mM Tris HCl pH8, 50mM NaCl, 1mm EDTA, 0.5mM phenylmethylsulfonyl fluoride (PMSF) and 0.8% Triton X-100 twice, then washed twice more without Triton X-100. Inclusion bodies were then solubilised overnight in 6M guanidine HCl and 5% β-mercaptoethanol at 4°C with stirring. Solubilised protein was obtained by centrifugation at 4°C, 10000g for 15

minutes. Excess salt was dialysed against 4L of refolding buffer (25mM Tris-HCl pH 8, 5mM $CaCl_2$, 5mM L-cysteine and 0.9M guanidine). Guanidine was reduced in each buffer change until guanidine was removed in final buffer of 20mM Tris-HCl pH 7.4, 2.5mM KCl. Solubilised protein was analysed by SDS-PAGE and western blot.

2.4.7 Nickel agarose affinity purification for crystallography

Recombinant His tagged proteins were purified from cell supernatants by affinity purification to nickel-nitrilotriacetic acid (Ni-NTA) resin (QIAGEN). Cell supernatants were mixed with Ni-NTA resin then adjusted to pH 8.0 and incubated at 4°C with rotation for 2 hours. The slurry was then pelleted by centrifugation at 4000g (Hereaus Multifuge 3s-R) for 10 minutes at 4°C and the supernatant was aspirated. The slurry was then washed twice with wash buffer (50mM NaH_2PO_4, 300mM NaCl, 20mM Imidazole pH 8.0) and pelleted at 14000 rpm (Eppendorf 5415C) for 1 minute. The protein was eluted by resuspending the Ni-NTA slurry in elution buffer (50mM NaH_2PO_4, 300mM NaCl, 250mM Imidazole pH 8.0) then centrifuging at 14000 rpm (Eppendorf 5415C) for 1 minute and collecting the supernatant. All reagents were purchased from Sigma unless stated.

2.5 Cell culture

2.5.1 Cell lines

Human HEK 293 cells – The human embryonic kidney cell line were used which were derived in 1977 (Graham et al. 1977). HEK 293 cells are known and used in this study for their quick growth rate, high transfection efficiency and high protein expression (Baldi

et al. 2005; Jordan, Köhne & Wurm 1998). Cells were kindly donated by Grant Logan, Children's Medical Research Institute, Westmead.

Human U2OS cells – Are a human bone osteosarcoma epithelial cell line derived in 1964 (Ponten & Saksela 1967). Little is known about their proteome profile however were selected in this study for their adherent large flat morphology ideal for microscopy (Niforou et al. 2008). Cells were generously donated by Dr Helen Rizos, from the institute for Cancer research, Westmead millennium institute, NSW, Australia.

2.5.2 Cell culture and passaging

HEK 293 cells and U2OS cells were cultured in Dulbecco's modified Eagle's medium (DMEM with High glucose and pyruvate)(Life Technologies), also supplemented to contain 10% heat inactivated foetal bovine serum (Life Technologies, USA), 80 units/ml penicillin and 80µg/ml streptomycin and 1.6mM L-glutamine all purchased from Life Technologies. Cells were incubated at 37°C supplemented with 5% CO_2 in a humidified incubator and passaged to 90% confluency before passaging. Cells were passaged by washing the cells with sterile PBS (Amresco), then detaching the cells from the flask by incubating with 0.05% trypsin EDTA (Life Technologies) diluted in PBS (Amresco) for 2 minutes. Residual trypsin was inactivated by adding 10mls of fresh media then centrifuging for 3 minutes to pellet cells and aspirate the supernatant. Cells were then resuspended in fresh media and propagated in a new tissue culture vessel (Becton Dickinson).

2.5.3 Calcium phosphate transfection of eukaryotic cell lines

All human cell lines were transiently transfected with purified plasmid DNA by using the calcium phosphate method (Gorman 1985). Cells were seeded into 10cm tissue culture dishes, 6, 12 or 24 well tissue culture dishes (Becton and Dickinson) the previous day so that cells were approximately 80% confluent at the time of transfection. The following day the media was replaced 2hours before transfection. For cells seeded in a 6 well dish a mixture containing 4µg of plasmid DNA, 16µl of 2M $CaCl_2$ (Sigma) diluted to a total volume of 125µl in 0.1% TE was prepared. The DNA calcium mixture was then added drop wise with aeration to a mixture containing 125µl of 2x HEPES buffered saline (HBS) and 1.25µl Na_2HPO_4 (pH 7.1) and incubated at room temperature for 20 minutes. The DNA complexes were then added to the cells evenly and incubated at 37°C in 5% CO_2 for 4 hours. The media was aspirated then washed with warm saline (0.9% w/v NaCl) (Baxter) and replaced with fresh media for up to 48 hours. The reactions were scaled up or down according the cell surface area in each tissue culture dish.

2.6 Cell staining

2.6.1 Rab5 staining

A polyclonal rabbit anti Rab5 antibody (AbCam) and secondary conjugated Alexa fluor (AF) 568 IgG goat anti rabbit (H+L) (Molecular probes, Life Technologies) were used to demarcate Rab5 positive endosomes within U2OS cells. Briefly adherent cells seeded in 35mm flourodishes (World Precision Instruments) were washed 3 times in warm PBS for 1 minute. The cells were then incubated with 4% paraformaldehyde (PFA) (Sigma) in PBS for 15 minutes at 37°C. The cells were washed 3 times in PBS for 1 minute then

permeabilised with 0.1% Triton X-100X-100 (Sigma) in PBS for 1 minute. The cells were washed again 3 times in PBS then blocked in 2% heat inactivated goat serum in PBS for 1 hour. The serum was removed and then stained with the polyclonal rabbit anti human Rab5 antibody (AbCam) 5µg/ml diluted in blocking solution for 1 hour. Cells were washed 3 times in PBS then stained with a secondary polyclonal goat anti rabbit-AF568 antibody (molecular probes) 1µg/ml for 1 hour. The cells were washed 3 times in PBS then visualised in glycerol (90%) in PBS (Sigma). A no primary antibody control was performed by omitting the primary polyclonal rabbit anti Rab5 antibody staining step and staining with the secondary polyclonal goat anti rabbit-AF568 antibody.

2.6.2 DRAQ5 staining

Live or fixed U2OS cells were stained with DRAQ5 (Abcam) to visualise the nucleus. To fix cells, the media was removed and cells were washed 3 times in warm PBS, incubated with 4% PFA in PBS for 15 minutes then washed again 3 times in PBS. DRAQ5 was diluted in PBS to a working concentration of 5µM then added to the cells and incubated at 37°C for 15 minutes. For live cell staining DRAQ5 was added directly to media at the same concentration. The cells were washed 3 times in PBS then mounted in glycerol-based mounting media (Sigma) for fixed cells or left in media or PBS for live cells.

2.6.3 Live cell Wheat Germ Agglutinin (WGA) staining

Live adherent U2OS cells were incubated with WGA conjugated to AF594 (Molecular probes, now Life technologies) directly into the media (5µM) at 37°C for 10 minutes.

Excess WGA-AF594 was removed by washing 3 times in PBS and were visualised immediately.

2.6.4 Fixed WGA staining

Seeded U20S cells were fixed by removing the media, washing 3 times in warm PBS, incubating with 4% PFA in PBS and then removing the PFA by washing 3 times for 1 minute with PBS. Cells were then incubated with WGA conjugated to AF594 (Molecular probes, Life technologies) in PBS (5µM) at 37°C for 10 minutes. Cells were then washed 3 times in PBS and visualised in glycerol (90%) in PBS.

2.7 Microscopy

2.7.1 WT-TNFR1-YFP and TRAPS MT TNFR1-YFP localisation with Rab5

U20S cells were seeded into 35mm fluorodish cell culture dishes (World Precision Instruments) overnight and then transfected the following day as per section 2.4.3. pcDNA3.TNFR1-YFP or pcDNA3.TRAPS-TNFR1-YFP constructs were transfected into the U20S cells then washed 4 hours post transfection with sterile saline (0.9% NaCl) (Baxter) and replaced with fresh media. The transfected cells were incubated for a further 16 hours then fixed and incubated with the Rab5 antibody and secondary goat anti-rabbit-AF568 as per sections 2.5.1. The cells were then washed and incubated with DRAQ5, then mounted in glycerol (90%) in PBS and visualised on an Eclipse TI live inverted widefield microscope (NIKON). Fluorescent tags were excited using a mercury arc lamp in combination with specific filter cubes (NIKON) for each fluorophore. Wild type and mutant TNFR1-YFP proteins were excited through a 495/10nm filter and emission was

detected using a 520/40nm barrier filter (NIKON). Cells stained with Rab5-AF568 antibodies were excited through a 540/25 excitation filter and detected though a 605/55nm barrier filter (NIKON). Nuclei stained with DRAQ5 were excited through a 660/55nm filter and detected through a 665/55nm barrier filter (NIKON). 20 random fields of view for each sample were acquired with a 60X objective NA 1.4.

2.7.2 Deconvolution and co-localisation analysis

Each image was deconvolved using AutoQuant software X2 (Media Cybernetics ver 2.2.1). 3D images stained with Rab5 were deconvolved using Blind 3D deconvolution on default settings. Deconvolved images were then imported into Imaris software (Bitplane ver 8.1) to perform co-localisation analysis using the Coloc tool. For each channel the isoline tool was used to define the intensity above the threshold. A co-localisation channel was then built and the appropriate statistics exported.

2.7.3 WT TNFR1-YFP and TRAPS mutant TNFR1-YFP localisation with WGA-AF596

U20S cells were seeded into 35mm fluorodish cell culture dishes (World Precision Instruments) overnight and then transfected the following day as per section 2.4.3. pcDNA3.TNFR1-YFP or pcDNA3.TRAPS.TNFR1-YFP constructs were transfected into the U20S cells then washed 4 hours post transfection with sterile saline and replaced with fresh media. The transfected cells were incubated for a further 16 hours then fixed and stained with WGA-AF596 as per sections 2.5.4. The cells were then washed and stained with DRAQ5 and afterward mounted in glycerol (90%) in PBS and visualised on an Eclipse

TI live inverted widefield microscope (NIKON). Cells stained with WGA-AF596 were excited through a 540/25nm excitation filter and detected with a 605/55nm barrier filter. Transfected wild type and TRAPS mutant TNFR1-YFP proteins were excited through a 495/10nm filter and emission was detected using a 520/40nm barrier filter. DRAQ5 stained nuclei were excited through a 660/55nm filter and detected through a 665/55nm barrier filter.

2.8 Flow cytometry

2.8.1 TRAPS vs WT TNFR1 and vTNFR vs WT TNFR1 cell death assay by flow cytometry (PI)

HEK 293 cells were seeded into 6 well dishes overnight at 7 x10^5 cells per well. The following day cells were transfected with 2µg of total DNA using the calcium phosphate method as in section 2.4.3. For the TRAPS vs WT TNFR1 cell death assay cells were transfected with pcDNA3-TNFR1-CFP (1µg) and pcDNA3-TRAPS-TNFR1-YFP (1µg). For the vTNFR vs WT TNFR1 cell death assay cells were transfected with pcDNA3.VARG4R- or pcDNA3.MPVJ2R- or pcDNA3.MYXT2- as either CFP or YFP (1µg) and pcDNA3-TNFR1-CFP or pcDNA3-TNFR1-YFP (1µg). pcDNA3, pcDNA3.CD27-CFP and pcDNA3.CD27-YFP were included as control samples and for cytometer setup. The cells were harvested 48 hours post transfection by pippeting the cells off the tissue culture dish and filtering through 90µm nylon mesh (SEFAR, Australia). Cells were transferred to a round bottomed tube and pelleted by centrifugation at 300g for 5 minutes. Cells were resuspended and washed twice in Saline (0.9% NaCl) (Baxter). Cells were then stained with PI (Life Technologies) (1.5µM) in Saline (0.9% NaCl) (Baxter) for 15 minutes at room

temperature. Cells were then analysed by flow cytometry on the LSRII (Becton Dickinson) analyser. CFP was excited using the violet laser (405nm), YFP and PI were excited using the blue laser (488nm). CFP emission was detected through a 460LP, 470/20nm BP filter, YFP emission detected through 505LP, 550/30BP filter and PI emission through a 550LP, 685 LP, 695/40 BP filter set. 30000 events were collected using FACS Diva software (Ver 6.0). Post analysis was performed using FlowJo (Ver 10.0.7). Statistical analysis was performed using Prism5 (GraphPad ver 5.03).

2.8.2 vTNFR cellular retention assay

HEK 293 cells were seeded into 6 well dishes and transfected as in section 2.5.3 with 1µg of pcDNA3, pcDNA3.CD27-YFP, pcDNA3.TNFR1-YFP, pcDNA3.TNFR2-YFP and 1µg of either pcDNA3.CD27-MycHis, pcDNA3.MYXT2-MycHis, pcDNA3.VARG4R-MycHis, pcDNA3.MPVJ2R-MycHis. The cells were harvested 48 hours post transfection by pippeting the cells off the tissue culture dish and filtering through 90µm nylon mesh (SEFAR, Australia). Cells were transferred to a round bottomed tube and pelleted by centrifugation at 300g for 5 minutes. Cells were resuspended and washed twice in saline (0.9% NaCl) (Baxter) and transferred to a 96 well plate (Becton Dickinson). The cells were fixed by incubating with 1% PFA for 10 minutes at room temperature and then washed twice in saline then once in 1X permeabilisation buffer (eBiosciences). Cells were then incubated with mouse anti-Myc-AF647 (1.5µg/ml) or Goat anti-mouse IgG-AF647 (1.5µg/ml) for 1 hour in permeabilisation buffer. Cells were washed 3 times in permeabilisation buffer then resuspended in saline and run on the LSRII (Becton Dickinson). YFP and AF647 were excited and detected as previously mention in section 2.8.1. 30000 events were collected using FACS Diva software (ver 6.0). Post analysis was

performed using FlowJo (Ver 10.0.7). Statistical analysis was performed using Prism5 (GraphPad ver 5.03).

2.8.3 CFP-YFP FRET

HEK 293 cells were transfected with either cyan fluorescent protein (-CFP) or yellow fluorescent protein (-YFP) fusion plasmid DNA by the calcium phosphate method as in section 2.4.3. The cells were harvested 48 hours post transfection by pippeting the cells off the tissue culture dish and filtering the cells through 90µm nylon mesh (SEFAR, Australia) to remove clumps then centrifuged at 300g. The supernatant was then removed and the cells resuspended in 1% paraformaldehyde in saline (0.9% NaCl) (Baxter). The cells were then run on a LSRII, 4 laser flow cytometer (Becton Dickinson). Excitation of CFP was achieved with a 405nm laser and detected using a 460 nm long pass (LP) and 470/20 nm band pass (BP) filter (in the 405 nm laser trigon detector). Standard YFP fluorescence was excited using the 488 nm laser and detected in the octagon detector using a 505 nm LP and 550/30 nm BP filters (in the 488nm-laser octagon detector). For the detection of fluorescence resonance energy transfer (FRET), CFP fusion proteins were excited with the 405nm laser and the emission of CFP excited YFP fusion proteins were detected with 530 nm LP and 546/10 nm BP filters in the 405 nm laser trigon detector separate from standard YFP excitation and emission. True FRET signals were obtained through compensation using FACS Diva software (Ver 6.0) with 30000 events collected for each sample. Post analysis was performed using FlowJo (Ver 10.0.7).

2.8.4 Statistical analysis

Statistical analysis was performed using GraphPad Prism 5 (GraphPad Software v5.03). To determine if statistical differences existed between samples a 1 way ANOVA was performed to test whether differences existed between samples. If a statistical difference was identified, a successive Dunnett's multiple comparisons test was performed to identify where statistical differences lie. A significance level of $p<0.01$, $p<0.05$, $p<0.5$ is represented by ***, ** and * respectively.

Chapter 3

Generation and characterisation of TRAPS mutations on TNFR biology

Chapter 3

3.1 Introduction

The biology of the TNFR1 receptor has been widely investigated and the pathways involved in TNFR1 signalling are well described (Aggarwal 2000; Aggarwal 2003; MacEwan 2002; Mathew et al. 2009; Schutze, Tchikov & Schneider-Brachert 2008). However mutations in TNFR1 associated with TRAPS and their involvement in pathology are still not completely understood. TRAPS is an autosomal dominant auto inflammatory disease, caused mutations in the extracellular domain of TNFR1 (McDermott et al. 1999). The majority of the mutations are single point mutations resulting in an amino acid change, often with multiple mutations affecting the same residue (Table 3-1). Interestingly, over 90% of the mutations reside in CRDs 1 and 2 with no mutations described in CRD 4 and only one mutation described in close proximity to the transmembrane region (Kriegel et al. 2003; Turner, Chaudhry & Nedjai 2012). (See Figure 1.5 and Table 3-1). No C-terminal TRAPS mutations have been described.

Patients harbouring TRAPS mutations present with a spectrum of clinical symptoms (Dodé et al. 2002; McDermott, Smillie & Powell 1997). These include fever, myalgia, arthritis, fasciitis, abdominal pain, skin patches, skin lesions, conjunctivitis, periorbital oedema and in severe cases amyloidosis (Lachmann et al. 2013; Lahaxe et al. 2010; McDermott, Smillie & Powell 1997; Quillinan et al. 2010; Rösen-Wolff et al. 2001; Williamson et al. 1982). Mutations associated with cysteine mutations are almost always found to be associated with more severe clinical symptoms, including amyloidosis (Hull et al. 2002; Lachmann et al. 2013). It is hypothesised that mutations more dramatically affecting the structure of TNFR1 such as cysteines involved in disulphide bridges, result

in more severe TRAPS phenotypes (Bulua et al. 2011; Hull et al. 2002). However the underlying mechanisms of how mutations result in the TRAPS phenotype is still not completely understood.

One possible explanation for the overactive inflammatory response is an inability of TRAPS mutant TNFR proteins to localise correctly within the cell accumulating within the endoplasmic reticulum (ER) and causing an ER stress response (Lobito et al. 2006). A number of TNFR TRAPS mutants (H22Y, C33G, T50M, C52F, R92P) fail to traffic to the cell surface, and instead, aggregate and localise within the ER (Lobito et al. 2006; Rebelo et al. 2006). These H22Y, C33G, T50M, C52F and R92P TNFR mutant proteins also fail to bind TNFα, and display a reduced efficiency to signal cell death or to activate the NF-κB pathways (Lobito et al. 2006; Siebert, Fielding, et al. 2005). Therefore, it is thought that TNFRs with TRAPS mutations activate inflammation in a ligand-independent pathway, possibly through the inflammasome or via an ER stress response (Bulua et al. 2011; Simon et al. 2010).

Although more work is needed to understand how TRAPS mutations result in the clinical inflammatory symptoms, TRAPS mutations also serve as natural occurring example of a mutational analysis in TNFR1. Because the majority of TRAPS mutations reside with CRD1 and the PLAD domain which are responsible for (or required for) WT TNFR self-association (Chan 2000), TRAPS mutations can also help better define how TNFR proteins function and interact with other proteins by identifying amino acid residues important to TNFR1 function. It also raises many interesting questions for proteins such as MYXT2 which are known virulence factors (Upton et al. 1991) and associate through the PLAD with cellular TNFRs to inhibit host cell death. For example, “how do the

presence of TRAPS mutations affect viral-cellular TNFR interactions, and what is the significance of TRAPS in terms of poxviral infection?" To begin to answer how TRAPS mutations affect the interaction of vTNFRs with cellular TNFRs, it was necessary to first understand how TRAPS proteins function in more detail in order to later compare interactions in the presence of vTNFRs. Therefore to characterise TRAPS mutations within the PLAD domain, 17 TRAPS mutations were selected and generated as YFP fusion constructs. These plasmids were then expressed in cell lines to assess the effect of each mutation on TNFR1 function *in vitro*.

3.2 Results

3.3 Generation of TNFR1 TRAPS-YFP mutants

To begin to investigate the biology of viral TNFRs and their interactions with cellular TNFRs, with respect to naturally occurring TNFR1 TRAPS mutations, TNFR1 PLAD domain mutations were generated by site-directed mutagenesis in wild type TNFR1 cDNA, in pcDNA3.TNFR1-YFP. In order to create the mutations in pcDNA3.TNFR1-YFP several specific mutagenic primers were needed. This study is investigating the function of the PLAD domain in TNFR1 biology, therefore a panel of mutations were selected from known cases of TRAPS in the INFEVERS database (http://fmf.igh.cnrs.fr/ISSAID/infevers/). At the beginning of this study only 25 mutations were known that had been described to be present within the PLAD of TNFR1 (INFEVERS database). Information about each mutation was compiled from the INFEVERS database, and literature, and assessed as to whether each mutation was relevant to the disease and assigned as a TRAPS mutation (Table 3.1).

Table 3-1 Reported TRAPS mutations

Traps mutation	Codon change	AA change	AA structural features	Associated Symptoms	Associated phenotype	Country of origin
D12E	GAT>GAG	Asp>Gln		Mild symptoms – only few occurrences of fever per year and lasting only 3 days	unknown	N/A
Y20D	TAT> GAT	Tyr>Asp	Affects highly conserved hydrogen bond between Y20 and D40	No shedding Arthralgia, severe abdominal pain, similar to TRAPS symptoms	TRAPS	Chinese (first TRAPS patient in china)
Y20H	TAT>CAT	Tyr>His	Affects highly conserved hydrogen bond between Y20 and D40	Abdominal pain, amyloidosis in kidneys (late onset), erysipelas-like eruption thigh. (sporadic symptoms)	TRAPS	Jewish/Polish/Italian
H22R	CAC>CGC	His>Arg		N/A	TRAPS	N/A
H22Q	CAC>CAG	His>Gln	Within β turn of loop 3	No amyloidosis, associated with juvenile idiopathic arthritis, no features of Traps	Juvenile idiopathic arthritis	Caucasian/UK
H22Y	CAC>TAC	His>Tyr	Within β turn of loop 3	No amyloidosis, variable reduced shedding, lifelong sporadic fever. Mild traps symptoms	TRAPS	Scottish/German and mixed northern European
C29Y	TGC>TAC	Cys>Tyr	Critical cysteine disulphide bond	N/A	TRAPS	N/A
C29F	TGC>TTC	Cys>Phe		fever, myalgia, abdominal pain, and skin lesions, lasting 2-3 weeks	TRAPS	N/A
C30R	TGT>CGT	Cys>Arg		Neurological disorder,	TRAPS	Irish/American
C30F	TGT>TTT	Cys>Phe		N/A	TRAPS	
C30Y		Cys>Tyr		N/A	TRAPS	
C30S	TGT>TCT	Cys>Ser (the most conserved cysteine residue)		Defective receptor shedding, TRAPS symptoms	TRAPS	French
C33G	TGC>GGC	Cys>Gly		TRAPS	TRAPS	Spanish
C33Y	TGC>TAC	Cys>Tyr		Defective shedding, amyloidosis in one patient, hernias	TRAPS	Mixed Irish/Caucasian/ Scottish
G36E	GGA>GAA	Gly>Glu		Raised acute phase markers	unknown	Spain

T37I	ACC>ATC	Thr>Ile		TRAPS	Germany
Y38S	TAC>TCC	Tyr>Ser	N/A	TRAPS	UK/Caucasian
Y38C	TAC>TGC	Tyr>Cys	Raised ESR, Leukocytosis, Long febrile fevers	TRAPS?, however some were asymptomatic	Netherlands
L39F	TTG>TTC	Leu>phe	N/A	TRAPS	
D42del	211-213 deletion	Asp>----	Amyloidosis, not severe inflammation, no shedding	TRAPS	Northern/Irish
C43R	TGT>CGT	Cys>Arg Within β turn of loop 3	N/A	TRAPS	Italy
C43Y	TGT>TAT	Cys>Tyr	N/A	Recurrent fever	France
C43S	TGT>TCT	Cys>Ser	N/A	TRAPS	UK
P46L	CCG>CTG	Pro>Leu Within β turn of loop 3	Defective shedding although less dramatic than others	TRAPS Low penetrance	African American/ northern European

For example the clinical history, symptoms, and prevalence of each TNFR1 PLAD mutation was used to exclude mutations irrelevant to TRAPS. Novel mutations such as those within introns, splice mutations and large deletions or insertions were also excluded as TRAPS mutations are almost exclusively single point mutations resulting in an amino acid change (Table 3.1). TRAPS is a dominantly inherited syndrome (McDermott et al. 1999), therefore spontaneous mutations and polymorphisms which share no inheritability were also excluded. A panel of 17 mutations were then identified within TNFR1 from which to create mutant TRAPS TNFR1 cDNAs by site directed mutagenesis (Figure 3.1A). The generation of some of these TNFR1 PLAD mutations were first attempted during my preceding honours research year. The remainder were generated in the course of my PhD studies (highlighted in orange); the complete set of TNFR1 mutants were then comprehensively verified for this PhD research. (Figure 3.1B).

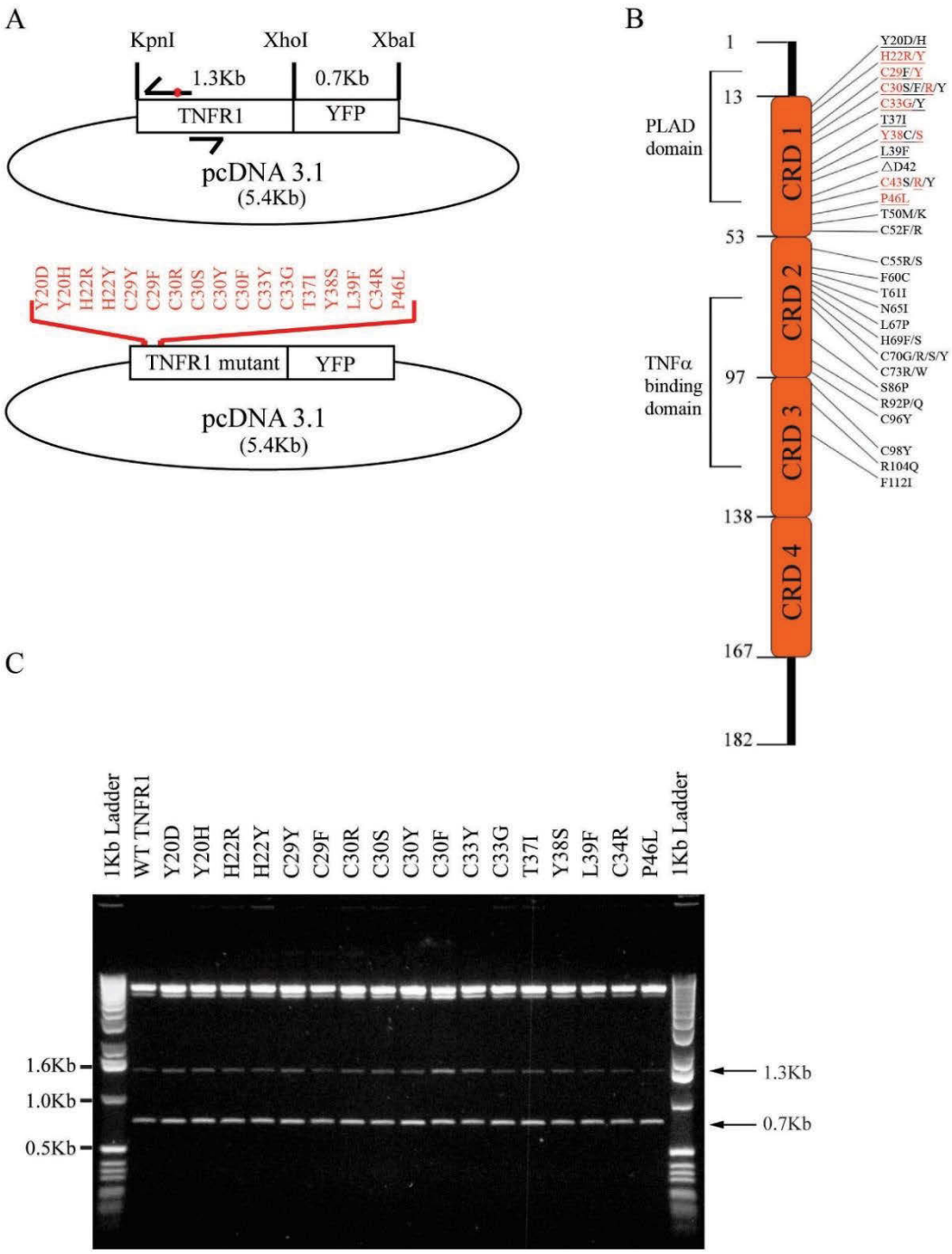

Figure 3.1 Generation of TRAPS-YFP mutations.

The generation of TRAPS mutations by site-directed mutagenesis. A) TRAPS mutations and site-directed mutagenesis primer location in pcDNA3.TNFR1-YFP. B) Linear representation of TNFR1 protein and location of TRAPS mutations. Selected TRAPS mutations generated in this study (highlighted red). C) Initial confirmation of generated TRAPS plasmids by restriction digest with *Kpn*I, *Xho*I and *Xba*I.

“Mutagenic primers” were designed i.e. with an altered nucleotide sequence, relative to the TNFR1 wild type cDNA sequence, such that, they would generate a specific amino-acid mutation; each forward primer generating a select mutation - out of a set of overlapping primers (Figure 3.1A). The forward and reverse primers contained 16-17 overlapping nucleotides and a further 10 TNFR1 wild type complimentary nucleotides, to permit annealing of the primers to the TNFR1 cDNA plasmid template. The primers were approximately 30 nucleotides in length and replicated bi-directionally around the pcDNA3.TNFR1-YFP plasmid to introduce the desired mutation. The cDNA sequence of TNFR1 (accession number M60275.1) within pcDNA3.TNFR1-YFP was used to model each primer pair.

Each of the selected TRAPS mutations was created through individual site-directed mutagenesis PCR reactions, essentially as per according to the manufacturers direction. (Invitrogen’s GeneTailor site-directed mutagenesis method). PCR reactions were performed in batches with primer pairs of similar annealing temperatures to introduce each mutation. The resulting PCR generated mutant TNFR1 cDNA from each site-directed mutagenesis reaction was identical in size to the starting wild type TNFR1 cDNA template, as judged by agarose gel electrophoresis (data not shown). To confirm each plasmid was, in fact TNFR1-YFP, as expected, the pcDNA3.TRAPS.TNFR1-YFP plasmids were digested with *Kpn*I, *Xho*I and *Xba*I restriction enzymes, which liberated/released the TNFR1 cDNA as well as the YFP cDNA insert, from the pcDNA3 vector and analysed by DNA gel electrophoresis. As expected, the cDNA fragment of 1.3 Kb for TNFR1 was observed for WT and each of the newly generated TRAPS mutant construct; a fragment of 0.7 Kb for the YFP fusion tag was also present (Figure 3.1C). This indicated that the TNFR1 and YFP cDNA sequences were all still of the expected size and that restriction

sites were unaltered. Further sequence confirmation was needed to verify that the specific mutations had been correctly introduced.

To determine whether each TRAPS mutation was successfully created in pcDNA3.TNFR1-YFP, each new plasmid DNA was sequenced. Both a forward (T7_Forward) and reverse YFP_Reverse) primer were used for sequencing, as these primers span the cDNA insert of TNFR1 and therefore permitted double strand sequence verification of the plasmid mutation. The sequence data clearly indicated that each of the selected TNFR1 mutations had successfully been introduced in to the origin of WT TNFR1 cDNA (Figure 3.2A), without secondary mutations occurring elsewhere within the TNFR cDNA i.e. potentially produced via the PCR reaction.

Since the plasmid sequencing data did not span the YFP fusion cDNA sequence, it was important to check for the potential of significant and unwanted additional PCR errors (i.e. outside of the TNFR1 cDNA) that could otherwise affect TNFR1 expression or detection of the mutant TNFR-YFP proteins, i.e. mutations that might alter YFP fluorescence. Therefore, to determine whether the TNFR1-YFP proteins could be detected via the presence of their YFP fusion tag, each plasmid was transfected into 293 HEK cells and the YFP fluorescence was detected by widefield fluorescence microscopy. Each TNFR1-YFP mutant as well as WT-TNFR1-YFP was observed to fluoresce when excited specifically for YFP with a 495/10 nm bandpass filter (Figure 3.2B). No auto fluorescence was detected from untransfected cells or cells transfected with pcDNA3 vector, meaning fluorescence detected was specific to TNFR1-YFP emission. All pcDNA3.mtTNFR1-YFP

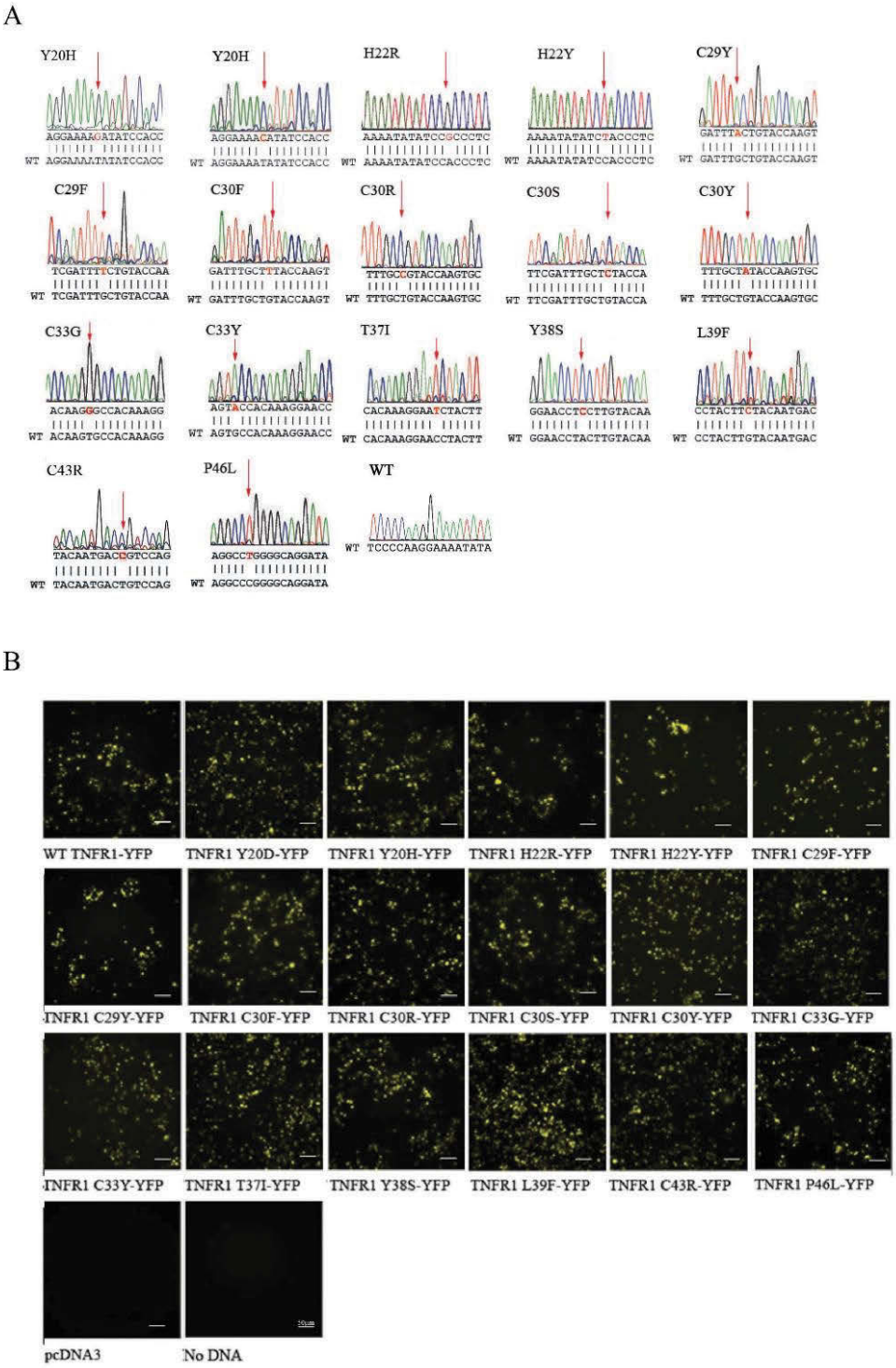

Figure 3.2 Confirmation of generated TRAPS-YFP plasmids.

A) TRAPS mutations confirmed by double strand sequence verification. B) Expression and visualisation of YFP expression on the Nikon TI widefield microscope. Expression of protein is 48hours post transfection in HEK 293 cells.

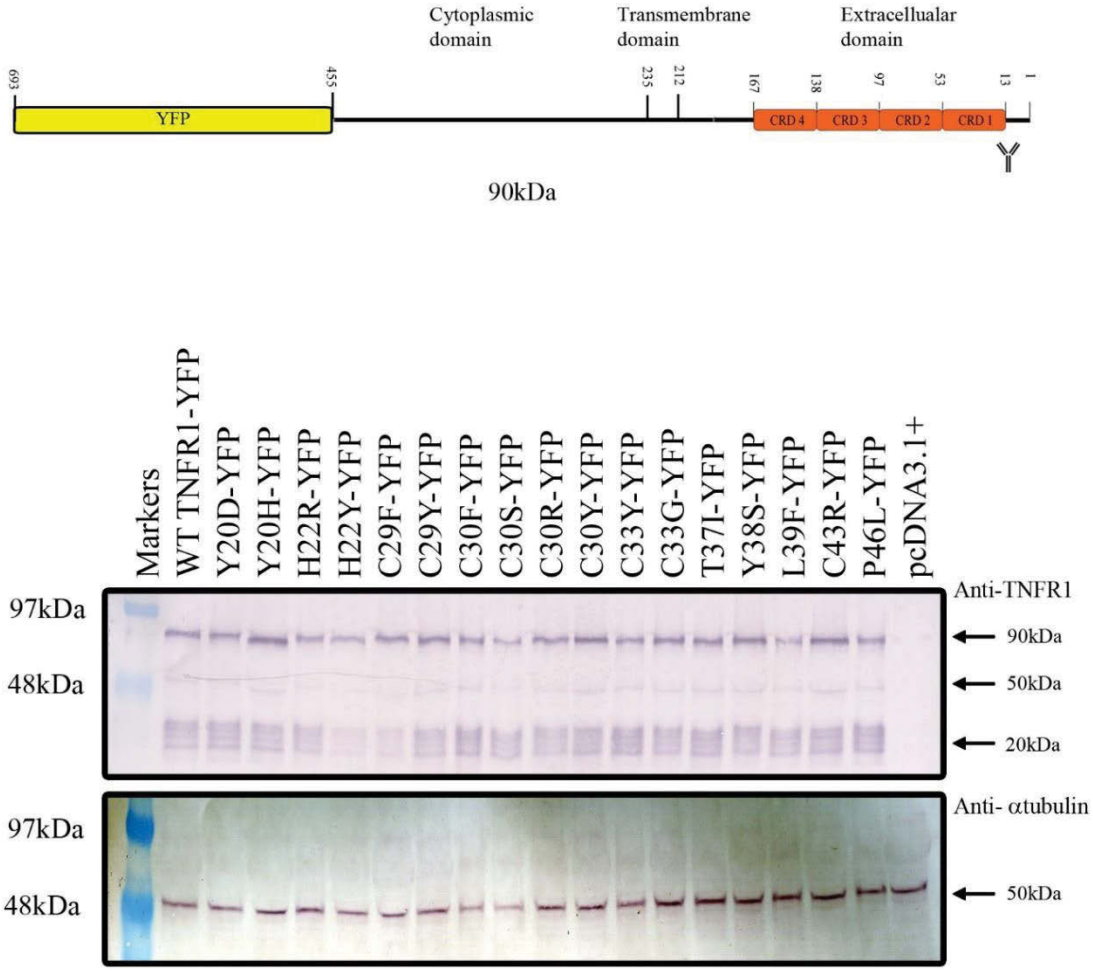

Figure 3.3 Confirmation of TNFR1 TRAPS-YFP expression.
Detection of TNFR1 TRAPS-YFP proteins by 12% PAGE and Western blotting. TRAPS proteins were expressed in HEK 293 cells, with lysates collected 72 hours post transfection. TNFR1 proteins were detected with an N-terminal (H5) anti-TNFR1 antibody. An anti-αtubulin antibody was used as a loading control for the same samples in a separate blot.

plasmids and pcDNA3.WTTNFR1-YFP appeared to be successfully expressed as indicated by YFP fluorescence.

Despite the presence of YFP fluorescence it was important to confirm the expression of a full-length TNFR1-YFP fusion protein. Thus a western blot was performed to detect

full-length proteins from transfected HEK 293 cells. Transfected HEK 293 cells lysates were prepared 72 hours post TF and analysed by 12% SDS-PAGE, with subsequent transfer to PVDF membranes. TNFR1 protein was then detected by immunoblotting with a 0.2μg/ml concentration of mouse anti-human TNFR1 (clone H-5; Santa Cruz) antibody followed by 1μg/ml conc. of secondary goat anti-mouse-AP conjugated antibody (Santa Cruz). The expected size of TNFR1 is between 55-60kDa (Loetscher, Schlaeger, et al. 1990) and since YFP is approximately 27kDa (Ganesan et al. 2006) , the TNFR1-YFP fusions proteins is expected to be approximately 80-90 kDa in size. Each TRAPS TNFR1-YFP protein and WT TNFR1-YFP gave a distinct band of approximately 85-90kDa, meaning that each protein was expressed and detected successfully (Figure 3.3). Another band of approximately 50-55kDa was also detected in the TNFR1 western blots, and this band was present in all of the samples except for the empty vector sample of unknown identity. A series of 4 additional smaller bands were also detectable in WT TNFR1 blots as well as all TRAPS mutant TNFR1 samples; these proteins ranged from 10-20 kDa in size (Figure 3.3). Since these bands were absent in the pcDNA3 control lane, these products appear to be specific to WT-TNFR1-YFP and TNFR1-TRAPS-YFP expression. Of note, these bands appear to be present in the manufacturer's western blots – as they are also evident in the product data sheet western blot images (data not shown). As a loading control, a separate SDS-PAGE gel was analysed by Western blotting with a mouse anti-α tubulin antibody (1μg/ml, Sigma) and an expected band of 50 kDa was observed in essentially the same abundance in each lane (Figure 3.3). Nevertheless, given that both TNFR1 WT and TRAPS mutant YFP fusions proteins appeared to be expressed in essentially similar abundance to each other, this indicated that the mutations had essentially no effect on the total overall levels of expression levels in HEK293 cells.

3.4 Generating TNFR1- and TNFR2-MycHis

In order to later analyse the interaction of cellular TNFRs with mutant TRAPS TNFR1 and/or vTNFR, a third non-fluorescent epitope tag was needed, in order to simultaneously detect all three constructs within the same experiment. Therefore WT-TNFR1 and -TNFR2 were subcloned to contain a C-terminal MycHis epitope Tag: (EQKLISEEDL/HHHHHH). The WT-TNFR1 and WT-TNFR2 cDNA sequences were obtained through double restriction digests with *Kpn*I and *Xho*I, then ligated into the *Kpn*I and *Xho*I sites of the pcDNA3.MPVJ2R-MycHis plasmid; this effectively substituted the TNFR1 or TNFR2 cDNA sequence for the original MPVJ2R cDNA sequence by creating an in-frame TNFR1- and TNFR2- MycHis fusion sequence (see Figure 3.4A).

To verify the TNFR1 and TNFR2 cDNAs had been successfully sub-cloned in the newly generated plasmids, and were of the correct size, a restriction digest was performed. pcDNA3.TNFR1-MycHis and pcDNA3.TNFR2-MycHis plasmids were digested with *Kpn*I and *Xho*I and analysed by agarose gel electrophoresis (see Figure 3.4B). Single digests with *Kpn*I or *Xho*I both linearized the plasmids, as evident by a single DNA band of approximately 7 Kb, meaning each enzyme only cut the plasmid once - consistent with the available restriction sites. The double digest resulted in a distinct band at 1.3 Kb representing the TNFR1-MycHis and TNFR2-MycHIs inserts of the expected sizes (Figure 3.4B). Each plasmid was also then double strand sequence verified to confirm the correct sequences (data not shown).

3.5 Generating CD27-CFP, –YFP and –MycHis

Finally, to compare the effect of either wild type TNFR1, TRAPS mutant TRAPS TNFR1 or vTNFR, another construct was needed, and CD27 was chosen as an internal comparison molecule. CD27 is a TNFRSF member which has not been reported to interact physically with wild type TNFR1, TNFR2 or vTNFRs. Moreover, since the interaction of TNFR1 PLAD domains is highly specific i.e. TNFR1 will not associate with TNFR2 (Chan et al. 2000a), it was hypothesised that CD27 would not associate with TNFR1, TNFR2 or vTNFRs, due to its low amino acid identity with TNFR1 or TNFR2 PLAD domain amino sequence. Additionally CD27 does not contain an intracellular death domain and is largely a co-stimulatory proliferative molecule on mature thymocytes (Gravestein et al. 1995), it therefore serves as an important non-death signalling control molecule, i.e. also for direct comparison to TNFR2.

To generate CD27-CFP, -YFP and –MycHis constructs, the cDNA sequence of human CD27 was amplified from a RNA lysate prepared from human peripheral blood mononuclear cells. The CD27 cDNA was generated by reverse transcription and subsequent PCR amplification of CD27 mRNA. An expected PCR product of approximately 700 bp was present from the PCR of the cDNA synthesis. No PCR products were present in the “no RT” reaction, or from the HeLa cell-specific control RNA (control template). This meant that the PCR amplification primers were specific to human CD27 as expected (Figure 3.5B). The PCR primers also introduced flanking 5’- *Kpn*I and 3’- *Xho*I restriction sites into the PCR product. These were subsequently used to ligate the PCR product into the same sites present within pcDNA3.MPVJ2R-MycHis, to create pcDNA3.CD27-MycHis, pcDNA3.CD27-CFP and pcDNA3.TNFR1-YFP (Figure 3.5A).

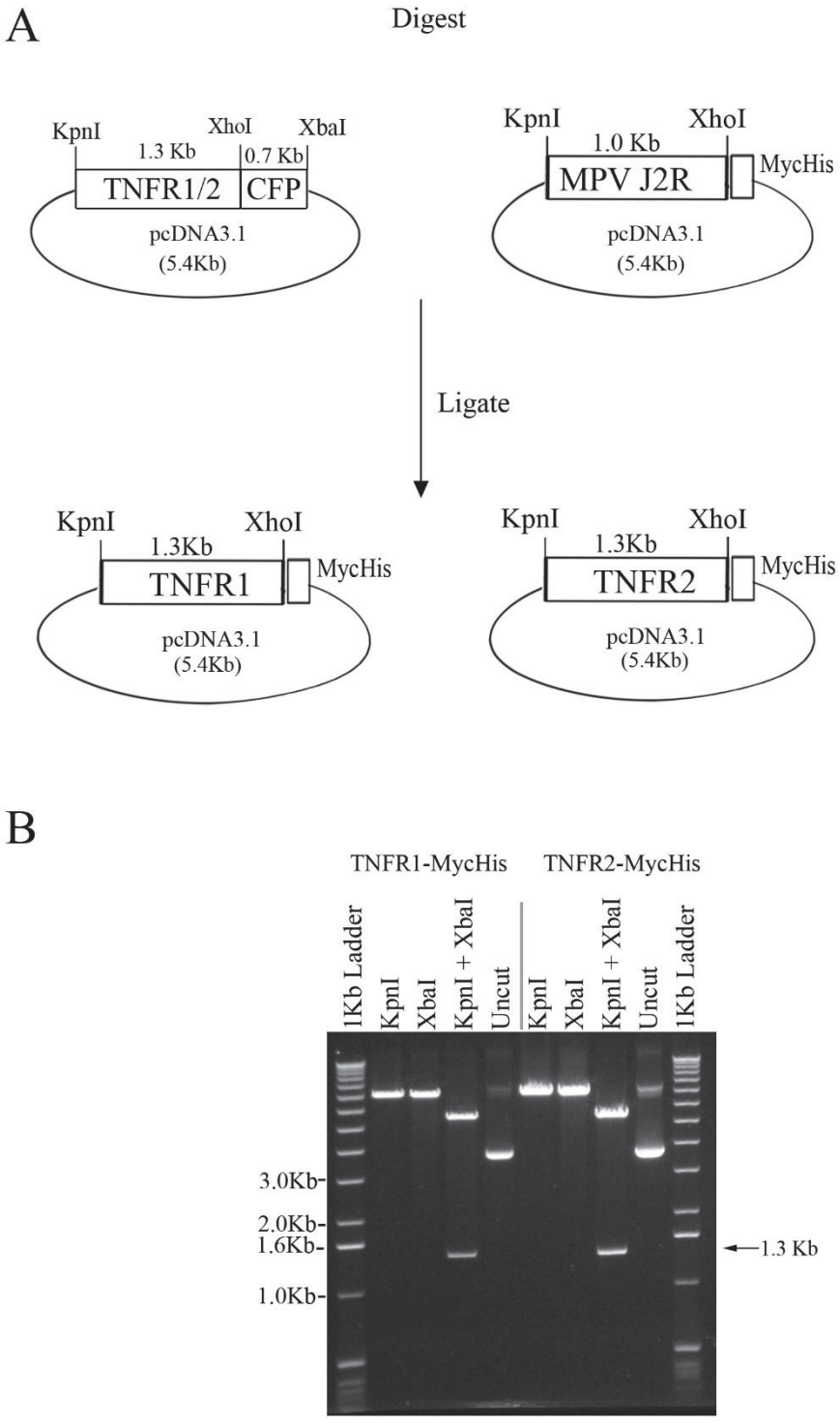

Figure 3.4 Cloning strategy and generation of TNFR1-MycHis and TNFR2-MycHis fusion expression plasmids.

A) Strategy used to subclone TNFR1 and TNFR2 cDNA sequences into the vector of pcDNA3.MPVJ2R-MycHis. B) Initial confirmation of subcloning of TNFR1 and TNFR2 cDNA inserts performed by restriction digest using *Kpn*I and *Xho*I.

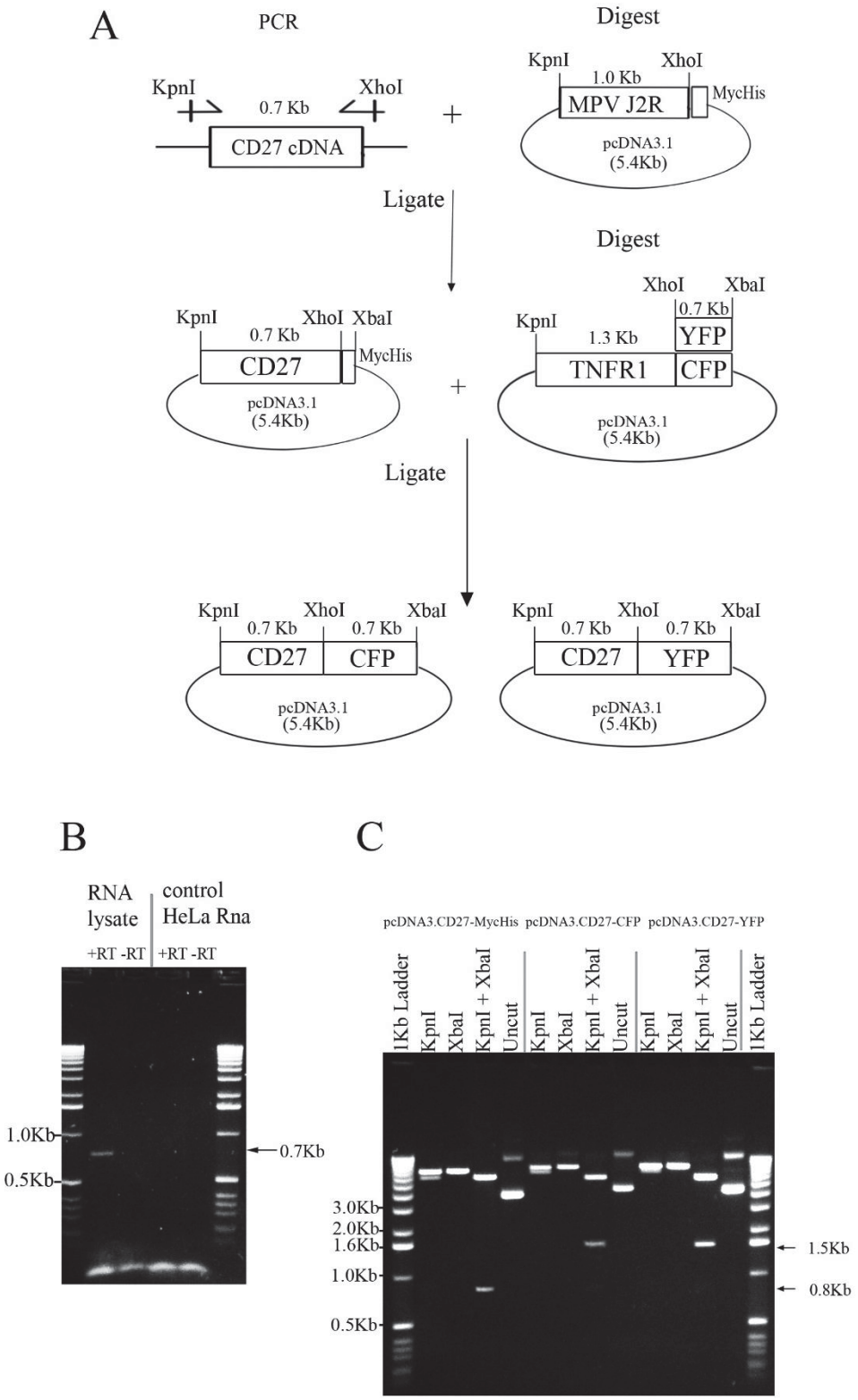

Figure 3.5 Generation of CD27-MycHis, -CFP and –YFP pcDNA3 plasmids
A) Diagram of PCR strategy used to amplify CD27 cDNA and subsequently subclone into pcDNA3.MycHis, pcDNA3.CFP and pcDNA3.YFP expression vectors. B) RT PCR of CD27 cDNA amplification. C) Initial confirmation of CD27 insert in generated pcDNA3.CD27-MycHis, pcDNA3.CD27-CFP and pcDNA3.CD27-YFP plasmids by restriction digest with *Kpn*I and *Xba*I.

To verify the inserts were of the correct sizes another restriction digest was performed using *Kpn*I and *Xba*I restriction enzymes to indicate the CD27 cDNA insert plus fusion Myc/His sequence. The restriction fragments were analysed by agarose gel electrophoresis (Figure 3.5 B). The double digests resulted in a restriction fragment of approximately 800 bp for pcDNA3.CD27-Myc/His and 1.5 Kb for both pcDNA3.CD27-CFP and pcDNA3.CD27-YFP (Figure 3.5C). The Myc/His epitope tag is 48 bp in length and both CFP and YFP sequences are 720 bp. When combined with the CD27 cDNA of 782 bp (accession NM_001242.4), this gave a predicted combined size of 830 bp from pcDNA3.CD27-Myc/His and a combined size of 1502 bp for pcDNA3.CD27-CFP and pcDNA3.CD27-YFP, respectively, exactly as seen in Figure 3.5B. These results indicated that CD27 cDNA had been successfully subcloned to create pcDNA3.CD27-Myc/His pcDNA3.CD27-CFP and pcDNA3.CD27-YFP plasmids. The plasmids were sent for double strand sequencing, which confirmed the CD27 inserts were correct, full-length, and in-frame with the Myc/His fusion tags (data not shown).

3.6 Localisation of WT TNFR1-YFP and Mt TRAPS TNFR1-YFP proteins

3.6.1 Multicolour microscopy set up

The subcellular localisation of WT TNFR1-YFP, compared to TRAPS mutant TNFR1-YFP proteins, was visualised by both widefield and confocal microscopy. Both WT and mutant TRAPS TNFR1 proteins were detected via the YFP fusion tag fluorescence. To observe where the TNFR1 proteins were localising, the subcellular organelles were

stained with fluorescent dyes or probes. For example, to determine the relative position of the nuclei, U20S cells were stained with DRAQ5 (Biostatus), and to identify endosomes a mouse IgG anti-human Rab5 antibody was used, together with a goat anti-mouse IgG secondary conjugated AF568 antibody. Similarly, to determine if TNFR1 proteins were localising at the cell surface, wheat germ agglutinin conjugated to AF594 (WGA-AF594) (Molecular probes) was used to highlight lipid membrane structures on cells. Due to recycling of membrane structures the labelling included structures such as the cell surface lipid bilayer, endoplasmic reticulum (ER), Golgi, and lipid vesicles, such as endosomes and lysosomes (Brown & Harris 2003; Kanazawa et al. 2008; Silva et al. 2006).

Each fluorophore was chosen so that the emission was detected separately in different fluorescence channels. Therefore to determine whether each fluorophore could be detected without "cross-bleeding" fluorescence emissions, each fluorophore was excited and detected within each of the fluorescence emission channels: (CFP/YFP/TRITC/Cy5.5). For this, U2OS cells were first grown in 35 mm glass bottom dishes and stained individually with WGA-AF594, DRAQ5, and rabbit anti-human Rab5

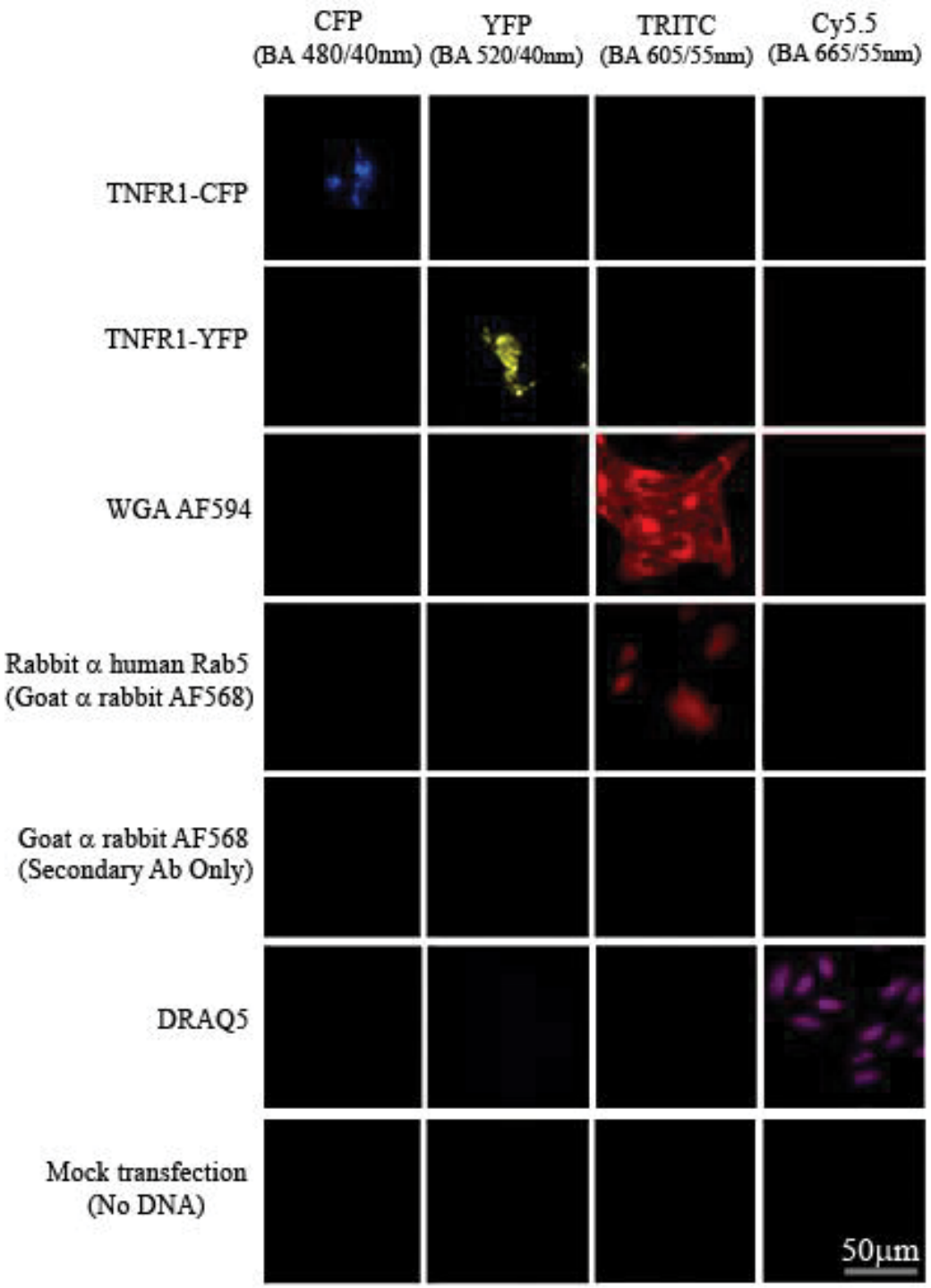

Figure 3.6 Multicolour microscopy set-up of fluorophore detection
Maximum intensity projection of detected fluorophores using U2OS cells. TNFR1-CFP protein (blue) detected in U2OS cell in the CFP channel only (Ex 430/20nm, BA 480/40nm). TNFR1-YFP protein (yellow) detected in U2OS cell in the YFP channel only (Ex 495/10nm, BA 520/40nm). U2OS cell membranes stained with WGA-594 (red) and Rab5 positive endosomes stained with rabbit α human Rab5 and secondary goat α rabbit-AF568 antibodies (red), detected only in the TRITC channel (Ex 540/25nm, BA 605/55nm). DRAQ5 stained nuclei in U2OS cells (purple) detected in the Cy5.5 channel only (Ex 660/55nm, BA 665/55nm).

then goat anti-rabbit-AF568, or transfected with either pcDNA3.TNFR-CFP or pcDNA3.TNFR1-YFP. Each fluorescence emission channel was then scanned for each sample (Figure 3.6).

TNFR1-CFP emission was only detected in the CFP channel (BA 480/40nm), TNFR1-YFP emission was only detected in the YFP channel (BA 520/40nm), and DRAQ5 emission was only detected in the Cy5.5 channel (BA 665/55nm) (Figure 3.6). Please note: although the WGA-AF694 emission and the Rab5/goat anti-rabbit-AF-568 antibodies were detected in the same channel, the localisation of each was to be determined in separate parallel experiments (Figure 3.6). No emission was detected for cells stained with only the secondary goat anti-rabbit AF-568 antibody, meaning that no non-specific staining was occurring with these reagents, and hence that the staining for Rab5 expressing endosomes was specific to the primary anti-human Rab5 specific antibody (Figure 3.6). No emission was detected for cells that were mock transfected ("no DNA" control transfection) which confirmed that there was no significant auto-fluorescence occurring in any of the microscope channels (Figure 3.6). Taken together, these results clearly indicate that the fluorescent signals detected from each of the fluorophores were representative of specific staining, and that the desired protein/fluorescence emissions could be used simultaneously (with the exception of WGA-AF694 and Rab5/goat anti-rabbit AF-568; which were to be used in parallel experiments).

3.6.2 WT TNFR1-YFP and TRAPS TNFR1-YFP cell surface detection.

WT TNFR1 is reported to exist as cell surface transmembrane receptors (Loetscher, Pan, et al. 1990) and also in compartmentalized intracellular vesicles, referred to as

"receptosomes" as reported more recently (Schneider-Brachert et al. 2004; Schutze, Tchikov & Schneider-Brachert 2008). The internalisation of TNFR1 and its ligand (TNF) rapidly triggers cell death (Schneider-Brachert et al. 2004). Rab5 positive receptosomes fuse with trans-Golgi vesicles, containing acid sphingomyelinase and cathepsin D, to form multivesicular endosomes that initiate pathways leading to cell death via Bid. U2OS cells transfected with pcDNA3.TNFR1-YFP, expressing WT TNFR1-YFP were analysed visually by widefield fluorescence microscopy. WT TNFR1-YFP was not found visually to be detectable as localising at the cell surface of cells stained with WGA-594. Instead, however, TNFR1-YFP fluorescence was easily detected as a punctate localisation throughout the cell (Figure 3.7). In addition some WT TNFR1-YFP were found expressed as punctate dots, with larger aggregates perinuclear (nuclei detected with DRAQ5). The aggregated localisation appeared to bear resemblance to the Golgi and/or ER structure (Terasaki et al. 1991; Terasaki et al. 1984). As expected no YFP fluorescence was detected in cells transfected with pcDNA3 empty vector, and there was no significant or obvious change in the morphology of these cells with or without transfection (Figure 3.7). Thus the transfection had little impact on the cells and YFP emission appeared to be specific to TNFR1-YFP. U2OS cells were also transfected with the TRAPS mutant expressing plasmids, pcDNA3.TRAPS.TNFR1-YFP, and stained with WGA-AF594 and DRAQ5. All TRAPS mutants localised as punctate structures throughout the cell, and many appeared to form larger aggregates, often adjacent to the DRAQ5-stained nuclei (resembling ER or Golgi).

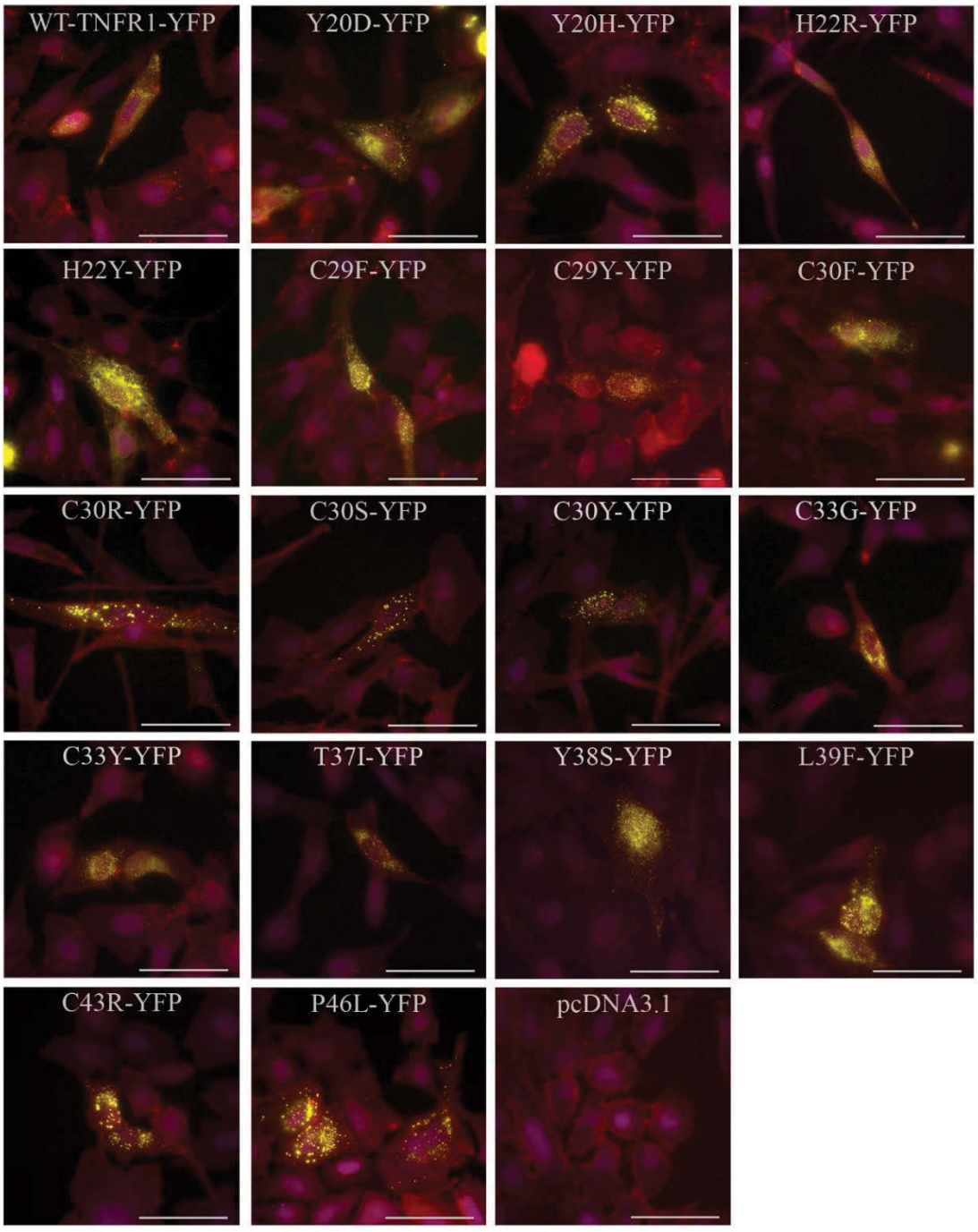

Figure 3.7 localisation of TNFR1-YFP proteins with WGA-594.
U2OS cells transfected to express either WT TNFR-YFP or mutant TNFR1 TRAPS-YFP proteins (yellow) and stained with cell surface marker WGA-594 (red). Nuclei are stained with DRAQ5 (purple). Images are maximum intensity projections of Z-dimension images, taken 16 hours post transfection using the Nikon widefield TI microscope and represent 20 fields of view from 4 individual transfections. Scale bar represents 50μm.

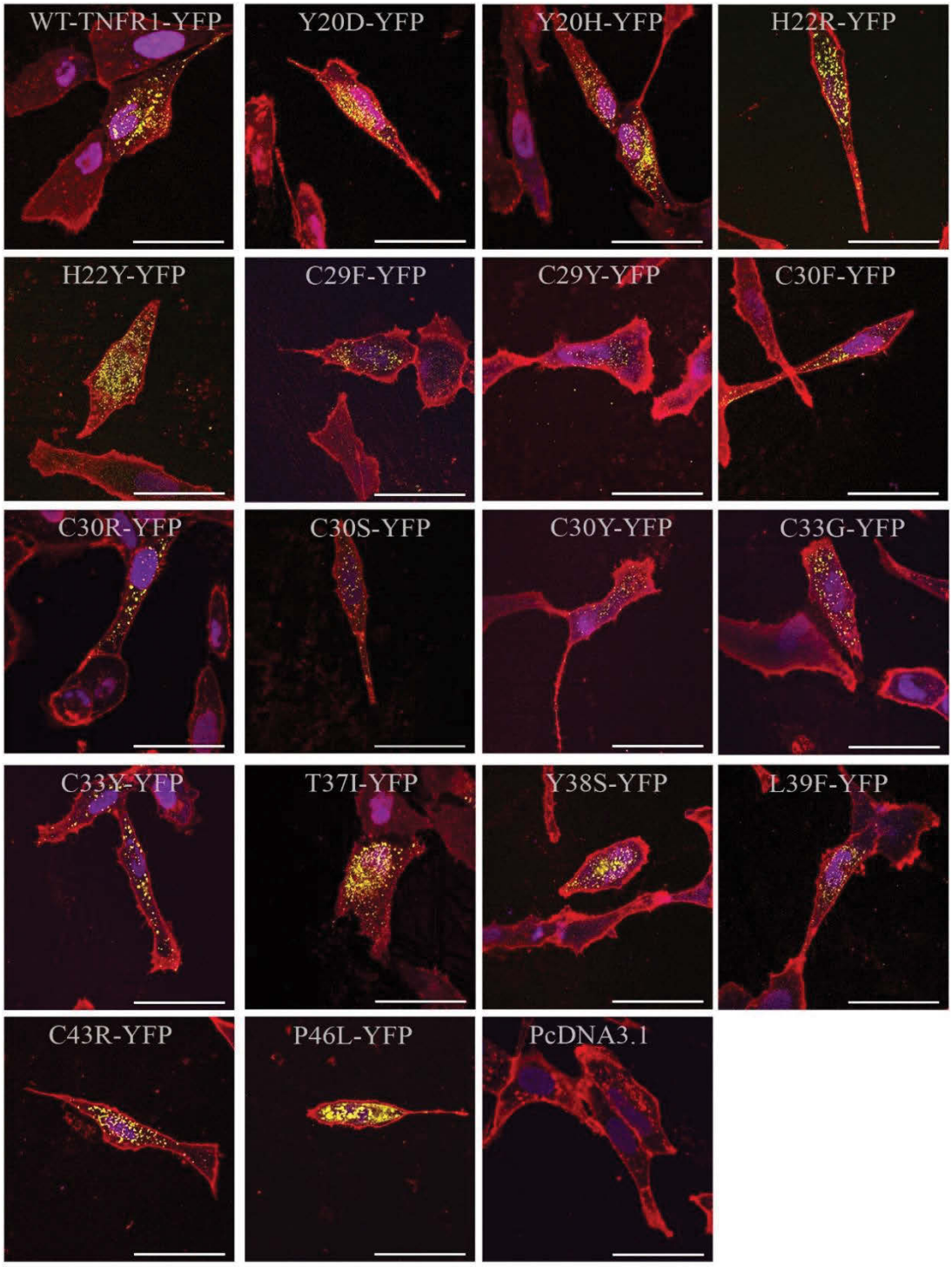

Figure 3.8 Confocal imaging of TNFR1-YFP localisation with WGA-594
Maximum intensity projections of U2OS cells expressing TNFR1-YFP proteins (yellow) stained with WGA-594 (red) to identify cell surface membranes and DRAQ5 (purple) to identify nuclei. Images taken 16 hours post transfection using the Nikon A1 confocal microscope with the same filter sets used as for the Nikon TI widefield. Images represent 20 fields of view from 4 independent transfections. Scale bar represents 50μm.

TRAPS TNFR1-YFP mutants C30S, C30R and C30Y tended to appear more punctate in their localisation (less diffuse localisation). However, because of out of focus light associated with widefield microscopy, and an inability of the widefield microscope system to clearly define the cell surface, a confocal microscopy system was used instead, to further clarify and verify these putative observations.

Using the same filter sets from the widefield microscopy system, again U2OS cells were transfected with pcDNA3.TNFR1-YFP or pcDNA3.TRAPS.TNFR1-YFP and stained with WGA-AF594 and DRAQ5. By utilising the confocal microscope the visualisation of WGA-AF594 was much more distinct and gave a clearer outline of the cell surface (Figure 3.8). Nevertheless, WT TNFR1-YFP could not be visually observed at the cell surface, and instead, it still was seen localising as a punctate morphology throughout the cell. Again these punctate structures formed larger aggregates often adjacent to the DRAQ5-stained nucleus in a Golgi/ER-like structure. Despite using confocal microscopy, the TRAPS TNFR1-YFP also failed to be clearly observed at the cell surface of the U2OS cells, and instead, were mostly localised as punctate proteins, throughout the cell, and, as with WT TNFR-YFP, they also tended to be found aggregating around nuclei (Figure 3.8). Thus TRAPS mutants C30S, C30R and C30Y did not appear to differ visually in their localisation compared to WT TNFR1-YFP, and other TRAPS mutants, even when examined by the confocal microscope detection system. This difference may be possibly due to a higher sensitivity and elimination of “out of focus” light in detection between the two detection systems.

All cells visualised by confocal microscopy were further analysed using Imaris Coloc (Bitplane ver 8.1) to determine if TNFR1-YFP proteins were co-localising at the cell

surface (Table 3-2). For this a threshold was set on each channel to identify the cell surface and TNFR1-YFP proteins. Automatic thresholding was unable to set a suitable threshold for the TRITC (red) channel, due to WGA-AF594 labelling of other membranous structures within the cell. Instead, a "Manual Threshold" was set based on the dimmest fluorescence signal detectable in each channels, i.e. to identify each YFP and WGA-AF594 signal. This was set on a representative image and kept consistent across all of the images analysed (Table 3-2). From the analysis values shown in Table 3-2 it was determined that 63.27% of TNFR1-YFP co-localised with WGA-AF594. Even more surprising, 84.01% of TRAPS Y20D TNFR1-YFP were found to co-localise with WGA conjugated AF594. This is in contrast to the localisation of TRAPS mutants Y20D (84.01%) and C33G (23.51%) with WGA, however, this was not represented in the captured images. Visual comparison of the representative images of Y20D and C33G (Figure 3.8) shows no localisation of TRAPS TNFR1-YFP at the cell surface. Therefore it was concluded that the analysis method was likely not very suitable for reporting co-localisation at the cell surface. This is likely due to labelling of the other membranous structures within the cell, including endosomes, and background labelling, causing analysis difficulties that were not easily resolved.

Finally, 3D modelling was performed in Imaris (version 8.1) to further visualise the TNFR1-YFP sub-cellular localisation, and to further consider the contrasting data (images versus data analysis). For this, surfaces were created in Imaris software for each fluorescence channel collected, and TNFR1-YFP fluorescence was rendered using the "spots" function (Figure 3.9). No WT TNFR1-YFP rendered spots could be seen localising to the cell surface, but instead, TNFR1-YFP was found localising throughout the cytoplasm, and on a membranous structure surrounding the nucleus resembling the ER

or Golgi (Figure 3.9). This is also true for TRAPS mutant Y20D and C33G TNFR-YFP, and all TNFR1-YFP proteins analysed. Only these two TNFR1-YFP mutants were analysed as they represented the most obviously different localization as evident in the Imaris Coloc analysis (Table 3-2) (TNFR1 Y20D 84.01% and TNFR1 C33G with 23.51%). Therefore, taken together, WT TNFR1-YFP could not be detected at the cell surface of U2OS cells, but instead appeared to localise as punctate proteins throughout the cell and aggregated around the nuclei, in a structure resembling ER and/or Golgi. This was also true for all analysed TRAPS TNFR1-YFP PLAD mutants, and as analysed by both widefield and confocal microscopy. Three-dimensional rendering analysis in Imaris further substantiated these results. Thus, no significant differences were found between mutants or WT TNFR1-YFP fusion proteins in terms of their sub-cellular localisation when expressed in pcDNA plasmid transfected cells.

3.6.3 WT TNFR1-YFP and TRAPS TNFR1-YFP proteins detection of Rab5 positive endosomes.

To determine if TRAPS mutant TNFR1-YFP proteins were localised within so called receptosomes, U2OS cells were stained with a Rab5 specific antibody, which was detected with a goat-anti mouse Ig conjugated to AF568. Rab5 is a marker of early endosomes (Zeigerer et al. 2012) and is involved in the processing of receptosomes in the endosomal pathway (Schneider-Brachert et al. 2004). To determine if TRAPS mutations alter the localisation of TNFR1, U2OS cells were transfected with pcDNA3.TNFR1-YFP or pcDNA3.TRAPS.TNFR1-YFP plasmids.

Table 3-2 Co-localisation analysis of TNFR1-YFP proteins and WGA-594

Sample	Threshold A[1]	Threshold B[2]	% of dataset colocalised	% of volume A above threshold colocalised	% of volume B above threshold colocalised	% of material A above threshold colocalised	% of material B above threshold colocalised
WT-TNFR1	406	273	0.48	2.41	65.64	2.61	63.27
Y20D	406	273	0.24	2.70	83.69	3.23	84.01
Y20H	406	273	0.75	5.54	57.41	5.65	55.90
H22R	406	273	0.26	5.50	43.85	4.52	40.67
H22Y	406	273	0.14	2.86	28.27	2.88	26.48
C29F	406	273	0.45	4.82	58.22	5.42	56.21
C29Y	406	273	0.21	1.69	27.51	1.74	22.92
C30F	406	273	0.09	1.73	69.70	2.12	67.69
C30R	406	273	0.16	1.46	39.87	1.49	33.33
C30S	406	273	0.36	7.06	97.64	9.81	98.28
C30Y	406	273	0.04	1.74	52.86	1.93	51.83
C33G	406	273	0.73	7.60	27.64	6.61	23.51
C33Y	406	273	0.12	2.81	37.42	2.75	32.16
T37I	406	273	1.54	14.33	84.39	16.60	92.04
Y38S	406	273	0.17	1.96	44.17	1.54	38.22
L39F	406	273	0.24	2.63	52.98	2.51	52.63
C43R	406	273	0.25	5.93	49.56	5.50	47.74
P46L	406	273	0.37	19.77	30.78	15.33	21.70

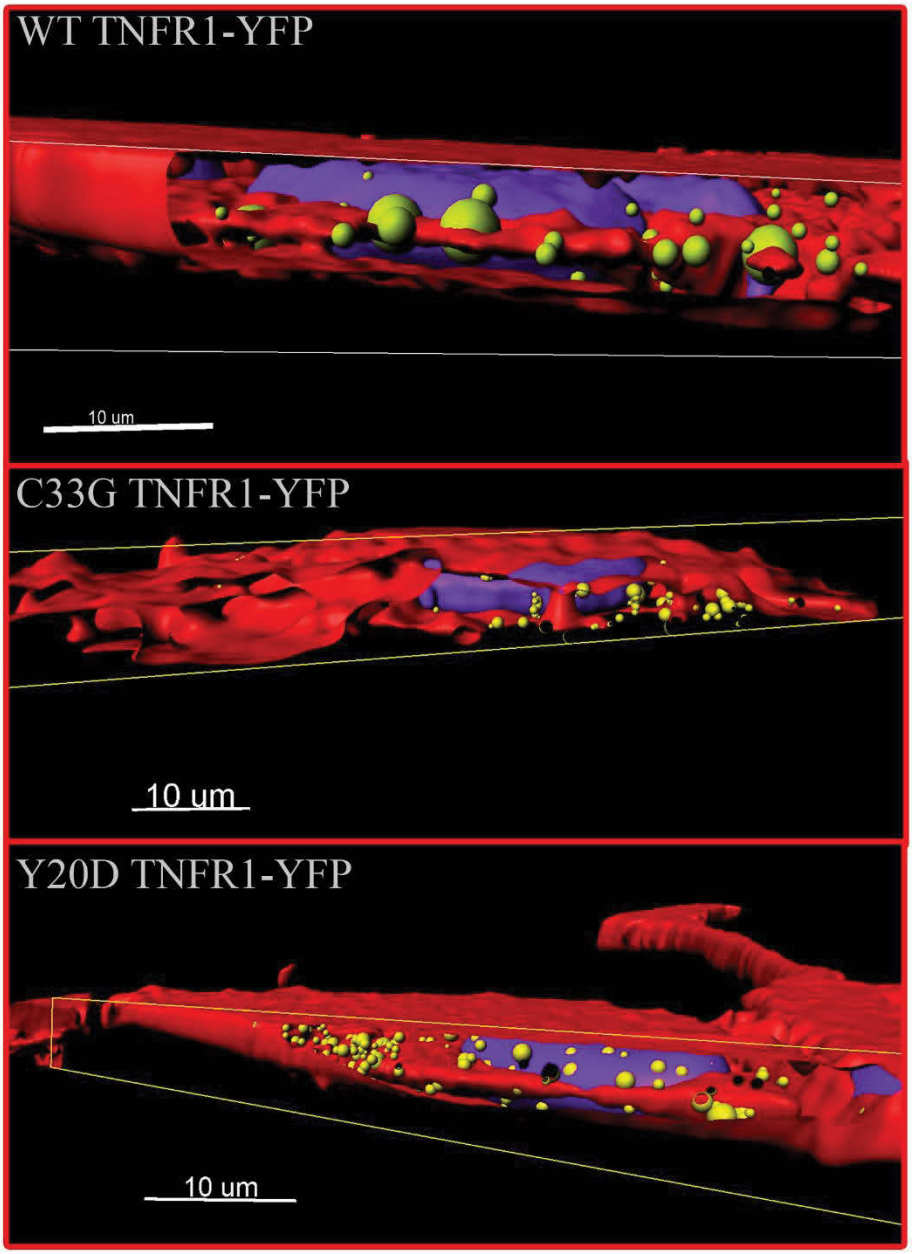

Figure 3.9 3D visualisation of TNFR1-YFP protein localisation with WGA-594
Imaris 3D rendering of the confocal images showing TNFR1-YFP proteins (yellow spheres) localising within WGA-594 stained (red surfaces) U2OS cells. Nuclei are stained with DRAQ5 (purple surface) as reference.

then stained for Rab5 and nuclei using DRAQ5 (purple) (detection of the nuclei was included as a point of reference within each cell). Images were captured using a Nikon (Eclipse Ti) widefield microscope. Images were deconvolved with the AutoQuant

software, using 3D blind deconvolution, which eliminates any “out of focus” light and spherical aberrations. From this WT TNFR1-YFP (yellow) was found to largely co-localise with Rab5 proteins on early endosomes (red). Of note, due to the yellow YFP signal being much brighter than the red Rab5 signal, co-localisation did not appear orange when overlaid (Instead still appeared yellow) (Figure 3.10). Nevertheless, all TNFR1 TRAPS mutants appear to co-localise with Rab5 positive endosomes (Figure 3.10). As expected, and reported in previous experiments, no YFP fluorescence was observed in the pcDNA3 “empty vector” transfections, and no differences were seen in the staining for Rab5 and nuclei amongst the control and TNFR1 WT and mutant samples. Thus YFP expression represents TNFR1-YFP and the YFP expression does not have an effect on the ability to detect Rab5 expression.

To determine any differences between samples with respect to co-localisation, an analysis was again performed using Imaris Coloc software tools. Since both YFP and Rab5 (AF568) emission was sharp and punctate, both channels could easily be successfully thresholded, for the co-localisation analysis. This analysis indicated that approximately 80% of WT TNFR1 was found to co-localise with Rab5-positive endosomes (Table 3-3). This was consistent with previous findings, which indicates that TNFR1 traffics intracellularly coincident with Rab5 positive receptosomes/endosomes (Schneider-Brachert et al. 2004). All TRAPS TNFR1-YFP were also

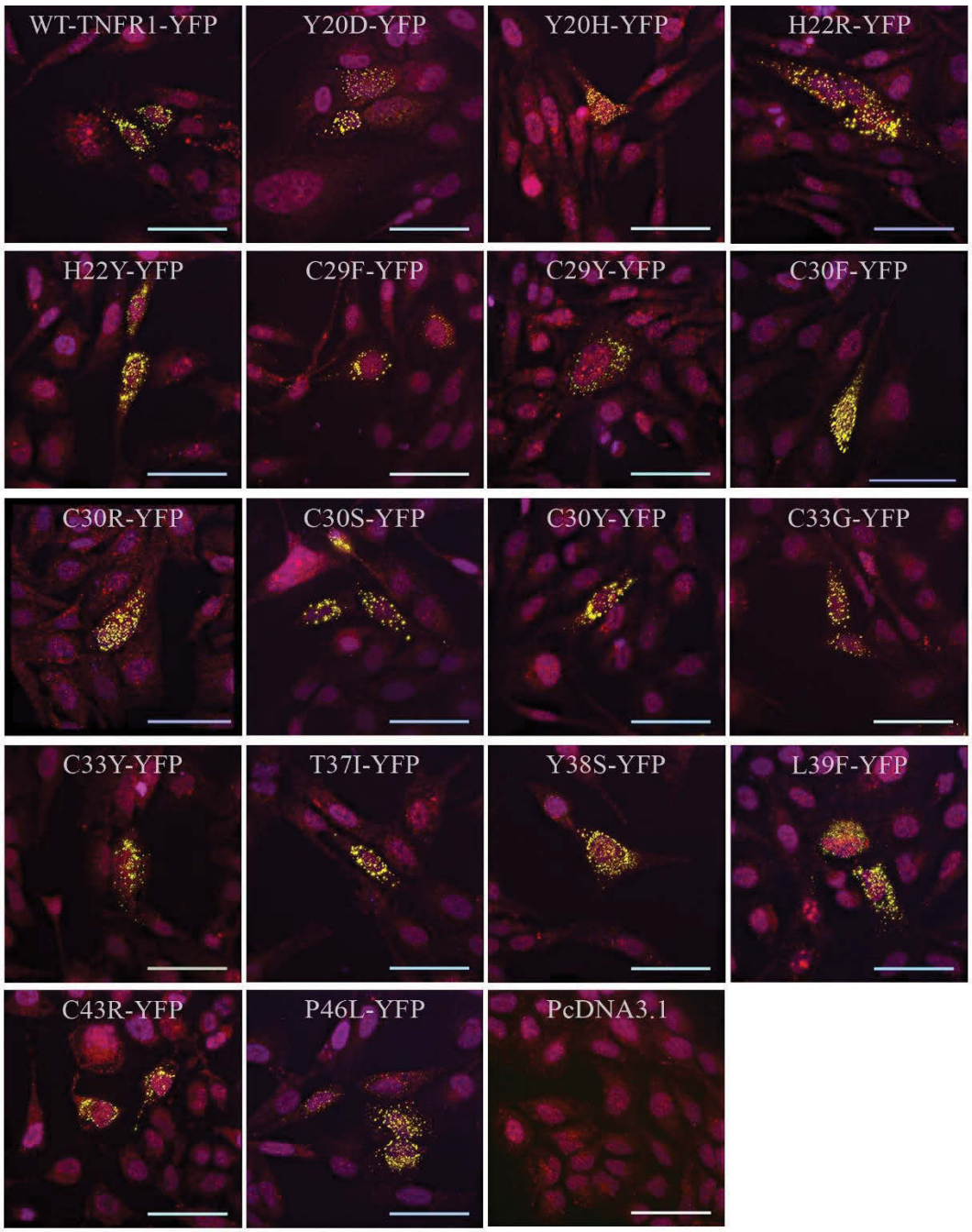

Figure 3.10 TNFR1 localisation with Rab5 positive endosomes.
U2OS cells expressing TNFR1-YFP proteins (yellow) 16 hours post transfection, stained with a rabbit anti human Rab5 antibody and secondary goat anti rabbit-AF568 (red). Nuclei are demarcated with DRAQ5 (purple). Images shown are captured using the Nikon TI widefield microscope and then processed through blind deconvolution using AutoQuant software. Images are representative of 20 fields of view from 4 independent transfections. Scale bar represents 50μm

Table 3-3 Co-localisation analysis of TNFR1-YFP proteins and Rab5 endosomes

Sample	Threshold A (Rab5)	Threshold B (TNFR1)	% of dataset colocalised	% of volume A above threshold colocalised	% of volume B above threshold colocalised	% of material A above threshold colocalised	% of material B above threshold colocalised
WT-TNFR1	750	18000	1.53	16.51	63.57	22.33	80.01
Y20D	750	18000	1.54	19.43	53.85	28.14	79.16
Y20H	750	18000	2.47	21.16	54.83	22.64	65.94
H22R	750	18000	1.51	14.46	61.23	23.17	82.87
H22Y	750	18000	1.73	22.93	52.73	25.06	65.90
C29F	750	18000	1.90	22.87	46.94	24.25	60.87
C29Y	750	18000	1.68	11.32	52.21	13.44	66.89
C30F	750	18000	1.57	16.04	58.05	20.96	78.80
C30R	750	18000	2.12	28.68	59.33	39.56	80.12
C30S	750	18000	0.60	20.1	42.82	25.86	68.57
C30Y	750	18000	0.41	9.98	49.47	12.57	71.23
C33G	750	18000	0.54	8.61	39.97	8.67	53.00
C33Y	750	18000	1.36	19.25	57.37	27.82	81.11
T37I	750	18000	1.13	37.45	44.70	42.43	63.20
Y38S	750	18000	0.48	4.46	41.42	4.93	63.00
L39F	750	18000	2.37	25.08	46.83	28.92	62.99
C43R	750	18000	0.79	11.37	55.34	13.00	69.93
P46L	750	18000	1.04	23.97	42.57	27.89	63.45

found to co-localise with Rab5 positive endosomes. In comparison, all of the TRAPS TNFR1-YFP mutants were found to have reduced co-localisation with Rab5 endosomes, with the exception of TRAPS mutants Y20D, H22R, C30F, C30R and C33Y which were similar to WT TNFR1-YFP (~80% co-localisation with Rab5; Table 3-3). TNFR1 TRAPS mutant C33G displayed the least co-localisation with Rab5 (53%) (Table 3.3). This might

indicate reduced TNFR1-induced cell death/signalling reported for this mutant as intracellular signalling for cell death is the result of TNFR1 internalisation and trafficking (Lobito et al. 2006; Schneider-Brachert et al. 2004; Schutze, Tchikov & Schneider-Brachert 2008). In all of the samples examined, only approximately 20% of Rab5 staining co-localised with TNFR1-YFP proteins (Table 3-3, % of material A above threshold colocalised), thus not all endosomes contained the expressed TNFR1-YFP proteins. However approximately 80% of WT TNR1 associated with rab5 (Table 3-3, % of material B above threshold colocalised). Interestingly and for the sake of clarity one could consider anything greater than or less than 5% difference in co-localisation from the WT to be a meaningful difference; this would suggest the following mutants vary from WT in their ability to colocalise with Rab5; Y20H, H22Y, C29F, C29Y, C30S, C30Y, C33G, T37I, Y38S, L39F, C43R, P46L. Notably these are not purely cysteine mutations, which are expected to change TNFR structure.

3.7 Comparison of TNFR1-induced cell death between WT TNFR1 and mutant TRAPS TNFR1

Over expression of TNFR1 is known to be sufficient to induce apoptosis (Boldin et al. 1995). MYXT2 is shown to inhibit TNFR1 induced cell death by associating with the TNFR1 cellular receptor (Sedger et al. 2006), however this still not well defined. By utilising the single point mutations in TRAPS TNFR1 proteins we can better understand this mechanism and also observe the effect of TRAPS mutation on the ability to subvert TNFR induced cell death. This is the focus of this thesis, however to first assess the effect

of TRAPS mutations on viral subversion, we needed to first assess the impact of the TRAPS mutations themselves on TNFR1 induced cell death.

To date only 3 TRAPS mutations have currently been examined for cell death: C33G, C33Y and H22Y. (Lobito et al. 2006; Rebelo et al. 2006; Todd et al. 2004). Thus this study was the first to assess the effect of the panel of TRAPS mutations across the PLAD. For this, we compared the effect of each of the TRAPS mutant as if they were expressed in cells that were heterozygous (i.e. expression both WT and mutant TNFR1 proteins) Thus, HEK 293 cells were transfected with plasmids to co-express WT TNFR1-CFP and –YFP, and compared to cells co-expressing WT TNFR1-CFP and MT TRAPS TNFR1-YFP. Cell death was measured by flow cytometry using propidium iodide (PI). The cell population was first gated on to exclude aggregates and debris (R1, red gate) (Figure 3.11A). Next we gated on single cells to eliminate doublet (R2, blue gate). Finally, a threshold was set on cells expressing both CFP and YFP TNFR-family molecule fusion proteins (R3, Green gate). Hence we were able to measure the extent of cell death (%PI positive) selectively, i.e. only in the TNFR1-YFP and -CFP expressing cells (Figure 3.11A). First we examined cells transfected with CD27-CFP, CD27-YFP, or pcDNA3 “empty vector”, to ensure that the laser voltages were set correctly and that the gating strategy was appropriate to accurately detect YFP/CFP expressing cells (Figure 3.11A). From this it was evident that there were two PI positive populations – both a PI dull and PI bright population. It was hence assumed that PI staining could detect both dead cells and cells that were associated with extracellular plasmid DNA. This did not impact significantly on the assay, as the dead/dying cells were a clearly distinct population; DNA-associated cells were a log less PI bright compared to the dead PI-high cells. Representative plots of each triplicate sample can be seen in Figure 3.B.

Expression of WT TNFR1-CFP and TNFR-YFP appeared to induce cell death in approximately 40% of cells (Figure 3.11B). In comparison, expression of some TRAPS mutations appeared to induce significantly less cell death, compared to WT TNFR1. For example, TNFR1 TRAPS mutations Y20H (31%), H22Y (34%), C29Y (33%), C30Y (30%), C33G (35%) C33Y (33%), T37I (35%), Y38S (35%) all caused reduced TNFR1-induced cell death (of transfected -CFP and -YFP double positive cells) (Figure 3.11C). These results appear to be consistent with previous results for TNFR1 H22Y (Lobito et al. 2006), C33G (Lobito et al. 2006) and C33Y (Rebelo et al. 2006), as these were found to cause reduced apoptosis. Interestingly TRAPS mutations that resulted in the substitution of large or small branched amino acids i.e. tyrosine, were found to have the most significant reduction in apoptosis (Figure 3.11C). This was also true for amino acid residues that were critical to the folding or structure of TNFR1 such as the cysteine - an amino acid critically involved in disulphide bridge formation. Therefore the greatest predicted changes in structure appeared to correlate with the greatest reduction in apoptosis inducing capacity, compared to WT TNFR1 transfected cells.

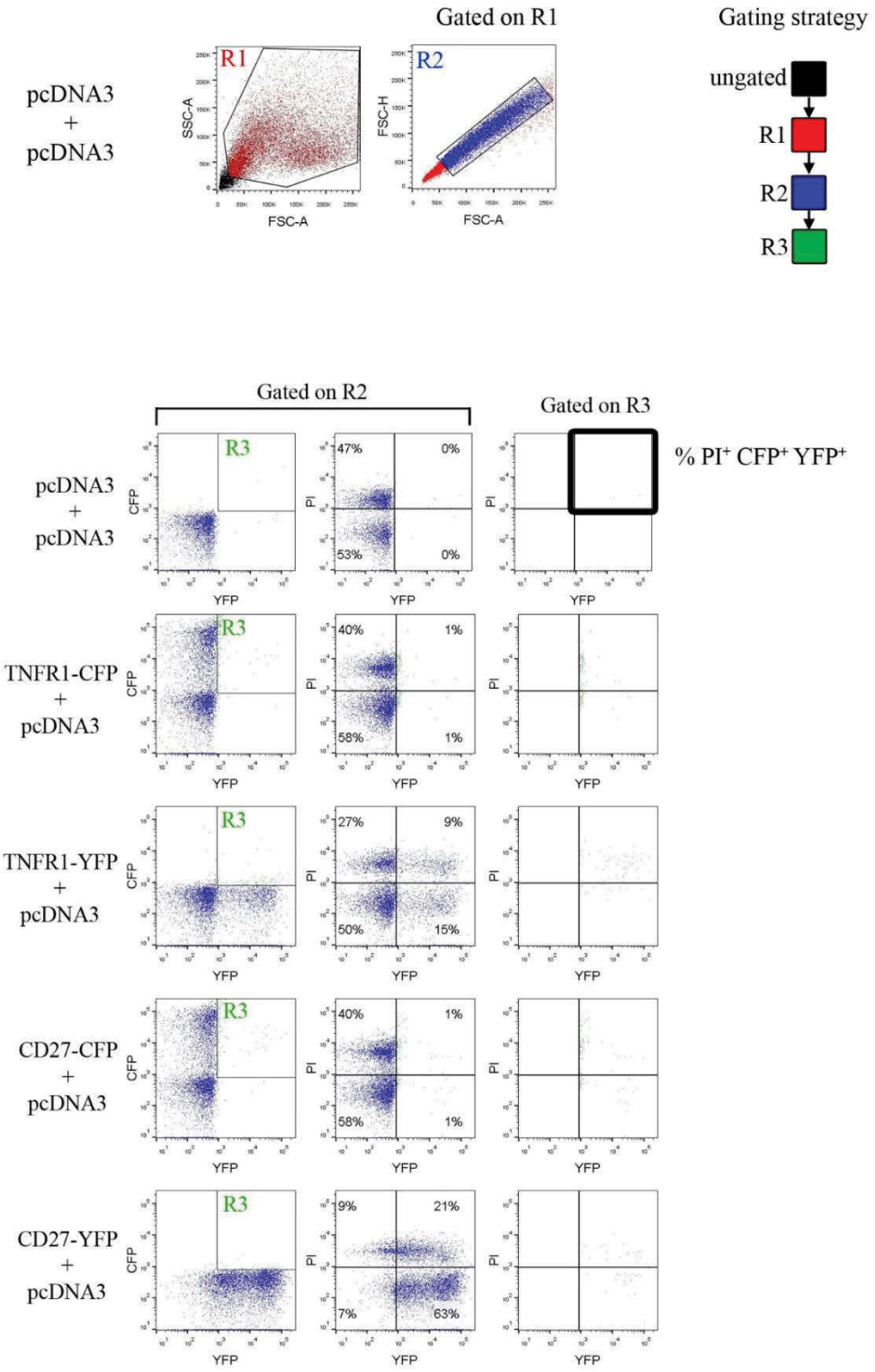

Figure 3.11A. Flow cytometry gating strategy and set up for TNFR1 and TRAPS induced cell death assay.

Transfected 293 HEK cells were first gated on (R1, red) to remove aggregates and debris in the FSC-A vs SSC-A dot plot. This population was then gated on to remove doublet cells (R2, blue), shown in the FSC-A vs FSC-H dot plot. The single cell populations was plotted in a CFP vs YFP dot and a gate was drawn on double positive cells (R3, green). Cell death was then assessed from the CFP/YFP double positive population in the top right quadrants showing YFP vs PI (dead cells) as a percentage of double positive CFP/YFP cells

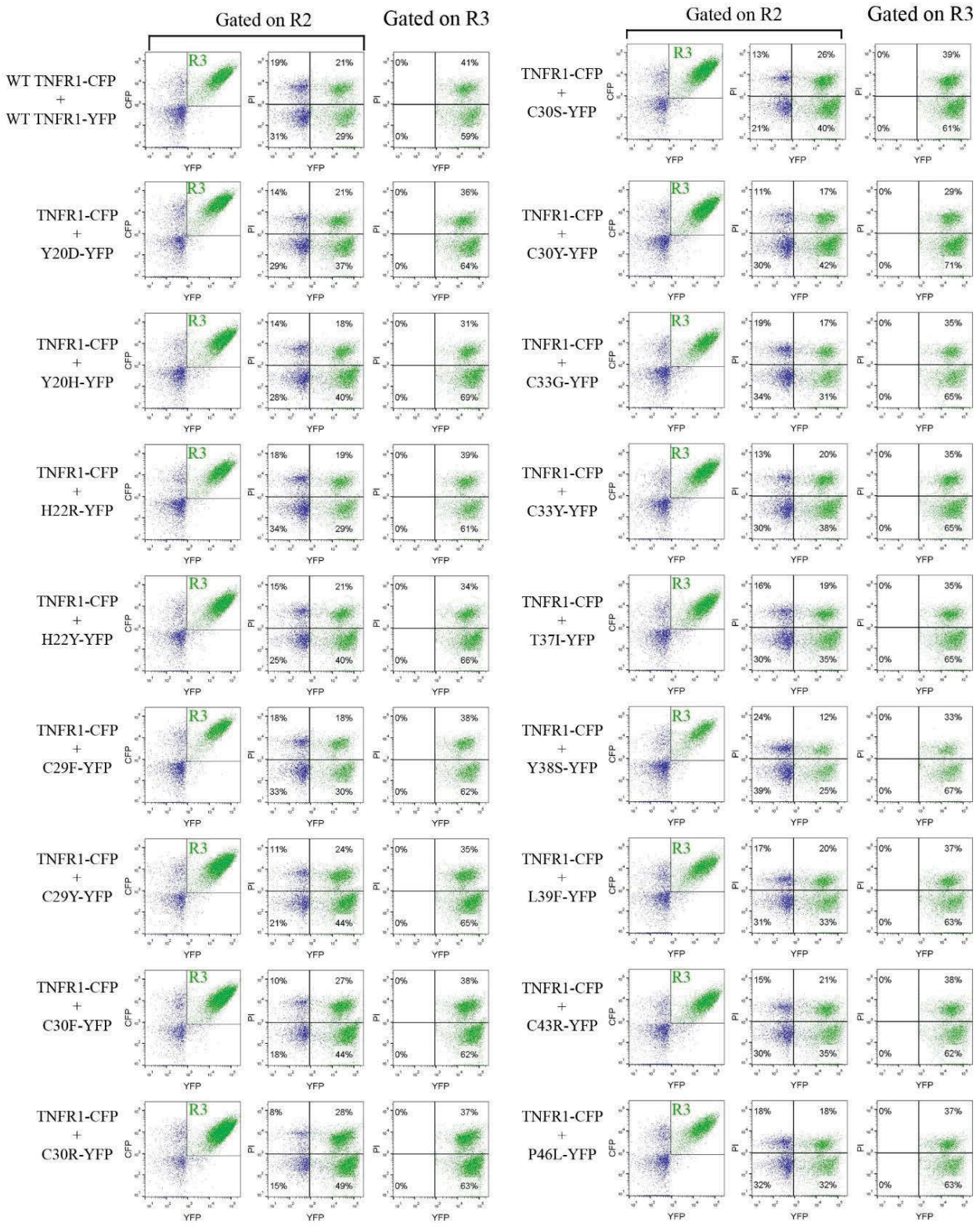

Figure 3.11 B Flow cytometry analysis of TNFR1-Induced cell death

293 HEK cells transfected to co express both WT TNFR1-CFP and either WT TNFR1-YFP or mutant TRAPS TNFR1-YFP were stained with PI and analysed for the percentage of cell death. Double positive cells for CFP and YFP were gated on (R3, green), and the amount of cell death was measured in $CFP^{+}YFP^{+}PI^{+}$ cells identified from the YFP vs PI dot plots in top right quadrant. Data shown represents 30000 events and the median data from three independent transfection experiments.

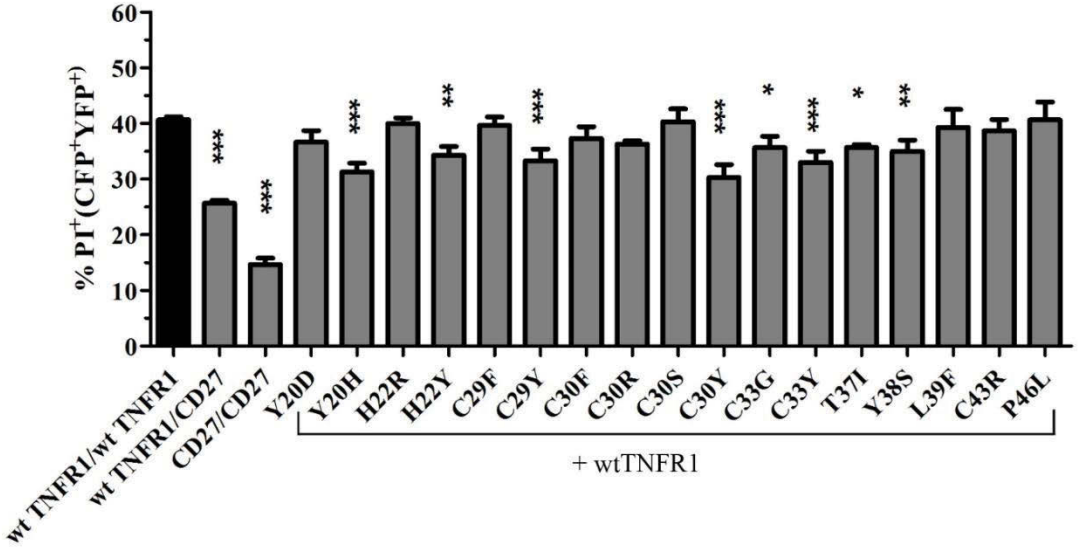

Figure 3.11C Statistical analysis of flow cytometry TNFR1-induced cell death assay.

A graphical summary representing the mean and standard deviation of three independent transfection experiments. Statistical analysis was performed in Prism using a 1 way ANOVA and Dunnett's Multiple Comparison Test to find differences between sample means. Comparisons of means were made against cells double positive for WT TNFR1 (black bar graph) and significant differences are asterisked. * = $P \leq 0.05$, ** = $P \leq 0.01$, *** = $P \leq 0.001$.

3.8 Discussion

Previous Studies on TRAPS mutations have only provided or characterised preliminary results of only a few TRAPS mutations at a time (Lobito et al. 2006; Siebert, Amos, et al. 2005; Todd, Radford, Ziegler-Heitbrock, et al. 2007). Therefore this study aimed to characterise a panel of known TRAPS mutations within the PLAD domain in which to later characterise their interaction with vTNFRs. The INFVERS database was used to source information about each of the reported mutations within the PLAD domain and whether the mutations were associated with TRAPS. The INFEVERS database is a registry of hereditary auto-inflammatory disorders listing mutations where users can submit

new novel mutations (Sarrauste de Menthia re et al. 2003). Although the sequences are verified by the editors, the TNFR1 mutations are not all necessarily associated with TRAPS, and may be TNFR1 polymorphisms (Aksentijevich et al. 2001). As TRAPS is defined as a dominantly inherited auto-inflammatory syndrome associated with TNFR1 mutations, of which the large majority are missense mutations (McDermott et al. 1999), only mutations from the INFEVERS database that fit this criteria were selected within the PLAD. Any mutations not found to be clinically associated with TRAPS from publications and reports were also excluded such as mutation D12E (Havla et al. 2013). TRAPS is found to present clinically similar to a number of other auto-inflammatory disease such as Familial Mediterranean fever which involves mutations associated with the pyrin gene and in fact, in some cases it has been found patients carry both mutations (Granel et al. 2007; Lachmann 2011). Thus mutations with no found association with TRAPS were excluded from the study. This resulted in a panel of 17 TRAPS mutations to characterise as well as investigate the interactions with viral TNFRs MYXT2, VARG4R and MPVJ2R.

Each of the 17 TRAPS mutations were successfully generated though site directed mutagenesis and double strand sequence verified along the whole cDNA insert for any this secondary mutations. This was to ensure that any differences observed, were attributable to only the desired TRAPS mutations.

Each TRAPS mutant TNFR1-YFP was successfully expressed in human U2OS cells and HEK 293 cells. Expression was observed initially via the presence of each YFP fusion tag then verified for the expression of the full length TNFR1 proteins through PAGE and Western blotting using an anti-TNFR1 antibody to an epitope (H5) in the N-terminal domain. It

was not known if TRAPS mutations would affect the detection of the expressed TRAPS proteins, as it was possible that the mutations may alter the epitope recognised by the antibody. Regardless, each TRAPS mutant was successfully detected using the anti-TNFR1 antibody. It could be observed that the relative expression of each of the proteins remained essentially consistent across each of the TRAPS mutations suggesting that the TRAPS mutations did not differ in expression between each of the TNFR1-YFP TRAPS proteins. This was also reflected visually by the low power microscopic images of the YFP detection, in that each TRAPS mutant was expressed essentially consistent across the panel of TRAPS mutations. The expression also did not differ from WT-TNFR1-YFP suggesting that none of the mutations had a significant effect on TNFR1 expression.

One of the growing hypothesis of TRAPS molecular pathology suggests that the increased inflammation caused by the mutations is TNFα-independent, possibly caused by intracellular retention of the mutant proteins (Lobito et al. 2006; Todd, Radford, Daffa, et al. 2007). TRAPS mutants are not found to localise to the cell surface but instead are retained within the endoplasmic reticulum (ER) (Lobito et al. 2006; Simon et al. 2010). In addition TRAPS mutations are unable to bind TNF and self-associate to form aggregates rather than associate with WT TNFR1 (Lobito et al. 2006; Todd et al. 2004). It is hypothesised that the intracellular aggregation and retention triggers intracellular signalling through the JUN N-terminal kinase, mitogen activated protein kinase (MAPK) pathways resulting in production or reactive oxygen species (ROS) (Bulua et al. 2011; Lobito et al. 2006). It is possible that the accumulation of TRAPS proteins in the endoplasmic reticulum (ER) may trigger an ER stress response to create the inflammatory state, as it has recently been found that ER stress can activate the NLRP3 inflammasome releasing pro-inflammatory cytokines such as IL-1β (Menu et al. 2012).

To visualise the localisation for the panel of PLAD TRAPS TNFR1 proteins, each generated TRAPS plasmid was transfected into human U2OS cells. To visualise whether the entire panel of TRAPS mutants localised to the cell surface, each sample was stained with WGA-AF594; a lectin that binds to sialic acid and N-acetylglucosaminyl residues predominantly found in the plasma membrane (Marth & Grewal 2008). Sialic acid and N-acetylglucosaminyl residues are also found on the ER and Golgi complex and are involved in endocytosis, trafficking and protein folding, therefore residual staining of intracellular membrane structures were also evident (Helenius & Aebi 2004; PARODI 2000). All TRAPS mutant TNFR1-YFP proteins as well as WT TNFR1-YFP proteins were found as punctate localisation within the cell and aggregating in a cellular sub-compartment near the DRAQ5 stained nuclei. This structure beared resemblance with the endoplasmic reticulum or Golgi. As WGA-594 is observed as diffuse localisation at the cell surface, out of focus light that is detected from the widefield detection system made it difficult to discern whether any of the TRAPS mutant TNFR1-YFP or WT TNFR-YFP proteins were also localising at the cell surface. Therefore it was decided to record the same experiment using a confocal microscopy system using the same filter sets to eliminate the out of focus detected light (Jonkman & Brown 2015). The confocal visualisation of the WGA-594 markedly improved the definition of the cell surface plasma membrane however neither WT-TNFR1-YFP nor any of the TRAPS mutants were observed to localise at the cell surface. The absence of TNFR1-YFP at the cell surface is most likely due to the level of sensitivity of detection of the microscope systems. The lack of WT TNFR1 localisation observed by confocal microscopy has also been reported previously but has been confirmed through flow cytometry to localise at the cell surface (Lobito et al. 2006; Todd et al. 2004). Further analysis using Imaris' co-localisation

software was performed but was unable to accurately analyse the co-localisation of the TNFR1-YFP proteins with WGA-AF594. This was reflected by the large differences between mutants reported in the co-localisation output, not reflected by the observations from the static images. This was largely due to the staining of the WGA-AF594 and the labelling of other membranous structures such as endosomes, ER and Golgi which confounded the co-localisation results. To verify the co-localisation data of the TNFR1-YFP proteins and TRAPS TNFR1-YFP proteins, the greatest differences observed between two TRAPS mutations Y20D and C33G from the co-localisation output were rendered in 3D to give a greater spatial awareness of where the TNFR1-YFP proteins were localising. No TNFR1-YFP for Y20D or C33G was clearly observed to localise at the cell surface and no obvious difference could be discerned between the two TRAPS mutants and therefore it was determined that co-localisation analysis was not suitable with WGA-AF594. Regardless all TRAPS mutants as well as WT-TNFR1-YFP appeared to again aggregate around a structure and location resembling the ER or Golgi. This was consistent with previous initial reports of the WT TNFR1 and TRAPS mutant C33G and C33Y localising in a perinuclear structures resembling ER or Golgi (Lobito et al. 2006; Todd et al. 2004). It was found that the TRAPS TNFR1 mutants largely localised to the ER whereas WT TNFR1 localised to the Golgi (Lobito et al. 2006). This work builds upon this data and shows that the entire panel of PLAD TNFR1 mutations aggregate and localise in a structure resembling the ER. Although this data correlates with previous reports of TRAPS mutants (Lobito et al. 2006; Todd et al. 2004), a possible contribution to the formation or aggregation of the TNFR1-YFP receptors may be due high-level expression of TNFR1 due to the CMV constitutive promoter, especially as WT TNFR1-YFP was also found perinuclear but is well described at cell surface (Siebert, Fielding, et al. 2005; Wang et al. 2003; Wilkinson & Akrigg 1992). High-level expression and retention

of TRAPS TNFR1 proteins is also observed in leukocytes from TRAPS patient containing the C33Y mutation (Todd, Radford, Daffa, et al. 2007). The plasmid overexpression in our expression system may simulate ligand-independent signalling of TRAPS TNFR1 proteins and represent the over-sensitivity of TRAPS patient cells in response to inflammatory stimuli (Todd, Radford, Daffa, et al. 2007).

It is reported that signalling of cell death by TNFR1 can occur intracellularly through endosomal pathways in compartments termed" receptosomes" (Schneider-Brachert et al. 2004). As WT-TNFR1-YFP and all TRAPS TNFR1-YFP proteins were observed in punctate localisation throughout the cell as well as aggregating within an ER or Golgi like structure, human U2OS cells were stained with an endosomal marker Rab5 known to be present as part of the receptorsome complex (Schneider-Brachert et al. 2004). The Rab5 staining of positive endosomes was detected as small punctate structures throughout the cell. On initial observations the punctate expression and localisation of WT TNFR1-YFP and TRAPS TNFR1-YFP appeared to co-localise. However because the YFP expression of TNR1-YFP was much brighter in intensity than the fluorescence from the secondary AF654 conjugated antibody to anti-human Rab5, an obvious overlap of the two colours was not observable (i.e. an orange overlay in colour of the YFP shown in yellow and Rab5 shown in red). However an overlap in fluorescence emission (colour) does not equal co-localisation and is a subjective measure of co-localisation, an example of this is when fluorescence detected in the Z-dimension may be behind another probe but not necessarily in the same coordinates as another fluorophore leading to a false impression of co-localisation due to the viewing/detection point (For review on co-localisation methods see (Dunn, Kamocka & McDonald 2011)). To give a more accurate representation of co-localisation, each image of the TRAPS and WT TNFR1-YFP proteins

with Rab5 were analysed using the analysis software Imaris (Bitplane). Because both fluorescence emission was punctate and defined, the image analysis proved much more accurate in defining, detecting and comparing each fluorescence emission. Both WT TNFR1-YFP and each of the TRAPS TNFR1-YFP mutants were observed to co-localise with Rab5 throughout the cell. However with the exception of mutants H22R, C30R and C33Y which showed ~80% of TNFR1-YFP co-localising with Rab5 (similar to WT TNFR1-YFP localisation), the TRAPS mutants displayed a reduced co-localisation with Rab5 (~50-60% of YFP localised with Rab5). Although it has initially been described that selected mutants C33G and C33Y aggregate within the ER and retain signalling capacity (Lobito et al. 2006; Todd et al. 2004), these results show that almost all of the panel of TRAPS mutations within the PLAD domain traffic less through the endosomal pathway. Amongst the mutations however, C33G displayed the greatest difference to WT TNFR1-YFP co-localisation with Rab5 (80% vs 53% respectively) suggesting a greater effect of the mutation on localisation. The reduced co-localisation may possibly lead to reduced signalling capacity for the mutants that display reduced co-localisation with Rab5 as trafficking of TNFR1 receptors within the endosomes/receptosomes is known to trigger cell death pathways (Schneider-Brachert et al. 2004).

To test the effect of TRAPS mutations on TNFR1 induced cell death, each of the TRAPS mutations was expressed in HEK 293 cells and stained with propidium iodide (PI) to compare against WT TNFR-YFP measured by flow cytometry. PI stains dead cells on the principle that dying cells are characterised by DNA fragmentation and loss of nuclear content (Crompton et al. 1992; Riccardi & Nicoletti 2006). PI then intercalates with the DNA where its emission increases 20-30 fold and becomes longer in wavelength emission (Crompton et al. 1992). Because the transfection procedure relies on the

precipitation and uptake of the DNA complexes, it was observed that the transfected cells exhibited a background level of PI fluorescence. This however did not prove problematic as staining of true dead cells (shown in WT TNFR1-YFP overexpressing cells) revealed that PI florescence was more intense and distinct from background staining. In WT TNFR1-YFP/CFP double transfected cells, TNFR1 induced cell death was observed in approximately 40% of cells. TRAPS mutant TNFR-YFP proteins were expressed with WT TNFR1-CFP to replicate the biological heterozygous expression of TRAPS proteins and this largely resulted in reduced TNFR induced cell death compared to WT TNFR1-YFP and WT-TNFR1-CFP co-expressing cells. Of note TNFR1 TRAPS mutations Y20H (31%), H22Y (34%), C29Y (33%), C30Y (30%), C33G (35%) C33Y (33%), T37I (35%), Y38S (35%) caused statistically reduced cell death. This was consistent with initial reports of TNFR1 H22Y (Lobito et al. 2006), C33G (Lobito et al. 2006) and C33Y (Rebelo et al. 2006), displaying reduced cell death in both cell lines in vitro and human cells *ex vivo* containing TRAPS mutations.

It has previously been reported that certain TRAPS mutations (R92Q and C43S) display a reduced signalling capacity (D'Osualdo et al. 2006; Siebert, Fielding, et al. 2005). It may be possible that TRAPS mutations render the TNFR1 protein dysfunctional, essentially diluting out the expression and WT signalling of TNFR1 within the cell. However the data presented in this chapter shows differences among the TRAPS PLAD mutations in their capacity to induce cell death which suggests that the mutations have varying functional effects on TNFR1 biology. This is also supported by the overwhelming presence of mutations within the functional domains of TNFR1 (Aksentijevich et al. 2001), the large clinical spectrum of symptoms (Lahaxe et al. 2010) and responses to treatment observed (Dodé et al. 2002; Nedjai et al. 2009) for different TRAPS mutations indicating differing

effects attributed by the mutations rather than a dysfunction. Further to this, in a murine model expressing mutations C33Y or T50M it was shown that the mutant TNFR1 proteins activate JNK and p38 Mitogen activated protein kinase (MAPK) signalling cooperatively with WT TNFR1 (Simon et al. 2010). Therefore the differences observed between TRAPS mutations inducing cell death are most likely attributable to the mutations either in their structure or localisation.

Chapter 4

Characterisation of vTNFRs and inhibition of TNFR-induced cell death

Chapter 4

4.1 Introduction

MYXT2 was the first well characterised viral TNFR, and in fact vTNFRs were discovered (Upton, DeLange & McFadden 1987) even before cellular TNFR1 or TNFR2 cDNAs were cloned (Gray et al. 1990; Loetscher, Pan, et al. 1990). To date MYXT2 still remains the best characterised vTNFR binding protein and neutralises rabbit TNFα with a high affinity in a species specific manner (Upton et al. 1991). It quickly became evident that vTNFRs also existed amongst other poxviruses, also binding and neutralising TNFα with a very high affinity but varying specificities for TNF and LTα (Hu, Smith & Pickup 1994; Loparev et al. 1998; Massung et al. 1994; Smith et al. 1996a). Almost all orthopoxvirus genomes have been found to contain at least one vTNFR ORF or remnants of a vestigial vTNFR ORF (Sedger 2005), with strains of cowpox virus such as Brighton Red containing up to 4 known CRM- or vTNFR proteins (Loparev et al. 1998; Saraiva & Alcami 2001; Shchelkunov 2003; Smith et al. 1996a). However, for all of the known vTNFRs the focus has remained on the mechanism of these proteins to bind and neutralise soluble TNFα (Gileva et al. 2006; Schreiber, Sedger & McFadden 1997; Smith et al. 1996a).

Structure is often very strongly associated to function and the discovery of a PLAD (pre-ligand assembly domain) in MYXT2 led to the discovery a second mechanism in which vTNFRs interact with cellular TNFRs (Sedger et al. 2006). MYXT2 is very efficient in binding and neutralising rabbit TNF however this interaction is shown to be strictly species specific (Schreiber & McFadden 1994). The intracellular activity of MYXT2, not only indicated MYXT2 able to associate with “human” TNFR1 and TNFR2, but it also protected against “human” TNFR-induced cell death. This suggested a more nonspecific

means of inhibition, as MYXT2 does not inhibit and neutralise soluble human TNF (Sedger et al. 2006). As the PLAD is highly conserved amongst other TNFR super family members (Chan 2000; Kramer et al. 2007) including vTNFRs (Sedger et al. 2006), it is predicted that vTNFRs other than MYXT2 are also able to associate with cellular receptors and inhibit cell death similarly (Sedger et al. 2006). Because the intracellular subversion of TNFRs is not species-specific, it may prove as a more important mechanism for poxviruses with a broader host range such as Monkeypox virus (Parker & Buller 2013). To begin to answer these questions, first the intracellular mechanism of TNFR inhibition for other vTNFRs requires further characterisation, and more in depth investigation - the focus of this chapter.

4.2 Results

4.3 Generation of viral TNFR plasmids for mammalian expression

A pcDNA3.MYXT2-MycHis plasmid was created previously through PCR amplification of the MYXT2 ORF (NCBI accession: AAA46632) cloned into *Bam*HI and *Xho*I restriction sites in pcDNA3.1-MycHis (Sedger et al. 2006). Plasmids pUC19.VARG4R-MycHis and pUC19.MPVJ2R-MycHis were designed and codon optimised for optimal expression in *Homo sapien* and *Mus musculus* cells by Sarah Sherwood, a previous PhD student in this lab. The sequence for VARG4R was codon optimised from the VAR India 1967 strain sequence (NCBI accession: NP_042240.1). The sequence for MPVJ2R was synthesised and codon optimised using the MPV 1996 Zaire strain sequence (NCBI accession: AF380138.1). The sequences were synthesised by Codon devices Inc. USA and cloned into pUC19 plasmids, between the *Kpn*I and *Xho*I restriction sites 5'-3' (data not shown). Due to restrictions in working with the ORFs of VARG4R and MPVJ2R were synthetically

synthesised with WHO smallpox committee approval, dealing not involving an intentional release (DNIR) from the office of the gene technology regulator (OGTR) approval and UTS Biosafety approval.

Plasmids pcDNA3.VARG4R-MycHis and pcDNA3.MPVJ2R-MycHis were created by previous PhD student Sarah Sherwood (data not shown). For this the ORF of VARG4R and MPVJ2R from Puc19.VARG4R-MycHis and Puc19.MPVJ2R-MycHis were subcloned into corresponding restriction sites (*Kpn*I and *Xho*I) in the multiple cloning site of pcDNA3.MycHis (Figure 4.1). This created the VARG4R and MPVJ2R ORFs in frame with a 3' MycHis fusion tag in pcDNA3.MycHis (Figure 4.1A). The ORF sequences were then double strand sequence verified (data not shown).

4.4 Generation of pcDNA3.MYXT2CFP, pcDNA3.VARG4RCFP and pcDNA3.MPVJ2R.CFP

Plasmids pcDNA3.VARG4R.CFP, pcDNA3.MPVJ2R.CFP were generated by digesting pUC19.VARG4R-mycHis and pUC19.MPVJ2R-mycHis with *Kpn*I and *Xho*I to remove the viral TNFR ORFs (Figure 4.1A), for sub cloning into the subsequent restriction sites in pcDNA3.TNFR1-CFP i.e. replacing the TNFR1 cDNA with VARG4R and MPVJ2R ORFs (Figure 4.1A). This produced VARG4R and MPVJ2R in-frame with the cDNA sequence of CFP to express the vTNFR as fluorescently tagged proteins. Similarly plasmid pcDNA3.MYXT2-CFP was generated by sub cloning the MYXT2 ORF from pcDNA3.MYXT2-mycHis by digesting with *BamH*I and *Xho*I (this was necessary as the ORF of MYXT2 contains an internal *Kpn*I restriction site).

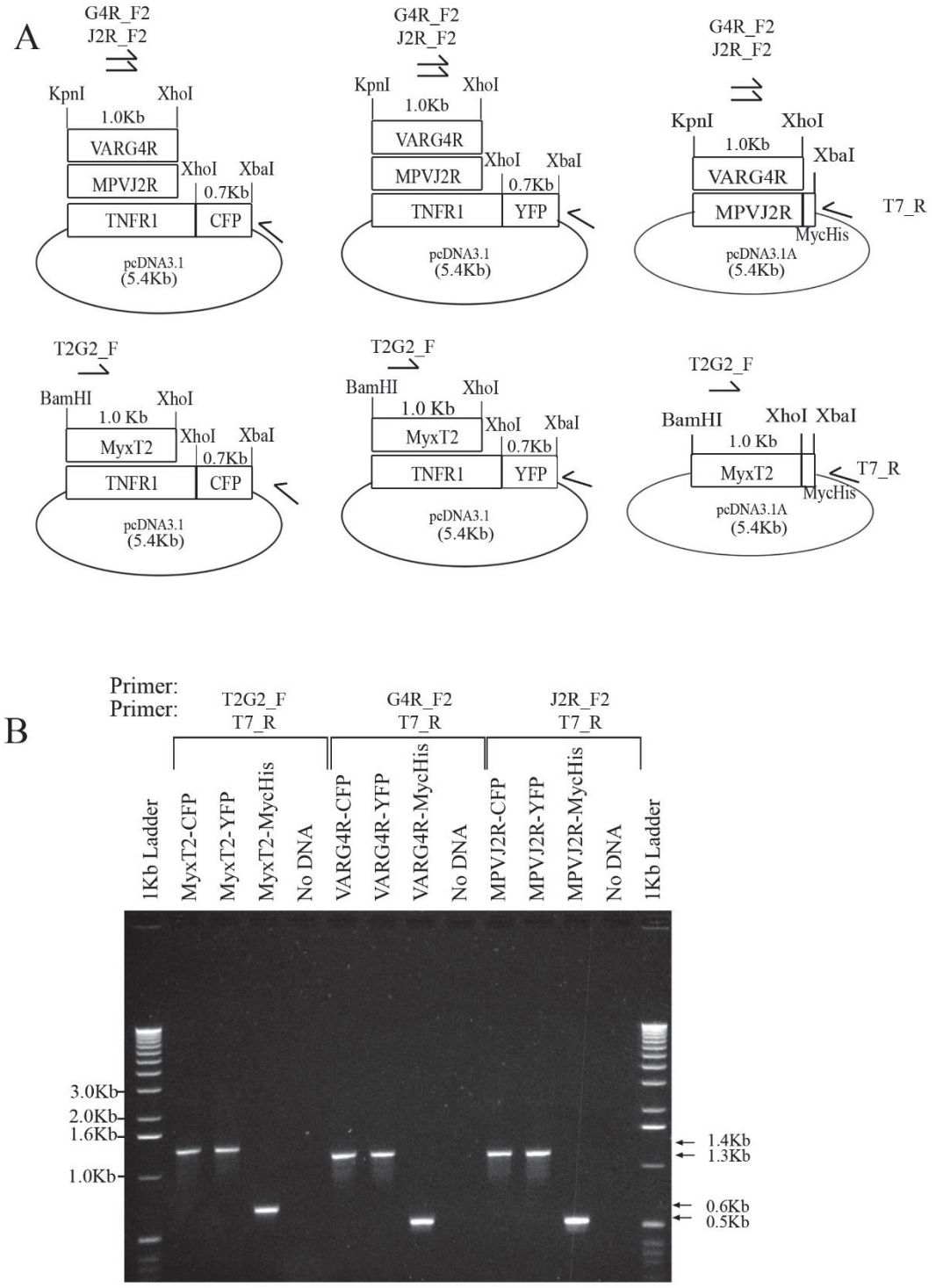

Figure 4.1 Cloning strategy for MYXT2, VARG4R and MPVJ2R-MycHis, -CFP and –YFP plasmids.

The synthesised vTNFR ORFs of VARG4R and MPVJ2R from the pUC19 vector were subcloned into the vectors of pcDNA3.TNFR1-CFP, -YFP and the pcDNA3.MycHis plasmid using *KpnI* and *Xho*I restriction sites. MYXT2 was originally PCR amplified from the Myxoma virus and subcloned into pcDNA3.MycHis as described in (Sedger et al. 2006). The MYXT2 ORF was then subcloned into pcDNA3.TNFR1-CFP and pcDNA3.TNFR1-YFP using restriction sites *Bam*HI and *Xho*I replacing the TNFR1 cDNA. A PCR was performed to confirm successful subcloning into the newly generated plasmids. Primers specific to each of the ORFs and a reverse primer nested in the vector were used.

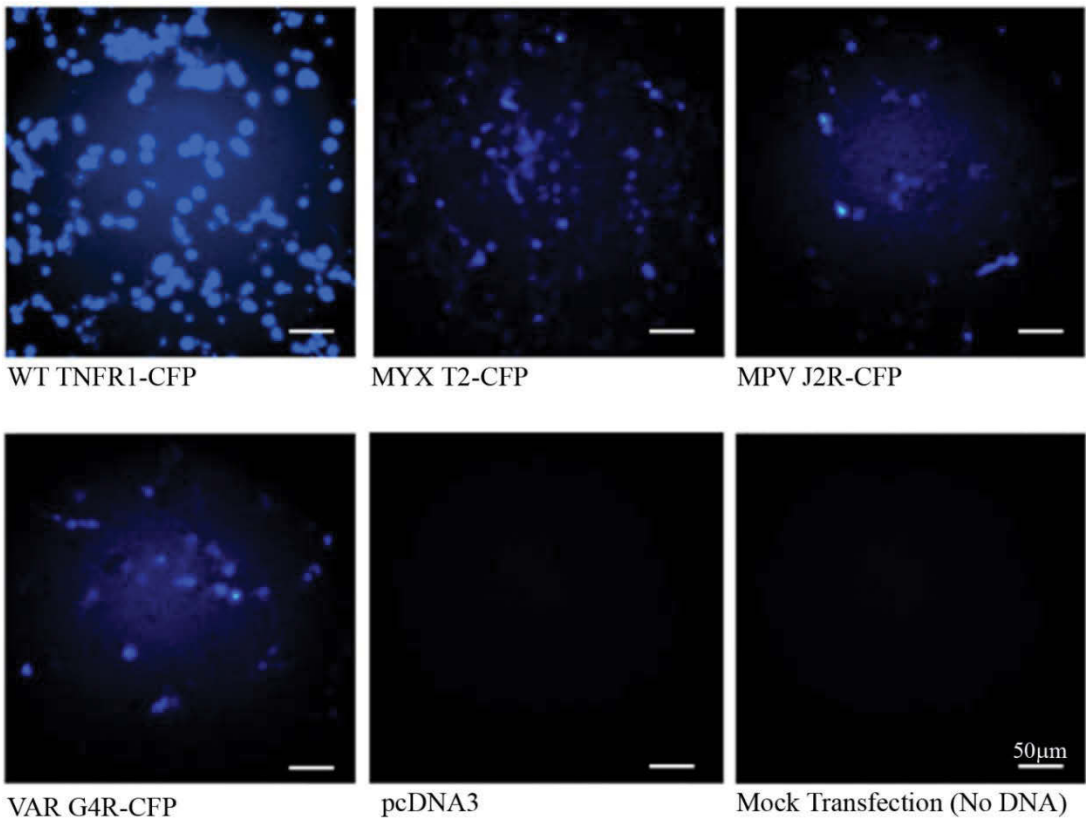

Figure 4.2 Microscopic evidence of vTNFR expression via CFP detection
Each vTNFR was expressed in 293 HEK cells and examined by widefield microscopy at 20x (NIKON TI eclipse). Expression was observed 48 hours post transfection and compared to TNFR1-CFP expression. Empty pcDNA3 and mock transfections were also included. CFP (blue) was detected in the CFP channel (Ex 430/20nm, BA 480/40nm).

Plasmids pcDNA3.VARG4R-YFP, pcDNA3.MPVJ2R-YFP and pcDNA3.MYXT2-YFP were designed and cloned by Sarah Sherwood. From this pUC19.VARG4R-MycHis and pUC19.MPVJ2R-MycHis were digested with *Kpn*I and *Xho*I removing the vTNFR ORFs, which were then subcloned into the same restriction sites in pcDNA3.TNFR1-YFP (i.e. replacing the TNFR1 cDNA) (Figure 4.1A). This created VARG4R and MPVJ2R as fusion constructs as in-frame 3' -YFP cDNA sequences (Figure 4.1A). Plasmid pcDNA3.MYXT2-YFP was subcloned by digesting pcDNA3.MYXT2-mycHis with *BamH*I and *Xho*I instead. This was ligated into the same restriction sites in pcDNA3.TNFR1-YFP (i.e. replacing the TNFR1 cDNA in pcDNA3.TNFR1-YFP) (Figure 4.1A).

To verify that the vTNFR-CFP plasmids had been generated correctly, a PCR was performed to confirm the presence of the MPVJ2R, VARG4R and MYXT2 cDNA. The vTNFR-YFP and vTNFR-MycHis plasmids previously created by Sarah Sherwood had been already been double strand sequence verified, however they were included again in the PCR for confirmation and comparison against the newly created pcDNA3.MYXT2.CFP pcDNA3.VARG4R.CFP and pcDNA3.MPVJ2R.CFP plasmids (Figure 4.1B). Each plasmid was amplified using an internal forward primer specific for each MPVJ2R primer (J2R_F2), VARG4R primer (G4R_F2) and MYXT2 primer (T2G2_F) and a common reverse primer (T7_R) residing in the plasmid (Figure 4.1A). PCR of pcDNA3.MYXT2.CFP, pcDNA3.VARG4R.CFP plasmids amplified a band of approximately 1.3kb which is the combined total size of the viral TNFR cDNA and CFP cDNA sequence (Figure 4.1C). The PCR product from pcDNA3.MYXT2-CFP was 1.4kb as the T2G2_F primer nested closer to the 5' end of the ORF (Figure 4.1C). The PCR products from pcDNA3.MYXT2.YFP, pcDNA3.VARG4R.YFP and pcDNA3.MYXT2-YFP were also approximately 1.3kb and 1.4kb respectively, as the YFP and CFP sequences are of the same length 720bp (Figure 4.1C).

The PCR products from pcDNA3.VARG4R-MycHis, pcDNA3.MPVJ2R-MycHis and pcDNA3.MYXT2-MycHis were approximately 0.5kb as the MycHis epitope tag is only 46bp compared to the sequence of CFP or YFP. Therefore given that the primers were specific to the vTNFR ORFs and the PCR products from the previously verified plasmids pcDNA3.MYXT2.YFP, pcDNA3.VARG4R.YFP and pcDNA3.MYXT2-YFP were of the same size it suggested that pcDNA3.MYXT2.CFP pcDNA3.VARG4R.CFP and pcDNA3.MPVJ2R.CFP were successfully created.

4.5 Confirmation of MYXT2-CFP, VARG4R-CFP and MPVJ2R-CFP fluorescence

To confirm pcDNA3.MYXT2-CFP, pcDNA3.VARG4R-CFP and pcDNA3.MPVJ2R-CFP were sub cloned in-frame and expressed a functional fluorescent protein, each plasmid construct was transiently transfected into 293 HEK cells. The CFP fluorescence of each protein was then detected by widefield microscopy using an inverted Nikon Eclipse TI microscope (Figure 4.2). pcDNA3.TNFR1-CFP was included as a positive control and a pcDNA3 empty vector (no fluorescence) and mock transfections included as negative controls. CFP fluorescence was detectable in cells transfected with MYXT2-CFP, VARG4R-CFP and MPVJ2R-CFP, as well as for the positive control TNFR1-CFP (Figure 4.2). No fluorescence was detectable from the pcDNA3 empty vector, and mock transfection controls, meaning CFP fluorescence was specific to CFP fusion proteins. Therefore pcDNA3.MYXT2-CFP, pcDNA3.VARG4R-CFP and pcDNA3.MPVJ2R-CFP all appeared to express CFP fusion proteins. To ensure pcDNA3.MYXT2-CFP, pcDNA3.VARG4R-CFP and pcDNA3.MPVJ2R-CFP did not contain secondary mutations from the cloning process, each plasmid ORF was double strand sequence verified. Each pcDNA3.MYXT2-CFP,

pcDNA3.VARG4R-CFP and pcDNA3.MPVJ2R-CFP construct was verified to be of the correct sequence and moreover in frame (data not shown).

4.6 MYXT2, VARG4R and MPVJ2R inhibit cell TNFR induced cell death

It is well known that vTNFRs have the ability to bind and inhibit specific soluble TNF [for review see (Sedger 2005)], however only MYXT2 has been identified to inhibit TNFR-Induced cell death (Sedger et al. 2006). Since this interaction was shown to occur in a species non-specific manner with MYXT2, whether this function is also a characteristic of VARG4R and MPVJ2R proteins is unknown. The ability of VARG4R and MPVJ2R proteins to inhibit human TNFR-induced cell death was therefore examined. This provides an interesting comparison as each protein comes from viruses with very different host ranges – VAR restricted to solely humans (Arita & Henderson 1968) and MPV exhibiting a broad host range (Fields, Knipe & Howley 2007). Using flow cytometry, TNFR-induced cell death was assayed by propidium Iodide (PI) in 293 HEK cells. Cells co-transfected with either MYXT2, VARG4R or MPVJ2R and overexpressed human TNFR1 were then examined. These samples were then compared against 293 HEK cells overexpressing TNFR1 and CD27 proteins, another TNFRSF member not known to have any impact on TNFR induced cell death (Gravestein et al. 1995).

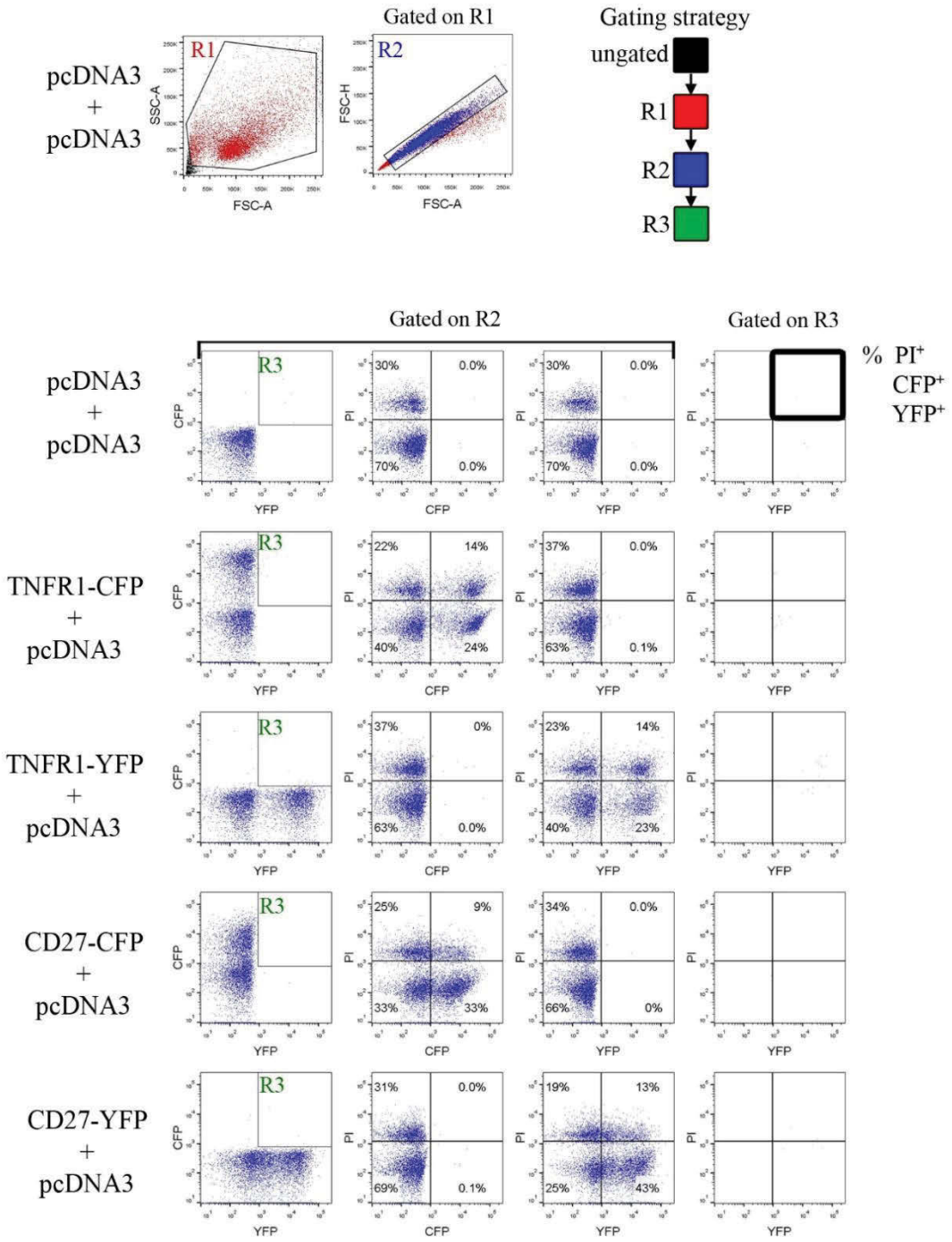

Figure 4.3A Flow cytometry set up and gating strategy for vTNFR inhibition of TNFR-induced cell death assay

Transfected 293 HEK cells were analysed by first gating on the population (R1, red) to eliminate cell debris. Single cells were then sub gated on (R2, blue) to exclude doublet cells. Double positive cells expressing CFP and YFP were then gated on (R3, green), then analysed for cell death by measuring the percentage of PI positive cells in YFP vs PI dot plots. $CFP^+YFP^+PI^+$ cells (dead cells) were identified in the top right quadrants of the YFP vs PI dot plots. Percentages represent proportion of CFP^+YFP^+ cells in each quadrant.

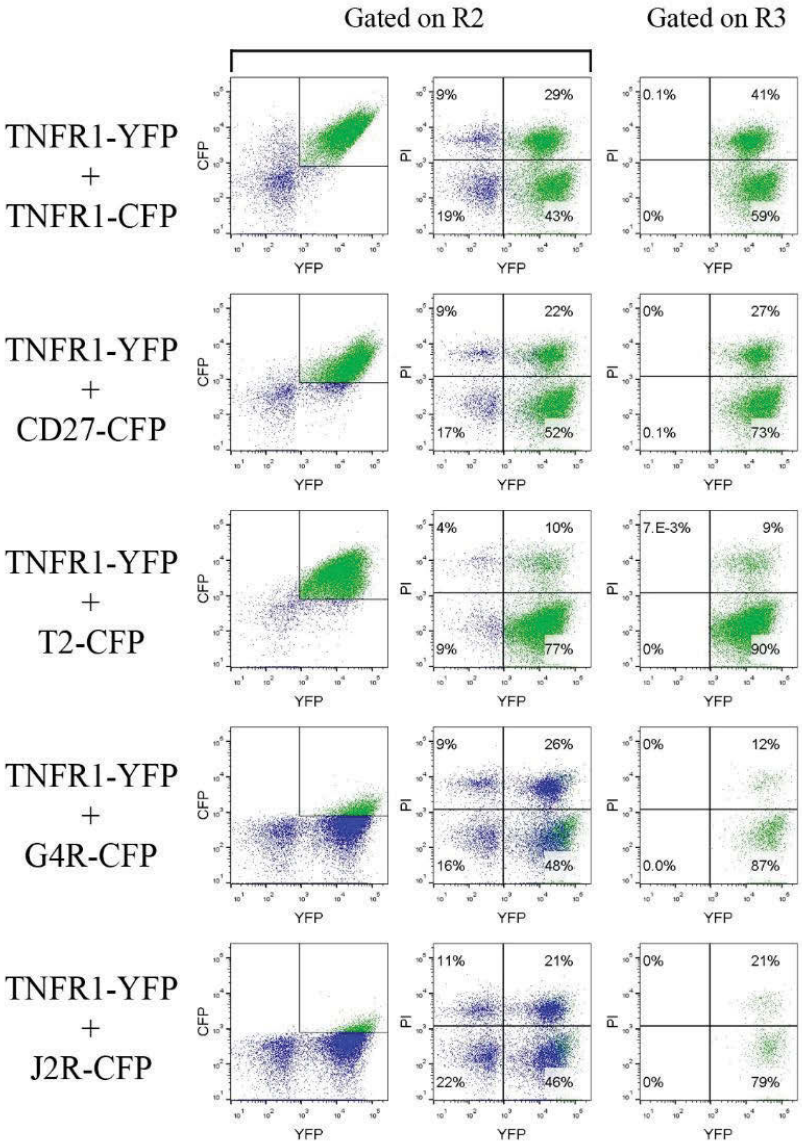
Gated on R2
Gated on R3
TNFR1-YFP + TNFR1-CFP
TNFR1-YFP + CD27-CFP
TNFR1-YFP + T2-CFP
TNFR1-YFP + G4R-CFP
TNFR1-YFP + J2R-CFP
CFP
YFP
PI
9%
29%
19%
43%
0.1%
41%
0%
59%
9%
22%
17%
52%
0%
27%
0.1%
73%
4%
10%
9%
77%
7.E-3%
9%
0%
90%
9%
26%
16%
48%
0%
12%
0.0%
87%
11%
21%
22%
46%
0%
21%
0%
79%

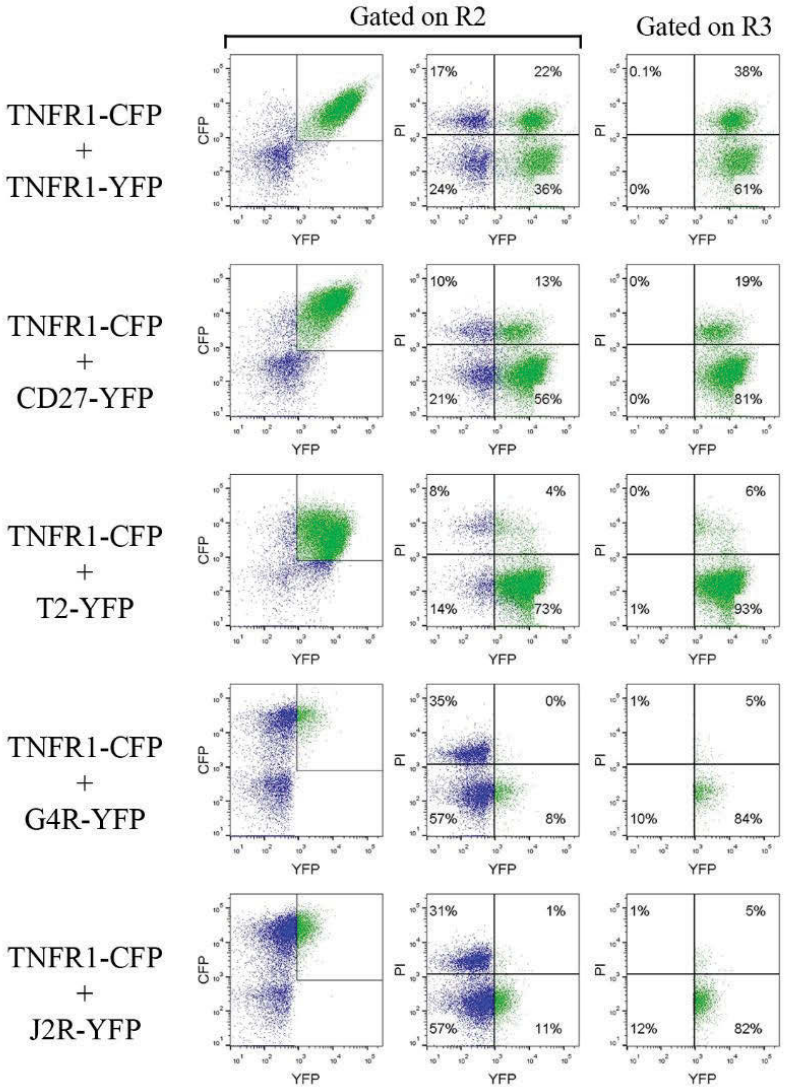

Figure 4.3B Flow cytometry analysis of vTNFR inhibition of TNFR-induced cell death

Transfected 293 HEK cells co-expressed WT TNFR1 and either MYXT2, VARG4R or MPVJ2R. Cells were then stained with PI and analysed for cell death. Data represents the median transfection experiment of independent triplicate transfections with 30000 events collected for each sample. Transfections are examined 48 hours post transfection. Cells were transfected to express TNFR1-YFP and each of the vTNFR-CFP proteins. The experiment was then repeated using the inverse CFP and YFP plasmids.

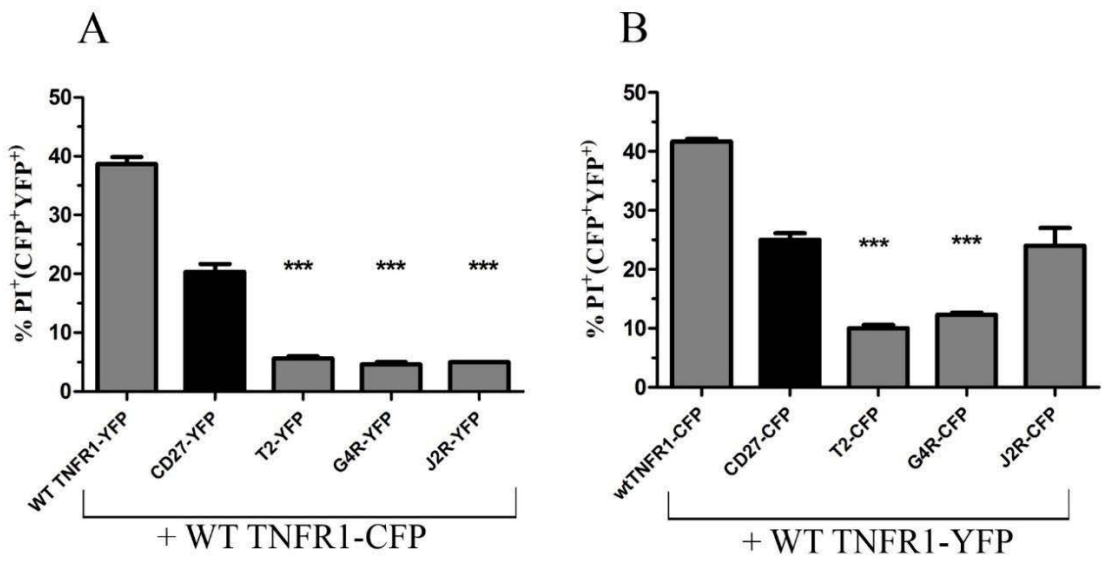

Figure 4.3C Statistical comparisons of vTNFR inhibition of TNFR1-induced cell death

Graphical representations of means and standard deviations from the independent triplicate transfections for each sample. Means of samples were assessed for differences using a one-way ANOVA then Dunnett's multiple comparisons test to compare each of the means against cells co-transfected with WT TNFR1 and CD27 (black control column). The level of statistical significance are asterisked. * = $P \leq 0.05$, ** = $P \leq 0.01$, *** = $P \leq 0.001$. T2 represents MYXT2-CFP, G4R represents VARG4R and J2R represents MPVJ2R.

To ensure repeatable and accurate results the experiment was performed in triplicate and both configurations C-terminal CFP or YFP fusion proteins i.e. TNFR1-YFP and MYXT2-CFP or TNFR1-CFP and MYXT2-YFP. Firstly, to ensure the correct and optimal laser set up, a series of controls were used. The cell population was first gated using a FWD vs SSC plot to exclude cell aggregates and debris (R1, red gate) then subsequently gated on to only include single cells and ensure only co-transfected single cells were examined (R2, blue gate) (Figure 4.3A). A third gate (R3, green gate) was drawn on cells positive for PI, CFP and YFP determined from WT TNFR1 co-transfected cells (Figure 4.3A). The analysis of dying cells was assessed from the quadrant identifying $PI^+CFP^+YFP^+$ cells (Figure 4.3A). Cells expressing single colour controls, TNFR1-CFP, TNFR1-YFP, CD27-

CFP and CD27-YFP were used to obtain the correct voltages and correct compensation for CFP, YFP and PI (Figure 4.3A). From this it was apparent that two positive PI populations were present; a PI high and PI low population likely being residual DNA on cells stained with PI. A log difference existed between PI low and PI high (dead) cell populations, allowing cell death to be measured (Figure 4.3A).

Cells expressing both TNFR1-YFP and TNFR1-CFP proteins exhibited cell death in approximately 40% of cells, which was consistent with previous experiments (Chapter 3.7) (Figure 4.3B). Less cell death was observed in cells co-expressing TNFR1 and CD27 (in either CFP or YFP configurations) with only approximately 25% of cells appearing to undergo cell death (Figure 4.3B). This was most likely due to less expression of TNFR1 to induce cell death (half the total amount of DNA pcDNA3.TNFR1-CFP or YFP transfected). Since the same amount of transfected TNFR1 plasmid DNA was used to compare the effect of vTNFR on TNFR1 induced cell death, cells expressing TNFR1 and CD27 were used as the comparison (black columns in graph Figure 4.3C). When expressed with TNFR1-CFP, all vTNFRs, MYXT2-YFP, VARG4R-YFP and MPVJ2R-YFP, inhibited TNFR-induced cell death, with only approximately 6% of cells dying for each sample (Figure 4.3C). This was statistically significant in comparison to TNFR1-CFP/CD27-YFP (Figure 4.3C). When the inverse CFP and YFP constructs were used with TNFR1-YFP, MYXT2-CFP inhibited TNFR1-induced cell death significantly (~9%) (Figure 4.3B and Figure 4.3C). By comparison VARG4R-YFP was observed to also inhibit TNFR-induced cell death with 12% of cells PI^+ (Figure 4.B and Figure 4.3C). Surprisingly, MPVJ2R-CFP was not observed to significantly rescue cells from TNFR-induced cell death with approximately 24% of cells becoming PI^+ (Figure 4.3B and Figure 4.3C), but this may have been possibly due to poor expression of MPVJ2R-CFP, as insufficient vTNFR protein being inadequate to rescue

cells from overexpressed TNFR1-YFP. Taken together, MYXT2, VARG4R and MPVJ2R all displayed the ability to rescue cells from human TNFR1-induced cell death.

4.7 Detecting vTNFR abundance in the presence of TNFR1 and TNFR2 overexpression.

With the evidence that MYXT2, VARG4R and MPVJ2R are able to inhibit TNFR1-induced cell death intracellularly, whether an association with human TNFR1 and TNFR2 also exists, was investigated. Although an association with human TNFRs is clearly demonstrated for MXYT2, it has not been shown for other vTNFRs. As an Indirect measure to test whether MPVJ2R and VARG4R proteins also interact with cellular TNFR1 and TNFR2 intracellularly, cells were transfected to express either MYXT2-MycHis, VARG4R-MycHis or MPVJ2R-MycHis in combination with TNFR1-YFP or TNFR2-YFP. Because MYXT2, VARG4R and MPVJ2R are known to be secreted from cells (Alejo et al. 2006; Gileva et al. 2006; Upton et al. 1991), I reasoned that vTNFR expression might be increased in cells overexpressing TNFR1 or TNFR2 as it might be retained within the cell to greater degree compared to lower expressed endogenous TNFR1 or TNFR2. Hence the expression of the vTNFRs was detected by an anti-Myc-AF647 (Cell Signalling technology) conjugated antibody and the correlating increase in abundance will be detected as an increase in MFI. Cells co-expressing vTNFR and TNFR1 or TNFR2 were compared against cells co-expressing CD27-Myc or CD27-YFP; CD27 being another TNFRSF member, which has no reported interactions with TNFR1 or TNFR2.

Therefore the relative abundance of MYXT2, VARG4R and MPVJ2R within cells was measured by flow cytometry. To detect MYXT2-MycHis, VARG4R-MycHis and MPVJ2R-

MycHis, cells were fixed then stained with a mouse anti-Myc-AF647 antibody. To exclude debris, FWD/SSC plots were first gated on (R1, red gate) and then a subsequent single cell gate was drawn from FWD-A/FWD-H plot to exclude doublet cells (R2, blue gate) (Figure 4A). From this cell population the mean fluorescence of AF647 was measured. First, cells transfected alone with CD27-Myc, CD27-YFP, or TNFR1-YFP, TNFR1-Myc, TNFR2-YFP, TNFR2-Myc and pcDNA3 "empty vector" were examined, to ensure that the laser voltages were set correctly and that staining for the Myc epitope tag was specific to the expressed proteins (Figure 4.4A). From this, it was observed that staining with anti-Myc-AF647 antibody resulted in a background fluorescence level slightly higher than in mock transfected cells stained with the isotype control antibody (goat anti-mouse IgG-AF647) (Figure 4.4A). All cells expressing the Myc fusion proteins i.e. CD27-Myc, TNFR1-Myc and TNFR2-Myc displayed a large increase in mean AF647 fluorescence (MFIs = 177, 166 and 224 respectively) which was clearly discernible above background AF647 fluorescence (MFI 7) (Figure 4A). As the anti-Myc-AF647 antibody staining resulted in slightly higher background fluorescence, all samples were compared to the anti-Myc-AF647 stained pcDNA3 (empty vector) examining sample in triplicate (Figure B).

Each plasmid pcDNA3 (empty vector), pcDNA3.CD27-MycHis, pcDNA3.T2-Myc, pcDNA3.G4R-Myc, pcDNA3.J2R-Myc was co-transfected with either pcDNA3 (empty vector), CD27-YFP, TNFR1-YFP or TNFR2-YFP plasmid in triplicate transfections. Each individual sample was then analysed using the same settings as the single colour control samples. Samples transfected with the vTNFRs were then statistically compared against samples when co-transfected with equal amounts (2ug) of pcDNA3 empty vector. When co-transfected with pcDNA3 (empty vector), CD27-Myc was detected by a large shift to

the right from the control (MFI 123 vs MFI 7) (Figure 4.3). pcDNA3.MYXT2-MycHis, when co-transfected with pcDNA3 resulted in a small increase of anti-Myc-AF647 intensity (MFI 21 vs MFI 7). Both VARG4R-Myc and MPVJ2R-Myc when co-transfected with pcDNA3 (empty vector) were only marginally detectable over the Myc antibody stained pcDNA3 transfected cells (empty vector) (MFI 13 and MFI 14 respectively, vs MFI 7) (Figure B and Figure C). pcDNA3.CD27-YFP when co-transfected with either pcDNA3.MYXT2-MycHis, pcDNA3.VARG4R-MycHis or MPVJ2R-MycHis was not expected to have any effect due to low sequence homology between proteins and the expectation was that no physical interaction would exist. As expected the MFI values for MYXT2-Myc (MFI 21), VARG4R-Myc (MFI 13) and MPVJ2R-Myc (MFI 14) remained virtually unchanged from the samples co-transfected with pcDNA3 empty vector. In contrast when TNFR1-YFP cDNA was co-expressed with pcDNA3.MYXT2-MycHis a significant increase in MFI of Myc-AF647 was observed (MFI = 108) compared to when co-expressed with pcDNA3 or CD27-YFP (Figure 4.4B). This increase indicated a higher level of MYXT2 intracellularly (Figure 4B and Figure 4C). VARG4R-MycHis and MPVJ2R-MycHis, when co-expressed with TNFR1-YFP displayed a slight increase in MFI (MFI = 19 and 18 respectively) (Figure 4B and Figure 4C), although this was not found to be statistically significant (Figure 4C). An increase in detection of the Myc-AF647 antibody was also observed in cells co-expressing TNFR2-YFP and MYXT2-MycHis proteins (MFI = 45) over cells co-expressing MYXT2-MycHis and CD27-YFP (MFI = 25) (Figure 4B and Figure 4C).

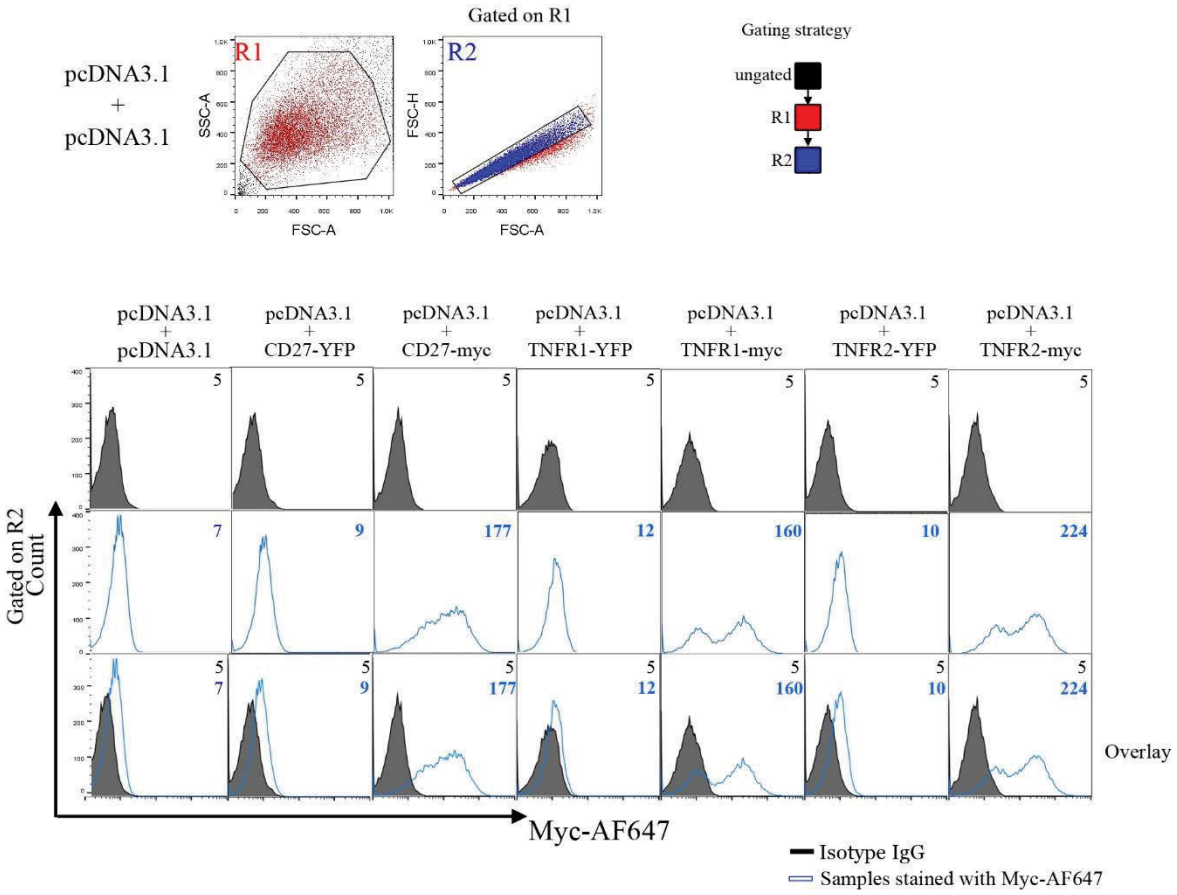

Figure 4.4A Flow cytometry gating strategy and single colour controls set up for detection of vTNFR intracellular abundance.

Transfected 293 HEK cells were analysed by first gating on the population (R1, red) to eliminate cell debris. Single cells were then sub gated on (R2, blue) to exclude doublet cells. The R2 subpopulation Expressing proteins containing a MycHis fusion tag were detected via an anti-Myc-AF647 antibody and detected in the Myc-AF647 channel. The same samples were stained in parallel with an isotype goat anti mouse IgG-AF647 control antibody.

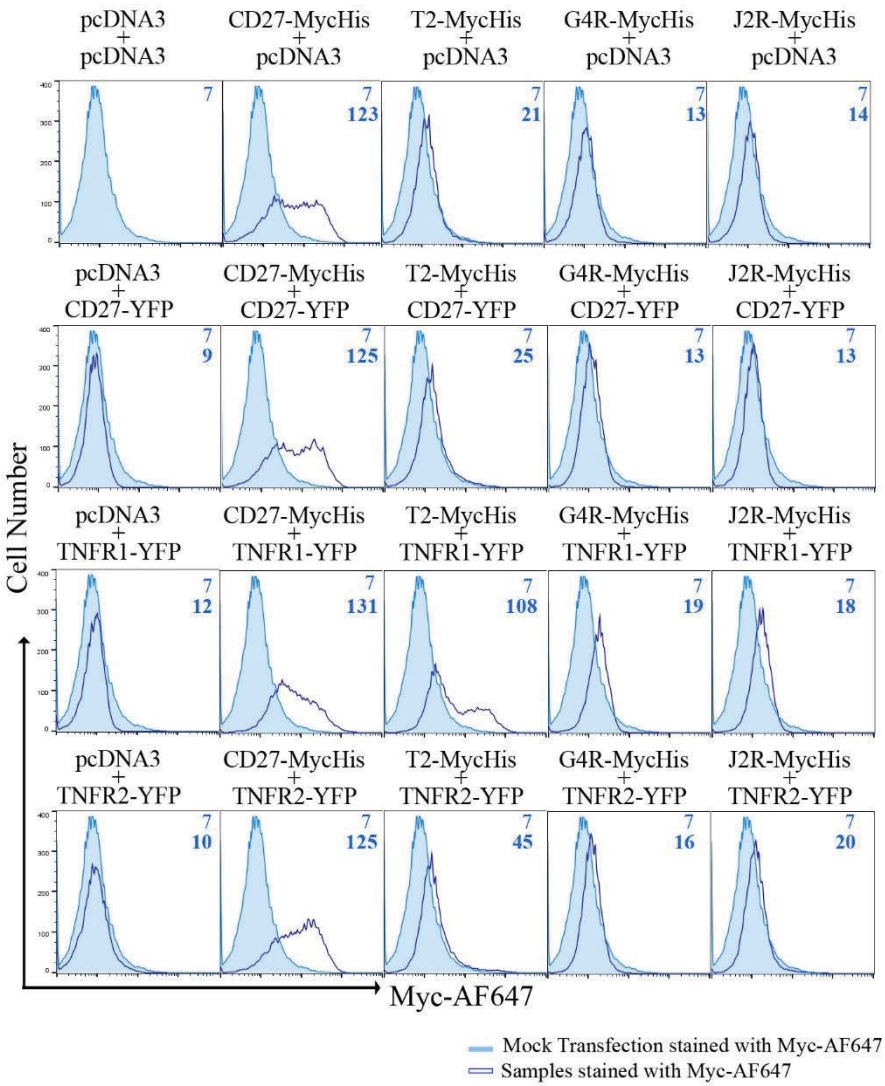

Figure 4.4B Analysis of vTNFR abundance by flow cytometry

The intracellular expression levels of MycHis fusion proteins in transfected 293 HEK cells. Singles cells (R2 sub-population) expressing fusion proteins containing MycHis epitope tags were stained with an anti-Myc-AF647 antibody (48 hours) post transfection. Each sample was compared to Mock transfected samples (light blue, solid histogram) stained with the same anti-Myc-AF647 antibody. Data shown is the median representative sample from three independent transfections. For each sample 30000 events were collected.

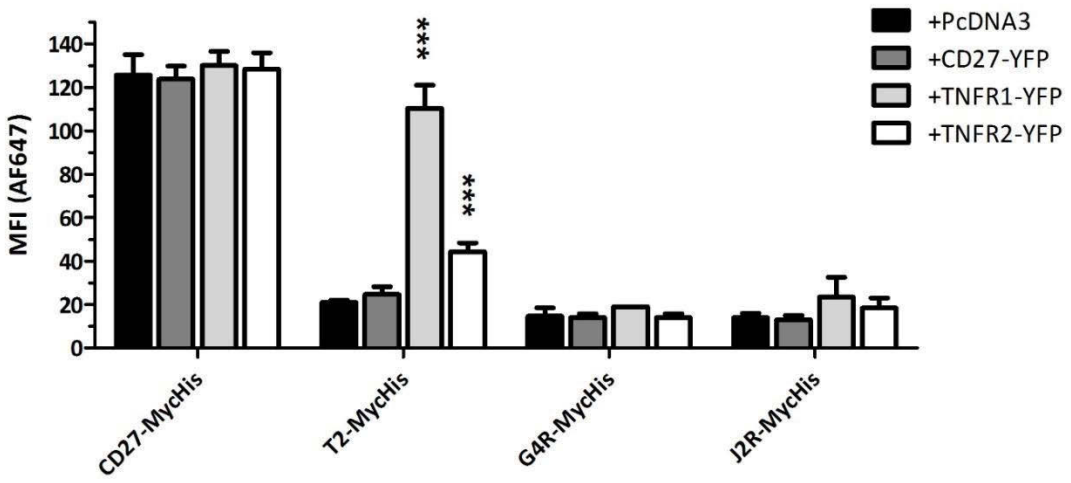

Figure 4.4C Statistical analysis of vTNFR intracellular abundance assay
Representation of means and standard deviations from the independent triplicate transfections for each sample. Means of samples were assessed for differences using a one-way ANOVA then Dunnett's multiple comparisons test. Each sample set of transfections i.e. CD27-MycHis, MYXT2-MycHis, VARG4R-MycHis and MPVJ2R-MycHis, were compared to expression with empty vector (pcDNA3) within the same set (black control column). The level of statistical significance are asterisked. * = $P \leq 0.05$, ** = $P \leq 0.01$, *** = $P \leq 0.001$.

Again a slight increase in MFI was observed in cells co-expressing VARG4R-MycHis and TNFR2-YFP (MFI = 16) or MPVJ2R-MycHis and TNFR2-YFP (MFI = 20). This, however, was not found to be statistically significant (Figure 4C). The Myc-AF657 MFI of CD27-MycHis remained consistent when expressed individually or with TNFR1-YFP or TNFR2-YFP indicating no interaction with the other TNFRSF members.

4.8 Bacterial expression of vTNFRs for crystallography

X-ray crystal structures are often considered the "gold" standard in terms of defining the nature of protein structures and their cognate binding partners. Therefore, no matter what functional assays are performed, an X-ray structure would be highly informative. Therefore the first step to achieve a structure determination is to generate purified

proteins. The only full length structure that has been solved for any of the vTNFRs is vaccinia virus (VV) CRM-E (Graham et al. 2007). Although a high resolution (2.0Å) structure was obtained, much information is still left to be inferred from the previous crystal structures of cellular human TNFR1 and TNFR2, such as binding sites for TNF (Graham et al. 2007). This is largely due to an inability to model TNF complexed with cellular TNFRs because of the hinge movement found in TNFR family members around the "50s loop" of the receptor (Graham et al. 2007; Mascarenhas & Kastner 2012). From sequence data, CRM-E is structurally different from other vTNFRs and only contains 3 CRDs whereas CRM-B and T2 molecules both contain 4 CRDs and a c-terminal SECRET domain involved in chemokine binding (Alejo et al. 2006; Graham et al. 2007; Saraiva & Alcami 2001).

To better understand the interaction of vTNFRs with cellular TNFRs it was planned to obtain the crystal structures of MYXT2, VARG4R and MPVJ2R either in complex with either human TNFR1 or TNFR2. For this a dual bacterial expression system was required and hence pETDuet -1 was utilised to express both vTNFR cDNAs with either TNFR1 or TNFR2 cDNA from the same plasmid vector in bacteria.

4.8.1 Generation of pETDuet.MyxT2, pETDuet.VARG4R, pETDuet.MPVJ2R

To express vTNFR proteins within *E.coli*, the ORF of MyxT2, VARG4R and MPVJ2R were first subcloned into a bacterial expression vector pProex-HTa between restriction sites *EcoR*I and *Xho*I. The pPRoEx plasmid contains an N-terminal His tag with a tobacco etch virus (TEV) cleavage site (Kim et al. 2004) and this created pProHis.MYXT2

pProHis.VARG4R and pProHis.MPVJ2R.pPROEx-HTa (Figure A). pProex-HTa was kindly donated by Dr Coulibaly (Monash University, Melbourne, Australia).

To co-express both vTNFR ORFs with human TNFR1 or TNFR2 in *E.coli,* a dual expression plasmid pETDuet-1 (El Mortaji et al. 2010) (also donated by Dr Coulibaly) was used because it contains two multicloning sites (MCS) and avoids the potential problems of incompatible plasmid expression in bacteria. Therefore plasmids pProHis.MYXT2 pProHis.VARG4R and pProHis.MPVJ2R were generated by PCR amplification using primers pProHis_F and either T2pPro_R, G4RpPro_R, J2RpPro_R (containing the restriction sites) to introduce restriction sites *BspH*I and *Hind*III, in either side of the vTNFR cDNA (Figure A). Thus the PCR fragments were purified and subcloned into pETDuet-1. For this pETDuet-1 was digested with *Nco*I and *Hind*III restriction enzymes and vTNFR ORF PCR fragments of pProHis.MYXT2 pProHis.VARG4R and pProHis.MPVJ2R were ligated into the corresponding sites the MCS1 of pETDuet-1 (Figure A). This cloning strategy was used because it introduced the N-terminal cleavable His tag from pProex-HTa. Thus this approach created plasmids pETDuet.MyxT2, pETDuet.VARG4R, pETDuet.MPVJ2R.

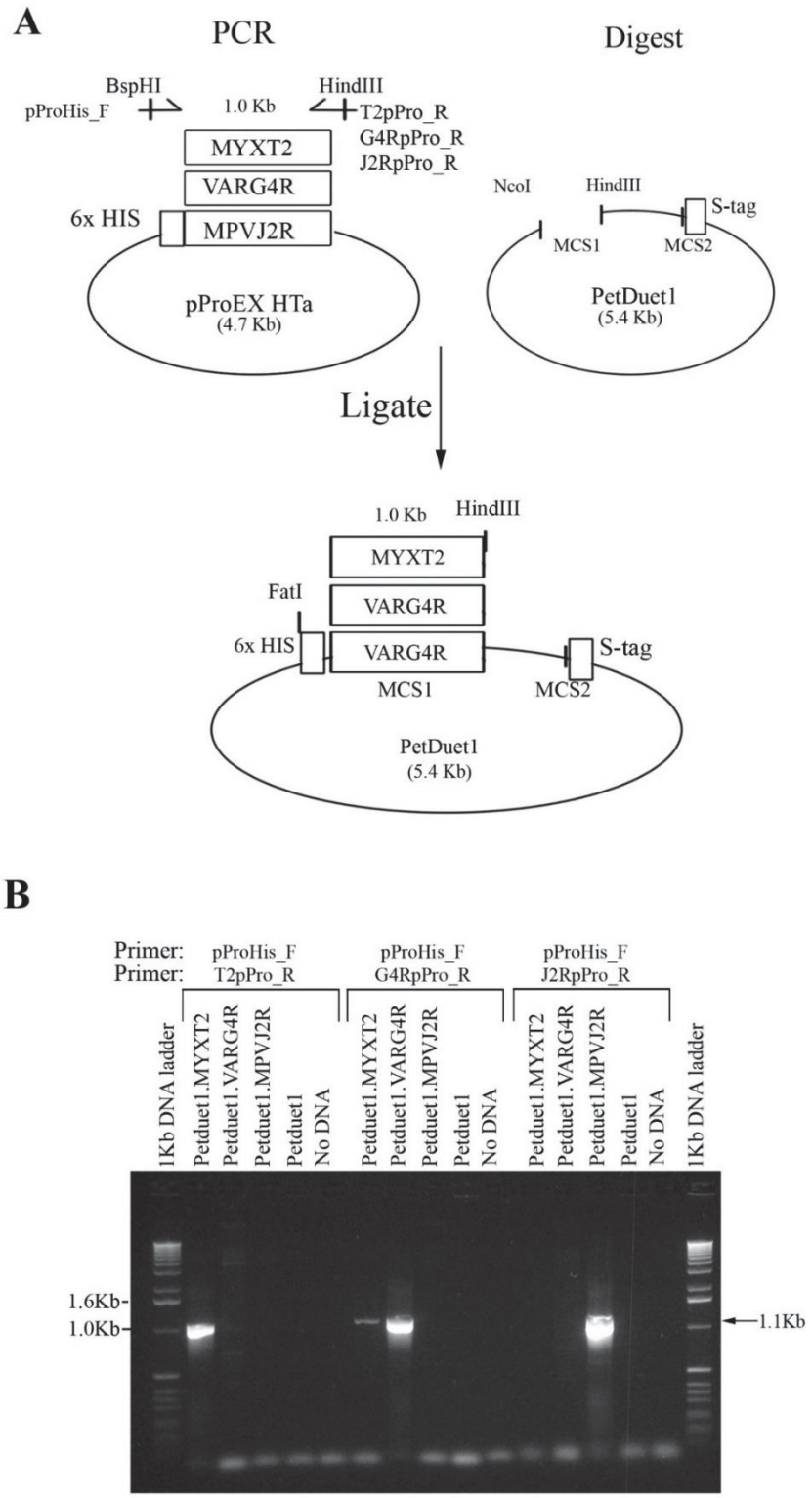

Figure 4.5 Cloning strategy and generation of pETDuet-1 vTNFR plasmids
A) The ORFs of MYXT2, VARG4R and MPVJ2R were first subcloned into the pProEx HTa vector then subsequently PCR amplified using flanking primers to introduce restriction sites BspHI and HindIII. The PCR amplified fragments were then subcloned into the pETDuet-1 vector to introduce the vTNFR ORFs and the N-terminal cleavable His tag in multicloning site 1. B) PCR amplification of each of the newly generated plasmids to confirm the presence of the vTNFR inserts.

To determine if the inserts had been correctly amplified and subcloned, a subsequent PCR of the ORFs were performed using a forward primer pPRoHis_F specific to the vector and a reverse primer specific to the viral ORF. A PCR product of approximately 1kb was produced from each pETDuet.MyxT2, pETDuet.VARG4R, pETDuet.MPVJ2R plasmid as expected (Figure B). An additional faint PCR product of 1kb was observed for pETDuet.MYXT2 using the G4RpPro_R primer (Figure B). This PCR product was not present in the no DNA control or vector only control and was therefore specific to amplification of MYXT2. This was present in repeated PCRs and is possibly due to primer mismatch of the template. All PCR products were of the correct size however and suggested that the subcloning was successful. To confirm the newly generated plasmids each construct was sequenced and double-strand sequence verified them to be correct data not shown.

4.8.2 Generation of pETDuet.TNFR1, pETDuet.TNFR2 plasmids

To generate pETDuet-1 plasmid with human TNFR1 and TNFR2, the cDNAs of TNFR1 and TNFR2 were first subcloned individually into the vector. The TNFR1 and TNFR2 cDNAs from pcDNA3.TNFR1-YFP and pcDNA3.TNFR2-YFP were obtained by plasmid restriction digest *Kpn*I and *Xho*I enzymes. The TNFR1 and TNFR2 cDNAs were then subcloned into the multi-cloning site 2 of pETDuet-1 which also introduced an in-frame C-terminal fusion S-tag. This created pETDuet.TNFR1 and pETDuet.TNFR2 plasmids (Figure A).

After bacterial transformation with the plasmids a number of bacterial clones were obtained. Three clones were selected at random and screened for the insert by restriction digest of the plasmid. For this each plasmid was cut with *Nde*I and *Xho*I enzymes to give an expected DNA fragment size of approximately 1.5kb (Figure B). This

fragment was observed for each double digest, from all bacterial clones (Figure B). Also each single digest resulted in a single linear fragment of approximately 7kb, indicating that each enzyme was only cutting once in the plasmid. Together this information suggested that pETDuet.TNFR1 and pETDuet.TNFR2 had been successfully generated.

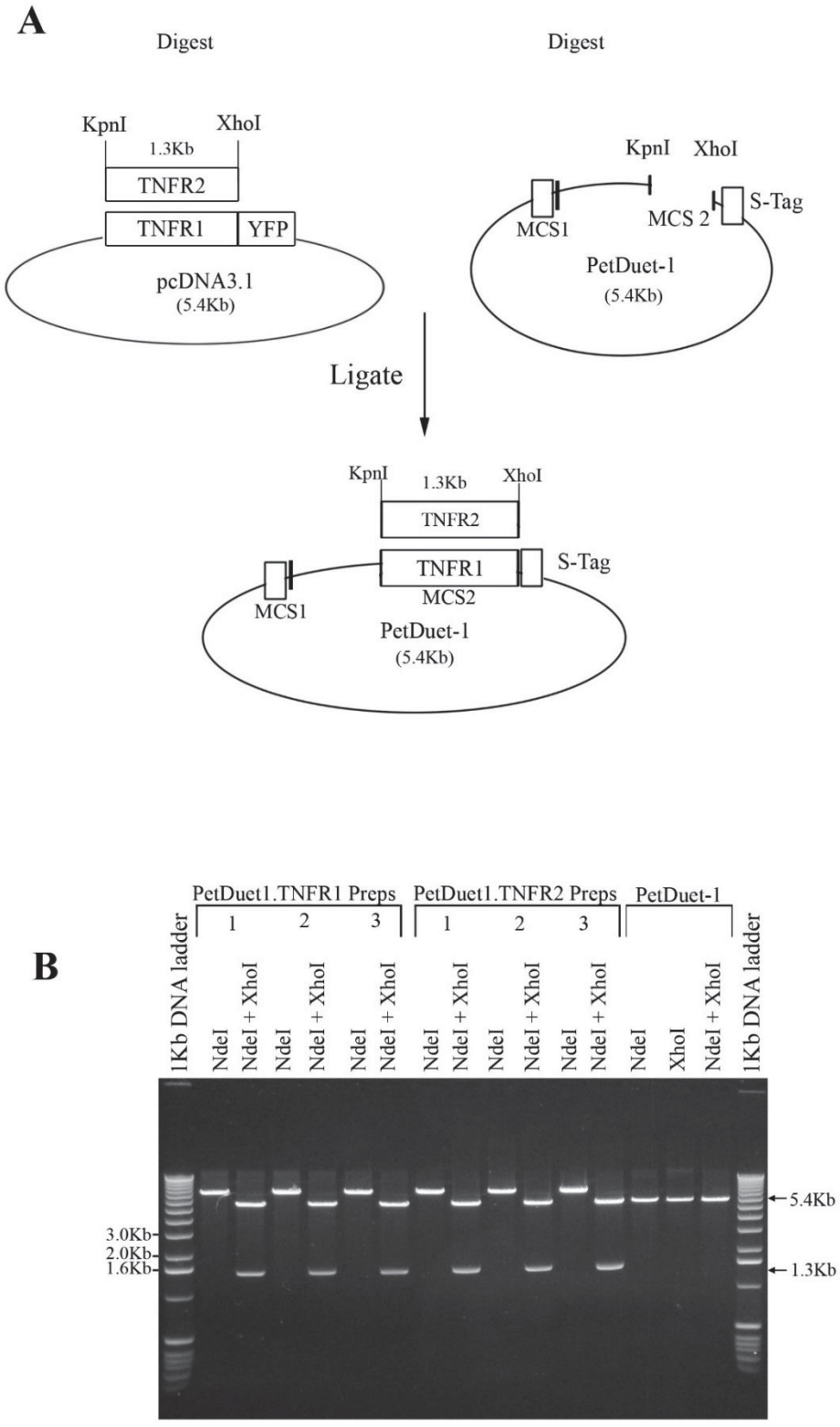

Figure 4.6 Cloning strategy and generation of pETDuet-1 cellular TNFR plasmids

A) The human TNFR1 and TNFR2 cDNAs from the pcDNA3.TNFR1-YFP and pcDNA3.TNFR2-YFP plasmids were subcloned into the restriction sites KpnI and XhoI of pETDuet-1 multicloning site 2. B) Bacterial clones were then screened for the TNFR1 and TNFR2 inserts by restriction double digest with NdeI and XhoI flanking the inserts.

A

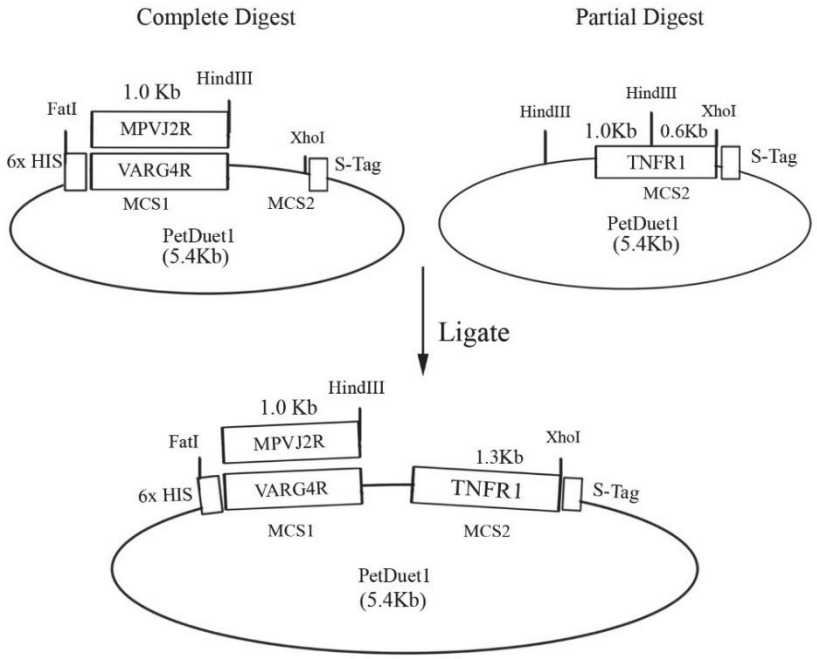

B

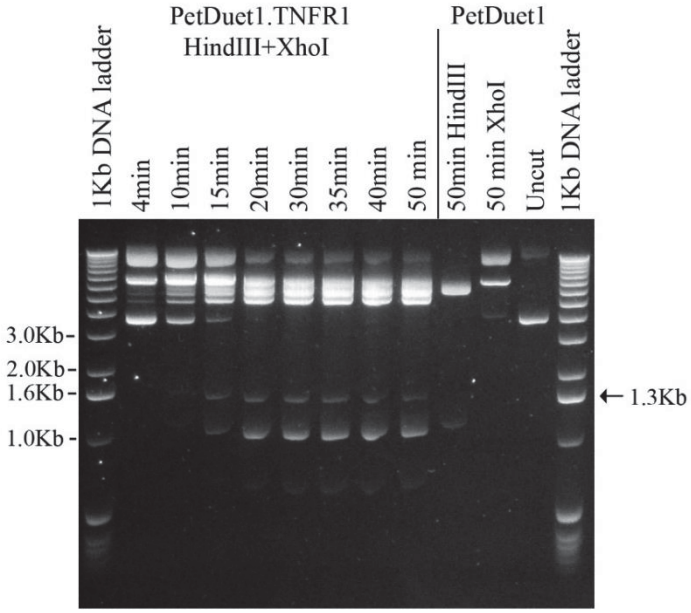

Figure 4.7 Strategy and generation of VARG4R and MPVJ2R co-expression plasmids with TNFR1.

A) The human TNFR1 cDNA from pETDuet.TNFR1 was subcloned into the VARG4R and MPVJ2R pETDuet-1 plasmids via a partial restriction digest with HindIII and XhoI. B) The DNA electrophoresis gel showing the different time points for each of the partial digests of pETDuet.TNFR1.

A single clone for each pETDuet.TNFR1 and pETDuet.TNFR2 plasmid was selected and sent for sequencing to verify the identity of the cDNA insert in each vector (data not shown) which confirmed that pETDuet.TNFR1 and pETDuet.TNFR2 were correctly generated and the TNFR1 and TNFR2 cDNA was cloned in-frame with the S-tag.

4.8.3 Generation of pETDuet.VARG4R.TNFR1, pETDuet.VARG4R.TNFR2, pETDuet.MPVJ2R.TNFR1 and pETDuet.MPVJ2R.TNFR2.

To enable co-expression of VARG4R or MPVJ2R with TNFR1, TNFR1 cDNA was subcloned into pETDuet.VARG4R and pETDuet.MPVJ2R. Due to common restriction sites within the ORFs of VARG4R, MPVJ2R and TNFR1 a different strategy was needed to subclone TNFR1 into the pETDuet-1 plasmids. For this pETDuet.TNFR1 was incompletely digested with enzymes *Hind*III, cutting 5' in the multi-cloning site as well as within TNFR1, and *Xho*I cutting 3' in the MCS i.e. after the TNFR1 cDNA (Figure A). A series of digestions were performed over time to isolate the TNFR1 insert of the correct size of approximately 1.3 kb (Figure B). From the 30 minute digest of pETDuet.TNFR1, the TNFR1 DNA fragment of approximately 1.3kb was isolated purified and subcloned into the multi-cloning site 2 of pETDuet.VARG4R and pETDuet.MPVJ2R. This resulted in the generation of pETDuet.VARG4R.TNFR1 and pETDuet.MPVJ2R.TNFR1 plasmids which were confirmed by DNA sequencing to be correct in sequence (data not shown).

For co-expression of VARG4R or MPVJ2R with TNFR2, pETDuet.TNFR2 was used to sub clone the cDNA of TNFR2 into pETDuet.VARG4R and pETDuet.J2R. pETDuet.TNFR2 was also digested with *Hind*III and *Xho*I, however, although it did not contain any conflicting internal restriction sites as in TNFR1. The cDNA of TNFR2 was then subcloned into the

multi-cloning site 2 of pETDuet.VARG4R and pETDuet.J2R, to create pETDuet.VARG4R.TNFR2 and pETDuet.J2R.TNFR2 (Figure A). A subsequent restriction digest was performed to assess whether TNFR2 had successfully been subcloned using *Hind*III and *Xho*I (Figure B). An additional single digest with *Hind*III and *Xho*I also resulted in a single linear fragment of approximately 8 kb for both pETDuet.VARG4R.TNFR2 and pETDuet.J2R.TNFR2 indicating that each enzyme was cutting once within the construct (Figure B). The *Hind*III and *Xho*I double digest resulted in two fragments, one of approximately 7kb in size corresponding to the pETDuet.VARG4R and pETDuet.MPVJ2R plasmid fragment and a band of approximately 1.3kb in size representing TNFR2 cDNA (Figure B). Taken together these data indicate that pETDuet.VARG4R.TNFR2 and pETDuet.J2R.TNFR2 were successfully generated. This was subsequently confirmed later by double strand sequence verification (data not shown).

4.8.4 Generation of pETDuet.MYXT2.TNFR1, pETDuet.MYXT2.TNFR2

To generate Pet.Duet1.MYXT2 as a co-expression vector with human TNFR1 and TNFR2, The cDNAs of TNFR1 and TNFR2 were subcloned into Pet.Duet1.MYXT2 through restriction digest and forced ligation. For this pETDuet.TNFR1 and pETDuet.TNFR2 plasmids were digested with *Nde*I and *Xho*I to remove the TNFR1 and TNFR2 cDNAs from the vector, and pETDuet.MYXT2 was also digested with *Nde*I and *Xho*I to create compatible ends for ligation. The TNFR1 and TNFR2 cDNA fragments were then ligated into pETDuet.MYXT2 to produce pETDuet.MYXT2.TNFR1 and pETDuet.MYXT2.TNFR2 (Figure A).

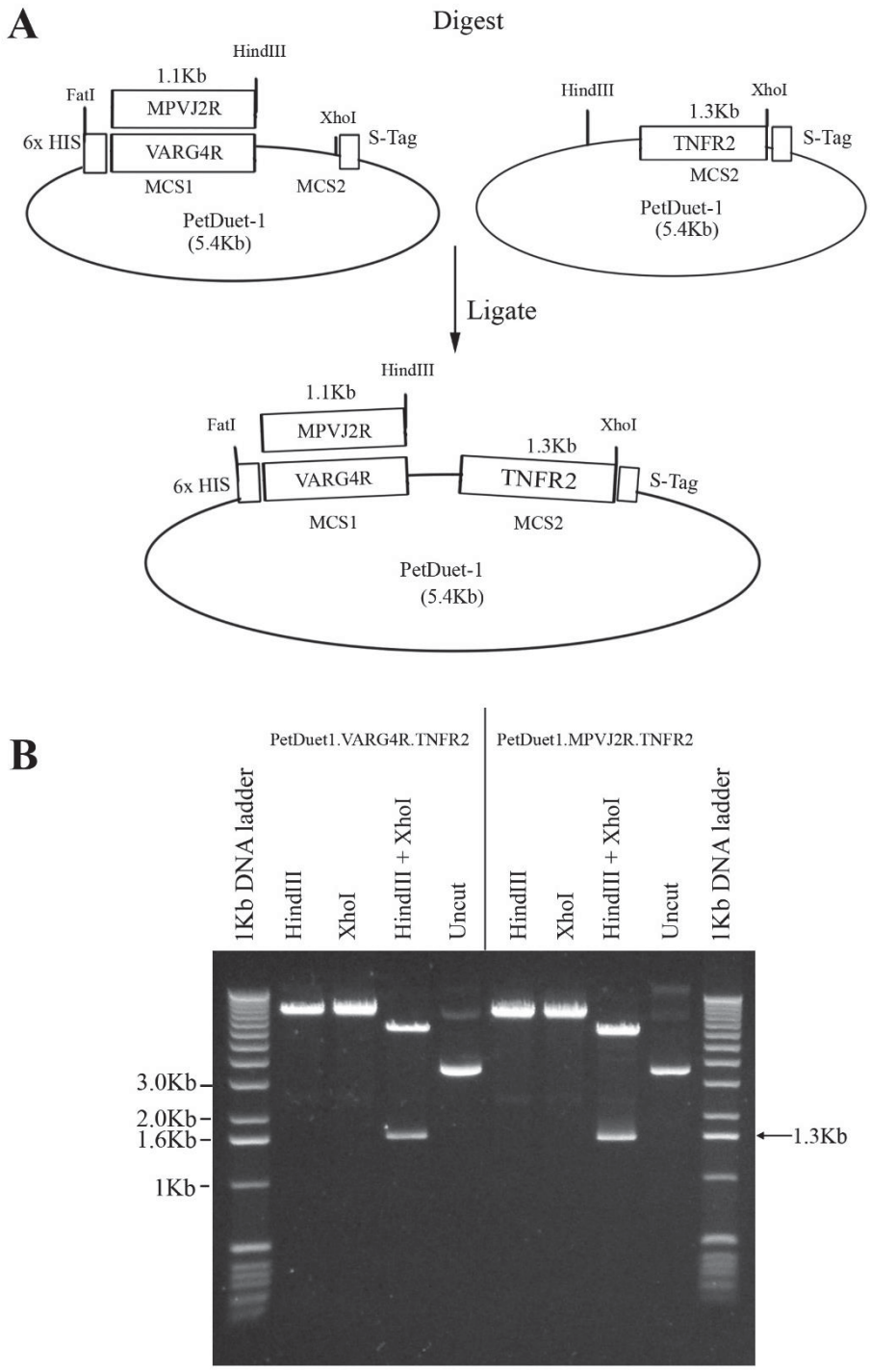

Figure 4.8 Strategy and generation of VARG4R and MPVJ2R co-expression plasmids with TNFR2.

A) The cDNA of TNFR2 from pETDuet-1 was subcloned into the restriction sites *Hind*III and *Xho*I of VARG4R and MPVJ2R pETDuet-1 plasmids. B) Confirmation of TNFR2 cDNA in newly generated VARG4R and MPVJ2R pETDuet-1 plasmids by restriction double digest with *Hind*III and *Xho*I.

The resulting plasmids were re-digested with *Nde*I and *Xho*I to confirm the presence of TNFR1 and TNFR2 (Figure B). An additional single restriction digest was performed with either *Nde*I or *Xho*I to ensure each enzyme was only cutting once within the plasmid represented by the linear plasmid of approximately 8kb in size (Figure B). Thus the presence of TNFR1 and TNFR2 cDNAs in the newly created plasmids, were indicated by the presence of a 1.3kb fragment observed in the *Nde*I and *Xho*I double digest (Figure B). The plasmids were also later confirmed by DNA sequencing, and found to be of correct sequence. These plasmids should permit enable correct dual expression of MYXT2 together with TNFR1 and TNFR2 in *E.coli*.

4.9 Bacterial co-expression of vTNFRs with cellular TNFRs

The co-expression of MYXT2, VARG4R and MPVJ2R proteins together with human TNFR1 or TNFR2 was attempted in BL21 (DE3) *E.coli.* Based on previous expression of CRM-E and the CRM-D SECRET domain proteins for crystallography, it was anticipated that expression of the vTNFRs with cellular TNFRs would be present within bacterial inclusion bodies (Graham et al. 2007; Xue et al. 2011). Therefore a similar method of protein expression based on these previous approaches was chosen. BL21 *E.coli* transformed with the pETDuet-1 dual expression plasmids were inoculated into LB broth containing ampicillin for plasmid selection and grown overnight. The following day cultures were subcultured into 1L of LB broth and further grown to log phase (O.D. 0.8). Isopropyl β-D-1-thiogalactopyranoside (IPTG) is a lactose metabolite that triggers transcription of the lac operon (Bahl et al. 1976) found in the pETDuet-1 vector. IPTG was therefore used to induce protein expression.

A

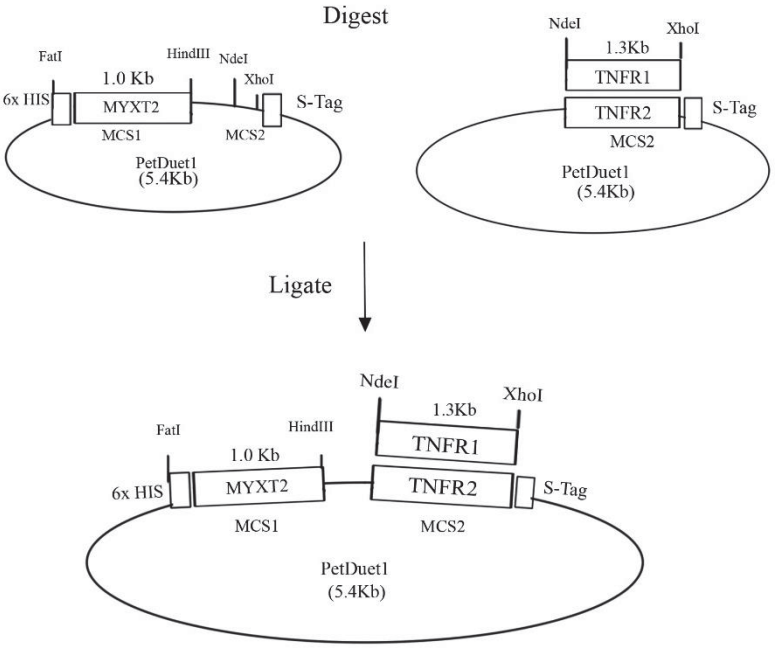

B

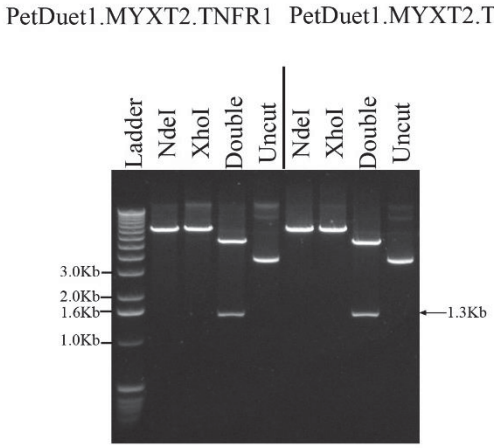

Figure 4.9 Design and generation of MYXT2/TNFR2 and TNFR1 pETDuet-1 co-expression plasmids

A) The cDNA of TNFR1 and TNFR2 from pETDuet-1 plasmids were subcloned into the multicloning site 2 of pETDuet.MYXT2 between *Nde*I and *Xho*I restriction sites. B) Restriction double digest to confirm the presence of the TNFR1 and TNFR2 cDNA in the newly generated pETDuet-1 co-expression plasmids.

When cultures had entered log phase 1mM IPTG was added to the media to induce expression. Protein expression was induced for a further 5 hours at 37°C and then the bacterial cells were harvested by centrifugation and analysed for protein expression by SDS-PAGE and Western blotting. From each bacterial pellet a soluble and insoluble fraction was purified, and analysed for protein expression. For this *E.coli* pellets were first lysed in 50mM NaH_2PO_4, 300mM NaCl, 10mM Imidazole and sonicated. The resultant soluble fraction and the insoluble fraction were separated, boiled in SDS loading buffer and examined by 12% SDS-PAGE. The vTNFR proteins expressed from pETDuet.MYXT2-His, pETDuet.VARG4R-His and pETDuet.MPVJ2R-His were examined by Western blotting using a mouse anti-Penta His antibody (QIAGEN), which was detected with a secondary rabbit anti-mouse alkaline phosphatase conjugated antibody. Unfortunately no protein was detected in either soluble or insoluble fraction (Figure). MYXT2-MycHis protein was expressed in human 293 HEK cells from pcDNA3.MYXT2-Myc/His as a positive antibody control to detect the His epitope and was detected as a band of approximately 50kDa in each western blot (Figure). Since capable of detecting the mammalian expressed MYXT2-MycHis protein, this suggested that the detection method was sufficient to detect the bacterial His fusion proteins being expressed, although the sensitivity of this method to detect Myc-tagged proteins is unclear.

The bacterial co-expression vectors pETDuet.MYXT2.TNFR1, pETDuet.VARG4R.TNFR1, and pETDuet.MPVJ2R.TNFR1 were also tested for expression of His-MYXT2, His-VARG4R and His-MPVJ2R, using the same method as described above, i.e. SDS-PAGE and Western blotting using mouse anti-Penta His antibody and secondary rabbit anti-mouse alkaline phosphatase conjugated antibody. Unfortunately, no proteins were detectable in these blots (data not shown). The same samples were also examined by Western blotting using

a mouse anti-human TNFR1 antibody with a secondary rabbit anti-mouse alkaline phosphatase conjugated antibody to detect any human TNFR1 proteins expressed. Unfortunately no TNFR1 protein was detectable in any of the samples, although the inclusion of a mammalian expressed TNFR1-MycHis protein did detect a 55kDa band, confirming the detection method was adequate to detecting human TNFR1 (Figure).

The analyses was repeated for pETDuet.MYXT2.TNFR1, pETDuet.VARG4R.TNFR1, pETDuet.MPVJ2R.TNFR1, transformed BL21 DE3 clones. Hence, the His-MYXT2, His-VARG4R and His-MPVJ2R proteins were not detectable either in soluble or insoluble fractions as detected with a mouse anti-Penta His antibody and secondary rabbit anti-mouse alkaline phosphatase (data not shown). The SDS-PAGE and Western blot was repeated using a rabbit anti-human TNFR2 and secondary goat anti-rabbit-alkaline phosphatase antibody to detect any expressed TNFR2. However, again only the positive control mammalian expressed human TNFR2 protein was detectable with a band of approximately 70-75kDa (Figure). It was also noticeable that a number of smaller bands present in these samples, which were of unknown identity but appear to be present in the manufacturers product insert (Woclawek-Potocka et al. 2013). These may also have possibly been degradation products, although though protease inhibitors were added to the lysis buffer and samples kept on ice to minimise this occurring.

The absence of vTNFR and cellular TNFR proteins detectable in bacterial lysates, despite a number of approaches, was taken to indicate that additional optimisation steps might be necessary for the expression in *E.coli*. The bacterial induction of proteins under the lac operon control within pETDuet-1 varies with increasing concentrations of IPTG, thus a range of concentrations were tested to optimise expression of viral and cellular TNFR

proteins. Therefore the expression was repeated under the same conditions, this time with a range of IPTG concentrations, increasing from 0.2mM to 1mM IPTG (Figure). The western blots again showed no protein bands detected, despite the varying IPTG concentrations, furthermore this was true in either soluble or insoluble fractions. Thus IPTG did not appear to have an effect on protein expression. Because CRM-E and CRM-D SECRET domain proteins were previously purified from *E.coli* inclusion bodies, it was possible that the proteins may be slightly toxic, or not fold well within *E.coli* (Miroux & Walker 1996). Therefore to avoid a rapid accumulation of protein the incubation period and temperature was optimised. Expression was performed at 20°C, 25°C and 30°C, i.e. to slow the rate of expression, rapid accumulation of protein and permit correct protein folding within *E.coli.* Regardless of all conditions tested again no protein was again detected from either soluble or insoluble fractions (data not shown). Finally the induction time was also varied from 4 hours to overnight at each temperature, but again protein was still not detectable at each time point (data not shown). Lastly another parameter that may help avoid accumulation of toxic proteins or incorrectly folding proteins, is to optimise the culture density at which induction of protein expression occurs. *E.coli* cells were therefore induced at a series of growth densities ranging from O.D. 0.5 to O.D. 1. However no protein expression was detected (data not shown).

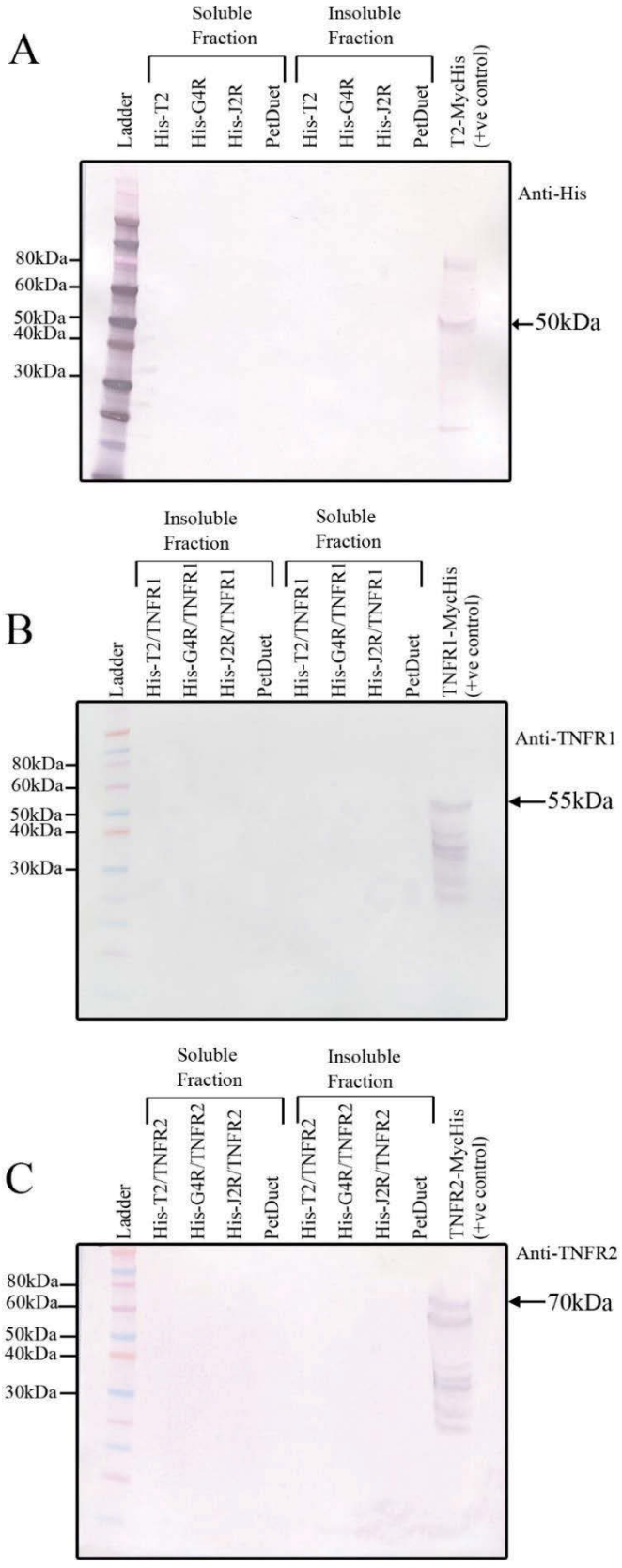

Figure 4.10 Detection of bacterial expressed vTNFR proteins

Screening for bacterial expressed vTNFRs and cellular TNFRs via 12% PAGE and Western blotting from insoluble and soluble bacterial fractions from dual expression pETDuet-1 vectors. A) Bacterial soluble and insoluble fractions were screened using an anti-Penta His antibody, B) anti-human TNFR1 antibody and anti-human TNFR2 antibody

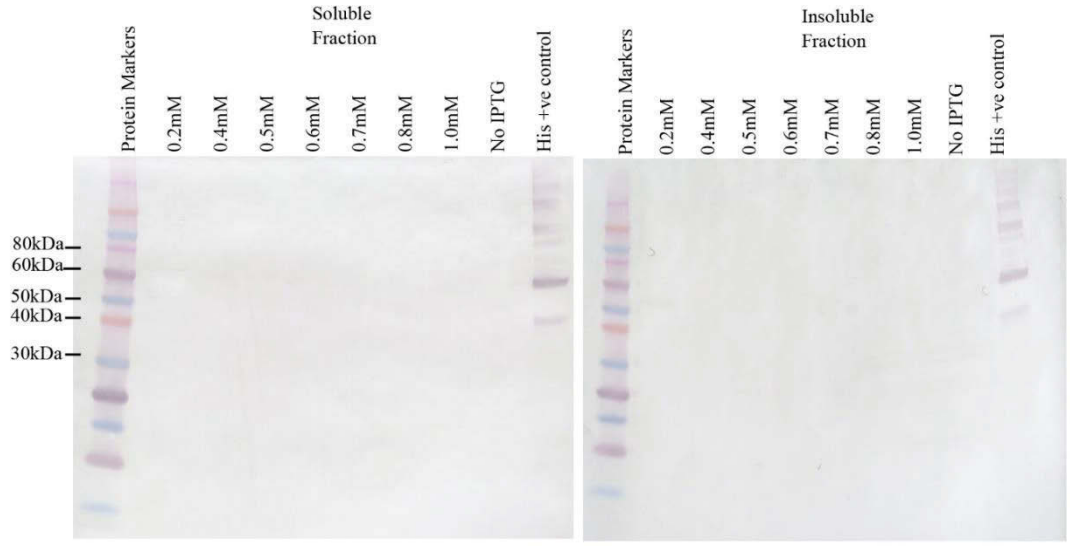

Figure 4.11 Optimisation of IPTG concentrations for bacterial expression
The bacterial induction of expression by IPTG was titrated from 0.2mM to 1mM then screened for the presence of vTNFR protein by 12% PAGE and Western blotting. Blots were probed using an anti-Penta His antibody and secondary rabbit anti-mouse alkaline phosphatase. Both soluble and insoluble lysates were screened from the expression. A purified recombinant His tagged protein (10ng loaded) was used as a positive antibody control.

Finally, in case the vTNFRs and cellular TNFRs were poorly expressed, and to ensure maximal detection of any expressed protein, each bacterial fraction was purified and concentrated. For this soluble fractions were harvested and purified using nickel agarose columns. Insoluble fractions were solubilised in 6M guanidine-HCl then dialysed against a reducing concentration of desalting buffer containing guanidine (25mM Tris-HCl pH 8, 5mM $CaCl_2$, 5mM L-cysteine and 0.9M guanidine). The fraction was then further concentrated using protein size-exclusion spin columns and the samples were loaded and run by SDS-PAGE and Western blotting. Again, no protein was detectable from either bacterial fraction for any of the pETDuet-1 constructs (Figure). Therefore despite these attempts no vTNFR or cellular TNFR proteins were able to be produced in bacteria at this time. Unfortunately this precluded the generation of any structural data.

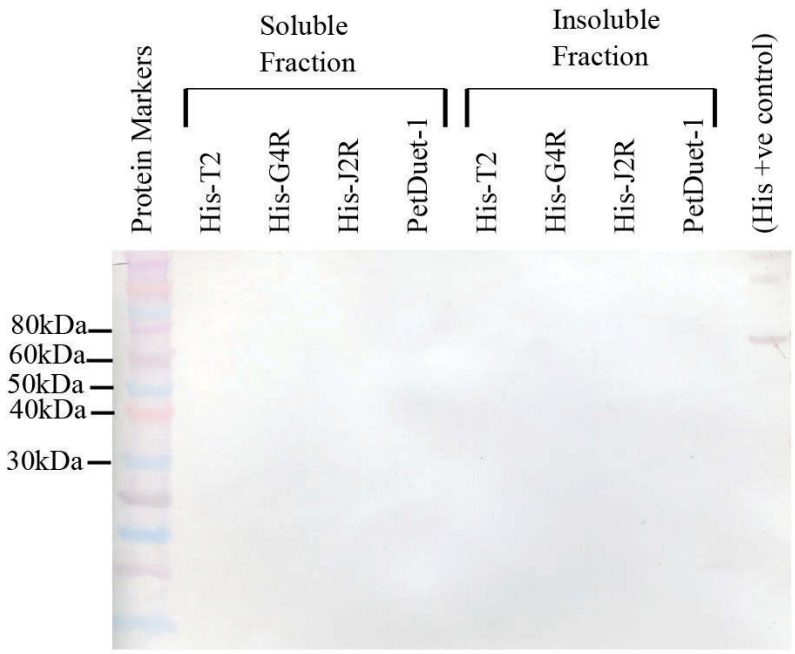

Figure 4.12 Screening of concentrated bacterial expressed vTNFRs
The soluble and insoluble fractions from the bacterial expression of vTNFRs from 1L cultures was purified by NI-NTA column affinity purification (soluble fraction) and Inclusion body purification (insoluble fraction). The resulting fractions were then further concentrated using spin columns and screened for vTNFR protein by 12% PAGE and Western blotting using an anti-Penta His antibody. A purified recombinant His tagged protein (10ng loaded) was used as a positive antibody control.

4.10 Discussion

To examine the interaction of MYXT2, VARG4R and MPVJ2R with human TNFR1 and TNFR2, each vTNFR were generated as both CFP and YFP C-terminal expression plasmids. These expression plasmids were then to be used in functional assays for the remainder of the chapter to characterise the effects of vTNFRs on TNFR biology. The presence of a fluorescent protein is an especially useful tool for the detection of a protein of interest, and can be used in a number of various assays to determine a proteins distribution, dynamics, history and association with other proteins (Snapp 2005). A major disadvantage of using fluorescent fusion proteins such as CFP and YFP is that are very large proteins,

and due this may affect functional domains in proteins by either disrupting folding of the protein or blocking functional sites. From published data on the use of fluorescently tagged human TNFR1 and TNFR2, it is known that the placement of CFP and YFP fusion tags to the N-terminus has the most significant effect disrupting TNFR self-association and binding of TNF (Chan et al. 2001). Placement of the fusion proteins at the C-terminus, however did not affect human TNFR signalling (Chan et al. 2001). Further to this it is known that mutations or alterations to CRD1 in TNFRs especially destabilises the structure of the receptor and also disrupts the formation of competent ligand receptors (Branschädel et al. 2010). As vTNFRs share a high homology to TNFRs in the N-terminal extracellular region (Graham et al. 2007; Sedger et al. 2006), it was hypothesised that C-terminal fusion proteins would have much more minimal affect to vTNFR function. This is consistent with mutational analysis of MYXT2 which showed that truncation of the up to half of the C-terminus had no effect on TNF binding and neutralisation, whereas deletions in any of the first 3 CRDs abolished TNF binding (Schreiber & McFadden 1996).

Because all of the functional assays in this thesis chapter were performed by transient transfections it was important to keep consistency in proteins expression and allow comparisons across experiments. For this a number of careful measures were implemented to keep consistency between experiments. All of the expression plasmids used for the functional assays of the vTNFRs and cellular TNFRs were expressed from the same backbone plasmid, pcDNA3. Thus the same regulatory elements such as the strong constitutive CMV promoter and bovine growth hormone poly A tail. The pcDNA3 CMV promoter, is a strong

constitutive and was used to induce high levels of protein expression (Wilkinson & Akrigg 1992). The CMV promotor was selected to best replicate viral expression, as viral replication favours viral protein expression and the shutdown of host protein synthesis (Fields, Knipe & Howley 2007). High level protein expression was also used to specifically induce cellular TNFR1-induced cell death within transfected cells (Boldin et al. 1995; Haridas et al. 1998). Furthermore because co-transfection assays were utilised, same amount of DNA for each plasmid and total amount of DNA was transfected within each sample to keep expression consistent. Despite this, it was observed in initial microscopic observations that the vTNFRs were less expressed compared to the cellular TNFRs. This was also evident in the flow cytometry data where vTNFR expression was significantly less, skewing the CFP vs YFP dot plots when co-expressed with cellular human TNFR1 or TNFR2. This may have largely been contributed by the fact that the vTNFRs are secreted as well as intracellular proteins (Hu, Smith & Pickup 1994; Schreiber, Rajarathnam & McFadden 1996), whereas cellular TNFRs are largely cell surface or intracellular. TNFR1 and TNFR2 are known to exist as soluble receptors, whether soluble TNFRs are a consequence of certain disease states, infection and the release from apoptotic cells, or rather apart of TNFR homeostasis is still unclear (Hawari et al. 2004; Xanthoulea et al. 2004). Regardless of the amount of expression however it was observed that when cells were transfected with both CFP and YFP, both plasmids were transfected into the same cell shown by the linear relationship in the flow cytometry data.

The cell death pathways for TNFR1 are well described and occur largely through the activation of caspases leading to DNA degradation and ultimately apoptosis

(Liu et al. 1996; Micheau & Tschopp 2003). The initial signalling complex requires the internalisation of TNFR1 and the subsequent recruitment of TRADD, FADD and caspase-8 to form a death inducing signalling complex (DISC) (Schneider-Brachert et al. 2004). The DISC then subsequently activates the caspase cascade involving caspase-8, caspase-3, caspase-9 and eventually caspase activated DNAse (Enari et al. 1998). MYXT2 is known to associate with TNFR1 and TNFR2 to subvert TNFR-induced cell death (Sedger et al. 2006). Despite this, little is known about how, where or even whether intracellular subversion of TNFR-induced cell death occurs for other poxviral vTNFRs. In this thesis chapter it was found that all of the vTNFRs, MYXT2, VARG4R and MPVJ2R were able to protect human 293 HEK cells from TNFR1-induced cell death. Like MYXT2 this interaction appears to be non-species specific for MPVJ2R, as it is not found to bind soluble human TNF but protect against human TNFR1-induced cell death (Gileva et al. 2006). With this evidence the mechanism of intracellular inhibition of TNFR1-induced cell death could be characterised further for each of the vTNFRs. The specific TNFR1 cell death pathway inhibited by MYXT2, VARG4R and MPVJ2R is still unknown but it is likely to be through the main activation of caspases. While signalling pathways were not investigated in this thesis, future work could include Western blotting for active caspase-8, live cell imaging using probes for molecules like TRADD, FADD and CAD or 2D mass spectrometry to similarly identify molecules involved in the pathway.

Using the evidence that MYXT2, VARG4R and MPVJ2R inhibit human TNFR1-induced cell death, whether VARG4R and MPVJ2R also associate with TNFR1 and TNFR2 to subvert TNFR-induced cell death was examined. Co-

immunoprecipitation and Western blotting is widely considered the gold standard in providing evidence for protein-protein interactions (Masters 2004). However because protein-protein interactions are very diverse the set of conditions are often very difficult to determine for each co-immunoprecipitation (Masters 2004), and furthermore no specific antibodies are available for VARG4R or MPVJ2R make this techniques even more difficult. Therefore as an alternative, an assay by flow cytometry was developed to indirectly test whether each of the vTNFRs was interacting with human TNFR1 and TNFR2 intracellularly. As each of the vTNFRs is secreted (Gileva et al. 2006; Sedger et al. 2006), It was hypothesised that if an intracellular interaction occurred between TNFR1 and TNFR2 and the vTNFRs, then more vTNFR may be retained rather than secreted with overexpression of TNFR1 or TNFR2. Therefore an increase in detection of each of the vTNFRs via a Myc epitope tag would be expected within the cell. The detection of the Myc epitope on the vTNFRs was also found to detect background endogenous Myc within the human cell lines. However this did not impede vTNFR detection as overexpressed Myc-tagged proteins were clearly detectable of this endogenous level. It was found that co-expression of TNFR1 and TNFR2 increased the detection of MYXT2 suggesting an increase of intracellular MYXT2. A slight increase in the detection of VARG4R and MPVJ2R was also detected however this was not considered statistically significant despite these proteins inhibiting TNFR1-induced cell death. It was unclear why this discrepancy was observed between MYXT2, VARG4R and MPVJ2R but could possibly be due to differing targets in the TNFR1 cell death pathway or even differences in the binding on/off rates with TNFR1 and TNFR2. The determination of where this interaction occurs would also provide further clues into how each

of the vTNFRs inhibits TNFR1-induced cell death. As TNFR1-induced cell death requires internalisation (Schneider-Brachert et al. 2004) vTNFRs may prevent TNFR1 internalisation or rather further downstream targeting specific cell death pathway molecules such as caspases. Time permitting this could be examined further by using specific cell death pathway inhibitors such as carbobenzoxy-valyl-alanyl-aspartyl-[O-methyl]- fluoromethylketone (Z-VAD-FMK) or overexpression of viral inhibitors such as CRM-A, an inhibitor of caspase proteases (Tewari et al. 1995). To also test whether the kinetics of vTNFR binding differs, future work could utilise methods such as surface Plasmon resonance or thermophoresis by virtue of the already generated CFP and YFP fusion proteins (Zillner et al. 2012). An increase in the protein on/off rates would make detection of intracellular retention difficult as protein may still be secreted and hence may explain the slight but not significant increases in VARG4R and MPVJ2R detection. Additionally an IP western blot may be required to confirm interactions of VARG4R and MPVJ2R with cellular receptors. This data confirms the previous evidence for MYXT2 inhibiting TNFR1-induced cell death (Sedger et al. 2006). In addition, this is the first evidence that shows VARG4R and MPVJ2R subverting TNFR1-induced cell death intracellularly, although whether this also occurs by associating with the receptor is still unclear.

To further characterise the association of vTNFRs with TNFR1 and TNFR2, it was planned to obtain crystal structures of MYXT2, VARG4R and MPVJ2R in complex with TNFR1 and TNFR2. To date the only structure of a vTNFR cellular TNFR homologue is the structure for Vaccinia virus CRM-E (Graham et al. 2007). A crystal structure for the 2L proteins from Tanapox virus has also been solved,

however these vTNFRs, although bind TNF, do not resemble cellular TNFRs and are more structurally related to the major histocompatibility complex (MHC) class proteins (Yang, West & Bjorkman 2009). Therefore the production of a crystal structure for either MYXT2, VARG4R or MPVJ2R would reveal a wealth of structural information as well as insight into binding sites of TNF, LTα and TNFRs. To obtain crystal structures, bacterial expression vectors were used to attain purified protein. Although mammalian expression of the proteins had already been achieved in this thesis, it was uncertain how modifications such as glycosylation would affect the formation of crystals. The structure and heterogeneity of carbohydrates in glycosylation prevents the formation of crystals forming (Chang et al. 2007). Each of the vTNFRs are expressed in mammalian hosts and are predicted to be extensively glycosylated (Loparev et al. 1998; Schreiber & McFadden 1996)(Sherwood, data not shown). In addition the use of a bacterial expression vector allows hi-yield expression over mammalian expression systems.

For bacterial expression ORFs of MYXT2, VARG4R and MPVJ2R were cloned into a bacterial expression vector, PetDeut-1. The advantage of this particular expression vector is that it allows dual expression of proteins from the same vector. It is unknown if stable heterodimers or heterocomplexes of vTNFRs with TNFR1 or TNFR2 form by mixing purified proteins, therefore to best simulate the co-expression of vTNFRs with TNFR1 and TNFR2 the co-expression vector pETDuet-1 was used to simultaneously co-express each vTNFR and cellular TNFRs. However as part of the cloning strategy each of the vTNFR ORFs were first subcloned into pProex-HTa containing an N-terminal cleavable His tag. The

subsequent subcloning from pProex-HTa into pETDuet-1 created the vTNFR pETDuet-1 plasmids to contain an N-terminal cleavable His tag from pProex-HTa. With the ability to remove the fusion tag this would generate the most likely representative crystal structures for each of the vTNFRs as well as allow easy purification of each vTNFR protein via nickel agarose affinity purification. Each of the vTNFRs was successfully cloned into pETDuet-1 into the multi-cloning site 1 together with either human TNFR1 or TNFR2 in multi-cloning site 2. Each of the plasmids were then double strand sequence verified to be correct and in-frame.

First attempts to express proteins from the pETDuet-1 dual expression plasmids were performed following the same methodology as previously used to express CRM-E and the CRM-D SECRET domain (Graham et al. 2007; Xue et al. 2011). However examination by SDS-PAGE and Western blotting using a rabbit anti-Penta His antibody and secondary goat anti-rabbit-alkaline phosphatase antibody revealed no protein was detected from both E.coli lysates and pellets. This was repeated with no detection of expressed protein from any of the vTNFR and TNFR1 or TNFR2 expression plasmids.

Both soluble and insoluble bacterial lysates were examined as it was not known whether the vTNFRs or cellular TNFRs would be secreted or contained in inclusion bodies. The human TNFR1 and TNFR2 receptors are both transmembrane proteins meaning their structure is incorporated into lipid bilayer. The previous expression and crystallisation of human TNFR1 and TNFR2 is only of the extracellular domain, largely to avoid problems associated with the hydrophobic domains preventing crystallisation (Mukai et al. 2010; Naismith et

al. 1996). Because the protein expression was of full length TNFR1 and TNFR2 it was likely that these receptors would be found in inclusion bodies. The vTNFRs can be found as both secreted and intracellular molecules so it was also unknown which bacterial fraction that may be contained in. In previous expression however both CRM-E and the SECRET domain of CRM-D were found in inclusion bodies (Graham et al. 2007; Xue et al. 2011). As CRM-E, CRM-D SECRET domain and both human TNFRs had been previously expressed in bacteria it was reasoned that each MYXT2, VARG4R and MPVJ2R expression in *E.coli* should be possible. Furthermore the same methodology was followed for Vaccinia CRM-E and Ectromelia virus CRM-D SECRET domain (Graham et al. 2007; Xue et al. 2011). Unfortunately why no expression was detectable from any of the vectors was unable to be determined within this study despite numerous attempts at optimising the expression conditions.

Because CRM-E and the CRM-D SECRET domain were both purified from insoluble inclusion bodies, it was hypothesised that the vTNFRs attempted to be expressed may be causing toxicity to the *E.coli* through rapid accumulation or misfolding. The addition of IPTG to the media of BL21 DE3 *E.coli* induces the overexpression of protein under control of the T7 promoter (Fernandez-Castane et al. 2012). Where the protein produced causes stress to the host *E.coli*, the plasmid expressing the recombinant protein can become unstable and lost, and E.coli not containing the plasmid will rapidly overgrow due to selection (Saida et al. 2006). This is especially true in cultures containing ampicillin as the *E.coli* will secrete beta-lactamase quickly accumulating in the media and breaking down the ampicillin, removing the selective pressure (Korpimaki, Kurittu & Karp 2003).

The rate of protein production is not dose-dependent, especially in the production of misfolded proteins (Fernandez-Castane et al. 2012). Therefore the optimal concentration required for protein expression was determined by titration of IPTG to increase the protein yield. Despite titrating the concentration of IPTG, from the lowest recommended concentration of 0.2mM up to 1mM (Fernandez-Castane et al. 2012) no protein was still detectable by SDS-PAGE and Western blotting.

Protein toxicity can occur due to the rapid overproduction of protein which may interfere with essential cellular processes (Baneyx & Mujacic 2004; Saida et al. 2006). Although the vTNFRs or cellular TNFRs should have no function in *E.coli*, the rapid production and accumulation can lead to protein misfolding and formation of inclusion bodies, stressing the homeostasis of the cell (Baneyx & Mujacic 2004). A method to overcome this is to slow the production of recombinant protein by reducing the temperature of the induction period (Dumon-Seignovert, Cariot & Vuillard 2004). For this, induction was carried out at less than optimal temperatures to slow growth and tested at 20°C, 25°C and 30°C. unfortunately no protein was again detectable from any of the expression clones for MYXT2, VARG4R and MPVJ2R with TNFR1 or TNFR2.

It was uncertain whether the Western Blot detection method was sufficient to detect the recombinant proteins. Therefore to maximise detection the *E.coli* cultures were scaled up to 1L broth cultures, then purified increase to protein yield. The soluble fractions were purified using a nickel agarose pull down to bind the N-terminal His tags contained on the vTNFRs. The insoluble fraction,

potentially containing inclusion bodies, were solubilised in 6M guanidine then refolded and concentrated using protein spin columns. Again no protein was detectable from each of the fractions by Western blotting and antibody detection of the N-terminal his tags. In terms of low sensitivity of the His antibody, if small amounts were present from the 1L cultures, it would be expected protein should be detectable from a 1L culture. However this was not the case, and the positive His antibody controls used for each of the samples were sufficiently detected. This led to the conclusion that no protein was being expressed from any of the generated pETDuet-1 expression vectors. As each of the plasmids were double strand sequence verified and in-frame containing intact transcription elements such as a promoter, Shine-Delgarno sequence and terminator sequence there was no obvious reason why expression was not occurring (Wang et al. 2012). Furthermore plasmids were re-cloned multiple times to ensure mutations outside of the subcloned sequences were not affecting expression. None of the reasons provided give reason for no bacterial expression at this present time, despite following similar methodology as previous reported.

Unfortunately without any purified protein for MYXT2, VARG4R, MPVJ2R and the human TNFR1 and TNFR2 no protein could be purified for X-ray crystallography. However alternate structural methods in the following chapter were utilised to gather more information of the interaction between vTNFRs and cellular TNFRs.

Chapter 5

Structural characterisation of TNFR interactions

Chapter 5

5.1 Introduction

In chapter 4 it was shown that vTNFRs MYXT2, VARG4R and MPVJ2R all possessed the ability to protect 293 HEK cells against human TNFR1 induced cell death. Because almost all vTNFRs share a high homology with cellular TNFRs within the PLAD domain (Figure 5.1) it is hypothesised that the inhibition of TNFR-induced cell death occurs through the association of the vTNFRs with cellular TNFR1 and TNFR2 requiring an intact PLAD (Sedger et al. 2006). In support of this, the deletion of the PLAD within MYXT2 abolishes the ability of MYXT2 to associate with TNFR2 and vastly diminishes the ability to associate with TNFR1 (Sedger et al. 2006). However, very little is still known about how MYXT2 protects cells from TNFR induced cell death and details of the mechanism.

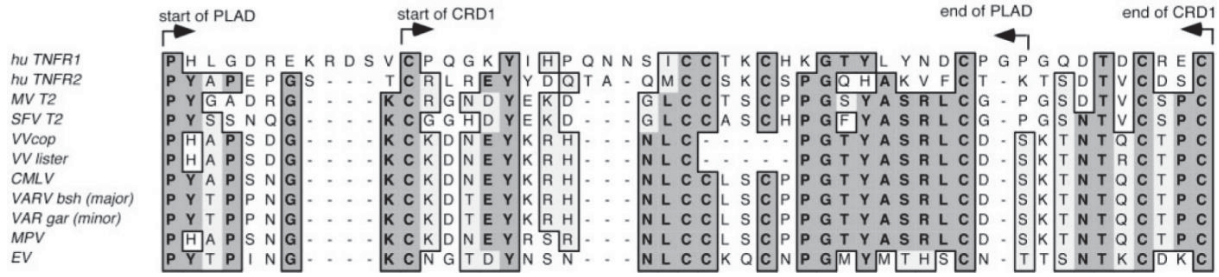

(Sedger et al. 2006)

Figure 5.1 PLAD alignments in poxviral and cellular TNFRs
vTNFR sequence PLAD alignments from Myxoma virus (MV T2), Shope fibroma virus (SFV T2), Vaccinia virus strains Copenhagen (VV cop) and Lister (VV Lister), camel pox virus (CMLV), Variola virus major strain Bangladesh (VARV bsh major), Variola virus minor strain Garcia (VAR gar minor), Monkeypox virus (MPV) and Ectromelia virus (EV) against human TNFR1 and TNFR2 PLAD sequences.

Human TNFR1 is well known to signal at the cell surface (Shih et al. 2011) as well as from intracellular endocytic vesicles referred to as “receptosomes” (Schneider-Brachert et al. 2004; Schutze, Tchikov & Schneider-Brachert 2008). However, even though the

signalling pathways for TNFR1 and TNFR2 are well described (Aggarwal 2000; MacEwan 2002) it is still uncertain how the activation of TNFR signalling occurs. Increasing evidence supports the model of TNFRs forming higher order complexes and aggregates that increase the ability of the receptor molecules to recruit adaptor signalling proteins such as TRAF2 and FADD (Boschert et al. 2010; Mascarenhas & Kastner 2012; Mukai et al. 2010). It has also been recently published that TRAPS mutations may disrupt these networks or aggregates, which possibly results in a less efficient signalling complex (Lewis, Valley & Sachs 2012). Cellular TNFRs are predicted to form a lattice-like network in association with TNFα in a 3:1 or 2:1 stoichiometry (Lewis, Valley & Sachs 2012). As TRAPS mutations are predicted to alter the conformation of the receptor, it was predicted for the R92Q mutation (a more benign mutation) that these structural changes cause stress within the lattice and disrupt its formation (Lewis, Valley & Sachs 2012). For TRAPS mutations involving residues such as cysteines within the PLAD domain, this effect may be exacerbated. The question relevant to this PhD project, however, is whether vTNFRs have the ability to disrupt these cellular TNFR lattice networks and whether vTNFRs function by associating with TNFRs, integrating amongst the network thereby disrupting signalling of cellular TNFRs. Whether viral subversion of TNFR signalling occurs by interacting with these complexes is yet to be determined.

Försters resonance energy transfer, sometimes referred to as fluorescence resonance energy transfer (FRET), is a powerful technique for determining the molecular proximity of molecules up to 10nm or 100 angstroms (Figure 5.2) (Sekar & Periasamy 2003). The principle of FRET is based on the phenomenon that molecules with overlapping excitation and emission spectra have the ability to excite one another (Figure 5.2). FRET is commonly used to map protein-protein interactions however by strategically labelling

proteins with fluorophores it can be used to determine structural features and stoichiometry's of protein complexes (Bujalowski & Jezewska 2012). For example, because TNFR1 was found as both a parallel and anti-parallel dimer (Naismith et al. 1996), FRET could be used to determine which conformation allows for a FRET signal when expressed as a TNFR-CFP/YFP fusion protein (Figure 5.3). Because the energy transfer between molecules is inversely proportional to the sixth power of the distance between donor and acceptor, FRET is extremely sensitive to small changes in donor-acceptor distance (Berney & Danuser 2003). The other major advantage of FRET is that it allows for the determination of molecular interactions within live cells in real time (He et al. 2003; Trón et al. 1984).

By pairing FRET with technologies such as flow cytometry you can analyse thousands of cells individually per second, and get a representation of protein-protein interactions over an entire cell population or sample. Furthermore gating allows analysis in subpopulations of cells within the sample. A positive or negative result from FRET can be difficult to define without the appropriate controls and correct flow cytometer detection set up. This is because the overlap in fluorescence spectra of the acceptor and donor (which permits FRET) also contributes to the detection of false positive FRET due to fluorescence cross bleeding. (Bujalowski & Jezewska 2012). Therefore in order to obtain an accurate FRET result there is a need to optimise the method for a given flow cytometer instrument, using a number of controls to ensure FRET detection is accurate and robust.

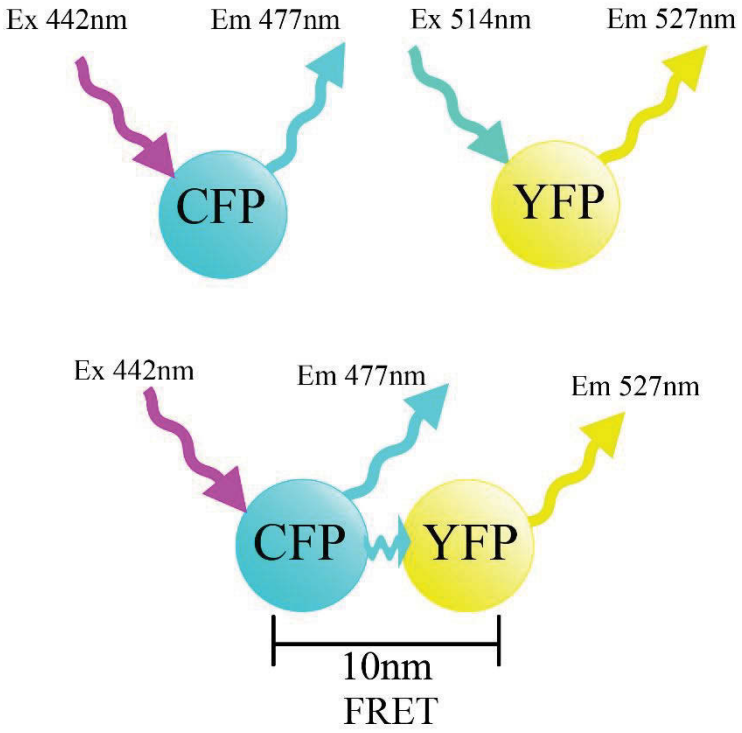

Figure 5.2 FRET excitation of CFP and YFP fluorphores
CFP contains a maximal excitation peak at 442nm which subsequently causes an emission at 477nm. YFP has a maximal excitation peak at 514nm and causes an emission maxima at 527nm. When CFP and YFP molecules are within 10nm distance, the excitation of CFP at 442nm again causes an emission maxima at 477nm, however some this energy can be transferred to excite YFP and cause emission from YFP at 527nm known as FRET.

The focus of this chapter is to develop a method of FRET by flow cytometry for the analysis of viral and cellular TNFRs. The experiments shown in this chapter sought to analyse whether TRAPS TNFR molecules are able to interact with WT TNFR1, as well as to determine if vTNFRs MYXT2, VARG4R and MPVJ2R, themselves form FRET dimers. The chapter lastly addresses vTNFR interactions with cellular TNFRs via a FRET detection system. In doing so, these results might provide further evidence of vTNFR association

with cellular TNFRs and an understanding of the mechanism of vTNFR subversion of cellular TNFRs.

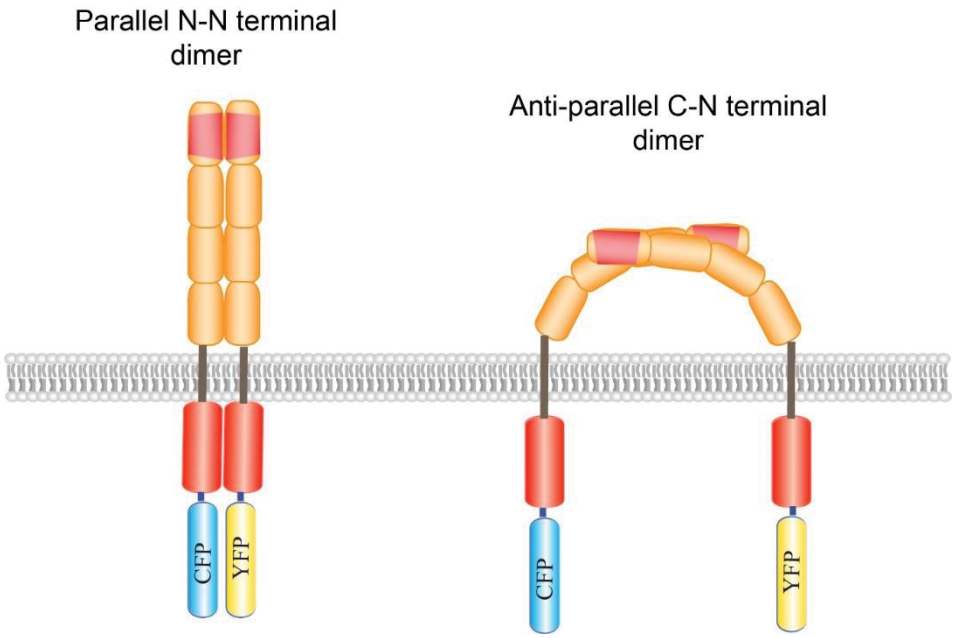

Figure 5.3 Possible predicted conformations of human TNFR1
From X-ray crystallography evidence (Naismith et al. 1996) there are two given structures which were solved. Based on this evidence and the placement of CFP and YFP C-terminal fusion tags, shown are the possible predicted conformations (parallel N-N) that may allow or (anti-parallel C-N) prevent FRET occurring.

5.2 Results

5.3 Set up and optimisation of FRET method by flow cytometry

The principle behind the FRET technique is the fluorescent energy of an acceptor and donor partner with overlapping excitation and emission spectra, that are capable of exciting the acceptor fluorophore thereby causing emission of a longer wavelength (Sekar & Periasamy 2003) (Figure 5.4). The method is very sensitive to distance with the energy transfer only occurring between fluorophores within small distances of up to 10nm (sometimes known as the Förster radius (Müller et al. 2013; Nagy et al. 1998).

FRET can therefore serve as an informative approach to gain structural information about protein interactions.

To set up the FRET by flow cytometry, human WT TNFR1, WT TNFR2, WT CD27 and viral MYXT2, VARG4R and MPVJ2R proteins were expressed from expression plasmids were generated as both -CFP and -YFP C-terminal fusion constructs (as shown in section 3.1). Therefore CFP was used as the donor fluorophore and YFP was used as an acceptor fluorophore to perform FRET. CFP and YFP share spectral overlap in their excitation and emission spectra which makes FRET possible (see Figure 5.4). CFP has a peak excitation wavelength at 436nm and a peak emission at 477nm which overlaps with the peak excitation of YFP at 527nm (Figure 5.1A). To ensure optimal detection of CFP and YFP, narrow bandwidth filters coupled with long pass mirrors to function as a more precise bandpass filter, were used in the LSRII cytometer (Figure 5.4). For the detection of CFP a 470/20nm bandpass filter coupled with a 460LP mirror was used to allow optimal detection of the CFP fluorophore emission (Figure 5.4). For YFP, a 550/30nm bandpass filter coupled with a 505LP mirror was selected to optimally detect YFP while excluding as much CFP emission (cross bleeding signal) as possible, from the 488 laser (Figure 5.4). FRET fluorescence was induced by exciting CFP with a 405nm laser which subsequently excited YFP, where the YFP FRET emission was detected on a separate detector (to CFP or 488nm laser excited YFP) via a narrow bandwidth 546/10 filter (Figure 5.4). Note that this detector is separate from the 488nm laser excited YFP emission and allowed differentiation of FRET YFP from the laser excited YFP (Figure 5.4).

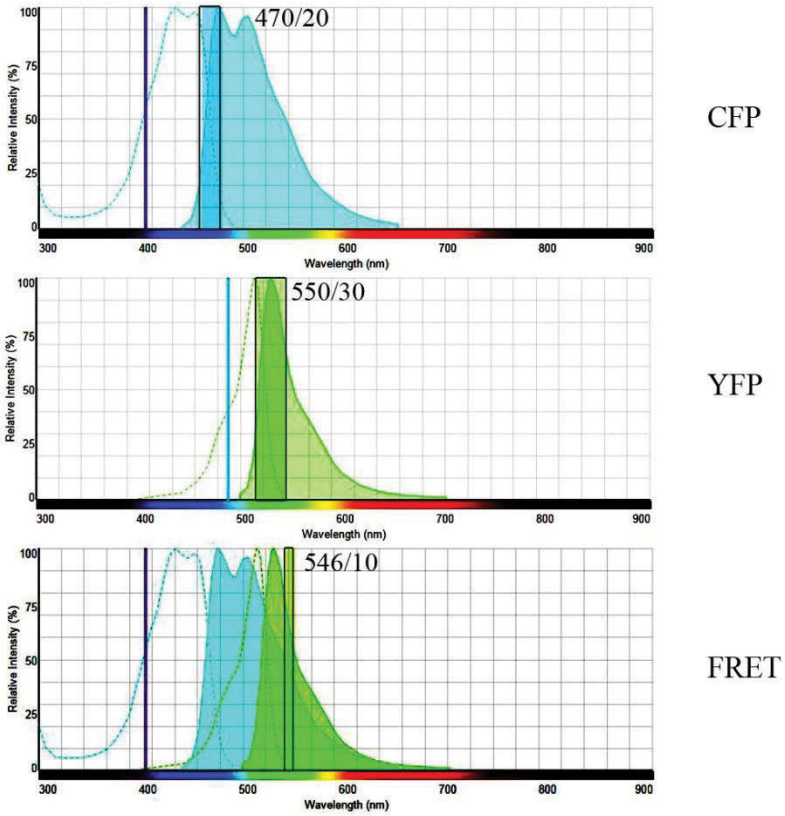

Figure 5.4 Spectral overlap of CFP and YFP flourophores
Shown is the excitation of CFP at 405nm (purple line) and excitation of YFP at 488nm (blue line) and the consequent emission peaks. Black outlined boxes represent the filter bandwidths used to detect CFP (470/20nm) and YFP (550/30nm) in the following flow cytometry set up. For the detection of FRET, CFP is excited using a 405nm laser and YFP emission (FRET emission) is collected off a separate detector using a narrow bandwidth filter (546/10nm).

As with the previous flow cytometry experiments in this research project, the voltages and gating needed to be established first to ensure correct detection of each fluorophore without fluorescence cross-bleeding. TNFR1-CFP, TNFR1-YFP, TNFR2-CFP and TNFR2-YFP singly expressed in transfected 293 HEK cells were used as "single colour controls" to establish the gating and correct voltage settings for accurate detection of FRET fluorescence (Figure 5.5). An initial gate (R1, red) was drawn around the cell population to also exclude aggregates and or debris. A second gate was then drawn to

distinguish single cells from doublets or clusters (R2, blue); single cells will be evident by the straight diagonal population on a FWD-A versus FWD-H dot plot (Figure 5.5). From this, CFP and YFP voltages were set using each of the single colour controls, ensuring CFP and YFP detection was occurring in the respective quadrants (Figure 5.5). Double positive cells for CFP and YFP were then gated on (R4, purple) to analyse FRET (Figure 5.5). However to determine the correct voltages required for FRET detection and also determine a positive FRET signal, it was realised that a reference point was needed for comparison, i.e. we needed to define a negative FRET fluorescence signal. Therefore an additional gate (R3, teal) was set on -CFP only cells (which should be negative for FRET), this permitted detection of bona-fide FRET positive signals within each sample (Figure 5.5).

Using 293 HEK cells transfected to co-express TNFR1-CFP and TNFR1-YFP it was evident that majority of cells (>70% of cells) were double positive for both CFP and YFP. This co-expression was almost always observed for all double transfected cells, for each of the CFP and YFP expression plasmids (Figure 5.6). Thus only a very few cells are CFP^+ only and hence, FRET fluorescence could not be compared to this minute population of CFP-positive cells within the co-transfection. To overcome this problem, addition of CFP-positive cells were spiked into in each sample (Figure 5.6). By comparing each sample with and without a spiked CFP-positive population of cells, it can be seen that the addition of the CFP only population creates a reference peak from which to compare a positive FRET signal. However, because of differences in brightness between molecules it was recognised that each sample needed to be spiked with the same population of CFP^+ cells.

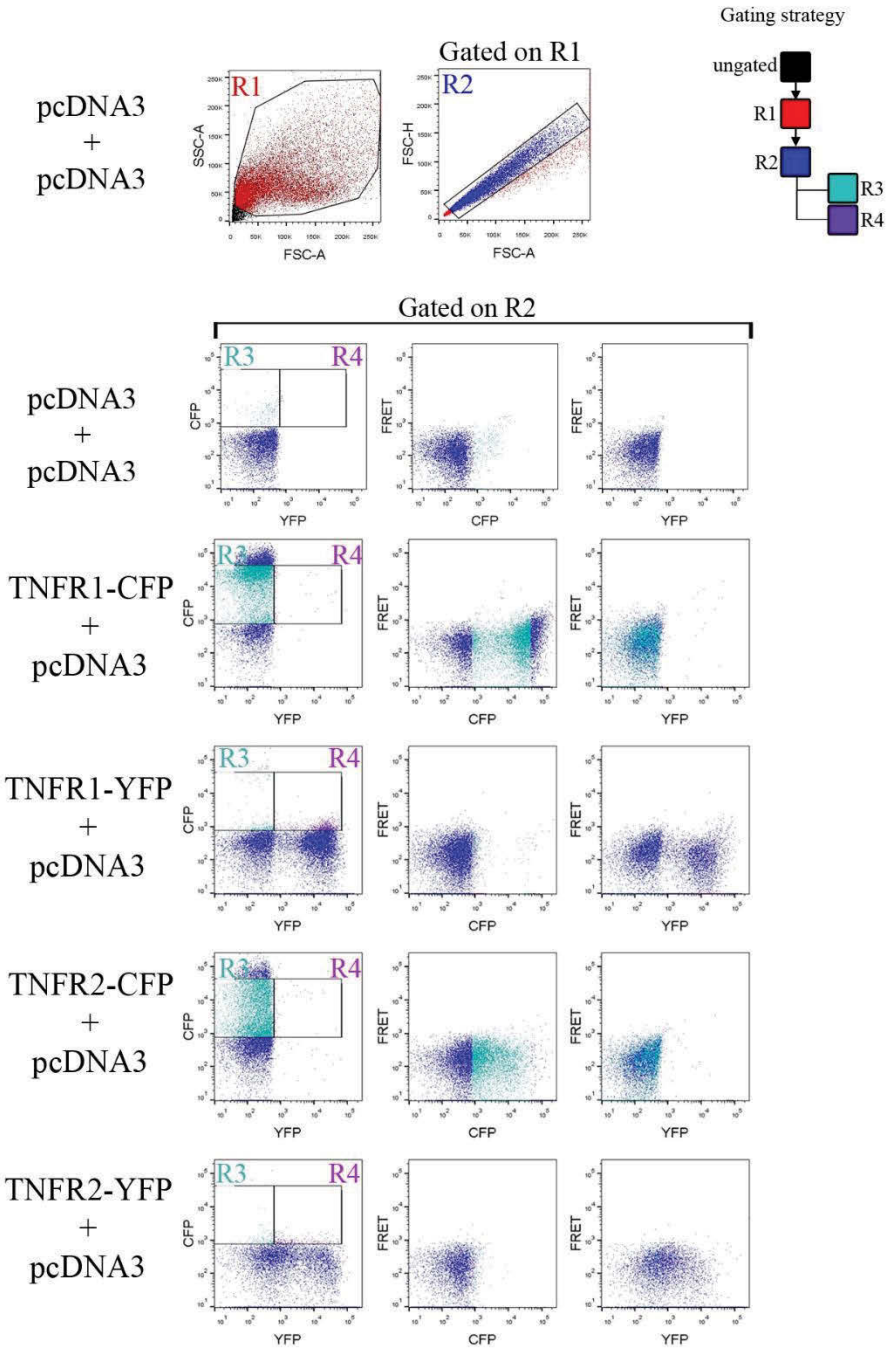

Figure 5.5 LSRII flow cytometry set-up for the detection of FRET

Single colour controls TNFR1-CFP, TNFR1-YFP, TNFR2-CFP and TNFR2-YFP expressing 293 HEK cells were used to set up the voltages and gating strategy required for FRET. A gate was first drawn to exclude cell debris (R1, red) and then another gate drawn to exclude doublet cells (R2, blue). The R2 population was then plotted in a CFP vs YFP dot plot and gates were then drawn to identify CFP (R3, cyan) positive as well as CFP and YFP double positive (R4, purple). Dot plots showing FRET vs CFP and FRET vs YFP are also shown to identify and set up voltages for positive and negative FRET emission signals.

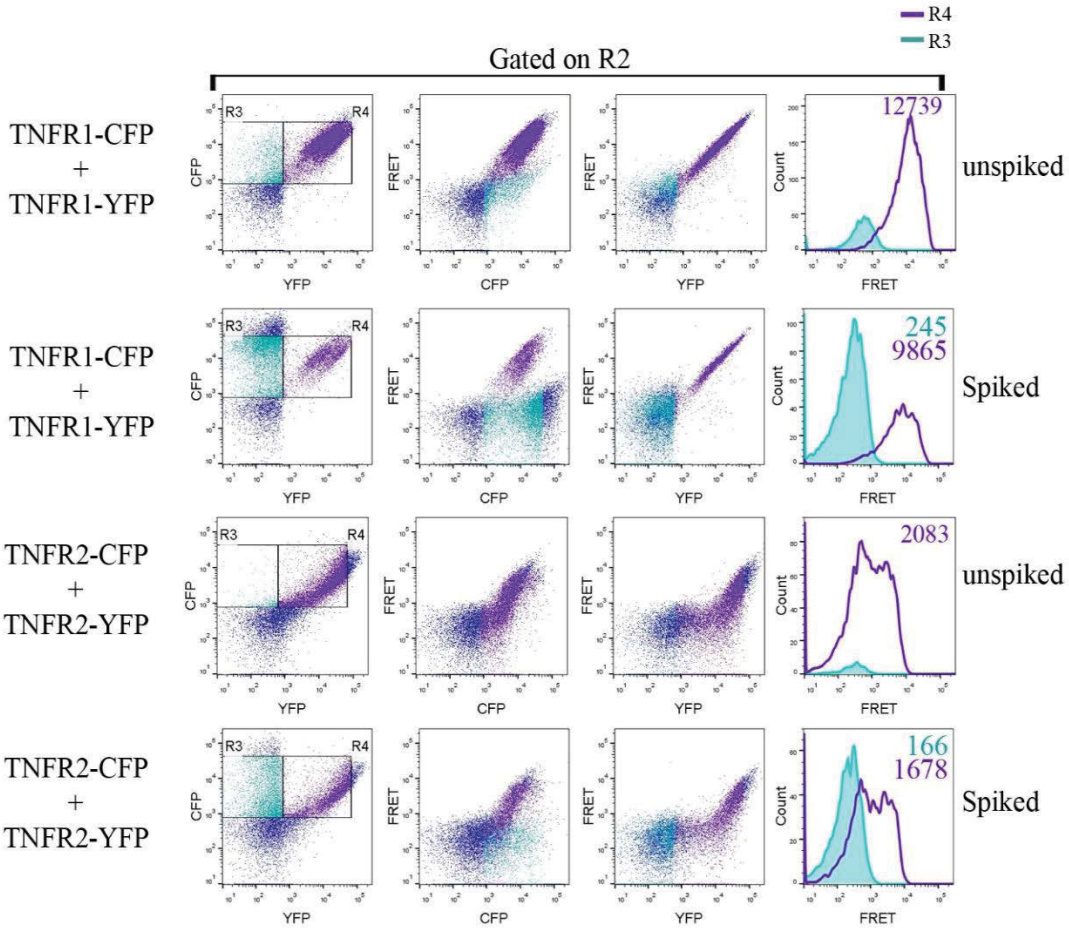

Figure 5.6 The requirement of a CFP spiked population for FRET detection.
A FRET signal can be detected from TNFR1-CFP/YFP double positive cells and TNFR2-CFP/YFP double positive cells. However as nearly all transfected cells are double positive for both CFP and YFP there is no negative FRET emission to compare the histogram against. Therefore a CFP only population spike in each sample is required, as an internal FRET comparison can used to set the voltages and compensation for the FRET channel. Shown are samples already compensated for CFP and YFP for simplicity. Numbers represent the MFIs of the matching colour coded histogram FRET peaks.

For example a TNFR1-CFP/TNFR1-YFP co-transfected sample needed to be spiked with TNFR1-CFP or a TNFR2-CFP/TNFR2-YFP sample needed to be spiked with TNFR2-CFP only cells. The inclusion of the CFP spiked cells permits the definition of a baseline to be set for the analysis. Due to the spectral overlap of CFP and YFP, detecting FRET emission also leads to the issue of also detecting CFP fluorescence. Although narrow band width filters were utilised in the flow cytometer to optimise detection, the FRET filters do not exclude all CFP emission. This can be observed in the uncompensated dot plots and fluorescence histograms (Figure 5.7). This is clearly seen with the spiked population of CFP positive cells as a false FRET signal is detected. It can be observed in the dot plots of FRET vs CFP and FRET vs YFP that the population of CFP only cells results in the population shifting into the FRET positive quadrants (Figure 5.7). This is especially evident for TNFR1-CFP/TNFR1-YFP cells, where the brightest CFP fluorescence begins to bleed through into YFP fluorescence as evident by the tailing of the population into the YFP positive quadrant of the dot plot (Figure 5.7). To minimise the effect of bleed through of the CFP fluorescence signals into both FRET and YFP compensation was needed. Compensation effectively subtracts the CFP fluorescence signal from the detection of YFP and FRET fluorescence signals electronically in the using the acquisition software DIVA (BD Ver 6.0) and the post-acquisition software FlowJo (Treestar Ver 10.0.8).

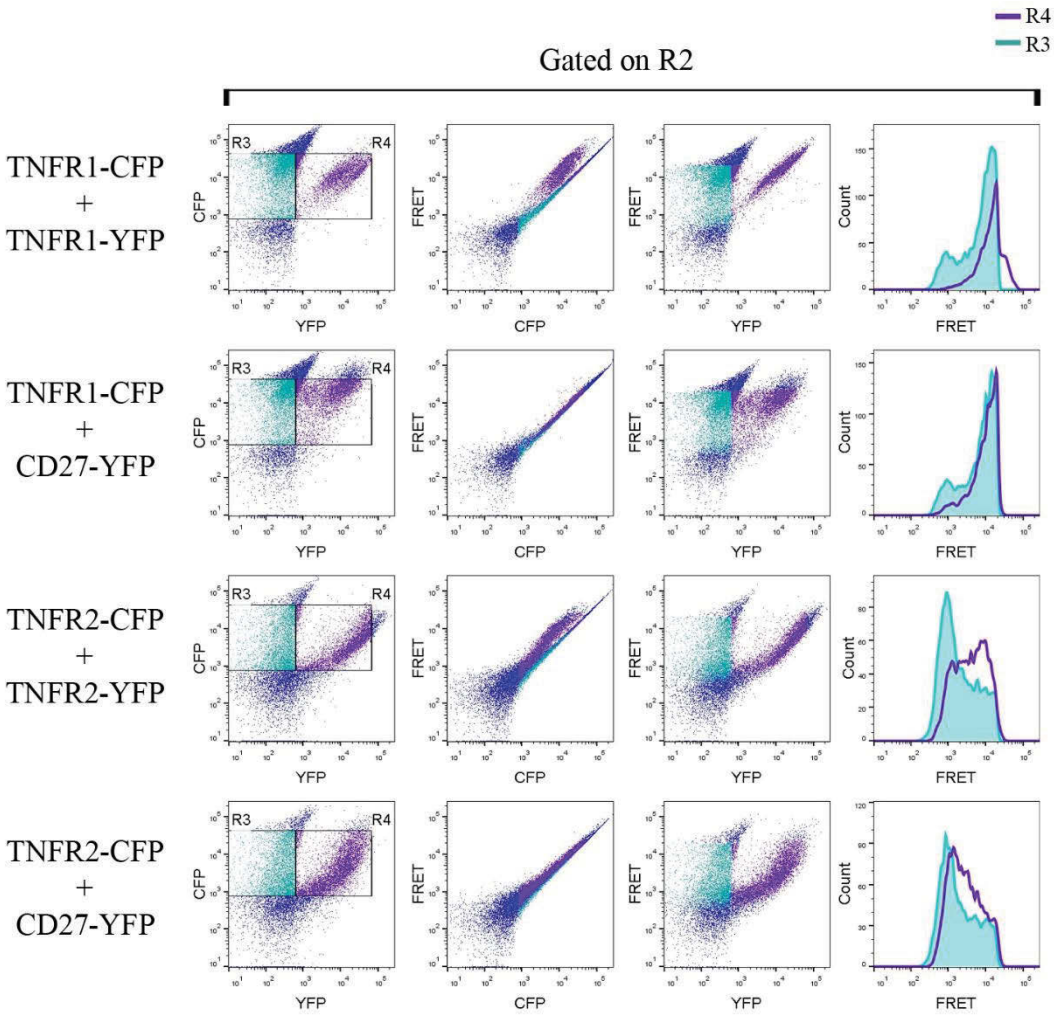

Figure 5.7 Compensation of CFP and YFP singals to determine FRET emission. Shown are 293 HEK cells co-expressing TNFR1-CFP and TNFR1–YFP or TNFR2-CFP and TNFR2-YFP and the resultant FRET signal without CFP and YFP compensation. In each sample a CFP only expressing population (either TNFR1-CFP or TNFR2-CFP) has been spiked. CFP only expressing cells are identified in the R3 gate (cyan) and double positive CPF and YFP cells are located in the R4 gate (purple).

The amount of compensation was assessed for each of the detection channels during acquisition and adjusted accordingly to correct for the false positive FRET and YFP signals. Once compensation was applied the bleed through of CFP fluorescence was dramatically reduced, allowing distinction of positive and negative FRET detection, this can be observed in the histogram comparing R3 (CFP spiked cells) and R4 (double positive cells) as well as in the dot plots of CFP or YFP vs FRET (Figure 5.8).

TNFR1 and TNFR2 form homotypic trimers and have been previously shown to cause a FRET emission detected by flow cytometry when expressed as C-terminal -CFP and -YFP recombinant fusion proteins (Chan et al. 2001). Therefore as expected a positive FRET signal was observed for double positive cells of TNFR1-CFP/TNFR1-YFP and TNFR2-CFP/TNFR2-YFP double positive cells and was used as a positive reference sample for all comparisons (Figure 5.8). TNFR1-CFP/TNFR1-YFP resulted in a mean FRET fluorescence of 9865 over compared to the CFP population which emitted a FRET MFI of only 245 for "CFP-only" spiked TNFR1-CFP expressing cells (Figure 5.8). Similarly, TNFR2-CFP/TNFR2-YFP co-transfected cells also displayed a clear FRET signal with a FRET MFI of 1678 compared to "CFP-only" spiked TNFR2-CFP expressing cells with an MFI of 166 (Figure 5.8). Thus a large shift in FRET MFI was very clear over the FRET signal evident in the CFP-only spiked population for both TNFR1 and TNFR2. This indicates that the C-terminus of TNFR1 dimers/trimers (and also TNFR2 dimers/trimers) were interacting with each other. Indeed the C-terminal of these molecules must be therefore physically within 10nm distance of each other.

For a negative control CD27-YFP was also co-expressed with TNFR1-CFP, or with TNFR2-CFP. CD27 and TNFR1 or CD27 and TNFR2 are not expected to associate with each other due to differences in structure and sequence homology – these molecules are not known to form heterodimers or hetero-trimers. Therefore when TNFR1-YFP was co-expressed with CD27-YFP, a slight FRET shift was observed, with a FRET MFI of 805 compared to the TNFR1-CFP only spiked cells which emitted a FRET MFI of only 245 (Figure 5.8). Similarly TNFR2-YFP/CD27CFP cells were detected with a FRET MFI of 408 versus TNFR2-CFP spiked cells with a FRET MFI of only 168 (Figure 5.8). Although a slight shift in FRET MFI was detected (over the CFP-only spiked cell population) this must

represent the background level or false FRET. This is likely to be due to the brightest CFP and in the double positive cells contributing to a false positive signal (Figure 5.8). Because of differences in molecule brightness this also meant that compensation needed to be optimised for each sample set (i.e. all cells co-expressed with TNFR1) within an experiment. In the same experiment it was necessary to have more than one comparison setting e.g. one for TNFR1 and one for TNFR2 samples.

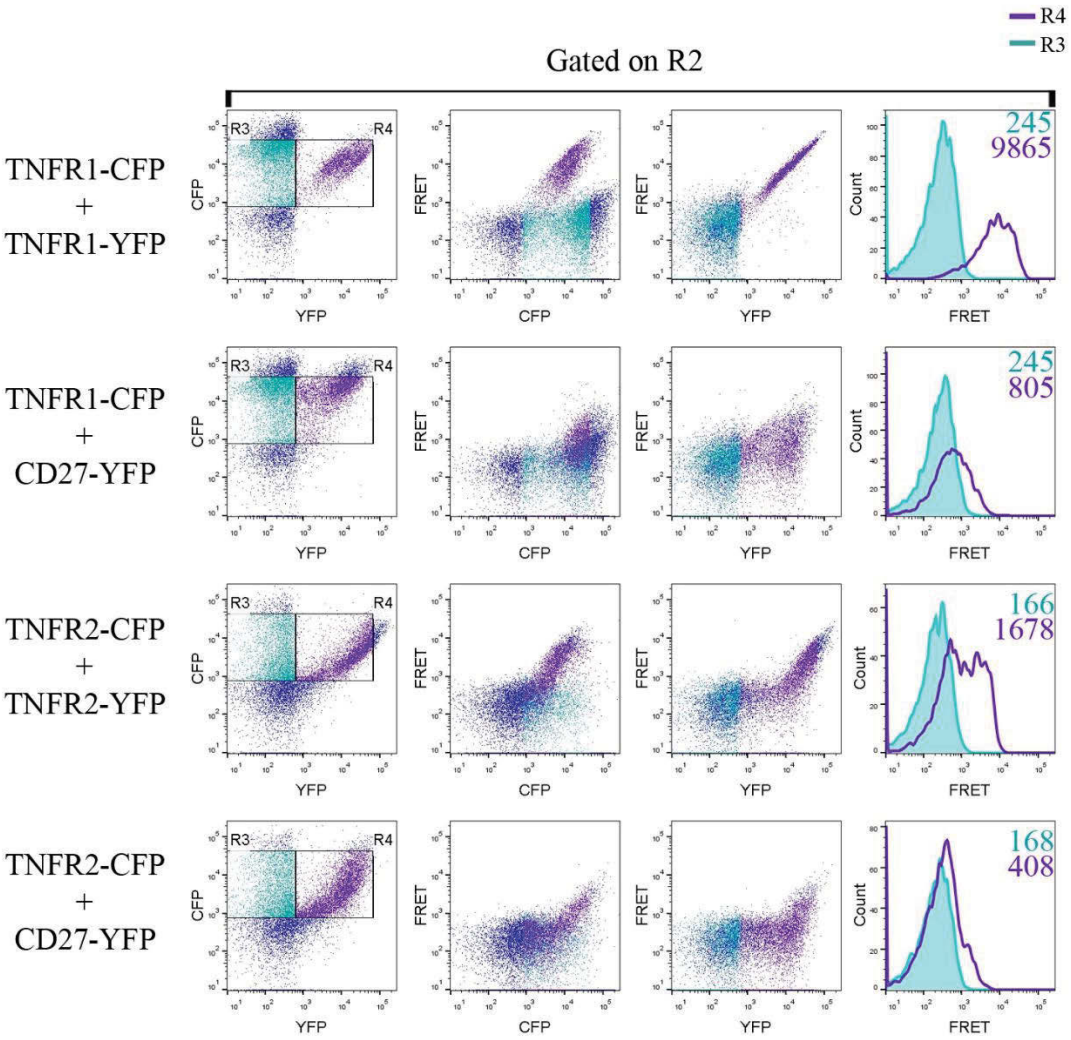

Figure 5.8 Differences in TNFR1 homologous FRET and TNFR2 homologous FRET

The optimised set up of FRET by flow cytometry reveals differences between cells co-expressing TNFR1-CFP and TNFR1-YFP, and cells co-expressing TNFR2-CFP and TNFR2-YFP. Numbers shown in each of the FRET histograms are MFIs of the respective colour coded cell populations i.e. CFP only cells (cyan) vs $CFP^{+}YFP^{+}$ cells (purple).

Without individually setting the compensation levels this would result in over compensation and hence subtraction of too much FRET signal (data not shown). Furthermore because TNFR1-CFP is always apparently much brighter in fluorescence more compensation was required than for samples expressing TNFR2-CFP or CD27-CFP. With the compensation settings now adjusted correctly for each sample set, FRET detection was now optimised for the LSRII flow cytometer and each of the sample sets to be analysed.

5.4 Comparison of TNFR1 FRET and TNFR2 FRET

TNFR1 and TNFR2 display various differences in their structure, especially in the C-terminal regions of each receptor: TNFR1 contains a death domain (Boldin et al. 1995) whereas TNFR2 contains TRAF-binding domains (Rothe et al. 1994). As TNFR1 and TNFR2 were both expressed as C-terminal fusion proteins with -CFP or –YFP, small differences in distance between these structures should be detectable by FRET. When TNFR1-CFP and TNFR1-YFP are co-expressed in cells a very large shift in FRET is observed with an MFI of 9865 vs a FRET MFI of TNFR-CFP spiked cells 281 (Figure 5.8). When TNFR2-CFP and TNFR2-YFP are co-expressed in cells, a shift in FRET is observed with a FRET MFI of 1678 vs 166 for the TNFR2-CFP spiked cells (Figure 5.8). Thus there are distinct differences for TNFR1 compared to TNFR2 (Figure 5.8). Also TNFR1-CFP/TNFR1-YFP cells exhibit a sharp FRET peak whereas TNFR2-CFP/TNFR2-YFP expressing cells display a broader FRET histogram which overlaps the CFP spiked population (Figure 5.8). This broader peak suggests that the TNFR2-CFP/TNFR2-YFP proteins adopt different conformations with differences in the distance between the C-terminal regions of TNFR2, i.e. the brighter FRET TNFR1-CFP/TNFR1-YFP proteins being closer together

compared to the less bright FRET cells containing TNFR2, being further apart in the C-terminal regions. This difference could also possibly represent cells with naive TNFR2 to ligand vs cells containing activated TNFR2, as activation from the binding of ligand by TNFR2 is known to induce a conformational change, bringing the C-terminal regions into closer proximity (Murali et al. 2005).

5.5 TRAPS TNFR1 can associate with WT TNFR1 but display differences in FRET

Traps TNFR1 mutants are predicted to alter the structure of WT TNFR1, especially those affecting amino acids involved in structurally important features e.g. cysteines involved in disulphide bonds (Rebelo et al. 2006). It is debated that because of the predicted changes in TNFR1 structure, that TRAPS mutant TNFR1 proteins are still able to associate or interact with wild type TNFR1 (McDermott et al. 1999). In a previous initial reports, TRAPS mutations H22Y, C33G, T50M, C52F, C88R, R92P, R92Q all displayed a greatly reduced FRET with WT TNFR1 (Lobito et al. 2006). Conversely, the TRAPS mutant T50K was judged to associate equally well with WT TNFR1 compared to homodimers of WT TNFR1 (Yousaf et al. 2005). Because different methods and mutations were analysed in the separate experiments it is difficult to assess whether all mutations exhibit an inability to interact with WT TNFR1. Therefore the panel of TRAPS mutations generated were used to evaluate differences between PLAD mutations to interact with WT TNFR1.

WT TNFR1 and TRAPS mutant TNFR1 interactions were examined in co transfected 293 HEK cells that had been transfected with pcDNA3.TNFR1-CFP and pcDNA3.TNFR1-YFP, or pcDNA3.TRAPS TNFR1-YFP. Single colour controls TNFR1-CFP. TNFR1-YFP, TNFR2-CFP,

TNFR2-YFP, CD27-CFP and CD27-YFP expressing cells as well as positive controls TNFR1-CFP and TNFR1-YFP, TNFR2-CFPand TNFR2-YFP co transfected cells plus negative FRET controls TNFR1-CFP and CD27-YFP, TNFR2-CFP and CD27-YFP were also included in each experiment. Each sample was repeated in triplicate transfections and the representative plot for each sample (Figure 5.9A). As expected TNFR1-CFP/TNFR1-YFP co-expressing cells (Gate R4) resulted in a significant positive FRET emission (FRET MFI 4305) compared to TNFR1-CFP spike cells (Gate R3) which produced a FRET emission with an MFI of 372 (Figure 5.9A). Cells co-expressing TRAPS mutant TNFR1-YFP proteins and WT TNFR1-CFP were then examined for a difference in FRET signals compared to WT TNFR1-CFP and WT TNFR1-YFP expressing cells. It was observed that all TRAPS TNFR1-YFP proteins resulted in a FRET emission when co-expressed with WT TNFR1-CFP (Figure 5.9A), likely indicating that TRAPS mutant receptors associate with WT TNFR receptors. However the brightness or strength of the detected FRET emission varied amongst the different mutants indicating differences in distance between CFP and YFP molecules of the TRAPS proteins. When compared against WT TNFR1-CFP/TNFR1-YFP (MFI 4305) statistically significant differences were observed for TRAPS mutants Y20D (MFI 3330), C29Y (MFI 5099), C30F (MFI 4659), C30R (MFI 2847), C33G (MFI 3621), C33Y (3562) and T37I (MFI 3436) (Figure 5.9A). All mutations except Y20D and T37I resulted in statistically significant differences in FRET compared to WT TNFR1 were mutations affecting cysteine mutations important to the structure and folding of TNFR1 (Fu et al. 1995; Rebelo et al. 2006; Tchernitchko, Goossens & Wajcman 2004). TRAPS mutation Y20D mutates the tyrosine involved in a highly conserved hydrogen bond between residues Y20 and D40 (Tchernitchko, Goossens & Wajcman 2004). This confirms our expectation that mutations that are most likely to affect the structure of TNFR1 alter the ability of TRAPS TNFR1 to interact with WT TNFR1. Also of note mutations C29Y and C30F were observed

to have higher emission of FRET (MFI 5099 and MFI 4659 respectively), compared to WT (MFI 4305). In each of the cases described above these differences were found to be statistically significant when comparing means of 3 independent transfections ($P<0.05$; Figure 5.B). Moreover, the results shown in the data figures were reproducible in independently repeated transfection experiments (data not shown).

Within in each FRET histogram showing overlays of CFP^+YFP^+ cells (Gate R4) with CFP^+ only spiked cells (Gate R3) it was evident that the histograms distribution of the R4 peak varied amongst each of the TRAPS mutants. For example in TNFR1 mutants C30R, it can be seen that the R4 peak becomes much broader and virtually splits into two populations, i.e. based on FRET brightness: a “FRET high” population and a “FRET low” population (Figure 5.9A). Two additional gates were therefore inserted consistently across all samples to identify the extent of this variation with respect to TRAPS mutations, and to measure the distribution of cells within each of these sub populations (gate regions R5 and R6). As WT TNFR presented as a single sharp FRET histogram, the midpoint of the two gates was determined from the tail of the WT TNFR1 homologous FRET histogram (Figure 5.A). WT TNFR1 contains a single sharp peak FRET emission without two distinct sub-populations. Nevertheless this set the distribution point at 25% of cells within R5 and 75% of cells within the FRET high R6 gate. WT TNFR1 was considered to be the standard from which to compare all of the TRAPS TNFR1-YFP mutants. Thus, it was clear from the analysis that the greatest differences from WT TNFR1 FRET were observed in TNFR1 Y20D (39%/61%), Y20H (33%/67%), C29Y (13%/87%), C30F (16%/84%), C30R (45%/55%), C33G (31%/69%), T37I (35%/65%), C43R (14%/86%) and P46L (16%/84%) (Figure 5.9A & B). Interestingly this effect correlated with the mutations that displayed differences in cell death described in

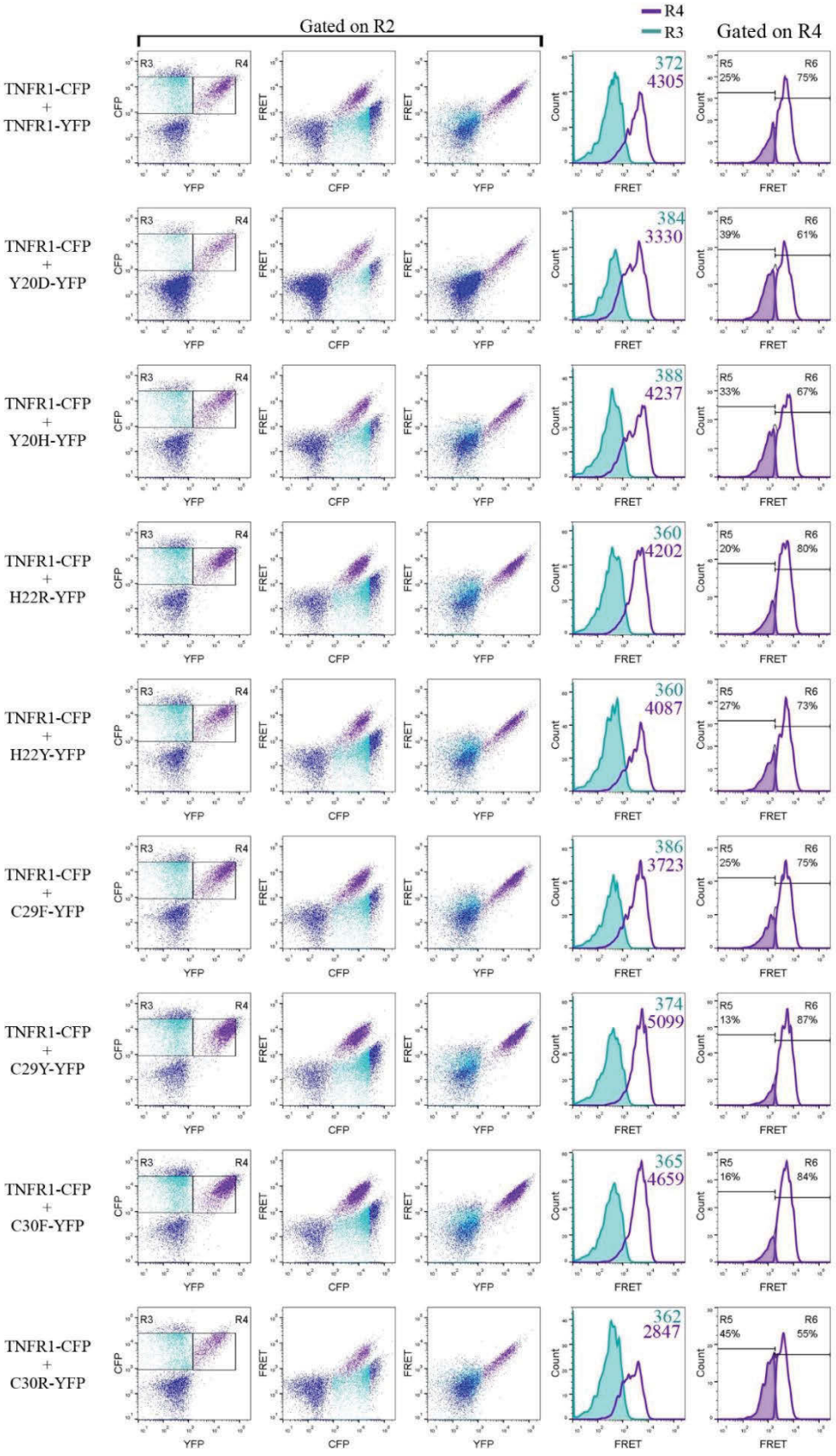
Gated on R2
R4
R3
Gated on R4
TNFR1-CFP + TNFR1-YFP
372
4305
R5 25%
R6 75%
TNFR1-CFP + Y20D-YFP
384
3330
R5 39%
R6 61%
TNFR1-CFP + Y20H-YFP
388
4237
R5 33%
R6 67%
TNFR1-CFP + H22R-YFP
360
4202
R5 20%
R6 80%
TNFR1-CFP + H22Y-YFP
360
4087
R5 27%
R6 73%
TNFR1-CFP + C29F-YFP
386
3723
R5 25%
R6 75%
TNFR1-CFP + C29Y-YFP
374
5099
R5 13%
R6 87%
TNFR1-CFP + C30F-YFP
365
4659
R5 16%
R6 84%
TNFR1-CFP + C30R-YFP
362
2847
R5 45%
R6 55%
R3
R4
CFP
YFP
FRET
Count

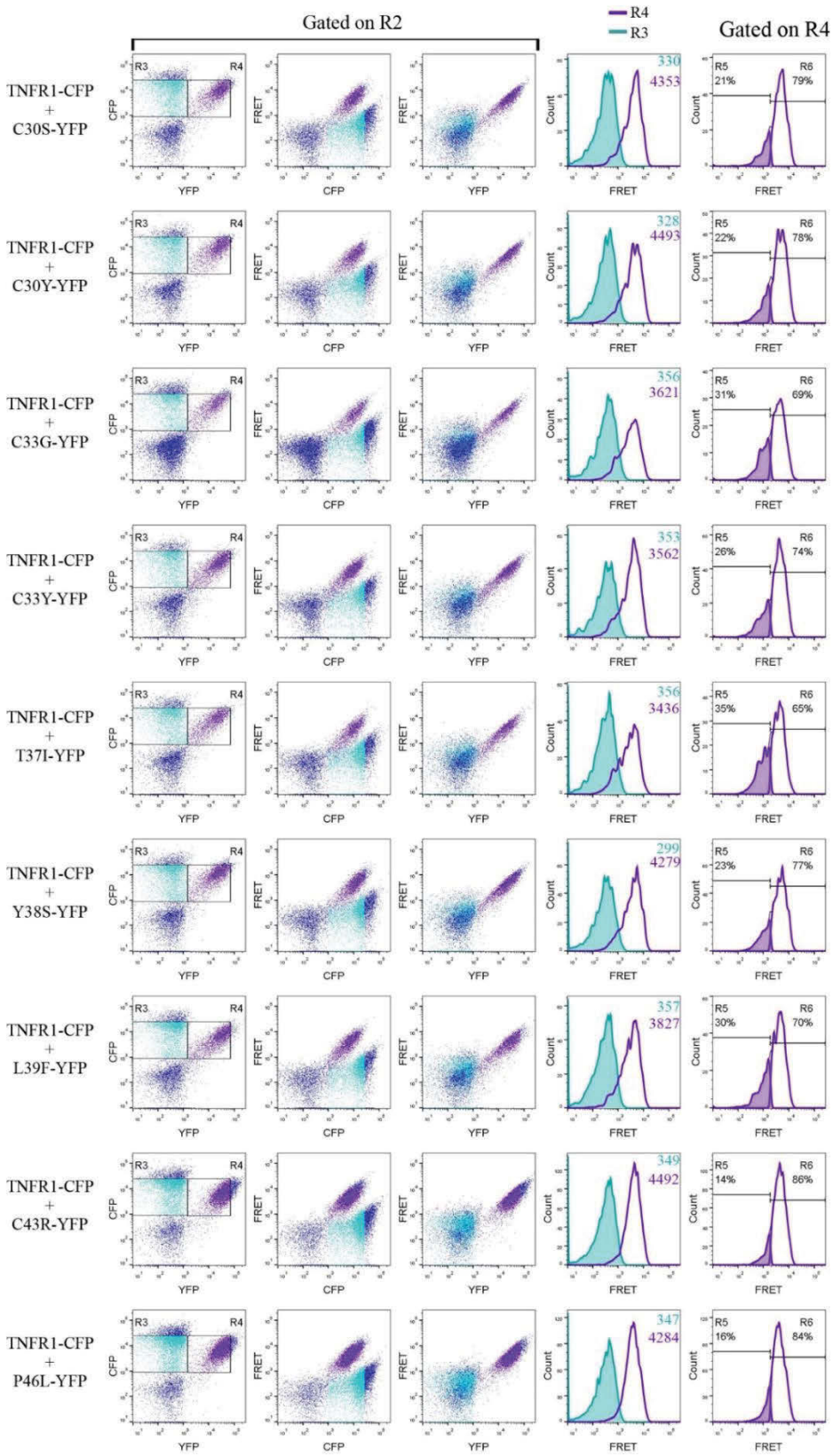

Figure 5.9A TRAPS TNFR1 and WT TNFR1 FRET by flow cytometry
Flow cytometric analysis of FRET between WT TNFR1-CFP and TRAPS TNFR1-YFP proteins in 293 HEK expressing cells. Cells were transfected with WT TNFR1-CFP and either WT TNFR1-YFP or TRAPS TNFR1-YFP then analysed for FRET 48 hours post transfection. Each sample was spike with a TNFR1-CFP only population identified in R3 (cyan) compared with each of the double positive CFP and YFP TNFR1 populations

(purple). The background level of FRET is denoted by the TNFR-CFP only population (cyan) in each of the CFP vs FRET, YFP vs FRET dot plots and FRET histograms. Each of the transfected TNFR1 and TRAPS co-expressing cells (R4, purple) were then compared to the pooled CFP only spiked populations. Numbers shown on histograms represent MFI of the matching colour coded cell subpopulation. Additional gates (R5, shaded purple, and R6 Bold purple outline) were drawn on each of the FRET histograms from the R4 subpopulation to determine differences in distribution of each FRET double positive population. The midpoint of the two gates was determined from the tail of the WT TNFR1 homologous FRET histogram, as WT TNFR1 presented as a single sharp histogram. Plots shown represent the median transfection from independent triplicate transfections with 30000 events collected for each.

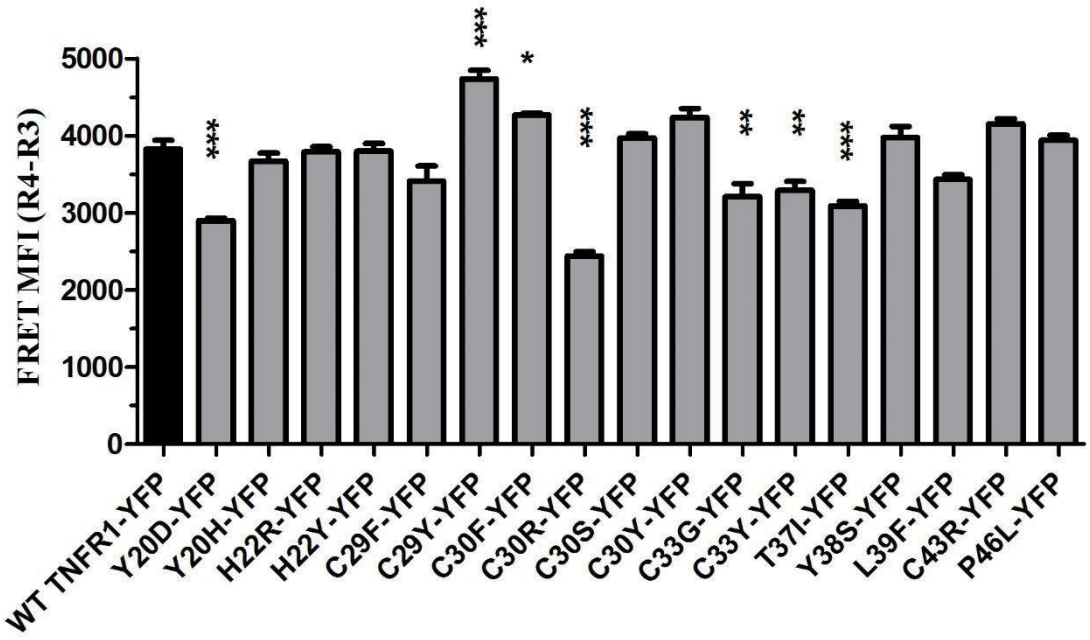

Figure 5.9 B Statistical analysis of FRET MFIs of TNFR1-CFP and YFP expressing cells

The FRET MFI values for the CFP only spiked population was deducted from the FRET MFI values of each double positive TNFR1-CFP and –YFP population for each triplicate sample. The Mean MFI value and standard deviation is shown for each triplicate transfection. A 1 way ANOVA and Dunnett's Multiple Comparison Test was performed to find differences between sample means. Comparisons of means were made against cells double positive for WT TNFR1 homologous FRET (black bar graph) and the level of significance is asterisked. * = $P \leq 0.05$, ** = $P \leq 0.01$, *** = $P \leq 0.001$.

Chapter 3 and may provide evidence that TRAPS mutations cause significant differences in interactions with WT TNFR1. This is due to the principle that FRET efficiency is related to acceptor donor distance (Nagy et al. 1998). This also further validates the flow cytometry FRET method and clearly indicates the sensitivity of the method, whereby effects of a single amino acid residue on protein structure, can be detected.

5.6 vTNFRs show no FRET with cellular TNFRs

MYXT2 is known to associate with human TNFR1 and TNFR2 subverting TNFR induced cell death (Sedger et al. 2006). This association was shown to require the PLAD domain, because a recombinant MYXT2 mutant protein lacking the PLAD displayed an inability to associate with TNFR1 and TNFR2 (Sedger et al. 2006). PLAD homologous domains exist in virtually all poxviral TNFR homologues (Figure 5.1). However it is still not known whether vTNFRs other than MYXT2 can inhibit TNFR-induced cell death. In addition, how MYXT2 (and other vTNFRs) interact with cellular TNFR1 and TNFR2 is still unclear. The distinct contacts involved in the interaction, or even the orientation of MYXT2 proteins relative to cellular TNFRs is yet to be determined. Interestingly the crystal structure of TNFR1 was found to exist as both a N-N parallel and C-N anti-parallel dimer (Naismith et al. 1996), therefore we propose that it might be possible that the interaction between vTNFRs and cellular TNFRs can occur in either orientation. We propose that FRET by flow cytometry can be used to indicate whether VARG4R and MPVJ2R, as well as MYXT2 associate with human TNFR1 and TNFR2 as well as determine the orientation of the MYXT2, VARG4R and MPVJ2R interaction with cellular TNFRs.

Transfected 293 HEK cells expressing TNFR1-CFP and MYXT2-YFP, or TNFR1-CFP VARG4R-YFP or MPVJ2R-YFP were compared to CD27-YFP and TNFR1-CFP or TNFR2-CFP co-transfected cells. Single transfected cells were also used to set voltages and compensation for FRET detection. Double positive TNFR1-CFP/TNFR1-YFP as well as TNFR2-CFP/TNFR2-YFP were used as positive FRET controls and each were observed to give a clear FRET (FRET MFI 6813 for TNFR1 and 1017 for TNFR2 respectively) over CFP-spiked cells (FRET MFI 291 and 181 respectively) (Figure 5.10A). When TNFR1-CFP and TNFR2-CFP were co-expressed with CD27 proteins (negative control) no FRET signal was observed for either TNFR1-CFP/CD27-YFP cells (FRET MFI 367 over CFP spiked cells FRET MFI 258) or TNFR2-CFP/CD27-YFP cells (FRET MFI 101 over CFP spiked cells FRET MFI 172). However when MYXT2-YFP was co-expressed with TNFR1-CFP, a small FRET signal was detectable over the TNFR1-CFP only spiked cells (R3) (FRET MFI 425 vs 261) (Figure 5.10A). Although the FRET MFI detected for TNFR1-CFP/MYXT2 double positive cells was only very slightly higher than that observed for TNFR1-CFP/CD27-YFP double positive cells, the FRET emission was comparable to TNFR1-CFP/CD27-YFP or TNFR2-CFP/CD27-YFP double positive cells (negative FRET controls) and thus not considered positive FRET (Figure 5.10A). Cells co-expressing TNFR1-CFP and VARG4R-YFP or MPVJ2R-YFP were also not detected as positive for FRET with an MFI of 388 and 262 compared to CFP spiked cells (R3) with a FRET MFI of 388 and 343 respectively (Figure 5.10A).

No convincing FRET emission was also seen for MYXT2, VARG4R or MPVJ2R when co-expressed with TNFR2 (Figure 5.10B). The FRET MFI of double positive cells (R4) for TNFR2-CFP/MYXT2-YFP was 97 vs CFP spiked cells with a FRET MFI of 161 (Figure 5.10B). Similarly FRET was not detectable for double positive cells expressing TNFR2-CFP/VARG4R-YFP with a FRET MFI of 166 or TNFR2-CFP/MPVJ2R-YFP proteins with a

FRET MFI of 177 compared to CFP spike cells with and MFI of 102 for both samples (Figure 5.10B).

Therefore taken together, although the FRET method was clearly efficiently detecting FRET fluorescence, a FRET emission was not detectable for any vTNFR when co-expressed with cellular TNFR1 or TNFR2. Since the FRET emission requires 2 molecules to be within approximately 10nm of each other (Berney & Danuser 2003), these data may mean that the receptors do not form the N-N heterodimer conformation. They may instead form N-C heterodimers. Alternatively the lack of FRET may simply indicate that the C-terminal regions of the proteins are greater than 10nm distance even in the N-N heterodimer conformation.

5.7 vTNFRs show no FRET with themselves or other vTNFRs

MYXT2 is known to exist as both a dimer and a monomer (Schreiber, Rajarathnam & McFadden 1996). The dimeric form of MYXT2, although more efficient in inhibiting soluble TNFα, was required in 2000 molar excess for 80% protection against TNFα induced apoptosis (Schreiber, Rajarathnam & McFadden 1996). Although MYXT2, VARG4R and MPVJ2R vTNFRs did not exhibit convincing positive FRET emission with human TNFR1 or TNFR2, it is possible that vTNFRs may be able to FRET as homodimers with themselves. Indeed MYXT2 is both a monomer and dimer and VARG4R is predominantly found as a dimer (Sherwood, data not shown)(Gileva et al. 2006). Therefore the FRET flow cytometry assay was used to examine the interactions of MYXT2, VARG4R and MPVJ2R. Each possible combination of MYXT2, VARG4R and

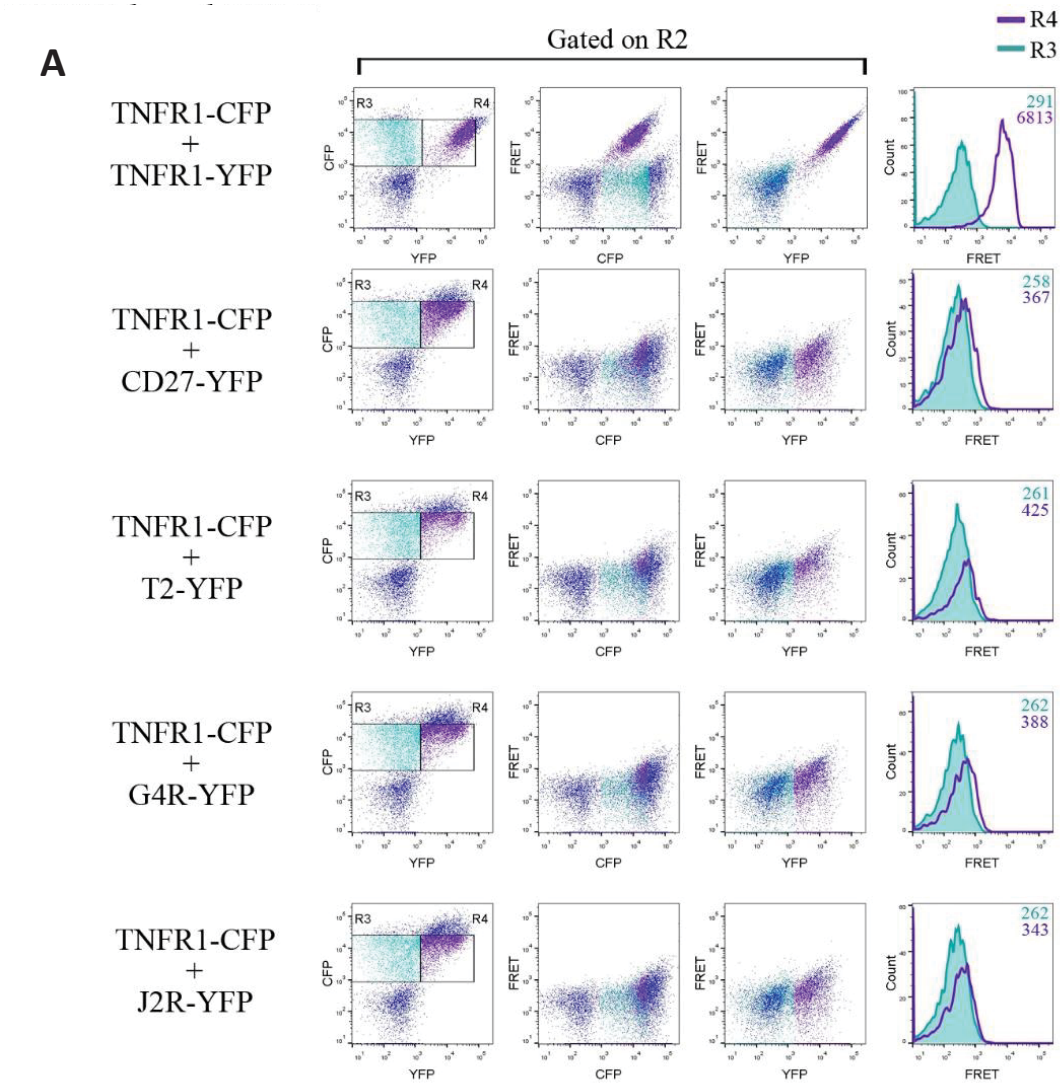

Figure 5.10 Detection of vTNFR-YFP FRET with WT TNFR1-CFP

B

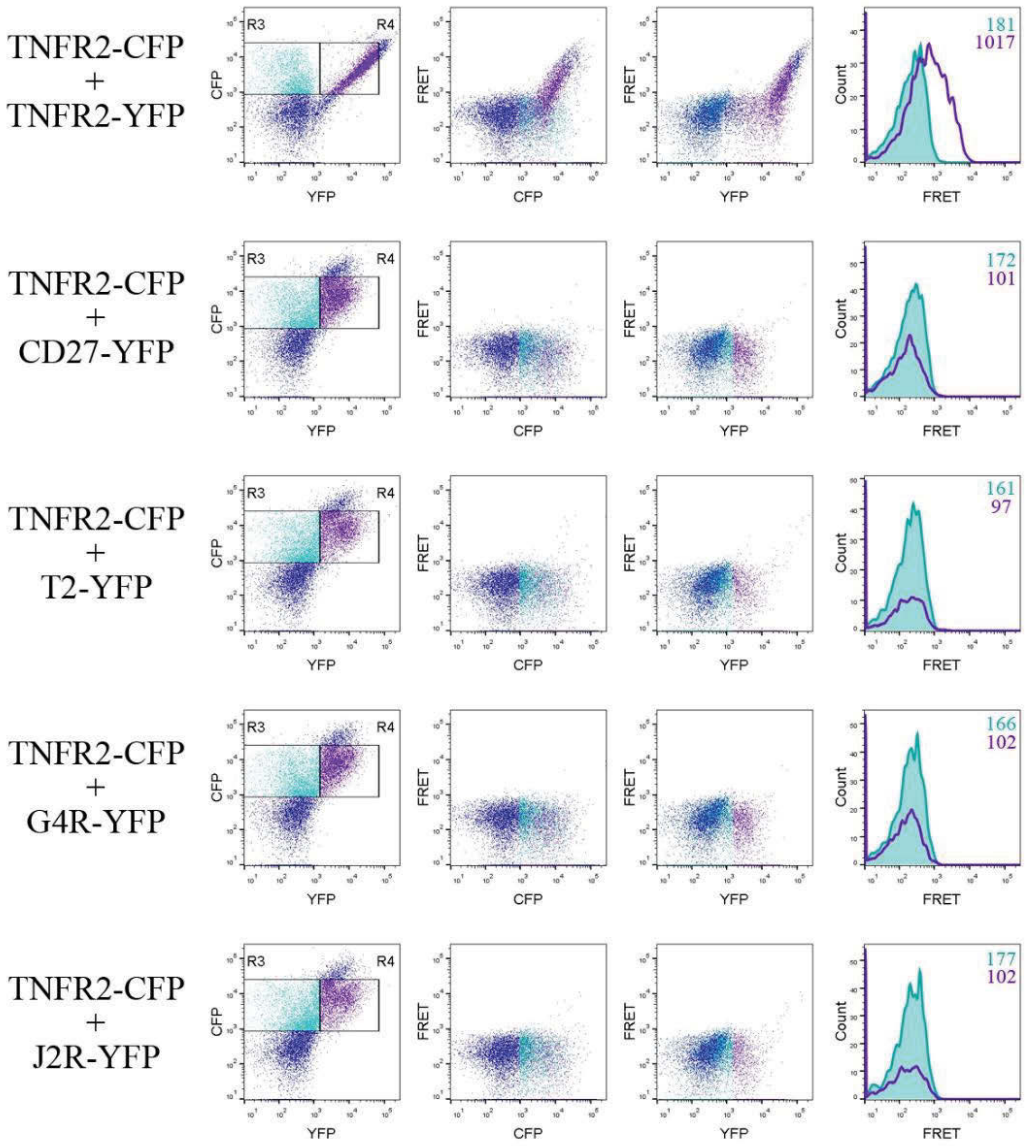

Figure 5.10 Detection of vTNFR-YFP FRET with WT TNFR1-CFP or TNFR2-CFP
Transfections were performed to co-express each of the vTNFRs with A) TNFR1-CFP and B) TNFR2 in 293 HEK cells. Analysis of FRET was then performed 48 hours post transfection with each of the samples spiked with a TNFR1-CFP (A) or TNFR2-CFP (B) only cell population. $CFP^{+}YFP^{+}$ expressing cells (R4, purple) were then compared to the background level of FRET in the CFP only expressing cells (R3, cyan). The level of FRET was determined by the shift from the CFP only cells in both the CFP vs FRET, YFP vs FRET dot plots and the FRET histograms overlays. The numbers shown in the FRET histogram overlays are MFI values for the respective colour coded cell populations and the data shown is the median representative transfection from independent triplicate transfections. 30000 events were collected for each of the samples analysed.

MPVJ2R-CFP and -YFP pair was examined, since it also remains possible that they could also form heterodimer due to their homology (Figure 5.11). No FRET emission was detected for MYXT2-CFP and MYXT2-YFP co expressing cells and in fact the FRET signal was comparable to the CD27-CFP only spiked cells (115 vs 137) (Figure 5.11). No FRET emission was also detected for cells co-expressing MYXT2-CFP and VARG4R-CFP or MPVJ2R-YFP with an MFI value of 139 and 137 over CFP spike cells (R3, teal) with a FRET MFI of 118 and 123 respectively (Figure 5.11). Similarly cells expressing VARG4R-CFP and VARG4R-YFP also did not FRET, with comparable FRET MFI values to the CFP-spiked cells (FRET MFI 125 vs 131 for CFP spiked cells). FRET was also not detected for VARG4R-CFP co-expressed with either MYXT2 or MPVJ2R (Figure 5.11). FRET MFI values for MPVJ2R-CFP cells were slightly higher than MYXT2-CFP and VARG4R-CFP cells with a FRET MFI of 148, 131 and 141 respectively, however, the FRET emission was still not significant when compared to the CFP spike population in each sample with a FRET MFI of 131 134 and 130 respectively (Figure 5.11). In summary no FRET emission was detected between any of the vTNFR pairs from the triplicate experiments. Thus no vTNFRs cause FRET emission even though MYXT2 (Schreiber, Rajarathnam & McFadden 1996) and VARG4R form homodimers (Sherwood, data not shown)(Gileva et al. 2006). One interpretation of this data is that N-N dimers exist but the C-terminal regions are not physically near enough to permit FRET emission. Alternatively, MYXT2, VARG4R and MPVJ2R may form anti-parallel N-C dimers. In support of this idea, the recent crystal structure of CRM-E reports the existence of an anti-parallel dimer (Graham et al. 2007).

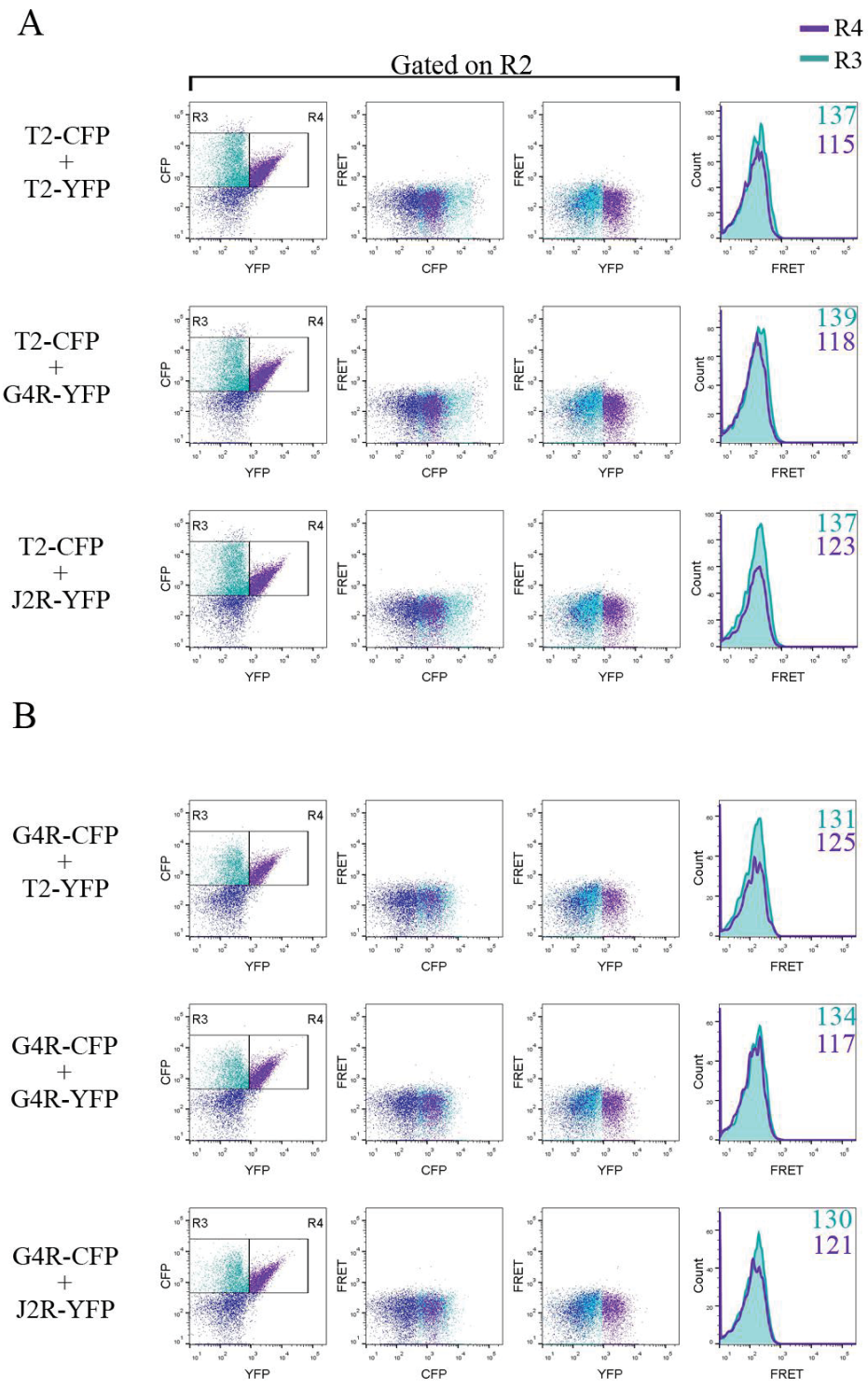
A
R4
R3
Gated on R2
T2-CFP
+
T2-YFP
T2-CFP
+
G4R-YFP
T2-CFP
+
J2R-YFP
R3
R4
CFP
YFP
FRET
Count
137
115
139
118
137
123
B
G4R-CFP
+
T2-YFP
G4R-CFP
+
G4R-YFP
G4R-CFP
+
J2R-YFP
131
125
134
117
130
121

C

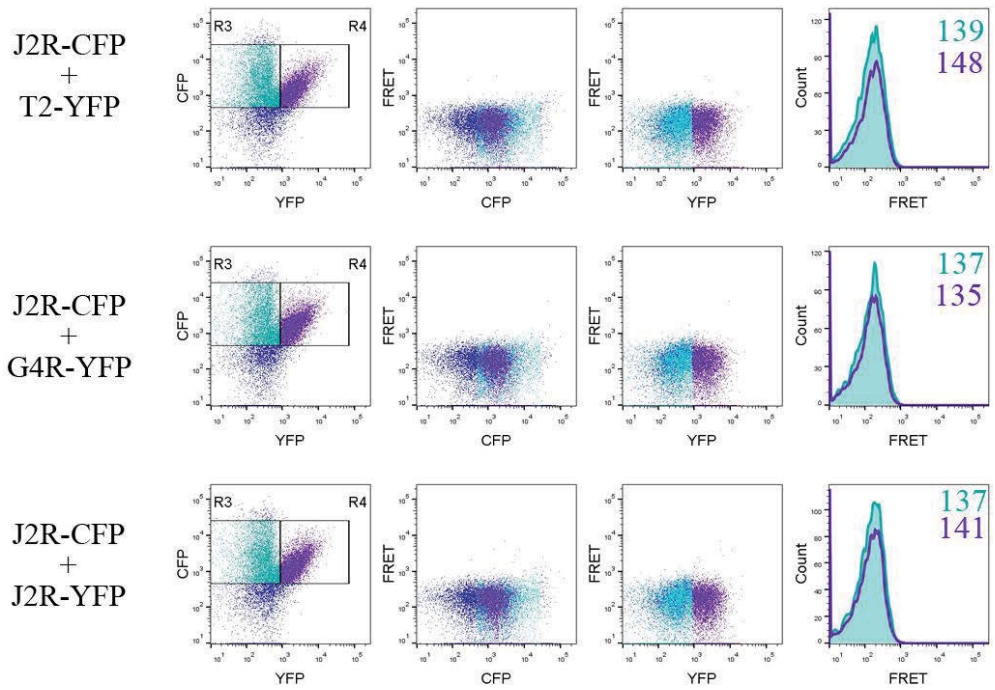

Figure 5.11 Flow cytometry analysis of FRET from cells co-expressing vTNFRs
Flow cytometry analysis of FRET between vTNFR-CFP and –YFP pairs in 293 HEK expressing cells. A) pcDNA3.MYXT2-CFP, B) pcDNA3.VARG4R-CFP or C) pcDNA3.MPVJ2R-CFP was co-transfected with each pcDNA3.MYXT2-YFP, pcDNA3.VARG4R-YFP and pcDNA3.MPVJ2R-YFP. FRET was then analysed 48 hours post transfection in $CFP^{+}YFP^{+}$ cells (R4, purple) and compared to a spiked population of CD27-CFP only cells (R3, cyan) (background level of FRET. A positive FRET emission was determined as a shift from the R3 population in each of the CFP vs FRET, YFP vs FRET dot plots and the FRET histograms overlays. The data shown is the median representative transfection from independent triplicate transfections with 30000 events collected for each sample. The numbers shown in the FRET histogram overlays are MFI values for the respective colour coded cell populations.

5.8 Comparative modelling of vTNFRs, and in complex with cellular TNFRs

Although no FRET emission was detected between MYXT2, VARG4R or MPVJ2R, with TNFR1 or TNFR2, a number of interpretations can be made about the orientations of the vTNFRs when associating with TNFR1 or TNFR2. FRET can only occur within 10nm, therefore an absence of FRET emission does not necessarily suggest that there is no literal association. In fact an association of MYXT2 has been previously demonstrated to physically interact with human TNFR1 and TNFR2 (Sedger et al. 2006). Using the results from the FRET experiments as well as the X-ray crystallography structures from TNFR1 (Naismith et al. 1996), TNFR2 (Mukai et al. 2010), CRM-E from vaccinia virus (Graham et al. 2007) and the so called C-terminal "SECRET" domain from Ectromelia virus (Xue et al. 2011), comparative modelling was used to explore possible structures of MYXT2, VARG4R and MPVJ2R with human TNFR1 and TNFR2. To generate full length models of MYXT2, VARG4R and MPVJ2R the modelling software UCSF Chimera (version 1.10.2) was used. To model each vTNFR, the target sequences for MYXT2 (E2CZP3), VARG4R (P34015) and MPVJ2R (V9NNY9) were obtained from the UNIPROT database. Each target sequence was then used to perform a BLAST search using Chimera's BLAST protein tool with the default settings to search the protein data bank (PDB: a database of known structures) for sequences similar to the MYXT2, VARG4R and MPVJ2R. Multiple template sequences can be utilised in Chimera to model each MYXT2, VARG4R and MPVJ2R. The sequences/structures with the highest sequence identity and E values (significance of target-template sequence alignment reported by template search) were used from each of the TNFR1, TNFR2, CRM-E and the SECRET domain structures as reference templates. MYXT2, VARG4R and MPVJ2R are all highly similar in sequence

similarity (~85% identity between VARG4R and MPVJ2R, ~50% between MYXT2 and VARG4R or MPVJ2R) and each containing CRDs and a SECRET domain. Therefore TNFR1 (PDB iD: 1TNR, the extracellular domain; chain R), TNFR2 (PDB iD: 3ALQ, the extracellular domain; chain W), and CRM-E (PDB iD: 2UWI; chain B of the dimer) were used to model the CRDs of each vTNFR. On the other hand the SECRET domain was modelled from the crystal structure of the SECRET domain of CRM-D from Ectromelia virus (PDB iD: 3ON9 chain B). Using Chimera's Match/Align tool each of the template models (TNFR1, TNFR2 and CRM-E) were first superimposed with TNFR2 (PDB iD:3ALQ) as the reference structure is used to orientate the molecules in the correct position and overlay each of the target sequences MYXT2, VARG4R and MPVJ2R. Note, the SECRET domain was not included in the superposition as it contained no homology to the other templates. The best aligning pair of proteins were matched using the Needleman-Wunsch alignment algorithm (Rose & Eisenmenger 1991) and a BLOSUM-62 matrix as recommended by the default Chimera settings. Matching was iterated by pruning long atom pairs until no pair exceeded 2.0 angstroms. Once the superposition was complete, a multiple alignment was performed to verify and refine the target sequence alignments to MYXT2, VARG4R and MPVJ2R against all of the template model sequences. The multiple alignment was performed using Clustal Omega (http://www.ebi.ac.uk/Tools/msa/clustalo/) on the default settings (number of guide-tree/HMM iterations = 1, using full distance matrix during initial alignment and using full distance matrix during alignment iteration.) (Sievers et al. 2011). From each of the multiple alignments the comparative modeller tool "Modeller (homology)" (Sali & Blundell 1993) was run via the web service using all template sequences PDB iDs:1TNR_R (TNFR1), 3ALQ_W (TNFR2), 2UWI_B (CRM-E) and 3ON9_B (CRM-D SECRET domain). All settings were run with default parameters, except the "thorough optimisation" parameter which was turned on and recommended for

multi-domain proteins. The results returned 5 generated models for each MYXT2, VARG4R and MPVJ2R and the predicted fit of each model was evaluated using the best scoring criteria provided by Modeller. “GA341” is a model score derived from statistical potentials; a value > 0.7 generally indicates a reliable model, >95% probability of having the correct fold (Melo, Sanchez & Sali 2002) (Table 5-1). zDOPE is a normalized Discrete Optimized Protein Energy (DOPE) score, it is an atomic distance-dependent with negative values indicating better models (Shen & Sali 2006) (Table 5-1). A score of the root mean square distances overlap of the α-carbon (RMSD) among the residues was also used to best verify the best predicted model, with lower values indicating better alignments to the template structures (Eramian et al. 2008) (Table 5-1). Thus using each of the evaluative scores, a predicted model was selected for each MYXT2, VARG4R and MPVJ2R (Figure 5.12). The lowest combined scores from the predicted models of MYXT2 was model 3, with a GA341 of 1.0 indicating a very reliable model and have correct folds, a zDOPE score of 0.02 indicating the most stable model and an RMSD of 5.246 which was most similar to the templates (Table 5-1). For VARG4R model 3 was also selected with the top scoring GA341, zDOPE and RMSD of 1.0, 0.06 and 3.354 respectively (Table 5-1). For MPVJ2R model 2 was selected with a GA341 score of 1.0, a zDOPE score of 0.06 and an estimated RMSD of 3.354 (Table 5-1). The zDOPE score was used with a heavier weighting than the RMSD score when selecting the models for each vTNFR, as it represents the most stable conformation rather than similarity to template represented by the RMSD.

Visually each model conformed to the structurally conserved folds found in TNFR1 and TNFR2 molecules forming 4 CRDs for each of the vTNFRs (Naismith & Sprang 1998) (Figure 5.12). The SECRET domain for each of the predicted structures also conformed

to the barrel beta sheet structure described in the analogous regions of CRM-D (Xue et al. 2011). Whilst CRD1 and CRD2 appear conserved amongst the three models CRD3 and CRD4 differ in the orientation and position of the alpha helices (Figure 5.12). As none of the template structures (TNFR1, TNFR2, CRM-E or CRM-D SECRET domain) spanned the domain between the SECRET domain and CRD4 of the vTNFRs, the residues spanning this region varied the most between each of the predicted structures (Figure 5.12). This was especially true for MPVJ2R as the domain between the SECRET domain and CRD4 distorted the molecule into a curved structure which may create steric hindrances when binding TNFα or binding to the human TNFR1 or TNFR2 receptors. Of note without a complete model or template of the any of the vTNFRs containing a SECRET domain, it is difficult to assess a true conformation of the residues between CRD 4 and the SECRET domain and hence without a template the models varied significantly.

Table 5-1 Statistical validation of predicted vTNFR models

vTNFR	Model	GA341	zDOPE	Estimated RMSD
MYXT2	1	1.0	0.04	9.521
	2	1.0	0.20	10.123
	3*	1.0	0.02	5.246
	4	1.0	0.14	4.171
	5	1.0	0.11	7.335
VARG4R	1	1.0	0.11	7.286
	2	1.0	0.12	3.948
	3*	1.0	0.06	3.354
	4	1.0	0.17	14.018
	5	1.0	0.12	4.247
MPVJ2R	1	1.0	0.10	3.099
	2*	1.0	0.09	3.044
	3	1.0	0.11	6.238
	4	1.0	0.13	6.605
	5	1.0	0.13	3.929

* Selected vTNFR model based on statistical scores

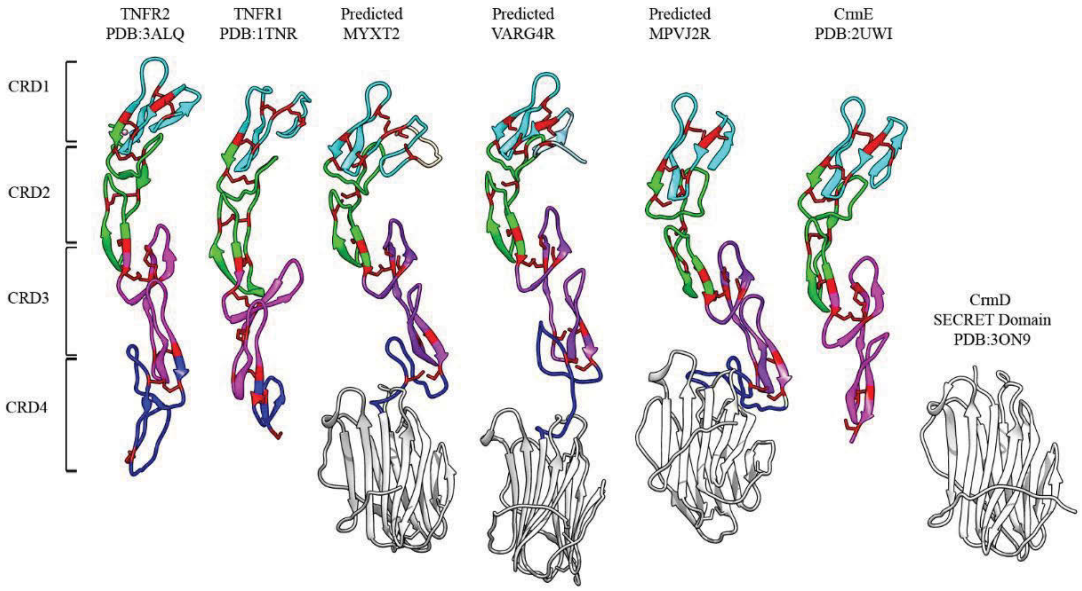

Figure 5.12 Comparison of predicted vTNFR models to X-ray crystallography structures of human TNFR1, human TNFR2, Vaccinia virus CRM-E and Ectromelia CRM-D SECRET domain.

The predicted full length models of MYXT2, VARG4 and MPVJ2R were generated in chimera using the TNFR1, TNFR2, CRM-E and the SECRET domain of CRM-D as templates. Models were constructed using the Modeller web based server tool within chimera to generate 5 models of each vTNFR. These models were then evaluated using the GA341, zDOPE and RMSD scores to select the model of best fit shown. Each CRD is colour coded in each predicted model; CRD1 (cyan), CRD2 (green), CRD3 (purple), CRD4 (blue).

5.9 Prediction of MYXT2, VARGAR and MPVJ2R structures in complex with TNFR1 and TNFR2

Since bacterial expressed proteins for crystal structures of MYXT2, VARGAR and MPVJ2R, were unable to be generated during the thesis project, a preliminary prediction of the docking of each of the vTNFRs with TNFR1 and TNFR2 were generated using the known PDB structures 1TNR (TNFR1) and 3ALQ (TNFR2). For each of the generated models of MYXT2, VARG4R and MPVJ2R, the selected model was saved into the PDB file format. Then each of the structures were submitted to a web-based program for the computational docking of the protein structures called ClusPro (Ver 2.0). ClusPro is

automated algorithm that evaluates billions of putative complexes, filtering and returning a number of structures with favourable surface complementarities (Comeau et al. 2004a). A receptor and ligand PDB model is uploaded to the server and then the ligand is rotated 70 000 times around the receptor. For each rotation, the ligand is translated in the X, Y and Z coordinates relative to the receptor, with the best scoring complementary model selected. The best 1000 rotations are then chosen that have the best surface complementary predicted structure based on a clustering algorithm (Comeau et al. 2004a). The program then returns ten of the best cluster size scoring models. However it reports that although a scoring system is applied it cannot meaningfully discriminate between the top 1000 from the starting 10^9 positions (http://cluspro.bu.edu/help.php). Consequently published structural data relating to ligand complementarity on TNFR1 (Naismith et al. 1996), TNFR2 (Mukai et al. 2010) and CRM-E (Graham et al. 2007) was used to pick the most relevant model out of the ten best scoring docking predictions. The most likely structures based on this data was then visualised using Pymol (ver 1.7.4.5) in the following results. Please note, that although the most probable structure was selected and visualised based upon evidence of cellular and viral TNFRs, each of the represented predicted structures from the ClusPro output could theoretically exist. It is Important to be mindful, that the structures represented below are computer predictions and further in vitro experimentation is always required to confirm them.

It is well known that TNFR1 and TNFR2 bind ligands, TNFα and LTα, with contact occurring within CRD2 and CRD3 (Marsters et al. 1992; Mukai et al. 2010; Naismith et al. 1996). Both TNFR1 and CRM-E from their respective crystal structures (Graham et al. 2007; Naismith et al. 1996) are reported to form two types of dimers in their crystal

packing; one dimer a parallel N-N terminal dimer and the other a C-N terminal dimer. Between these two structures the N-N dimers forms contacts within CRD1, and the anti-parallel dimer forms contacts between CRD1 and CRD3 (Graham et al. 2007; Naismith et al. 1996). Therefore models of MYXT2, VARG4R and MPVJ2R closest resembling these expected conformations with human TNFR1 and TNFR2 were selected from the output from ClusPro.

5.10 Predicted models of MYXT2, VARG4R and MPVJ2R with human TNFR1

Determination of the binding energies of the different conformations of TNFR1 with and without LTα show that the electrostatic forces between dimeric TNFR1 receptors is much less than the nonpolar forces, thus the hydrophobic forces are more prominent for the unligated form of TNFR1 (Mascarenhas & Kastner 2012). Thus as a result, each model was docked against the highest resolution dimer of TNFR1 from PDB (1EXT), and from the ClusPro output for each MYXT2, VARG4R and MPVJ2R complexed with human TNFR1, the hydrophobic favourable models were selected (Figure 5.13). MYXT2 was predicted to dimerise with TNFR1 in an N-C terminal orientation, with contact surfaces occurring between CRD1 of MYXT2 and CRD3 of TNFR1 (Figure 5.14). The main amino acid residues involved in the docking surfaces are R13, L19, H59, N58 in CRD1 of MYXT2 which form polar bonds to residues R77, E79, in CRD3 and E147, E161, Q113 in CRD3 of TNFR1 (Figure 5.14). The N-terminus of TNFR1 primarily makes contact through residues Q17, K32 and S63 in CRD1 with residues K112, D127, Y95 in CRD1 of MYXT2 (Figure 5.14). Thus, interestingly the orientation of the molecules are N-C terminal anti-parallel which appears to occlude the CRD2 and 3 binding sites for TNFR1.

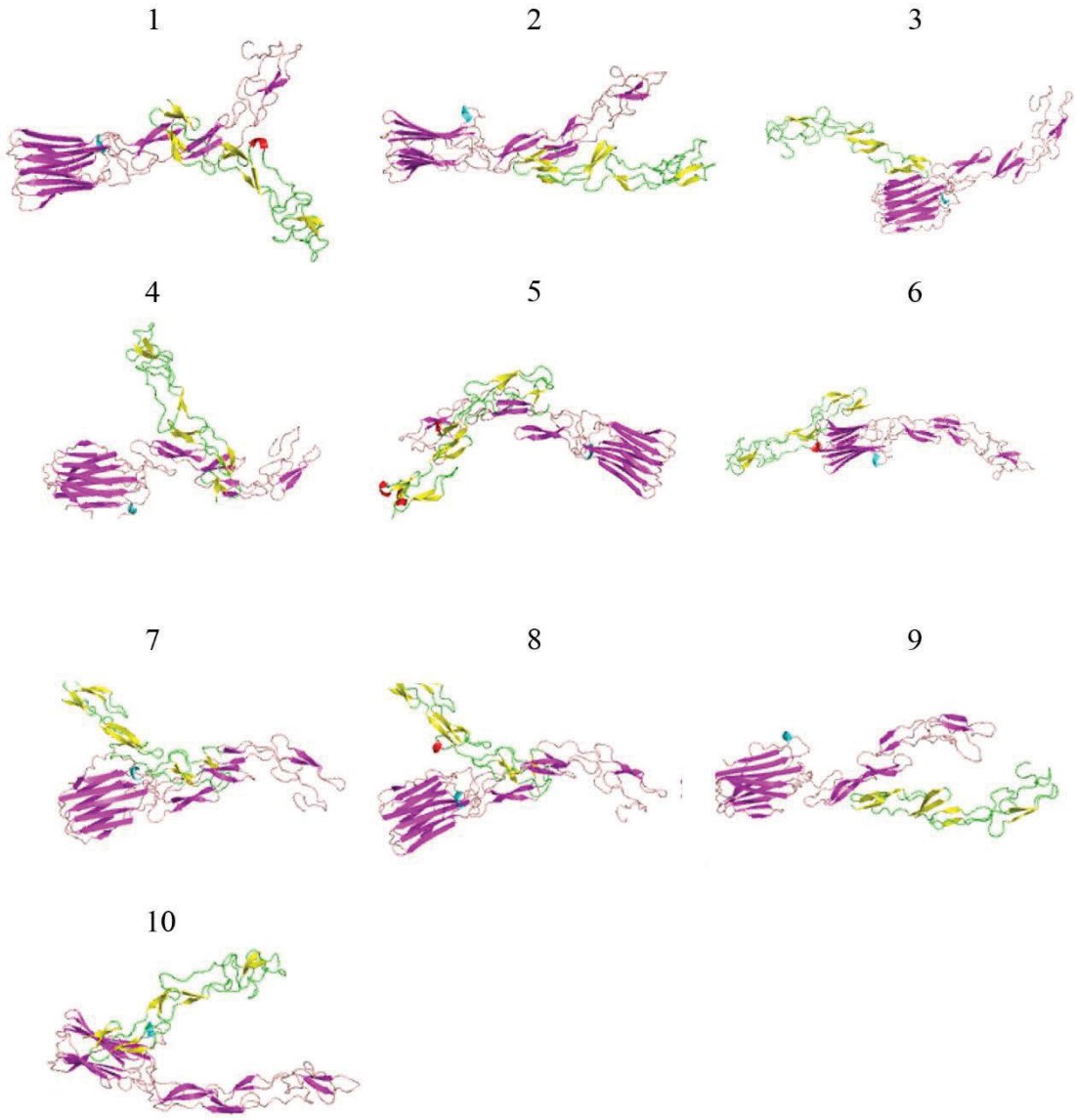

Figure 5.13 Top predicted docking surfaces between MYXT2 and the extracellular domain of TNFR1

The top ten predicted hydrophobic favoured docking surfaces shown between the PDB structure 1EXT (TNFR1) and the generated model of MYXT2, from the filtered ClusPro server output. MYXT2 from the Chimera generated model is shown in purple and the PDB extracellular domain structure of TNFR1 is shown in yellow.

Figure 5.14 Possible Interaction surfaces between MYXT2 and human TNFR1
Model 5 from the ClusPro output was selected due to the most likely interaction surfaces based on evidence from the X-ray crystallography structure of TNFR1 and known binding sites of each molecule. This model was then visualised and analysed for polar contacts using Pymol. A) Shows the full length view of the two molecules MYXT2 (yellow) and TNFR1 (purple) with polar contacts between amino acid side chains shown as cyan dotted lines. B) Shows the enlarged view of the contacts between CRD1 of TNFR1 and CRD3 of MYXT2. C) An enlarged view of the surfaces between CRD1 of MYXT2 and CRD3 of TNFR1. Amino acid side chains contributing to polar contacts are labelled.

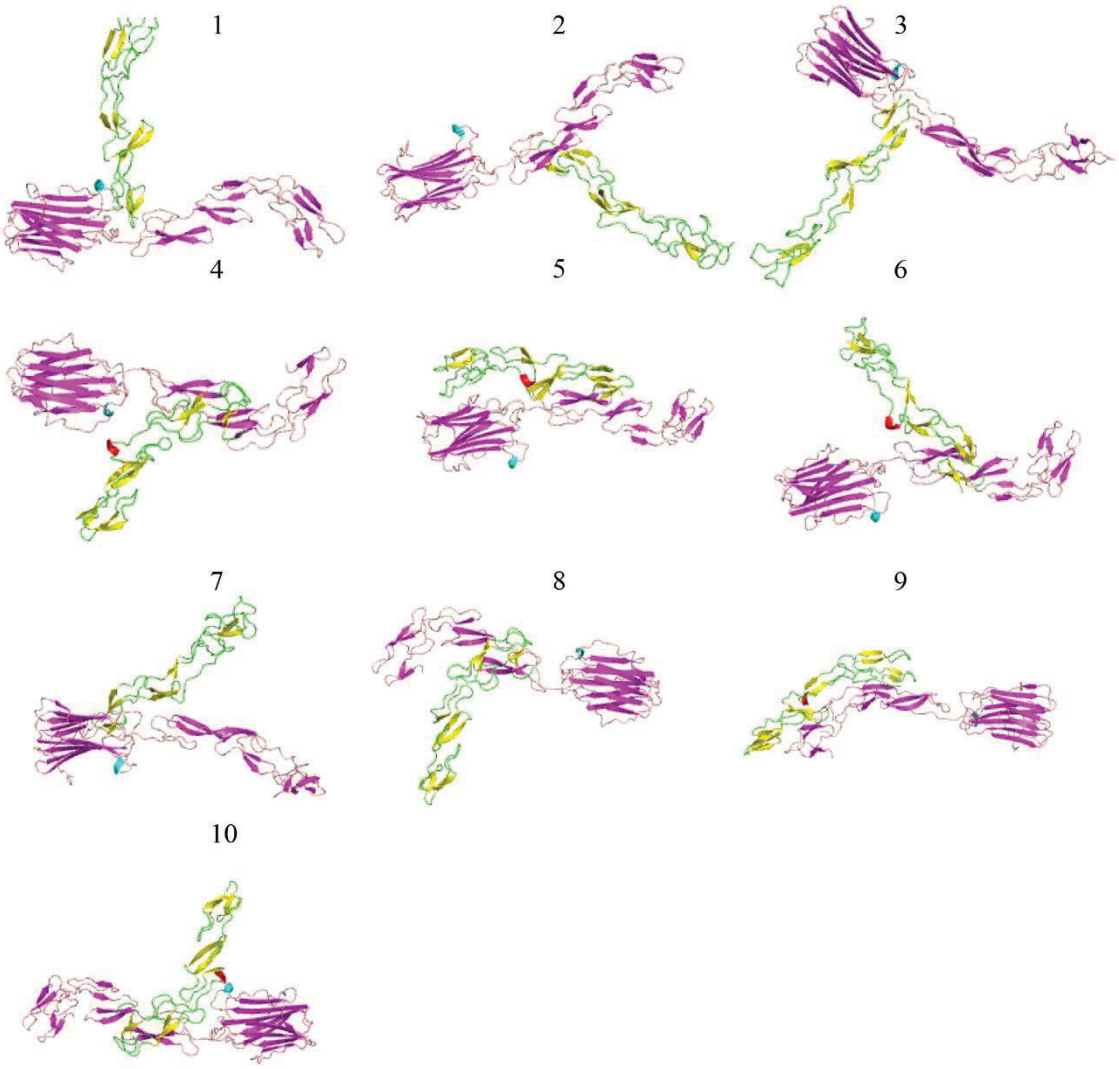

Figure 5.15 Top predicted docking surfaces between VARG4R and the extracellular domain of TNFR1

The top ten predicted hydrophobic favoured docking surfaces between the PDB structures 1EXT (TNFR1) and the generated model of VARG4R, are shown from the filtered ClusPro server output. VARG4R from the Chimera generated model is shown in purple and the PDB extracellular domain structure of TNFR1 is shown in yellow.

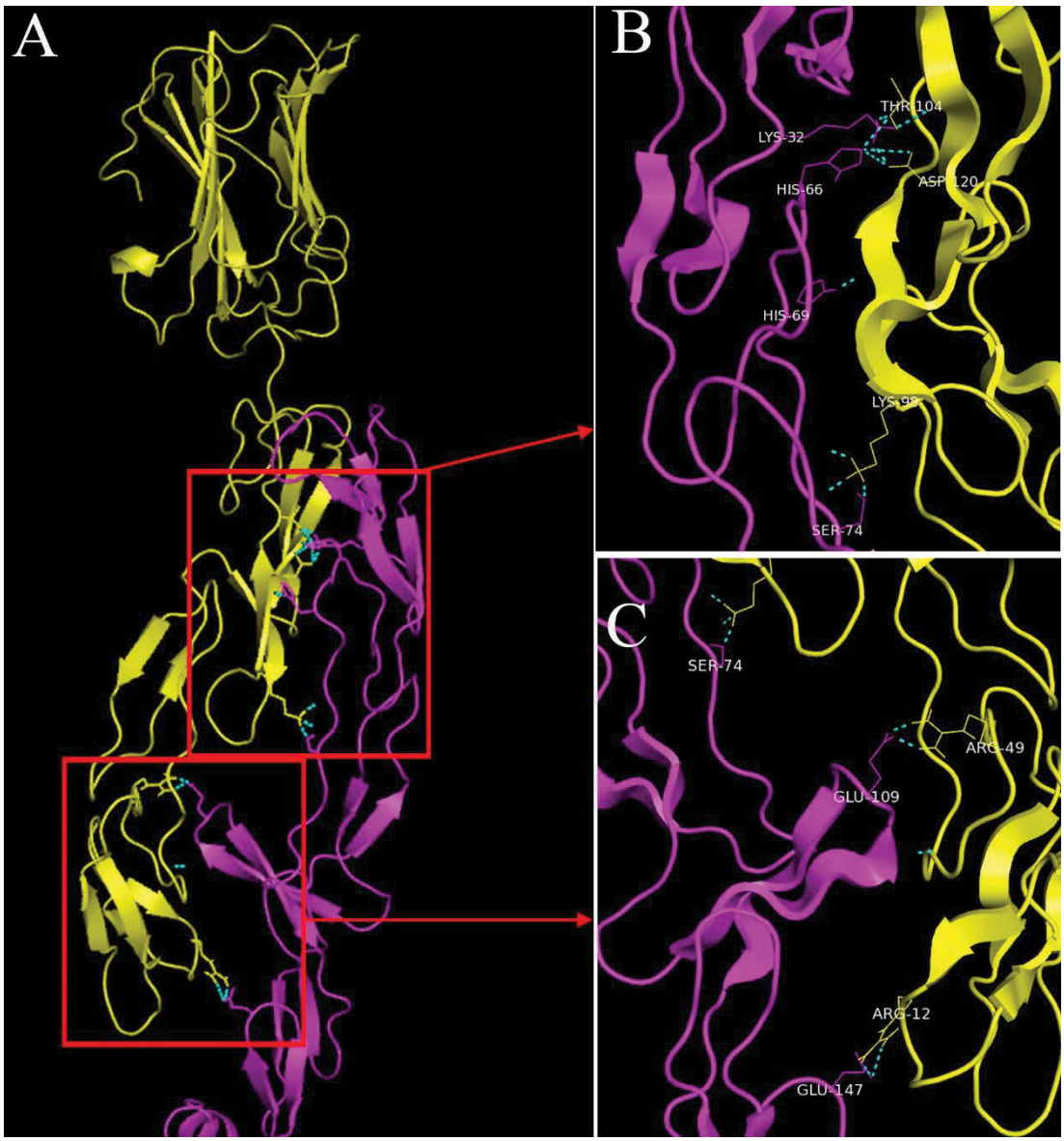

Figure 5.16 Possible Interaction surfaces between VARG4R and human TNFR1
Model 9 from the ClusPro output was selected due to the most likely interaction surfaces based on evidence from the X-ray crystallography structure of TNFR1 and known binding sites of each molecule. Using Pymol software, the structures were rendered and assessed for polar contacts. A) VARG4R (yellow) and TNFR1 (purple) is displayed in full length with polar contacts shown as cyan dotted lines. Enlarged views of the predicted interacting surfaces between B) CRD1 of TNFR1 and CRD3 of VARG4R and C) CRD3 of TNFR1 and CRD1 of VARG4R. Amino acid side chains contributing to polar contacts are labelled.

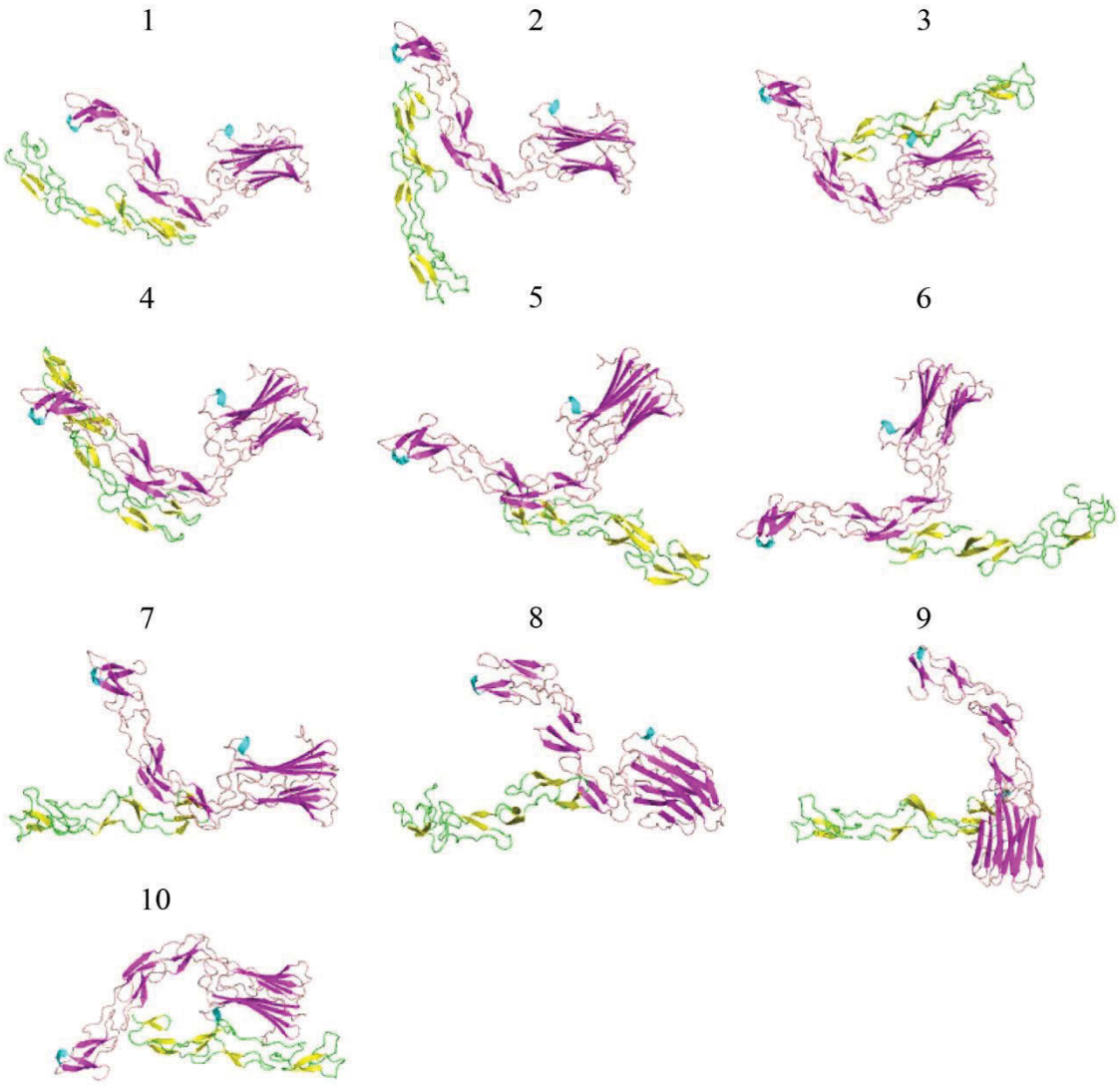

Figure 5.17 Top predicted docking surfaces between MPVJ2R and the extracellular domain of TNFR1

The top ten predicted hydrophobic favoured docking surfaces between the PDB structures 1EXT (TNFR1) and the generated model of MPVJ2R, are shown from the filtered ClusPro server output. MPVJ2R from the Chimera generated model is shown in purple and the PDB extracellular domain structure of TNFR1 is shown in yellow.

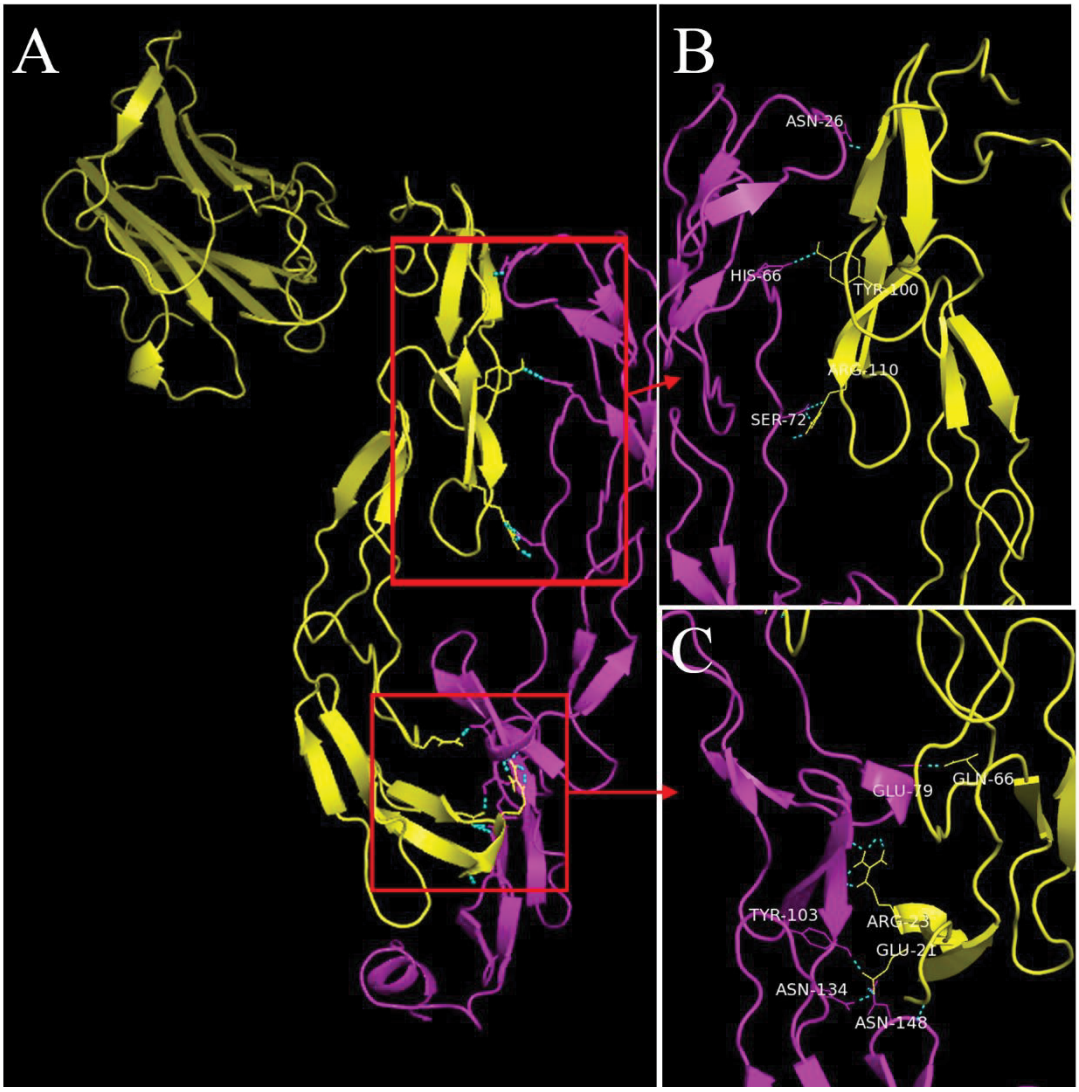

Figure 5.18 Possible Interaction surfaces between MPVJ2R and human TNFR1
Model 4 was selected from the ClusPro output based on evidence as likely interaction surfaces from the reported X-ray crystallography structure of TNFR1 and known binding sites of each molecule. A) Full length view of both the MPVJ2R (yellow) and TNFR1 (purple) are shown with polar contacts illustrated as (cyan) dotted lines. Enlarged views of the interacting surfaces between B) CRD1 of TNFR1 and CRD3 of MPVJ2R, as well as C) CRD3 of TNFR1 and CRD1 or MPVJ2R are shown. Amino acid side chains contributing to polar contacts are labelled.

This orientation also positions the SECRET domain of MYXT2 away from the N-terminus of TNFR1 (Figure 5.14). VARG4R similarly also was orientated in the anti-parallel conformation and contained primary contact surfaces between CRD1 and CRD4 of both molecules (Figure 5.16). The CRD1 of VARG4R involved residues R12 which interacted with E147 in CRD3 of TNFR1 (Figure 5.16). CRD3 of VARG4R formed polar contacts through amino acid residues K98 and D120 that creates multiple bonds with the side

chains of K32, H66, H69 and S74 in CRD1 of TNFR1 (Figure 5.16). A single polar contact was predicted between the CRD2 of both proteins and likely formed by amino acid residues R49 in VARG4R and E109 in TNFR1 (Figure 5.16). However because only two polar contacts are formed in CRD1 of VARG4R the additional contact formed in CRD2 may help stabilise the hetero-complex between VARG4R and human TNFR1 (Figure 5.16).

MPVJ2R is predicted to adopt a slightly different conformation compared to MYXT2 and VARG4R but is still expected to associate with TNFR1 in an anti-parallel N-C conformation (Figure 5.17). Three contacts are found between CRD1 of MPVJ2R involving amino acid residues E21 R23 Q66 that form contacts with amino acids E79, Y103, N134, and N148 in human TNFR1 CRD3 and CRD4 (Figure 5.18). Only two amino acid residues Y100 and R110 from CRD4 of MPVJ2R form polar contacts with N26, H66, S72 within CRD1 and CRD2 of TNFR1.

Thus From the output of ClusPro for all of the favourable hydrophobic positions of MYXT2, VARG4R and MPVJ2R with TNFR1, all models were predicted to be orientated in the anti-parallel conformation and not were observed in the N-N parallel conformation (Figure 5.13, Figure 5.15 and Figure 5.17).

5.11 Models of MYXT2, VARG4R & MPVJ2R with TNFR1 in complex with LTα

To determine the possible orientations and conformations of MYXT2, VARG4R and MPVJ2R, with TNFR1 in complex with LTα, each of the previously generated models

were submitted to ClusPro and docked with the PDB structures of TNFR1 (1EXT; unligated receptor and 1TNR; TNFR1 bound to LTα). First MYXT2 was docked against the full TNFR1 PDB structure 1TNR which is found ligated to LTα. The output from ClusPro of the 10 top scoring models yielded a variation in docking sites between MYXT2, TNFR1 and LTα (Figure 5.19). To eliminate biologically irrelevant models, (i) those in which the primary surface between the SECRET domain is the main docking surface and (ii) models which possibly would create significant steric clashes were eliminated (Figure 5.19). The SECRET domain is known to bind chemokines and can bind TNF independently of chemokines (Xue et al. 2011). Therefore it is highly unlikely that these models will bind TNFR1 within this domain.

The most favourable selected structure for MYXT2 is suggested to bind the CRD3 of TNFR1 interacts with CRD1 of MYXT2, and LTα through CRD3 of MYXT2 (Figure 5.20). Two major polar contacts are found to occur between the CRD1 of MYXT2 and CRD3 of TNFR1 and four polar contacts between the CRD3 of MYXT2 and LTα (Figure 5.20). The orientation of the MYXT2:TNFR1 hetero-complex is shown as N-C parallel and allows the binding of LTα and correlates with the findings that MYXT2 can similarly bind TNF whilst bound to TNFR1 and TNFR2 (Sedger et al. 2006). This conformation also allows the SECRET domain of MYXT2 to be orientated away the plasma membrane which theoretically allows easier access to bind to chemokines. From all of the top 10 scoring models returned by ClusPro, none were found in the parallel orientation, suggesting that the parallel N-N orientation may be less energetically favourable, and not likely to occur in nature or in vitro overexpression as examined in this thesis.

The selected optimal structure for VARG4R was also predicted to adopt a similar conformation with TNFR1 and LTα as described for MYXT2. VARG4R was predicted to interact with CRD1 contacting the CRD4 of TNFR1 (Figure 5.21). Interestingly more extensive contacts are observed between VARG4R and LTα than compared to MYXT2 with 5 predicted contacts occurring between amino acid residues Y88, K98, Y110, D120 and S223 of CRD3 and LTα (Figure 5.22). Overall the structure adopts an anti-parallel N-C conformation with the SECRET domain positioned away from the N-terminus of TNFR1 (Figure 5.22). None of the returned VARG4R docked models from ClusPro adopted a parallel N-N conformation (Figure 5.21).

Finally MPVJ2R was predicted to generate the most extensive contacts with TNFR1 and LTα. CRD1 of MPVJ2R creates strong polar contacts with CRD3 of TNFR1. The MPVJ2R amino acid residues involved in creating the contact surface include D20, R23, and Y22 with T124, H126 and T138 of TNFR1 (Figure 5.24). The contact surface with LTα involves thirteen polar contacts between the CRD3 of MPVJ2R and LTα. The surface of the interaction occurs between amino acid residues Y100, L104, R110, T116, Y122, S129 and T130 with residues H131, Y134 Q78, E127 of LTα. The orientation of the interaction is again expected to be N-C terminal anti-parallel, with respect to TNFR1. Once again the SECRET domain is positioned away from the N-terminus of TNFR1 (Figure 5.24). Although this would not likely create any steric clashes with TNFR1 or LTα this may be the result of distortion of the region adjoining the SECRET domain and CRDs of MPVJ2R created in the initial modelling of MPVJ2R.

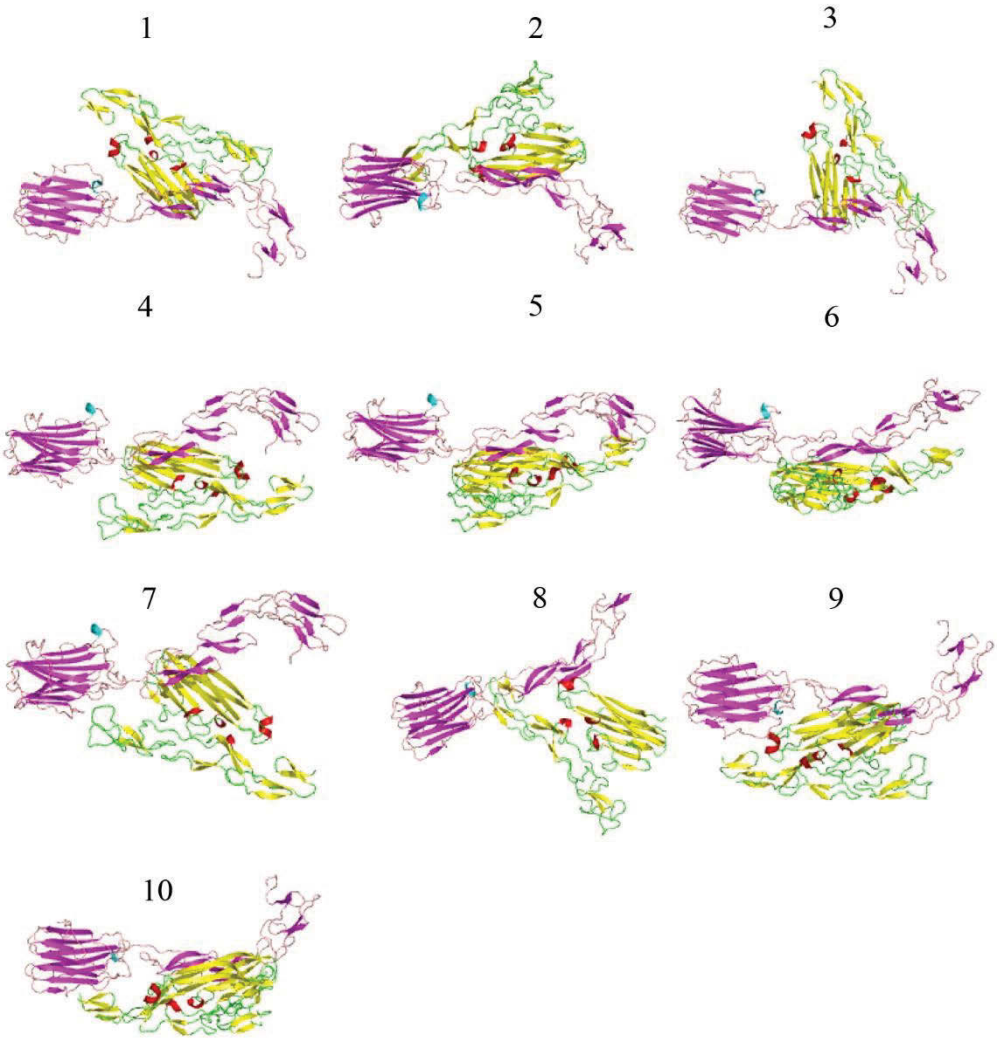

Figure 5.19 Top predicted docking surfaces between MYXT2 and the extracellular domain of TNFR1 in complex with LTα

The PDB structure 1TNR (TNFR1 in complex with LTα) (yellow) was docked with the generated model of MYXT2 (purple) from Chimera. The top returned hydrophobic favoured models are shown from the ClusPro server output.

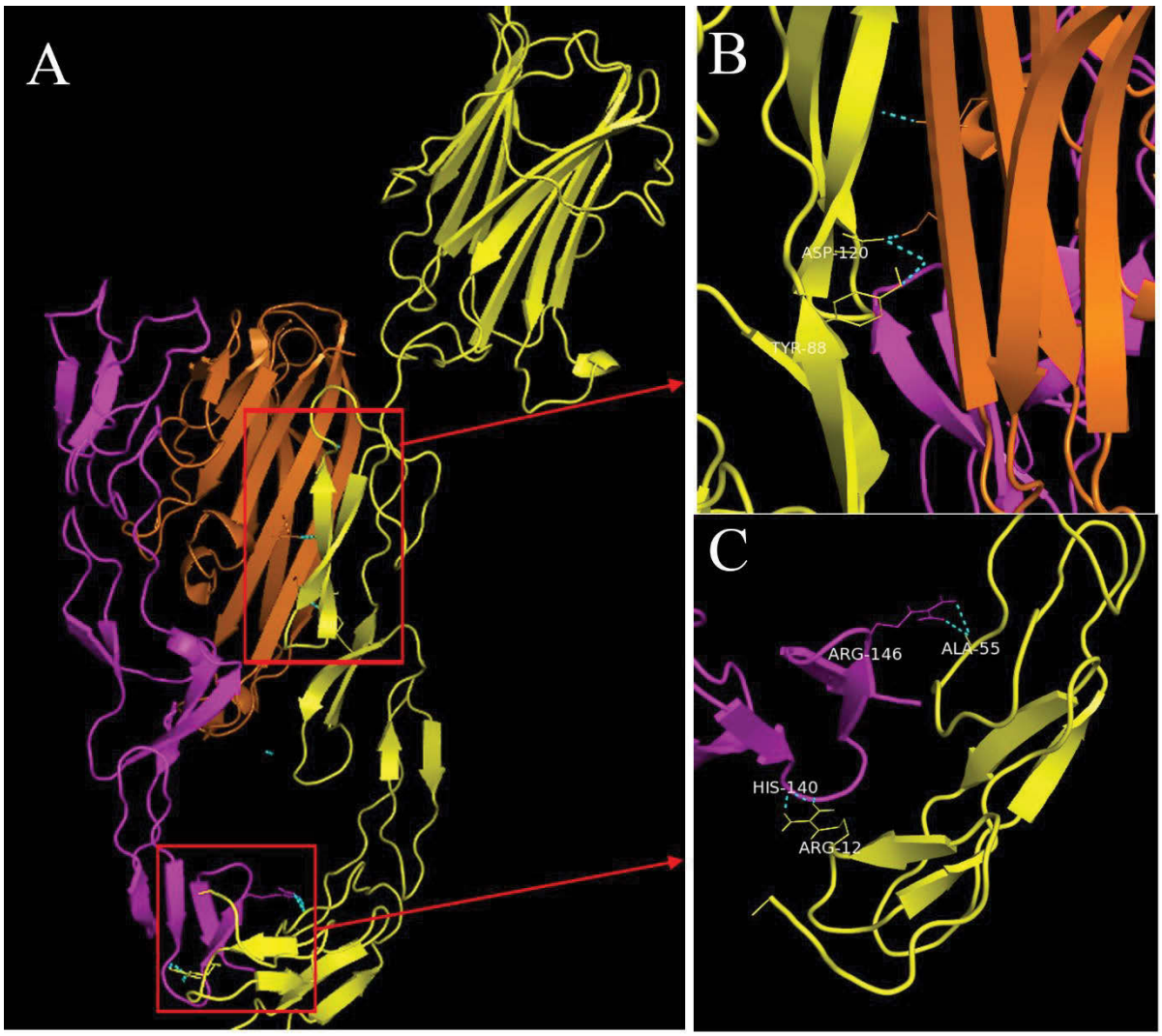

Figure 5.20 Predicted interacting surfaces of MYXT2 with TNFR1 in complex with LTα
Model 5 from the ClusPro Docking analysis was selected for further analysis in Pymol based on evidence from the X-ray crystal structures of TNFR1 and known binding sites of each molecule. A) Full view rendering of MYXT2 (yellow) in complex with TNFR1 (purple) and LTα (orange) is shown, with polar contacts shown as (cyan) dotted lines. B) An enlarged view of the surfaces of CRD1 of MYXT2 and also C) the CRD3 MYXT2 with each of the molecules is shown. Amino acid side chains contributing to polar contacts are labelled.

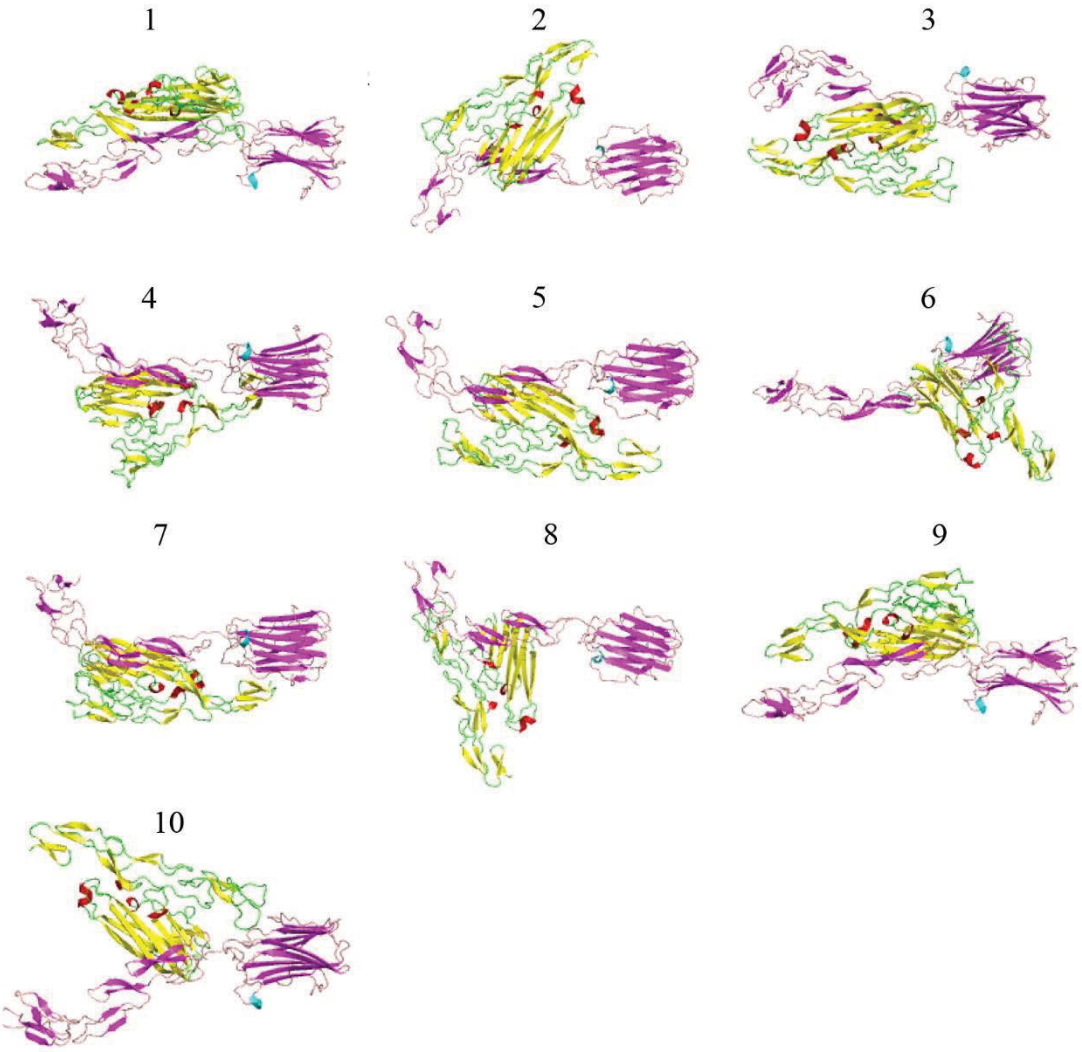

Figure 5.21 Top predicted docking surfaces between VARG4R and the extracellular domain of TNFR1 in complex with LTα

The PDB structure 1TNR (TNFR1 in complex with LTα) (yellow) was docked with the generated model of VARG4R (purple) from Chimera. The top returned hydrophobic favoured models are shown from the ClusPro server output.

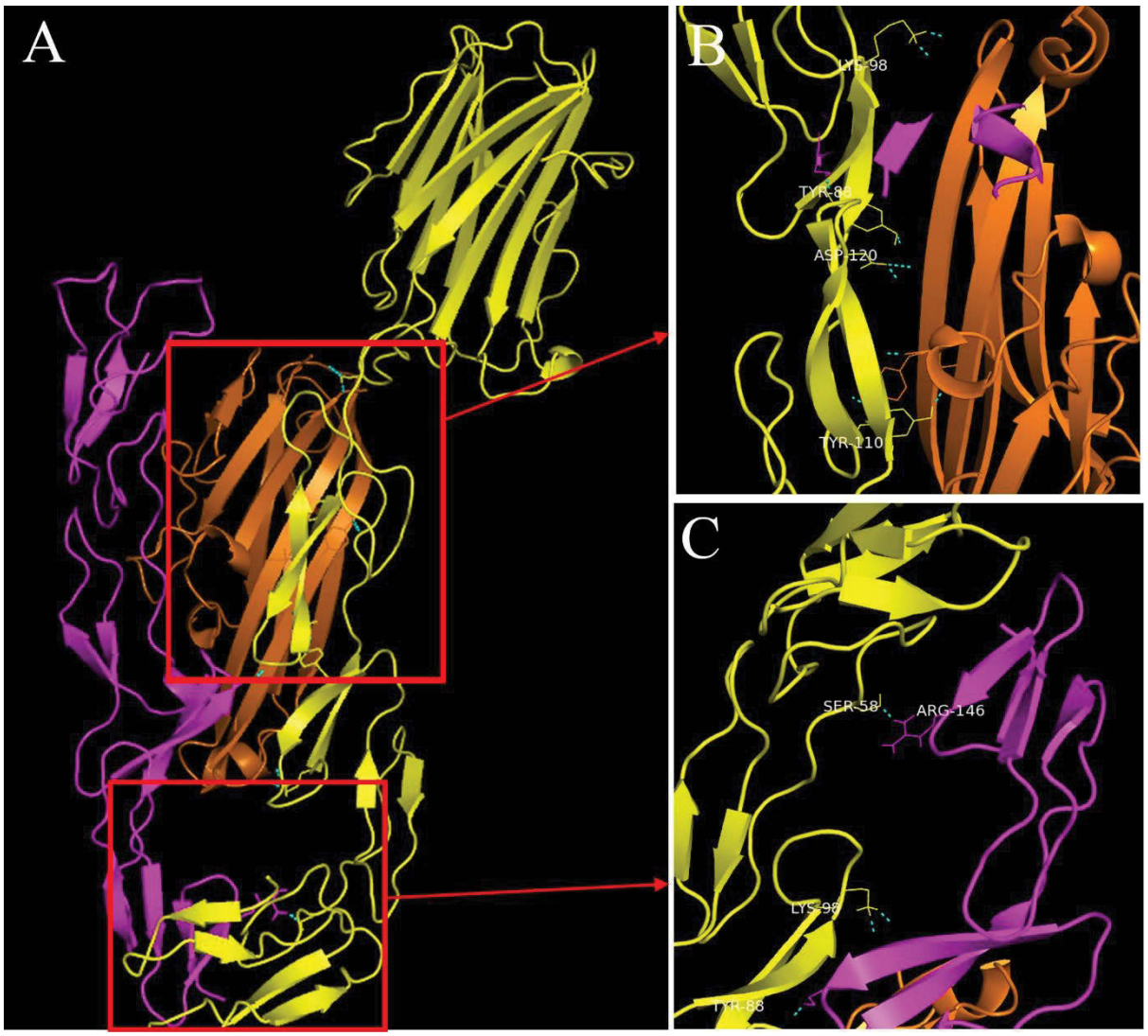

Figure 5.22 Predicted interacting surfaces of VARG4R with TNFR1 in complex with LTα
Model 1 from the ClusPro Docking analysis was selected for further analysis in Pymol based on evidence from the X-ray crystal structures of TNFR1 and known binding sites of each molecule. A) A 3D rendering in Pymol of VARG4R (yellow) in complex with TNFR1 (purple) and LTα (orange) is displayed, with polar contacts shown as (cyan) dotted lines. B) A detailed view of the surfaces of CRD1 of VARG4R and also C) the CRD3 VARG4R with each of the molecules is enlarged. Amino acid side chains contributing to polar contacts are labelled.

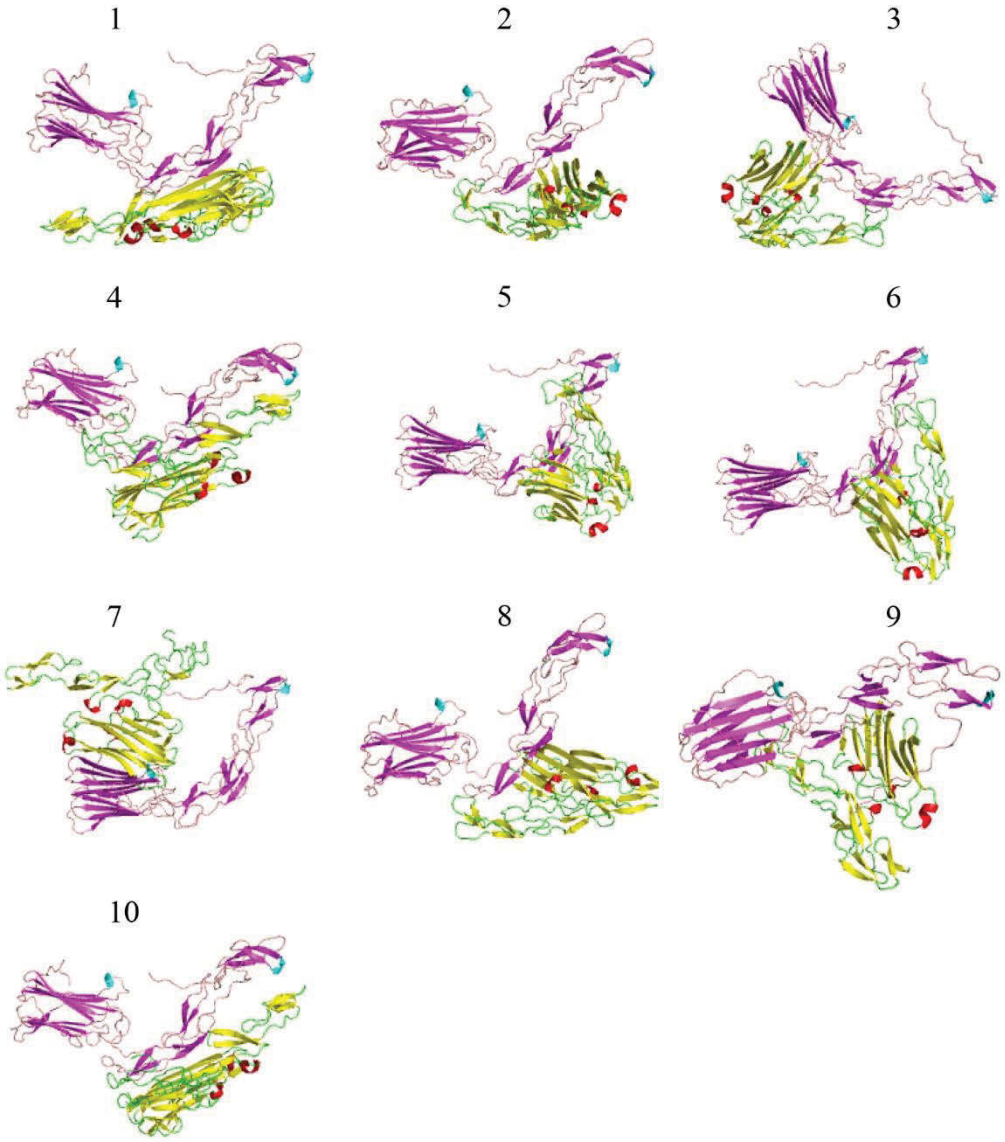

Figure 5.23 Top predicted docking surfaces between MPVJ2R and the extracellular domain of TNFR1 in complex with LTα

The PDB structure 1TNR (TNFR1 in complex with LTα) (yellow) was docked with the generated model of MPVJ2R (purple) from Chimera. The top returned hydrophobic favoured models are shown from the ClusPro server output.

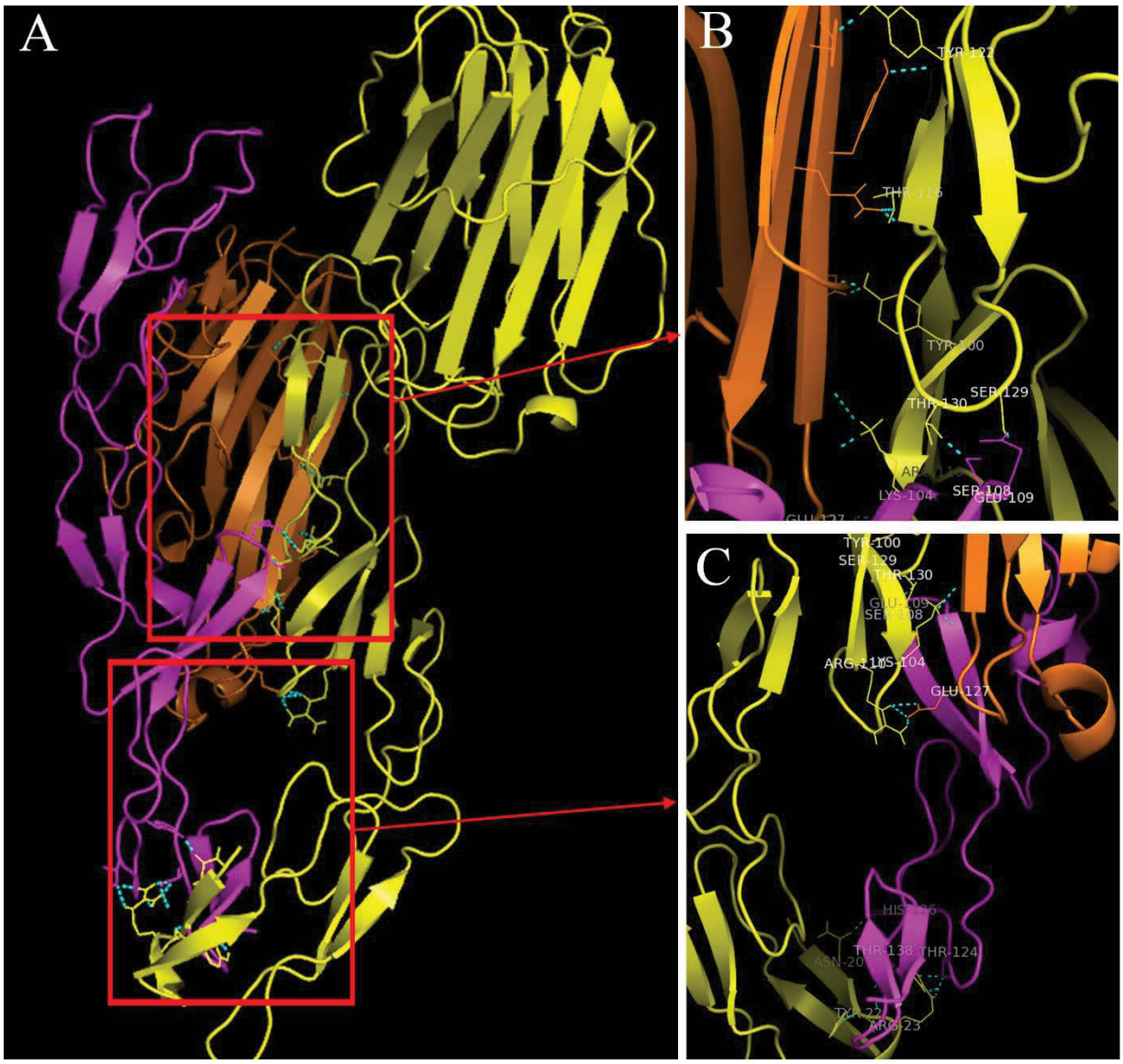

Figure 5.24 Predicted interacting surfaces of MPVJ2R with TNFR1 in complex with LTα
Model 4 from the ClusPro docking analysis was selected for further analysis in Pymol based on evidence from the X-ray crystal structures of TNFR1 and known binding sites of each molecule. A) A 3D rendering in Pymol of MPVJ2R (yellow) in complex with TNFR1 (purple) and LTα (orange) is displayed, with polar contacts shown as (cyan) dotted lines. B) A detailed view of the surfaces of CRD1 of MPVJ2R and TNFR1 as well as C) the CRD3 MPVJ2R with TNFR1 and LTα is enlarged. Amino acid side chains contributing to polar contacts are labelled.

5.12 Predicted models of MYXT2, VARG4R and MPVJ2R with human TNFR2 and TNFR2 in complex with TNFα.

To date only one structure of TNFR2 has been solved by X-ray crystallography shows a large complex of the extracellular domain of TNFR2 in association with TNFα (Mukai et

al. 2010). Although TNFR2 is homologous to TNFR1 and contains the canonical CRDs in the N-terminus, it differs from TNFR1 in how the CRDs are structured, especially CRD4 (Mukai et al. 2010; Naismith et al. 1996). Depending on how the structural disulphide bonds form each CRD and the number of bonds involved in each fold they are classified into either A, B, or C modules and numbered 1 or 2 (Naismith et al. 1996; Naismith & Sprang 1998). CRD3 and CRD4 in TNFR2 conform to slightly different folds compared to TNFR1 with TNFR2 CRD3 containing the A2, B1 modules compared to the A1, B2 in CRD3 of TNFR1 and CRD4 contains A1, B1 modules whereas TNFR1 contains an A1, C2 module (Mukai et al. 2010; Naismith et al. 1996; Naismith & Sprang 1998). Simulated docking was performed again in ClusPro for TNFR2 to predict the effect of these structural differences and the effect on association between the generated models of MYXT2, VARG4R and MPVJ2R.

Using the same settings in ClusPro as used for TNFR1, MYXT2 was model against the PDB model 3ALQ using chain W; one of the TNFR2 monomers from the TNFR2/TNFα complex (Mukai et al. 2010). The model that did not interact with the SECRET domain and most biologically relevant was selected. As with TNFR1, MYXT2 was observed to form an anti-parallel C-N dimer with TNFR2 although the main contacts with TNFR2 were largely seen to occur with CRD1 and CRD3 of TNFR2 (Figure 5.26). Five residues from the CRD2 in MYXT2 formed a contact surface involving residues Y95, N94, K112 and R105 with TNFR2 CRD1, and three residues K19, T57 and S56 formed a surface from CRD1 in MYXT2 with CRD3 in TNFR2 (Figure 5.26). The predicted conformation of these two molecules would occlude the TNFα an LTα binding site within TNFR2 and thus would need to undergo a dramatic conformation change to accommodate the ligand.

Interestingly VARG4R was observed to conform to a much more open conformation with TNFR2 compared to MYXT2 and only one contact surface was predicted between the two proteins where amino acid residues S117, T116, D120, S102 and T104 from CRD3 of VARG4R would form polar contacts with CRD1 in TNFR2 (Figure 5.28). This conformation although very open, is in an anti-parallel N-C conformation consistent with the other predicted structures of MYXT2 and MPVJ2R with TNFR1.

Also, MPVJ2R was also observed to form a unique dimer complex with TNFR2, again in the anti-parallel conformation. MPVJ2R was predicted to interact with TNFR2 predominately via CRD1 with numerous amino acid residues forming a contacts between CRD1 and CRD3 (Figure 5.30). R23, E21, Y22, K18 and Q66 from CRD1 create the main contacts of the interaction, however two residues from the loop region of MPVJ2R CRD3 (S106 and R110) also contribute to the association with CRD1 of TNFR2 (Figure 5.30). All other models from the ClusPro output of MPVJ2R with TNFR2 either created significant surfaces with the SECRET domain or would likely create steric clashes within the hetero-complex (Figure 5.29).

Human TNFR2 bound to TNFα using ClusPro against MYXT2, VARG4R and MPVJ2R was also investigated. However all of the filtered and top scoring models returned from each of the analysis resulted in models largely interacting with the SECRET domain of MYXT2, VARG4R and MPVJ2R. As it was stated previously the SECRET domain of CRM-D is known to bind chemokines and does so independently of binding with TNFα (Xue et al. 2011), therefore it was determined that the models were not likely valid representations of the complex/interaction (Data not shown).

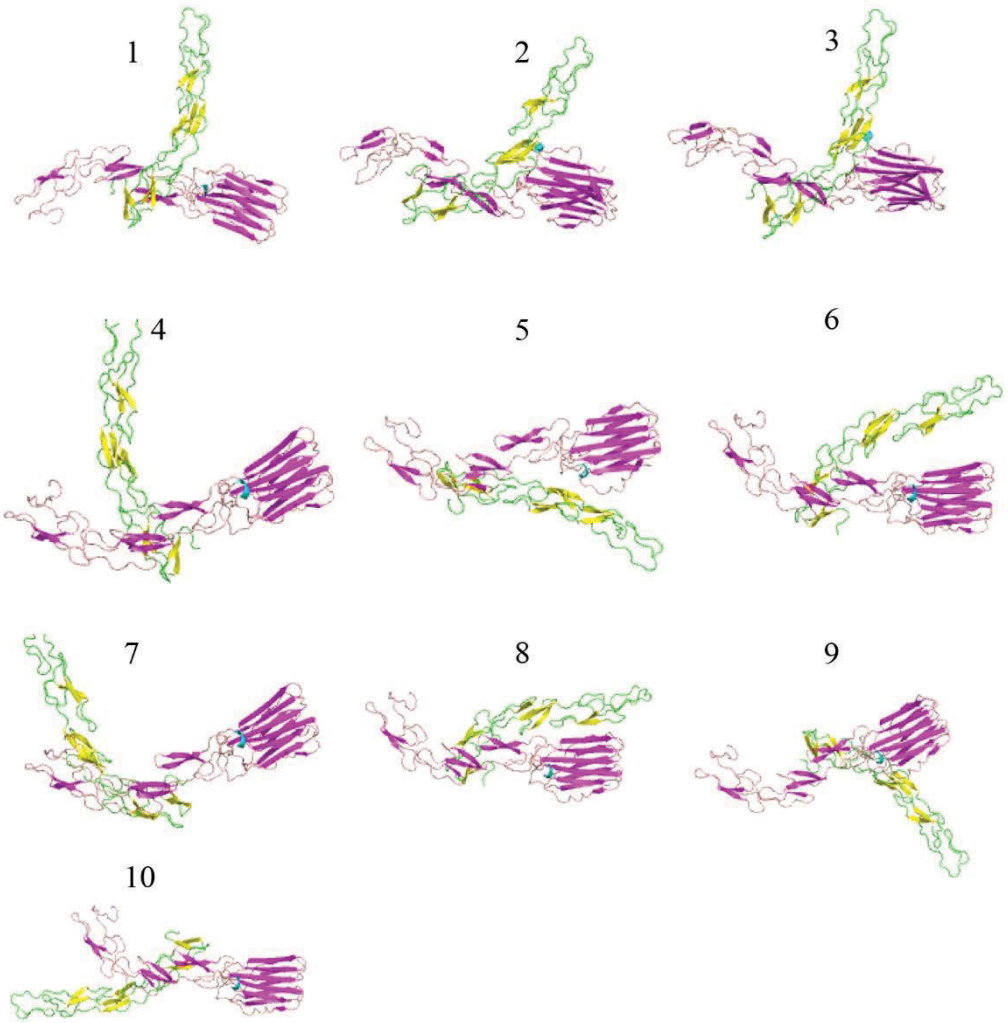

Figure 5.25 Top predicted docking surfaces between MYXT2 and the extracellular domain of TNFR2

The generated full length model of MYXT2 from Chimera was docked against the PDB structure; 3ALQ (TNFR2), using the ClusPro web server. The best computed hydrophobic favoured models are shown. MYXT2 is shown in purple and TNFR2 is shown in yellow.

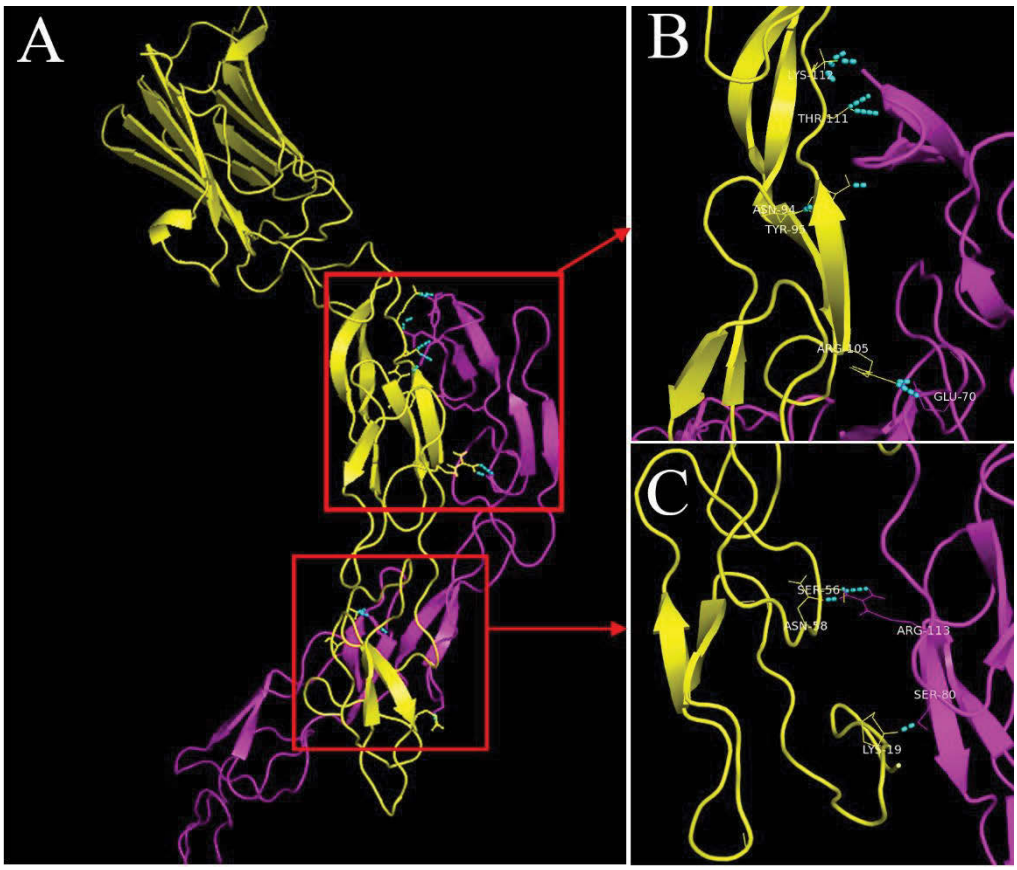

Figure 5.26 Predicted interacting surfaces of MYXT2 with human TNFR2
From the docking analysis from the ClusPro server, model 7 was selected using evidence based on the X-ray crystallography structure of TNFR2 and known binding sites of each molecule. A) A 3D rendered representation of the docking model was generated in Pymol showing MYXT2 (yellow) and TNFR2 (purple) and polar contacts were determined shown by (cyan) dotted lines. B) A detailed view of the predicted interacting surfaces between CRD1 of TNFR2 and CRD3 of MYXT2 as well as C) the CRD1 of MYXT2 with CRD3 of TNFR2 are enlarged. Amino acid side chains contributing to polar contacts are labelled.

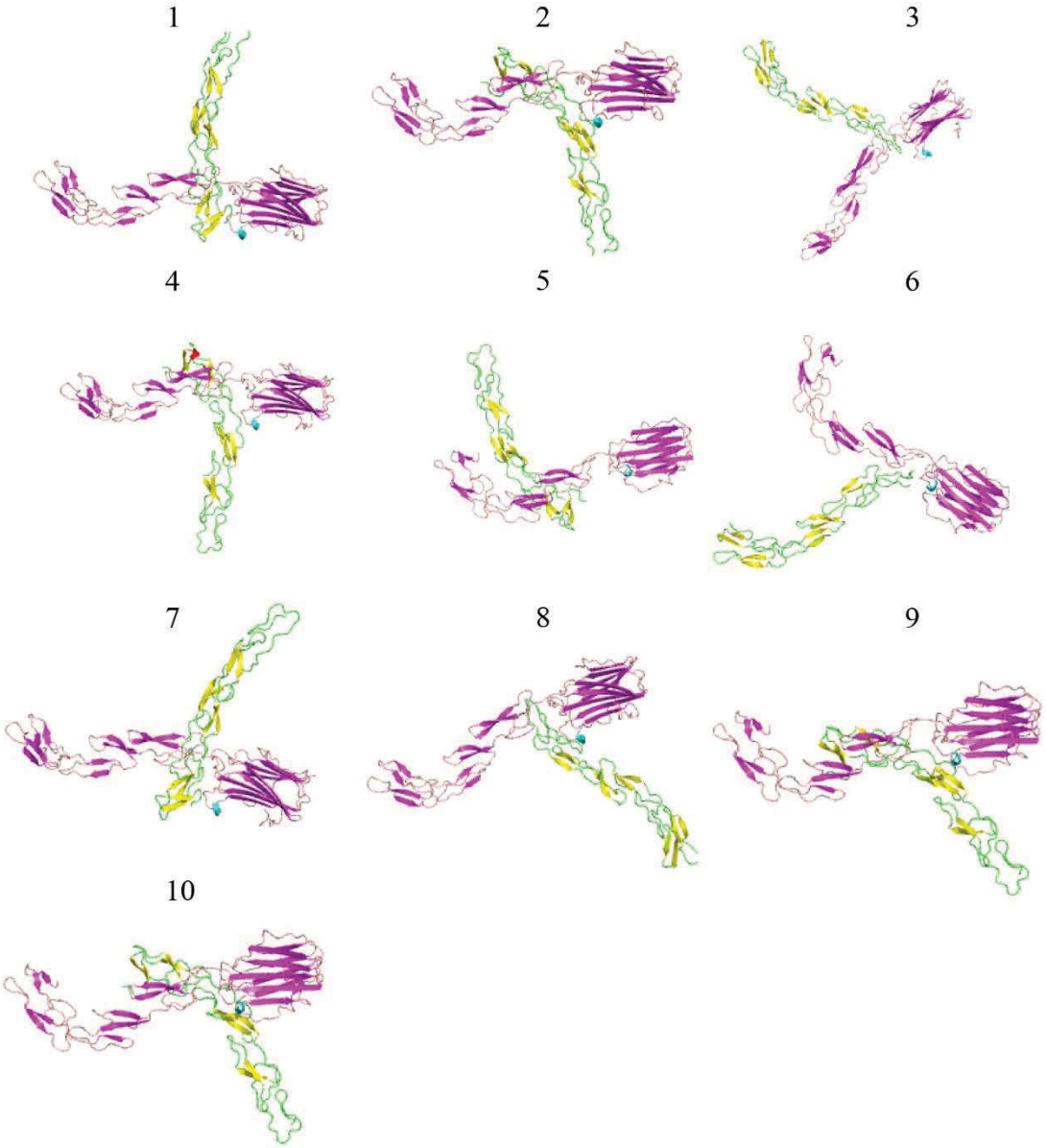

Figure 5.27 Top predicted docking surfaces between VARG4R and the extracellular domain of TNFR2

The generated full length model of VARG4R from Chimera was docked against the PDB structure; 3ALQ (TNFR2), using the ClusPro web server. The best computed hydrophobic favoured models are shown. VARG4R is shown in purple and TNFR2 is shown in yellow.

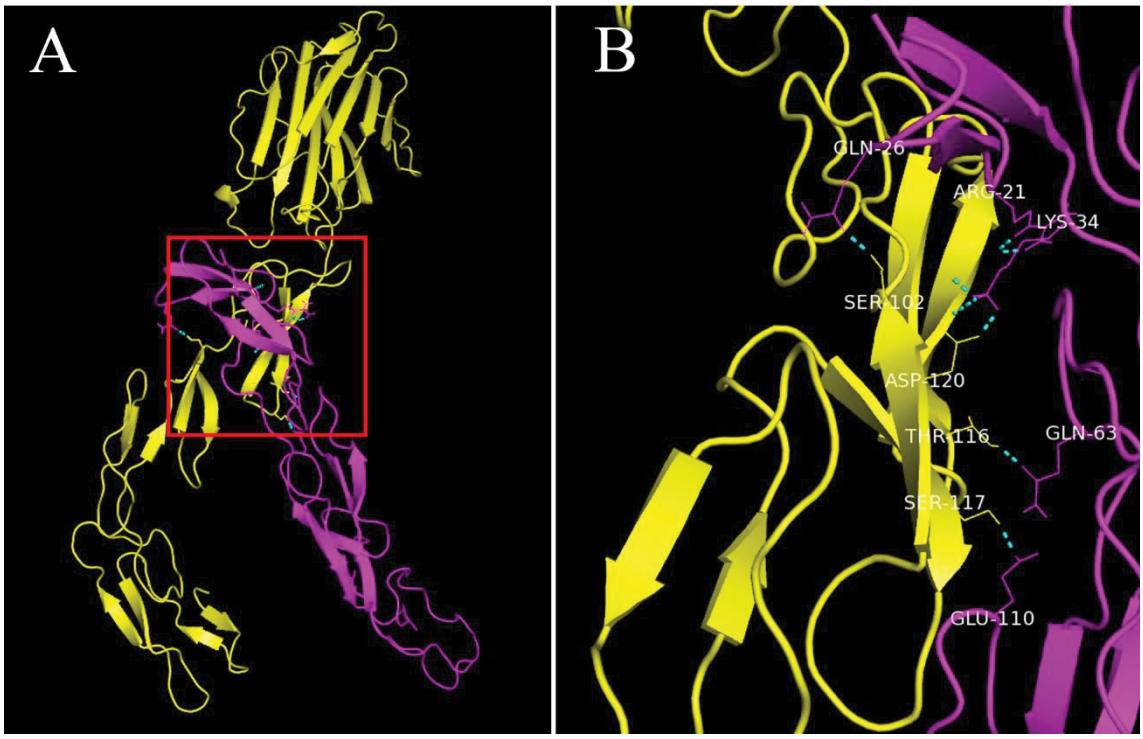

Figure 5.28 Predicted interacting surfaces of VARG4R with human TNFR2
From the docking analysis from the ClusPro server, model 5 was selected using evidence based on the X-ray crystallography structure of TNFR2 and known binding sites of each molecule. A) A full view representation of the docking model was generated in Pymol showing VARG4R (yellow) and TNFR2 (purple) with the predicted polar contacts determined by Pymol shown by (cyan) dotted lines. B) The single predicted surface of CRD1 of TNFR2 with CRD3 of VARG4R is shown in greater detail. Amino acid side chains contributing to polar contacts are labelled.

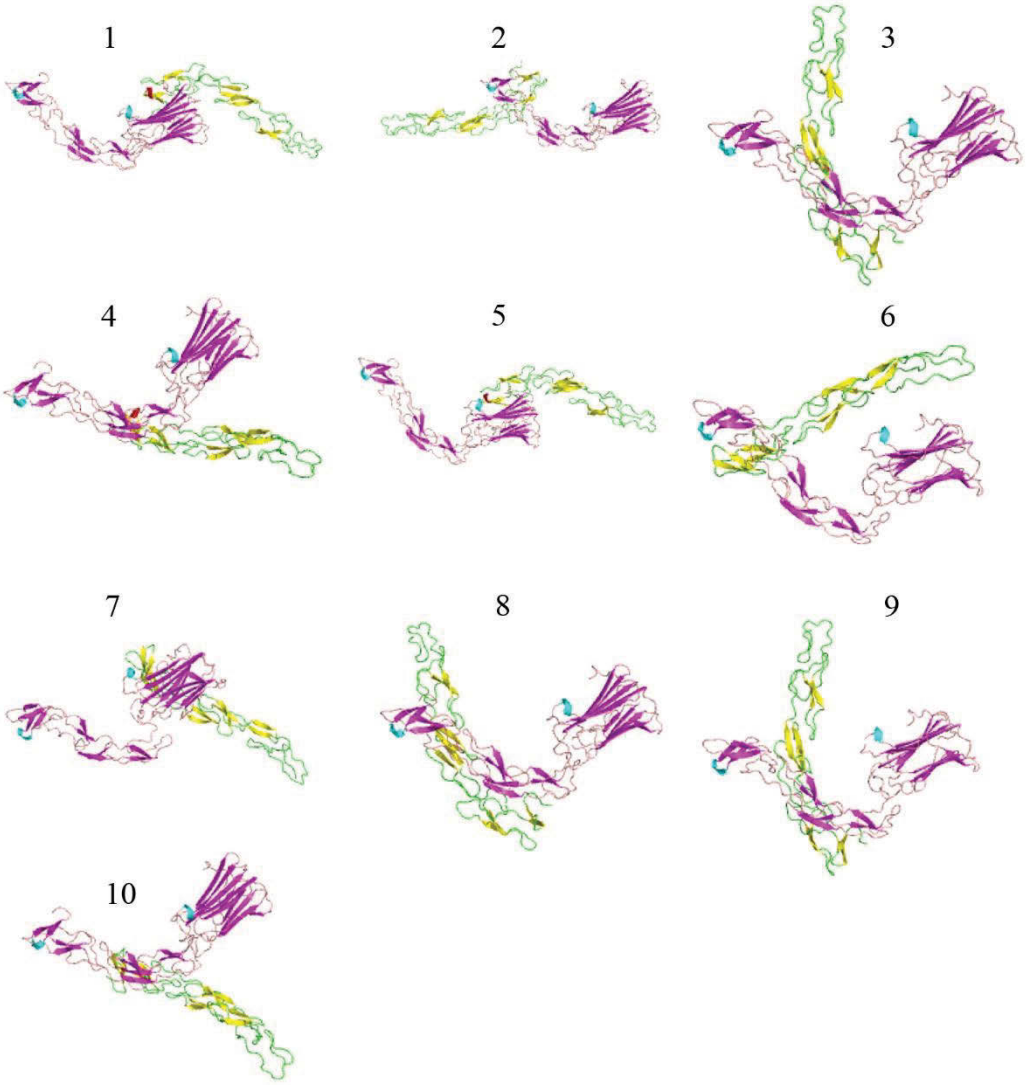

Figure 5.29 Top predicted docking surfaces between MPVJ2R and the extracellular domain of TNFR2

The generated full length model of MPVJ2R from Chimera was docked against the PDB structure; 3ALQ (TNFR2), using the ClusPro web server. The best computed hydrophobic favoured models are shown. MPVJ2R is shown in purple and TNFR2 is shown in yellow.

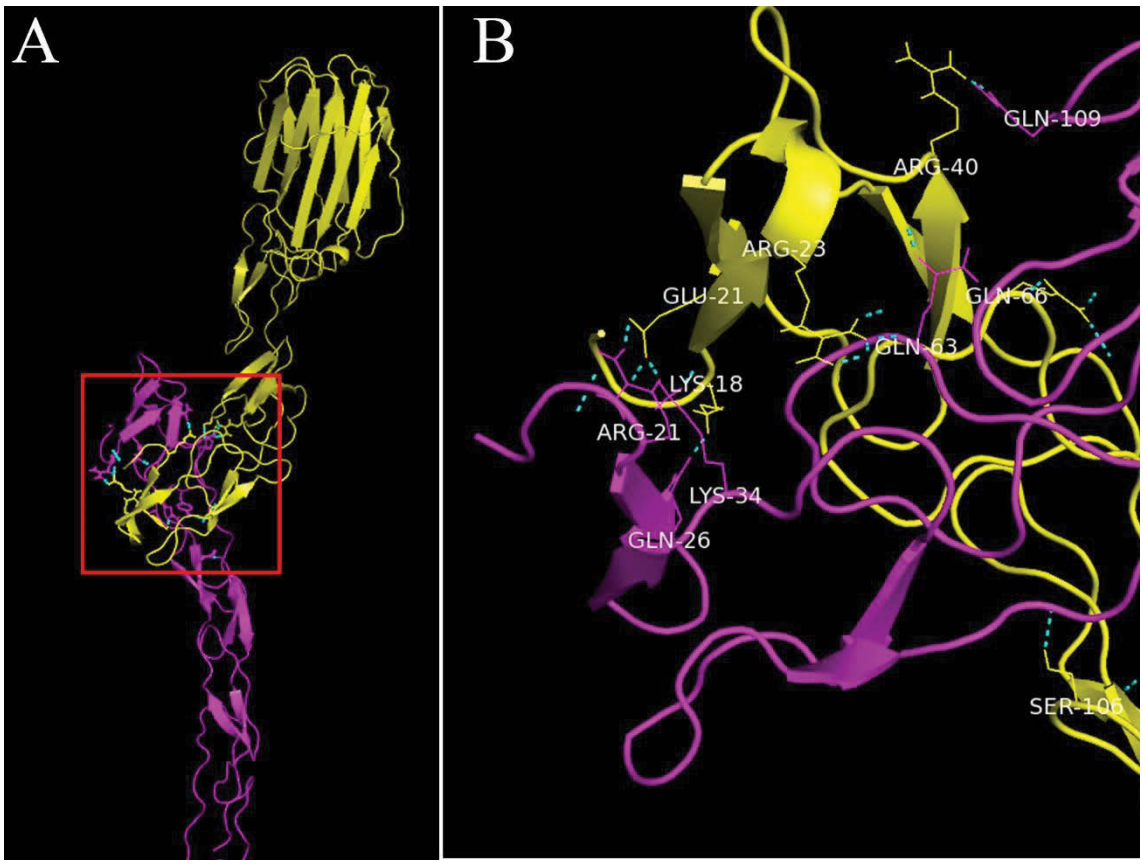

Figure 5.30 Predicted interacting surfaces of MPVJ2R with human TNFR2
From the docking analysis from the ClusPro server, model 2 was selected using evidence based on the X-ray crystallography structure of TNFR2 and known binding sites of each molecule. A) A full view representation of the docking model was generated in Pymol showing MPVJ2R (yellow) and TNFR2 (purple) with the predicted polar contacts determined by Pymol shown by (cyan) dotted lines. B) The interaction of the CRD1 from both molecules is shown in more detail with the amino acid side chains contributing to the polar contacts.

5.13 Predicted binding sites of MYXT2, VARG4R and MPVJ2R with human TNFα

It is well described that vTNFRs have the ability to bind TNFα (Sedger 2005), however a structure of the vTNFR-TNF complex with has not yet been determined. Modelling of the interaction of is challenging due to the range of movement that TNFR family CRDs exhibit between each domain (Graham et al. 2007; Mukai et al. 2010). This range of movement is described to be necessary for the conformational change in structure that

TNFR receptors when transition i.e. from the unligated state to a ligand bound complex (Mascarenhas & Kastner 2012; Murali et al. 2005). Nevertheless a predicted model of CRM-B with human and murine TNFs has been described, and is the only currently available model of the vTNFR-TNFα complex. From this model CRM-B is predicted to bind TNFα between the two monomers of the trimer (Nepomnyashchikh et al. 2010). To describe and compare possible contact surfaces between MYXT2, VARG4R and MPVJ2R, each vTNFR was docked against the trimer of human TNFα (PDB id: 3ALQ, chains ABC) using ClusPro. The ClusPro results from the blind docking analysis of MYXT2 returned ten models all of which displayed MYXT2 binding between the two monomers of TNFα within CRD2 and CRD3 of MYXT2 (Figure 5.31). This correlated well with the previous model of VARG4R (CRM-B) binding human TNFα (Nepomnyashchikh et al. 2010). The most likely biological predicted model was selected i.e. conformation based on TNFR1, TNFR2 and CRM-E, and analysed for the predicted contact amino acid residues displayed using Pymol (version 1.7.4.5) (Figure 5.32). The amino acids observed to form potential hydrogen bonds included L98, K99, Q101, within CRD2 and R124 and T123 within CRD3 (Figure 5.32). The amino acids were largely found in the loop structure of CRD3, very similar to the known 50s loop known to bind TNFα in TNFR1 and TNFR2 (Mukai et al. 2010; Mukai et al. 2009). The orientation of the VARG4R-TNFα complex is predicted the same N-C anti-parallel orientation predicted when bound to TNFR1 as in section 5.7 (Figure 5.32). This is in contrast to the model previously published of VARG4R (CRM-B) with human TNFα (Nepomnyashchikh et al. 2010) which denotes an opposite orientation of the VARG4R-TNFα complex.

VARG4R is predicted to bind the human TNFα trimer between the two monomers of the trimer (Figure 5.33). The main contact surface is created from VARG4R CRD2 and CRD3, and like MYXT2 is orientated in the opposite orientation to the previously published model of VARG4R (CRM-B) (Nepomnyashchikh et al. 2010). More specifically, the residues from VARG4R CRD2 N64 and K98 as well as Y110 in CRD3 created close polar bonds with human TNFα (Figure 5.34).

Finally, MPVJ2R despite the large variation in structure in CRD4 compared to MYXT2 and VARG4R, was predicted to bind TNFα in a very similar manner (Figure 5.35). The monomer of MPVJ2R bound TNFα between two of the TNFα monomers in the same orientation as MYXT2 and VARG4R. Extensive polar contacts are shown with TNFα with all residues residing in CRD3 of MPVJ2R. The amino acids involved included R110, T111, K104, Y100, D132 and Y122 also belonging to the loop structure of CRD3 (Figure 5.36).

In conclusion, taken together all the structures of vTNFRs, MYXT2, VARG4R and MPVJ2R were predicted to bind TNFα largely within the vTNFR CRD3 and CRD2, as expected from the mutational studies of MYXT2 (Schreiber & McFadden 1996). Each monomer for each of the vTNFRs was bound between two of the TNFα monomers however was found in the opposite orientation to which TNFR1 and TNFR2 are described to bind TNFα and LTα (Mukai et al. 2010; Naismith et al. 1996). Of Note this orientation allows the SECRET domain to be directed away from the plasma membrane (when the cellular TNFRs are localised at the cell surface), thus leaving the SECRET domain more accessible to bind free chemokines.

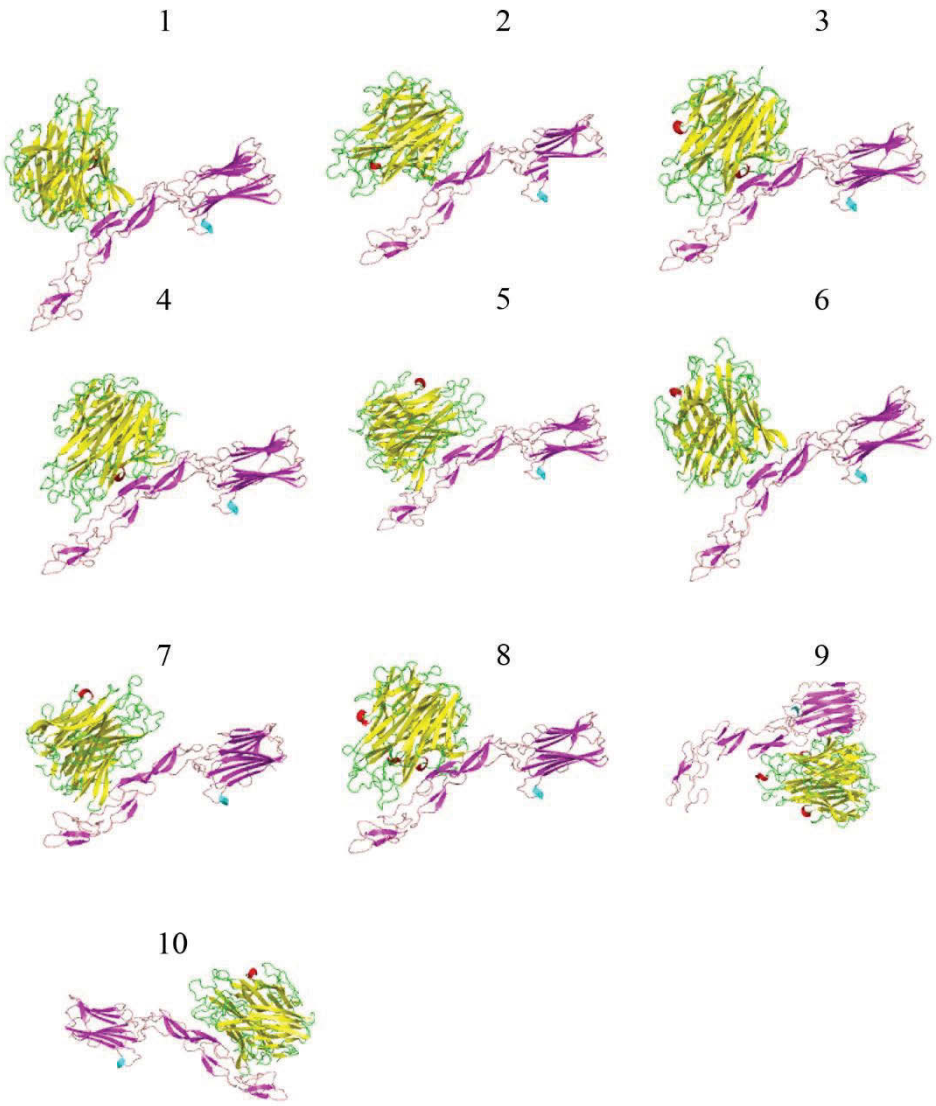

Figure 5.31 Docking predictions of MYXT2 with human TNF
The crystal structure of TNF (yellow) taken from the PDB structure 3ALQ (TNFR2 in complex with TNF) was analysed for possible docking sites with MYXT2 (purple). The top most likely orientations of both molecules were computed and are shown from the ClusPro server.

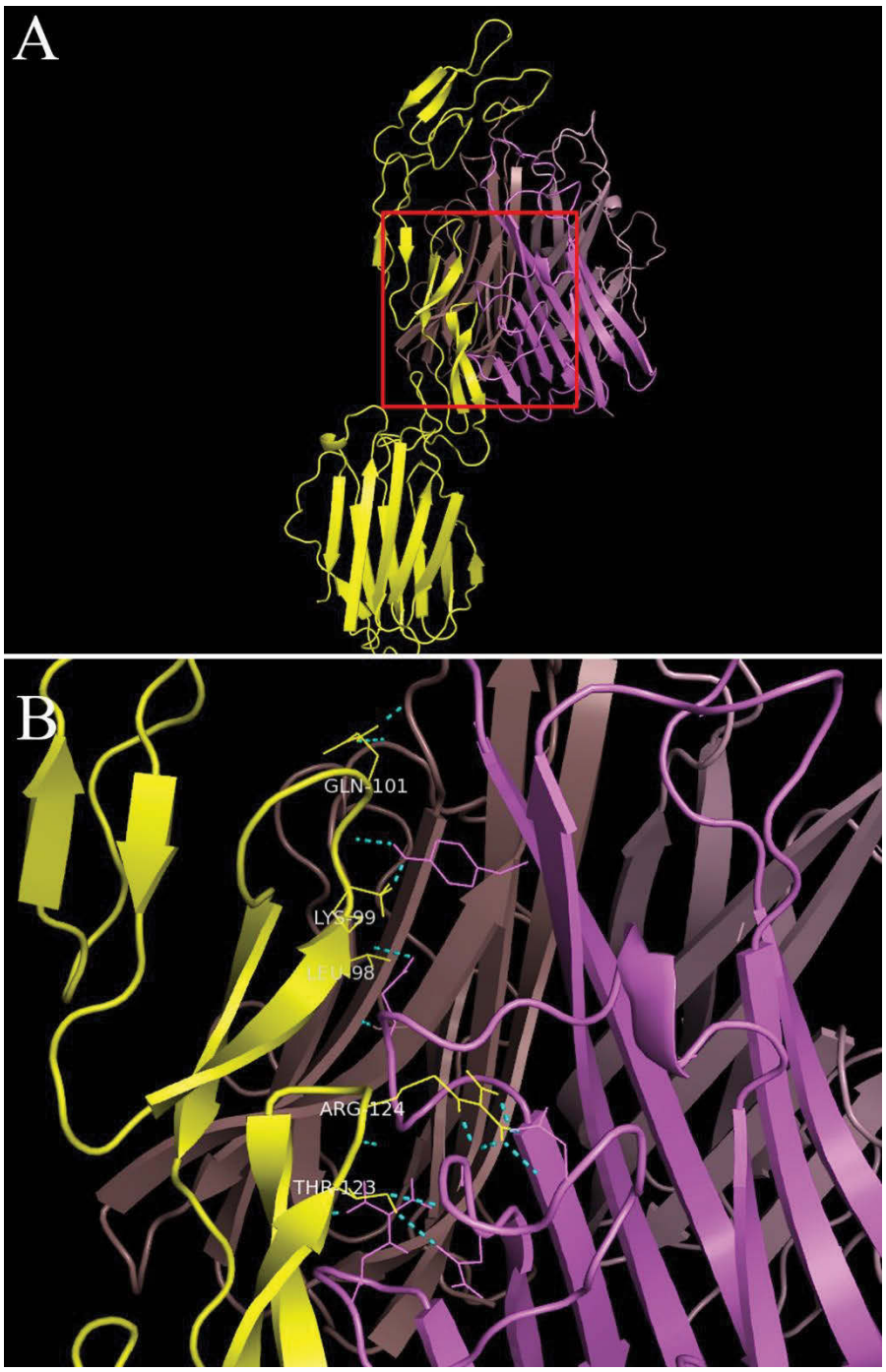

Figure 5.32 Predicted interacting surfaces of MYXT2 with human TNF
Using the evidence of known binding sites found in MYXT2 as well as the known binding sites found in TNFR1 and TNFR2, model 3 was selected from the ClusPro output to analyse in greater detail. A) A full view depiction of the interaction between MYXT2 (yellow) and human TNF (purple) was generated in Pymol and polar contacts (cyan) were predicted. B) An enlarged visual of the interaction surfaces between the two molecules is shown with the amino acids forming polar contacts depicted.

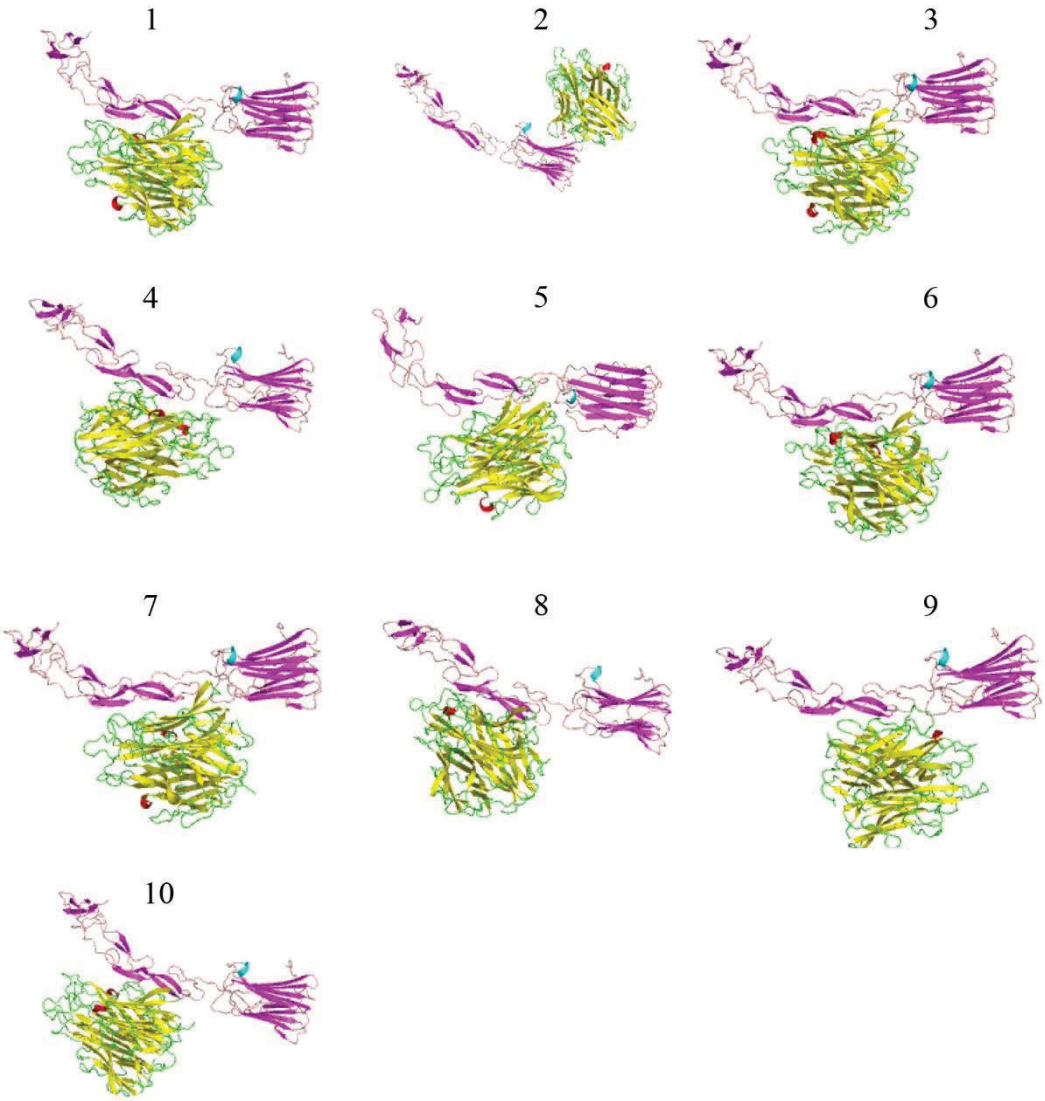

Figure 5.33 Docking predictions of VARG4R with human TNF
The crystal structure of TNF (yellow) taken from the PDB structure 3ALQ (TNFR2 in complex with TNF) was analysed for possible docking sites with VARG4R (purple). The top most likely orientations of both molecules were computed and are shown from the ClusPro server.

Figure 5.34 Predicted interacting surfaces of VARG4R with human TNF
Due to the high sequence identity of VARG4R and MYXT2, evidence of the binding site of TNF with MYXT2 was used select a likely docking model. As well as the using the known information of TNF binding sites in TNFR1 and TNFR2, model 1 was selected from the ClusPro output to analyse in greater detail. A) A full view depiction of the interaction between VARG4R (yellow) and human TNF (purple) was generated in Pymol and polar contacts (cyan) were predicted. B) An enlarged visual of the interaction surfaces between the two molecules is shown with the amino acids forming polar contacts depicted.

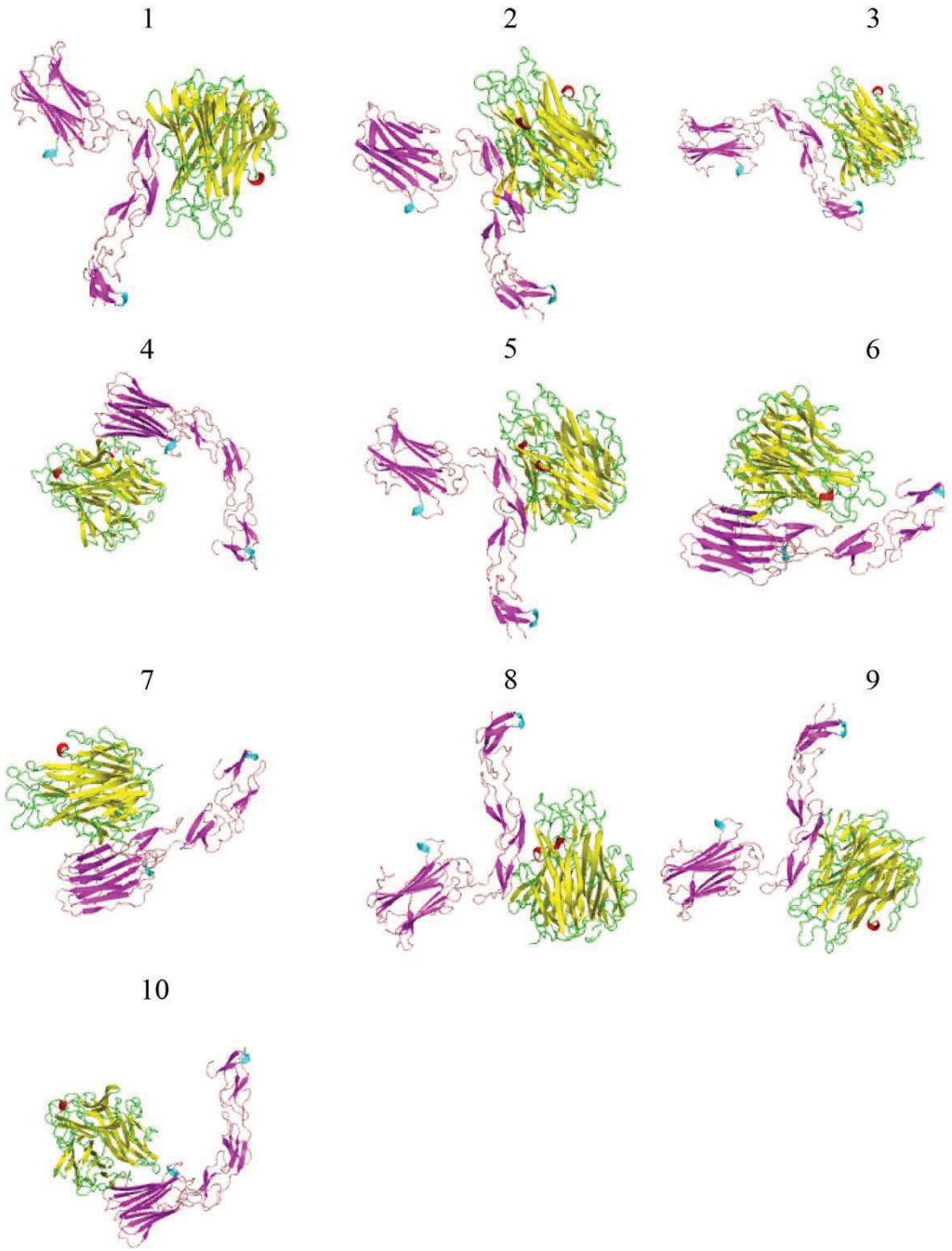

Figure 5.35 Docking predictions of MPVJ2R with human TNF
The crystal structure of TNF (yellow) taken from the PDB structure 3ALQ (TNFR2 in complex with TNF) was analysed for possible docking sites with MPVJ2R (purple). The top most likely orientations of both molecules were computed and are shown from the ClusPro server.

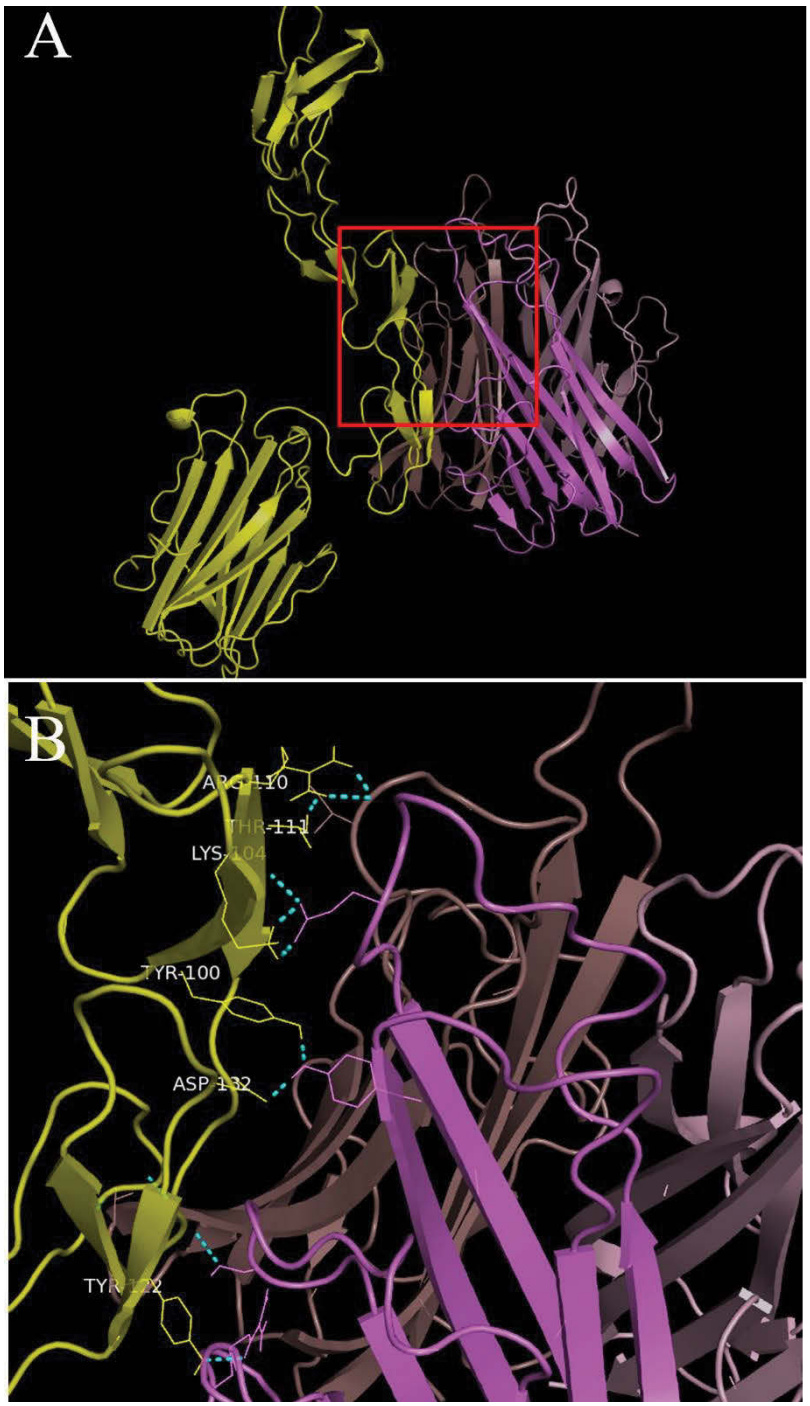

Figure 5.36 Predicted interacting surfaces of MPVJ2R with human TNF
Due to the high sequence identity of MPVJ2R and MYXT2, evidence of the binding site of TNF with MYXT2 was used select a likely docking model. As well as the using the known information of TNF binding sites in TNFR1 and TNFR2, model 1 was selected from the ClusPro output to analyse in greater detail. A) A full view depiction of the interaction between MPVJ2R (yellow) and human TNF (purple) was generated in Pymol and polar contacts (cyan) were predicted. B) An enlarged visual of the interaction surfaces between the two molecules is shown with the amino acids forming polar contacts depicted.

5.14 Discussion

As the generation of vTNFR and cellular TNFRs bacterial proteins for X-crystallography was unsuccessful, further evidence of the interaction between vTNFRs and cellular TNFRs was investigated using the previously generated C-terminal –CFP and YFP fusion constructs. A method of detecting FRET by flow cytometry was developed to determine the structural orientations of vTNFR-cellular TNFR complexes. Although X-ray crystallography is considered the "gold standard" for structural analysis (Smyth & Martin 2000), it is nonetheless also associated with various limitations. The formation of a fixed crystallised complex does not often easily form, and is usually created in harsh environments, sometimes in extreme pH and temperatures leading to formation of artificial conformations (Dunlop, Irvin & Hazes 2005). Furthermore membrane bound proteins are amongst the most challenging proteins to crystallise largely due to their hydrophobicity and the use of detergents often used extract them preventing crystal formation (Carpenter et al. 2008). In fact, due to this both, TNFR1 and TNFR2 crystal structures are not full length structures, only crystals of the truncated N-terminal extracellular regions (Mukai et al. 2010; Naismith et al. 1996). FRET, alternatively offers structural determination or protein-protein interactions within live cells, in real time, in the protein native state (Raicu & Singh 2013). The FRET method is very sensitive to minute changes in distance between the acceptor donor pairs and can even be used to determine the structure and orientations of large complex molecules (Bujalowski & Jezewska 2012). When paired with flow cytometry, FRET has the ability to deliver high-throughput structural information over whole cell populations (Dye 2005). FRET by flow cytometry permits detection on a single cell basis and allows for a sensitive and highly

rigorous assessment of protein interactions, and the large number of cells that can be examined by flow cytometry provides statistical reassurance (Dye 2005).

Advantageously, each of the vTNFRs and cellular TNFRs were previously generated as CFP and YFP C-terminal fusion constructs. CFP and YFP proteins have the ability to act as FRET acceptor/donor pairs due to spectral overlap in emission and excitation (He et al. 2003). Although inherent to the nature of the FRET method, the spectral overlap also creates complications in detection of FRET emission. This is especially true when using CFP and YFP, as CFP emission has a wide tailing emission spectra into the YFP emission spectra, which although needed to create FRET, is more than sufficient, causing bleed through into FRET YFP detection. Therefore to overcome the bleed through of CFP into FRET YFP, compensation of the CFP signal, along with a robust set of negative and positive controls were used to determine a true FRET signal. However to first determine this, a direct comparison within each sample was required, and therefore the addition of a CFP only positive population (i.e. a negative FRET population) was gated on and used as internal comparison. Due to differences in fluorescence brightness between samples, compensation settings were optimised for each sample set (e.g. TNFR1 co-transfected cells vs TNFR2 co-transfected cells) and spiked with matching CFP only samples i.e. a TNFR1-CFP spike for TNFR1-CFP containing samples. Because brighter CFP emission leads to greater CFP bleed through into YFP detection (He et al. 2003), greater bleed through was evident in samples containing for example TNFR1-CFP. To set a consistent compensation setting across all samples resulted in either over or under compensation and a skew of the results depending on the brightness of the samples. This optimisation, combined with very narrow bandpass filter sets to further optimally detect each

fluorophore resulted in a FRET detection system for human much more optimal for TNFRs than was previously described (Chan et al. 2001; Lobito et al. 2006).

Using the optimised FRET method, the interactions of TRAPS mutant TNFRs were analysed with WT TNFR1-CFP. Previous reports analysing the interactions of WT TNFR1 and TRAPS mutant TNFR1 failed to detect an association between TNFR proteins (Lobito et al. 2006). However from the data presented, it was shown that for all TNFR1 TRAPS mutants a FRET emission was detectable and that they were interacting with WT TNFR1. An association between TNFR1 has been shown via immunoprecipitation for the T50K TRAPS as well as R92Q by FRET (Lewis, Valley & Sachs 2012; Yousaf et al. 2005), however this is the first study to show an association for the entire panel of TRAPS mutations presented in this thesis. Although each mutant was shown to interact with WT TNFR1-CFP, a reduced FRET was detected from the cysteine TRAPS TNFR1 mutants C30R, C33G, C33Y, with the exception of mutants C29Y and C30F which had an increased FRET emission. TRAPS mutations involving cysteines are predicted to have the greatest effect on TNFR1 structure (Rebelo et al. 2006), as cysteine disulphide bonds are integral to the stability and rigidity of each CRD in the extracellular domain (Branschädel et al. 2010; Naismith & Sprang 1998). TRAPS Mutations Y20D and T37I also displayed reduced FRET with WT TNFR1, and although are not involved in intramolecular covalent bonds, are similarly also involved in highly conserved folds of TNFR1 or the formation of hydrogen bonds within the structure (Banner et al. 1993). Thus, as FRET emission is proportional to the distance between molecules (Berney & Danuser 2003), TRAPS mutations having the most dramatic effect on TNFR1 structure, would most likely be also changing the distance between CFP/YFP FRET pairs (i.e. a reduced FRET translating

to a greater distance between CFP and YFP of TRAPS TNFR1 and WT TNFR1 in the C-terminus, or vice versa)(Figure 5.37)

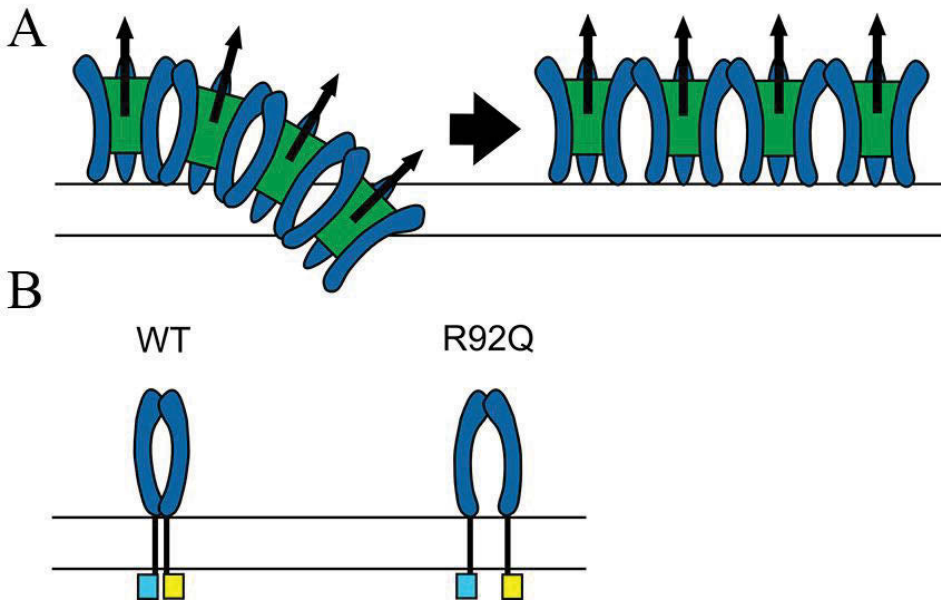

(Lewis, Valley & Sachs 2012)

Figure 5.37 TRAPS induced conformational change in TNFR1 and consequences on formation of higher order complexes.
A proposed model of receptor complexes based on reduced FRET of the R92Q TNFR1 mutant with WT TNFR1. Due to predicted steric conflicts with the membrane a conformational change must occur to alleviate the steric clash. This conflict is illustrated schematically in two dimensions for clarity. A) Adjacent ligand trimers are tilted at an angle of ~35°. To alleviate this steric conflict in higher order complexes, a conformational change must occur. B) The same conformational change is shown for the TNFR1 CFP/YFP FRET constructs.

In fact, modelling of the R92Q TRAPS mutation was shown to adopt an altered conformation compared to WT TNFR1 (Lewis, Valley & Sachs 2012). In addition the TRAPS R92Q mutation was also found to have a reduced FRET (Lewis, Valley & Sachs 2012). This suggested separation of the C-terminal regions, due to their involvement in the recruitment of signalling molecules (Figure 5.37), and may result in a deficiency to signal, consistent with reports and the evidence presented in Chapter 3 of reduced TNFR-induced cell death (D'Osualdo et al. 2006).

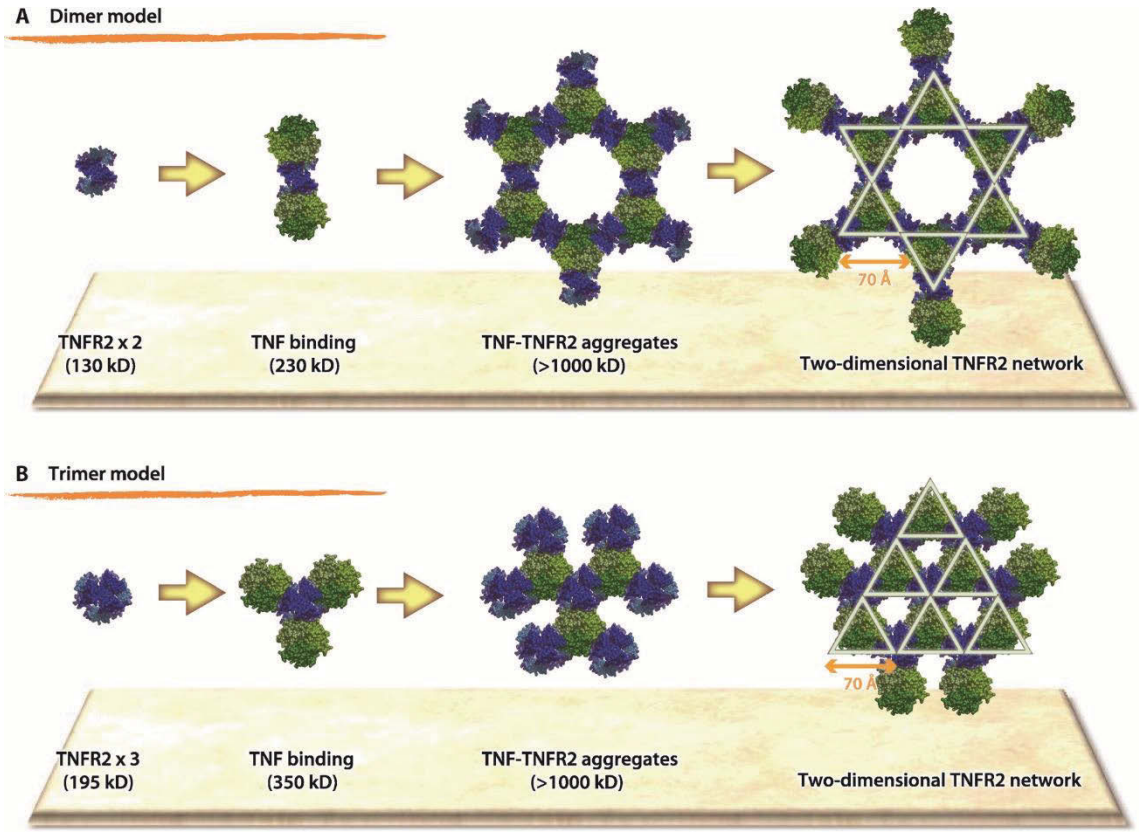

(Mukai et al. 2010)

Figure 5.38 Predicted 2D network formation of TNFR2
Based on the X-ray crystallography evidence and that TNFR2 receptors self-associated through the PLAD, two possible models are described for the formation of higher order complexes; A) a dimer model and B) a trimer model. TNFR2 (blue) is predicted to either form dimers or trimers through PLAD-PLAD interactions and the formation of larger complexes is centred on binding to TNF (green).

Because FRET by flow cytometry measures the protein-protein interactions over thousands of cells, it accounts for cell-to-cell differences in protein interactions between cells in a given sample. Therefore the FRET flow cytometry data represented is the sum of all protein interactions occurring within all cells analysed. The analysis of WT TNFR1 and TNFR2 homotypic FRET, although a positive FRET is detected from each, TNFR1 and TNFR2 show obvious differences in the dynamics of their interactions in their dimers or trimers. Cells co-expressing TNFR1-CFP and TNFR1-YFP proteins are detected with a very

bright, sharp FRET histogram, compared to TNFR2-CFP and TNFR2-YFP co expressing cells which are detected with a broad FRET histogram peak, overlapping the CFP only spiked population. As this represents the average protein interactions of the cells analysed, the large sharp FRET shift from FRET-negative cells suggests that TNFR1 is initially distant from other TNFR1 molecules, but once clustered/activated, form very close interactions in the C-terminal regions with nearly all FRET positive proteins existing in a state of either dimers, trimers or higher order complexes. In comparison TNFR2 exhibits a broad bimodal FRET histogram overlapping the FRET-negative CFP only population. This suggests that TNFR2 molecules are possibly initially much closer but once clustered or activated, form much more distant homotypic interactions compared to TNFR1. This may also be explained by the typical expression of each receptor and their signalling pathways. TNFR1 is highly expressed (Choi et al. 2005; Schwarz et al. 2013) and detected in nearly all cell types however is largely sequestered to the Golgi (Al-Lamki et al. 2001; Jones et al. 1999; Storey et al. 2002). TNFR2 is largely cell surface expressed and has a much more limited expression (Choi et al. 2005; Tartaglia et al. 1993). The accumulation of TNFR1 within the Golgi, as well as the observed trafficking within receptosomes (Schneider-Brachert et al. 2004) also observed in Chapter 3 would certainly allow closer interactions of TNFR1 especially when overexpressed. In comparison the distribution of TNFR2 on the cell surface and lower abundance on the plasma membrane may allow a more freely homogenous spatial arrangement of TNFR2. Indeed previously modelled complexes of TNFR2 suggests a spatial uniform arrangement of dimers or trimers on the cell surface of cells and once activated by ligand form a higher order lattice (Figure 5.38) (Mukai et al. 2010). This more uniform arrangement of TNFR2 in comparison to intracellular aggregation of TNFR1 would most likely lead to a more distant less efficient FRET transfer.

Similarly the FRET emission detected amongst each of the TRAPS mutations also displayed differences in their FRET histogram distributions compared to WT TNFR1. TRAPS mutations including Y20D, Y20H, T37I, C30R and C33G all displayed a more bimodal histogram in comparison to WT TNFR1. Based on the evidence and differences of FRET observed between WT TNFR1 and TNFR2, this may suggest that mutations such as C30R and C33G may disrupt the formation or arrangement of higher order complexes, causing a more spatial arrangement (Figure 5.38). Modelling of the R92Q mutation suggests an altered open conformation in the C-terminal regions of TNFR1, and the formation of higher order receptor networks creates steric hindrances unless a different network architecture is adopted (Figure 5.37) (Lewis, Valley & Sachs 2012). However the data presented in this chapter for TRAPS association with WT TNFR1, although sensitive enough to detect changes caused by a single amino acid changes, the FRET method used cannot distinguish between dimers trimers or higher order complexes. For this, either a different assay would be required such as protein crosslinking and Western blotting or the use of two-step FRET (He et al. 2005). Two-step FRET measures the FRET between three fluorophores or fluorescent fusion proteins such as CFP, YFP and red fluorescent protein (RFP). In this method CFP is excited using a laser which subsequently excites YFP and then excites RFP. Two-step FRET is able to differentiate between dimers, trimers and higher order complexes as, two step FRET i.e. CFP>YFP>RFP, only occurs when all three molecules are present in the complex and is also much more efficient than CFP>RFP FRET (He et al. 2005). In future work a TNFR1-RFP construct could be generated to establish two-step FRET and examine in more detail the differences between multimers of TRAPS complexes. Additionally differences between the two populations of TNFR1 protein complexes could be analysed further by FACS sorting then analysing

each population further by proteomics. This may possibly reveal differences in signalling complexes associated with the receptor complexes using techniques such as 2D gels and mass spectrometry.

FRET by flow cytometry was also used to determine the orientations and associations of MYXT2, VARG4R and MPVJ2R with TNFR1 and TNFR2. Each vTNFR was generated as both CFP and YFP C-terminal constructs therefore FRET was able to be performed with either set of fluorescent fusion proteins with both TNFR1-CFP/YFP and TNFR2-CFP/YFP. However due to the unknown lower expression observed in the Chapter 4 for the vTNFR-CFP constructs, FRET was performed using the vTNFR-YFP constructs as FRET acceptors instead. For each of the vTNFRs no convincing FRET was detectable with either TNFR1 or TNFR2. Considering that TNFR1-CFP emission is very intense, it was expected that the excitation of the vTNFR-YFP proteins would be more than sufficient. In addition because MYXT2 is known to associate with human TNFR1 and TNFR2 (Sedger et al. 2006), the absence of FRET detection is therefore most likely to be associated with receptor orientations and positions of the CFP-YFP molecules. Firstly It is important to remember that FRET only occurs within 10nm distance of the acceptor an donor (Trón et al. 1984). Therefore considering that both full length human TNFR1 and TNFR2 are transmembrane and also much larger in size in comparison to the vTNFRs, it was uncertain whether an N-N parallel dimer would allow the C-terminal regions in close enough proximity to permit FRET (Figure 5.39). Secondly it is also important to consider the conformations of each of the C-terminal regions for cellular and vTNFRs. Although cellular TNFRs and vTNFRs often depicted as linear molecules for simplicity, the tertiary structures of the C-terminal regions for cellular TNFRs and vTNFRs is much more complex. MYXT2, VARG4R and MPVJ2R each contain a SECRET domain in the C-terminal

region which is predicted from modelling to form a globular “barrel-like” structure as found in CRM-D (Antonets, Nepomnyashchikh & Shchelkunov 2010; Xue et al. 2011). For FRET to occur, CFP and YFP must be precisely positioned in such that their dipole moments are nearly parallel to one another (Inoué et al. 2002; Rosell & Boxer 2003).The attachment of YFP to the C-terminus may position the YFP molecules away from CFP in TNFR1/TNFR2 greater than 10nm, regardless of whether an association is occurring (Figure 5.39). Another consideration is the effect of the YFP proteins on the structure of each of the vTNFRs. Each of the vTNFRs is approximately 30kDa, compared to YFP which is approximately 27 kDa (Figure 5.39). This is a relatively large fusion protein compared the vTNFRs and may affect the structure of each resulting in a negative FRET detection. The alternative to this is an interaction in the opposite orientation i.e. an N-C anti-parallel dimer or complex (Figure 5.39). This orientation would also position the CFP and YFP molecules greater than 10nm apart resulting in no FRET emission. To test an anti-parallel conformation it may be possible to create an N-terminal fusion construct for example for the vTNFRs which may FRET with the C-terminal CFP of TNFR1 or TNFR2. Although it has been previously demonstrated that fluorescent fusion proteins (in particular CFP and YFP) attached to the N-terminus of the TNFR1 and TNFR2 disrupt the folding of the protein resulting in a loss of FRET (Chan et al. 2001). Furthermore this may also only be functional with evenly sizeable proteins to position the fusion CFP/YFP proteins, and will also heavily depend on the conformations of each of the proteins.

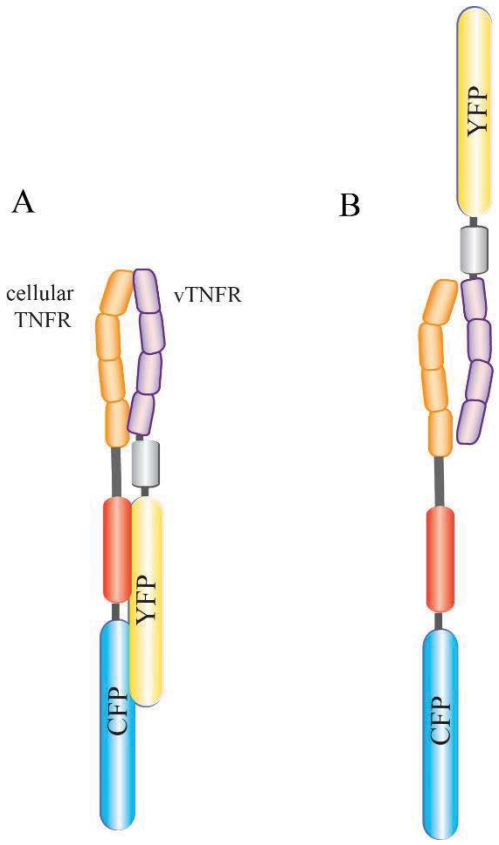

Figure 5.39 Possible orientations of cellular TNFR and vTNFR FRET pair interactions. The evidence of no FRET between either TNFR1 or TNFR2 with any of the vTNFRs suggest that alternate conformations or orientations may be possible to the predicted N-N parallel dimers. MYXT2 is known to physically associate with TNFR1 and TNFR2 therefore an absence of FRET may be due to the C-terminal CFP and YFP fusion proteins being; A) too far apart due to size differences or conformational differences or B) orientated away from each other due to a C-N anti-parallel dimer as found with CRM-E and TNFR1.

Secreted MYXT2 is found as both a dimer and a monomer (Schreiber, Rajarathnam & McFadden 1996), therefore it was hypothesised that a FRET may be detectable between MYXT2 dimers. On the other hand VARG4R is primarily found as a dimer and MPV primarily as a monomer (Sherwood, data not shown)(Gileva et al. 2006). Therefore it was also hypothesised that VARG4R would likely FRET as a dimer pair where as MPVJ2R would not, due to being monomeric. However this was not observed with no FRET detectable for each of the co-expressed vTNFR-CFP/YFP homo-dimers. Due to the highly conserved PLAD domain amongst pox viral TNFRs and the requirement of the PLAD to form homotypic interactions in TNFR family members (Chan 2007; Chan et al. 2000a),

heterodimers were also tested for FRET between MYXT2, VARG4R and MPVJ2R, but again FRET was not detectable. As for vTNFR interactions with TNFR1 and TNFR2, the absence of FRET did not necessarily mean no interaction. Even though homodimers of the vTNFRs are of equal sizes it is still unknown how or where the interactions are likely to occur. It is often predicted that vTNFR self-association occurs in the parallel N-N conformation due to PLAD homology, however the solution X-ray crystallography structure for CRM-E is found as an anti-parallel dimer (Graham et al. 2007). This would position the vTNFRs C-terminal regions containing the CFP and YFP fusion tags at a distance far greater than 10nm and result in no FRET. Another possible explanation maybe whether dimers or higher order complexes are even formed intracellularly. The monomer and dimer for MYXT2 is only described from the secreted proteins. As flow cytometry only assays FRET within cells, it is possible that the dimeric complex only forms extracellularly once secreted, and therefore FRET would not be detectable in this method as it is extracellular. Therefore although the FRET results of vTNFR with cellular human TNFRs and themselves remain inconclusive they also simultaneously suggest a number of possible conformations and orientations which could be further investigated.

To explore possible conformations and interactions of vTNFRs with cellular TNFRs, predictive modelling was used to support the findings of the FRET results in this chapter. To date no full length vTNFR structure containing a C-terminal SECRET domain has been published. Therefore using the previously solved structures for human TNFR1 (Naismith et al. 1996), human TNFR2 (Mukai et al. 2010), Vaccinia virus CRM-E (Graham et al. 2007) and the SECRET domain of Ectromelia Virus CRM-D (Xue et al. 2011), predicted models of the full length for MYXT2, VARG4R and MPVJ2R were generated. The 3 best scoring representative models of MYXT2, VARG4R and MPVJ2R all displayed high similarity to

the tertiary structures of TNFR1, TNFR2 and CRM-E. This was not surprising as the conserved cysteine amino acid residues within each vTNFR create the rigid structures found in each CRD (Graham et al. 2007; Naismith & Sprang 1998). The greatest differences between each of the models was observed in CRD4 which appeared particularly disordered. This was not unexpected as this region is poorly covered by each of the templates used. The crystal structure for TNFR1 although contains all 4 CRDs, the 4th CRD is highly disordered in this structure (Naismith et al. 1996). Full length CRM-E only contains 3 CRDs (Graham et al. 2007) and therefore only TNFR2 contains a complete 4th CRD from the extracellular region (Mukai et al. 2010). The problem with TNFR2 crystal structure is that it was solved bound to human TNF. The ligand bound state of TNFR1 and TNFR2 require a large conformational change in the receptor, especially in CRD4 of the extracellular region to allow recruitment of signalling molecules and correct positioning of the C-terminal regions (Mascarenhas & Kastner 2012). Therefore whether vTNFRs also require a conformational change to bind ligand or the receptor is unknown, and the TNFR2 model may bias these predicted models within CRD4. The SECRET domain, due to high homology between vTNFR C-terminal regions also resembled the SECRET domain of Ectromelia CRM-D. Even though each model was energetically favourable and returned a high model quality based on statistical algorithms, a criticism of comparative homology is that the predicted models generated will always bias towards the templates used to create them (Eramian et al. 2008). Even though this is true, depending on the different algorithms used it will also include information that is independent from the template such as molecular and mechanical force restraints (Das et al. 2007; Zhang 2007). Given that each of the vTNFRs share a high homology at the sequence level to each of the human cellular TNFRs, and that protein structure is much more conserved than DNA or amino acid sequences (Lesk & Chothia 1980), It is likely

that the models generated will closely represent the true structures of MYXT2, VARG4R and MPVJ2R.

Using the generated models of MYXT2, VARG4R and MPVJ2R possible interactions with human TNFR1 and TNFR2, as well as in complex with TNF and LT, were investigated. The computer predictions of the docking models were then used to support the data and hypothesis of the FRET experiments in this thesis chapter. ClusPro is a web-based service that uses an automated rigid-body docking and discrimination algorithm to generate billions of putative conformations (Comeau et al. 2004b). Filtering is then performed and involves the use of empirical free energy evaluation methods that select the top ten conformations with the lowest desolvation and electrostatic energies. However amongst these top structures the method scoring of models cannot discriminate meaningfully between them (Comeau et al. 2004a), therefore the most likely predicted interaction site was selected based on in vitro data and published reports of the vTNFRs and cellular TNFR1 and TNFR2. It is important to note that although the docking model selected may best correlate with the published data, each of the models is still a computer prediction and therefore any of the top models could represent the native interaction.

The vTNFR molecules were first docked against TNFR1 and each were found to interact via the PLAD domain. However for each of the docking models returned by ClusPro, each were orientated in the anti-parallel N-C conformation. For the docking models selected each MYXT2, VARG4R and MPVJ2R primarily made contact surfaces between CRD1 containing the PLAD and the CRD4 of TNFR1. This positioned the SECRET domain away from the N-terminus of TNFR1. These data may possibly explain the absence of FRET

observed between TNFR1 and the vTNFRs, as this orientation would not be capable of creating a FRET signal between the C-terminal CFP and YFP fusion proteins of the VTNFRs and human TNFR1. In addition, as TNFR1 is membrane bound this orientation may be more relevant than an N-N parallel dimer as an N-N parallel dimer would likely create hindrances with the plasma membrane. The positioning of the SECRET domain in the C-N anti-parallel conformation away from the plasma membrane would also allow easier access to bind free chemokines, which has been described for VARG4R (Alejo et al. 2006; Antonets, Nepomnyashchikh & Shchelkunov 2010). Although cell surface detection of MYXT2 was found to not interfere with the binding of TNF to TNFR1 or TNFR2, it is uncertain whether MYXT2 at the cell surface is also associated with each of the human cellular receptors (Sedger et al. 2006). Based on the evidence of the predicted docking models the anti-parallel conformations appears to occlude the TNF binding site found within TNFR1. Whether vTNFRs can undergo a conformational change to accommodate TNF is unknown, however the further docking modelling with TNFR1 in complex with LTα suggests that it may be possible. However even though suggested docking models appear conceivable from ClusPro, it is important to note that *In vitro* evidence has not described binding of MYXT2, VARG4R and MPVJ2R to LTα, although CRM-B from Cowpox virus is unable to bind LTα (Smith et al. 1996a). In support of the anti-parallel conformation each of the vTNFRs was also found to bind the TNF trimer in the same anti-parallel conformation. Therefore it may be possible for the vTNFRs to simultaneously bind TNFR1 and TNF.

Each of the vTNFRs was also modelled with TNFR2. However the docking structures were each found to vary and adopt a very open conformation with TNFR2. MYXT2 and VARG4R were both predicted to bind TNFR2 via CRD1 with the CRD3 of TNFR2 primarily.

MPVJ2R on the other hand was predicted to have a single contact surface between CRD1 and the CRD1 of TNFR2. These models again were predicted in the C-N anti-parallel conformation. The variations in interaction surface may be due to the crystal structure of TNFR2 and its complex with TNF. In this conformation the PLAD domains of TNFR2 are separated from each other by greater than 30 angstroms and the CRD4 exhibits great flexibility to accommodate TNF (Mascarenhas & Kastner 2012; Mukai et al. 2010). Therefore how relevant the docking models are with TNFR2 is questionable. Further evidence of this was found when trying to predict docking models of TNFR2 in complex with TNF. Each of the returned models was found with interaction surfaces with the SECRET domain which is highly unlikely, due to its function in binding chemokines and low homology to TNFR1 and TNFR2 (Antonets, Nepomnyashchikh & Shchelkunov 2010; Xue et al. 2011).

Although the docking modelling provides strong evidence that each of the vTNFRs in an anti-parallel C-N conformation, as well as a possible explanation for the absence of FRET between vTNFRs and TNFR1 and TNFR2, it is always important to remember that further *in vitro* experimentation is always required to confirm computer predictions. The models may provide evidence for complementary surfaces and orientations, however these alone are based on extrapolations of the models generated from templates of TNFR1, TNFR2, CRM-E and the SECRET domain of CRM-D. Therefore the predictions of the docking modelling will always be limited by the accurateness of the models generated and will always contain a bias towards the template (Eramian et al. 2008; Sali & Blundell 1993). Together with the evidence presented for the FRET in this chapter it suggests that each of the vTNFRs is most likely to adopt an anti-parallel C-N conformation and interact with cellular TNFRs via contacts primarily in CRD1 containing the PLAD. Although no

FRET was detectable between vTNFRs and human cellular TNFRs, the use of more strategically placed fluorescent tags on either the vTNFRs or TRAPS TNFRs may allow FRET analysis in future experiments. Considering the sensitivity of the assay as observed between individual TRAPS mutations this would reveal much more in-depth mutational analysis of the vTNFR interaction with cellular TNFRs.

Chapter 6

General discussion

Chapter 6 – General discussion

TNF and its respective receptors, TNFR1 and TNFR2 play one of the most diverse roles in mammalian biology. TNF has an essential role in mediating innate immunity as a potent inflammatory molecule with powerful anti-viral and anti-microbial activity. However in addition to its role in immunity it also plays an essential role in mammalian development, neurobiology and physiological processes of cellular homeostasis. Due to its pleiotrophic nature, TNF and the TNFRs have some of the most complex and diverse signalling pathways and cellular interactions of any of the known cytokines. Although it is one of the most studied cytokines and we know a great deal about the functions of the TNFRs, there is still much that still needs to be answered. Some of the benefits from better understanding basic TNFR biology have been demonstrated through the development of anti-TNFs as a therapeutic. The prototype member of anti-TNF therapeutics is Etanercept, which is a recombinant extracellular domain protein of the TNFR2 receptor linked to the Fc region of human IgG1 (Tsimberidou et al. 2003). These TNF antagonists have revolutionised treatment for inflammatory diseases such as rheumatoid arthritis, ankylosing spondylitis, ulcerative colitis, Crohn's disease and psoriasis. However because these agents block all of the functions of TNF by preventing it binding to the receptors, it also blocks many of the beneficial biological functions. As a result treatment is usually associated with increased risk to infections (Tresch et al. 2009), and development of lymphoma in younger patients (Lopez-Olivo et al. 2012). In addition these biologics are only relatively new on the therapeutic market and their long term use and side effects are still relatively unknown (Sedger & McDermott 2014).

Poxviruses have developed a unique mechanism to inhibit the TNFR pathway by encoding their own homologous TNFRs which can be secreted to bind soluble TNF. These genes have been captured from host genomes and have evolved a specialised functions to efficiently inhibit TNF and TNFRs (Alcami 2003; Benedict, Banks & Ware 2003). Their importance as an host defence mechanism and demonstrated virulence factor for viruses such as Myxoma virus (Upton et al. 1991) is reflected by presence of vTNFRs genes in all orthopoxvirus genomes (Epperson, Lee & Fremont 2012; Loparev et al. 2001; Reading, Khanna & Smith 2002; Smith et al. 1996a). A function for the soluble vTNFRs in binding soluble TNF has been described and characterised for nearly all currently known orthopoxviral vTNFRs, however MYXT2 is still the only known vTNFR in which an intracellular function of TNFR inhibition has been described (Sedger et al. 2006). This intracellular mechanism appears to subvert TNFR-induced apoptosis independently of TNF and may be a more specific means of inhibiting the functions of TNFR signalling. However much is still unknown about the interaction of MYXT2 with cellular TNFRs, and this thesis aimed at further characterising the interactions of vTNFRs; MYXT2, VARG4R and MPVJ2R, with human TNFRs. This was aided by using naturally occurring TNFR mutants from a syndrome known as TRAPS (McDermott et al. 1999), especially in regards to defining the interactions requiring the highly conserved PLAD domain. It was hypothesised that by better understanding the interactions of vTNFRs with cellular TNFRs that it may lead to the design of more specific anti-inflammatories based on the interactions of vTNFRs, as well as furthering our basic understanding of human TNFR biology.

In Chapter 3 the effect of PLAD domain mutations found in TRAPS, were first examined on normal TNFR1 biology. The interesting phenomenon concerning TRAPS, is that the

TNFR1 missense mutations defining TRAPS are exclusively found in the extracellular domain and overwhelmingly located within CRD1 and CRD2 (Aksentijevich 2014; Lachmann et al. 2013; Masson et al. 2004). The presence of mutations largely in CRD1, also stresses the importance of the PLAD to TNFR1 biology resulting in pathogeneses. The PLAD has been described as a vital component stabilising interactions required for TNFR self-assembly, subsequent ligand binding and signalling (Chan et al. 2000a). Therefore it is not surprising that these TRAPS mutations in the PLAD domain result in pathogenesis. The question remains, why particular mutations translate into more severe pathological effects that represent the wide clinical spectrum seen in TRAPS patients. It is hypothesised that more severe effects on TNFR1 are represented by mutations that have a greater effect on the structure, such as cysteine mutations forming backbone disulphide bonds integral to TNFR1 structure (Kimberley et al. 2007; Lahaxe et al. 2010; Nowlan et al. 2006). Indeed cysteine mutations such as C33G/Y, C30F/R/S/Y and C43R are all associated with the development of more severe symptoms such as systemic amyloidosis (Hull et al. 2002). Examination of TRAPS mutations *in vitro* and *ex vivo* reveals that TRAPS mutations exhibit altered association with WT TNFR1 receptors and localise and aggregate intracellularly within the ER (Lobito et al. 2006; Todd, Radford, Daffa, et al. 2007). It is hypothesised that the TRAPS mutations cause misfolding of the TNFR1 receptor and retention within the ER, altering signalling and possibly triggering an ER stress response resulting the activation of the inflammasome (Bulua et al. 2011). However this has only been described for a few TRAPS TNFR1 mutations, therefore the localisation of the entire panel of TRAPS mutations generated within this thesis were examined. It was found that for each of the PLAD TRAPS mutations, each failed to be detected at the cell surface and instead localised within Rab5 positive endosomes aggregating in a structure resembling the ER. However this

was also true for WT TNFR1 and is consistent with the fact that WT TNFR1 is principally localised in the Golgi and signalling cell death from within Rab5 positive endosomes or "receptosomes" (Jones et al. 1999; Schneider-Brachert et al. 2004; Storey et al. 2002). On further examination, however it was found that all TRAPS mutations except H22R, C30R and C33Y had reduced co-localisation with Rab5 positive endosomes compared to WT TNFR1. This indicated that the TRAPS mutations were causing altered intracellular trafficking and possibly altered cell death signalling induced by the compartmentalisation into Rab5 endosomes (Schneider-Brachert et al. 2004; Schutze, Tchikov & Schneider-Brachert 2008). Although the microscopy of WT and TRAPS TNFRs may have not been sensitive enough to detect the TNFRs at the cell surface, it has been previously reported that TRAPS mutations fail to localise at the cell surface (Lobito et al. 2006; Siebert, Fielding, et al. 2005). Whether this is true for all PLAD TRAPS TNFR1 mutations is still unknown, and something that could be assayed in future work, possibly through surface staining with probes and detection through more sensitive methods such as flow cytometry.

As a result of the above findings, the panel of TRAPS mutations were next assayed for the ability to cause TNFR1-induced cell death. In comparison to WT TNFR1 it was found that mutations affecting cysteine mutations including C29Y, C30Y, C33G, C33Y and mutations such as Y20D known to disrupt critical hydrogen bonds displayed a reduced ability to cause TNFR-induced cell death. This correlated with previous reports for TRAPS mutations C33Y and C33Y (Lobito et al. 2006; Rebelo et al. 2006) and suggested that mutations most critical to TNFR1 structure exhibited more aberrant cell death signalling. Taken together with the finding that TRAPS mutations exhibit altered trafficking and aggregation in an ER like structure, it may possibly explain some of the observations in

varying success in treatment of TRAPS patients. It is often found that the efficacy of biologics in TRAPS patients varies on a case by case basis (Jesus et al. 2008; Nedjai, Quillinan, et al. 2011; Nowlan et al. 2006). If TRAPS mutations exhibit intracellular TNF-independent signalling then the effect of these biologics is likely to be ineffective as they act extracellularly. Biologics would instead treat the symptoms in the short term caused by overexpression of cytokines as a result of aberrant signalling (Nedjai, Hitman, et al. 2011; Nowlan et al. 2006; Turner, Chaudhry & Nedjai 2012). In fact it is advised with caution to treat TRAPS patients with particular biologics such as infliximab which have shown to have a pro-inflammatory effect (Nedjai et al. 2009). A deficiency in apoptosis signalling may promote/favour the NFκB signalling pathways as observed for TRAPS mutations T50M, T50K and P46L (Nedjai et al. 2008; Yousaf et al. 2005). In fact ER stress is known to induce ligand independent NFκB activation (Hongxiu & Xin 2008; Pahl & Baeuerle 1997; Pahl et al. 1996). In future work the exploration of the death pathways involved would be particularly useful in determining a more specific treatment for TRAPS patients as well as other disease caused by misfolded proteins. In addition it could also lead to more tailored classes of anti-inflammatories used to target specific pathway intermediates.

In chapter 5 the interactions of TRAPS proteins with WT TNFR1 was investigated via FRET detection. It was found that the majority of TRAPS mutations in the PLAD including C29Y, C30F, C30R, C33G, C33Y and T37I exhibited differences in FRET emission when co-expressed with WT TNFR1. All of the mutations that exhibited differences were found to be affecting amino acid residues critical to the conserved structure of TNFR1 or the formation of stabilising hydrogen bonds (Naismith et al. 1996; Rebelo et al. 2006). In previous reports it was shown that TRAPS mutations, H22Y, C33G, T50M, C52F, C88R,

and R92Q display a reduced capacity to associate with WT TNFR1 (Lewis, Valley & Sachs 2012; Lobito et al. 2006). Furthermore these particular mutations all still are capable of forming higher order complexes (Lobito et al. 2006). The increased or decreased FRET efficiency displayed by the PLAD TRAPS mutations in this study suggests that the formation of the higher order complexes is altered, with the C-terminal regions either in closer proximity for mutations C29Y and C30F (i.e. increased FRET) or further apart for mutations C30R, C33G, C33Y and T37I (i.e. reduced FRET). The differences in FRET could also be observed by changes to the FRET histograms of each mutations. Mutations resulting in reduced FRET were observed with a bimodal FRET histogram, also suggesting differing formation of the higher order complexes. Modelling of the R29Q TRAPS mutations predicts that due to structural backbone perturbations, the formation of higher order complexes is stressed, forcing an altered conformation of the C-terminal regions (Lewis, Valley & Sachs 2012). This altered conformation is predicted to alter the signalling architecture of the receptor complexes and is likely to affect the consequent downstream signalling pathways (Lewis, Valley & Sachs 2012). This supports the observations of reduced cell death seen in this study for the majority of the TRAPS PLAD mutations. The greater the structural changes induced by more severe mutations such as the cysteine mutations, may reflect greater alterations in TNFR1 receptor complexes and thus more aberrant signalling, biology and observed symptoms for these mutations (Aksentijevich et al. 2001; D'Osualdo et al. 2006; Lahaxe et al. 2010; Lobito et al. 2011). Because single amino acid changes display an ability to change the formation of receptor complexes and alter signalling, a likely hypothesis would suggest that vTNFRs may function in a similar manner and disrupt the formation of larger complexes through their association of TNFR1 or TNFR2. However because the vTNFRs, although homologous to cellular TNFRs, differ much more than a single amino acid change and it would be

expected to have a much greater effect on signalling. The common observation shared amongst TRAPS mutations is that aberrant signalling, trafficking and interactions occur independently of TNF bound to the receptor (Lewis, Valley & Sachs 2012; Lobito et al. 2006), which reinforces the importance of receptor interactions and self-association in TNFR signalling and biology. It may suggest that new anti-inflammatory therapeutics may be more beneficial to target the receptor directly rather than TNF. Therefore the interactions of vTNFRs and how they interact with cellular TNFRs was investigated further to better understand how TNFR subversion occurs.

The ORFs of MYXT2, VARG4R and MPVJ2R were generated as CFP and YFP C-terminal fusion proteins to characterise the intracellular inhibition of TNFRs and interactions with human cellular TNFRs. MYXT2 shares the highest homology to CRM-B family molecules (~50% sequence identity) (Hu, Smith & Pickup 1994), including VARG4R and MPVJ2R. Therefore it was hypothesised that VARG4R and MPVJ2R may also function intracellularly to inhibit TNFR-induced cell death. It was found that the co-expression of MYXT2, VARG4R and MPVJ2R proteins with TNFR1 significantly reduced TNFR1-induced cell death. Although the intracellular mechanism of MYXT2 intracellular inhibition has previously been described, this was the first assay to show the same function for VARG4R and MPVJ2R by flow cytometry. Surprisingly although Monkeypox virus has the ability to infect humans, the secreted soluble form of MPVJ2R fails to bind and neutralise human TNF and even rat TNF (Gileva et al. 2006) despite its natural host reservoir in rodents (Lourie et al. 1975; Parker & Buller 2013). Therefore if MPVJ2R is a true virulence factor for Monkeypox virus, then the intracellular mechanism of TNFR inhibition may be more important than the species-specific inhibition of soluble TNF. However as Variola virus was only ever known to infect humans (Arita & Henderson 1968; Fenner 1993) it

may suggest otherwise, as it is also found to inhibit TNFR1-induced cell death. Viral host specificity although is much more complex than this, and the success of viral replication and infection is dependent on a myriad of other viral and host proteins and processes (Bandín & Dopazo 2011; Fields, Knipe & Howley 2007; Shchelkunov, Blinov & Sandakhchiev 1993), leaving this assumption still possible. Based on the evidence that each of the vTNFRs were inhibiting TNFR-induced cell death intracellularly, an assay was developed to also determine if an interaction was also occurring between vTNFRs and human cellular TNFRs. It was hypothesised that if human cellular TNFRs were over expressed via transient transfection, then the co-expression with vTNFRs would cause an accumulation of vTNFRs rather than being secreted if an interaction was occurring between the two proteins. Thus an increase in vTNFR detection would suggest intracellular retention. From these data it was found that MYXT2 intracellular abundance significantly increased when co-transfected with TNFR2 and even more so when co-expressed with TNFR1. An increase in VARG4R and MPVJ2R abundance was also detected when co-expressed with TNFR2 and TNFR1, however this was not considered statistically significant. This suggested that MYXT2 was interacting with human TNFR1 and TNFR2 in support of the intracellular inhibition of TNFR1-induced cell death. Although VARG4R and MPVJ2R was not considered statistically significant it may still suggest the same as a small increase was detected. The differences in the detected abundance of each of the different vTNFRs may reflect different dynamics of interactions. If the vTNFR interaction displayed differences in half-life kinetics then the vTNFRs may still be secreted contributing to differences in detected vTNFR abundance. In future work it would be ideal to test which of the cell death pathways are being inhibited via TNFR1 interactions and whether this is shared amongst the three pathways. For example the activation of caspases is the primary cell death pathway activated by

TNFR1 (Fotin-Mleczek et al. 2002; Schneider-Brachert et al. 2004), therefore an assay could be developed to measure the various amounts of cleaved pro-caspase 8 (the active form) to examine the inhibition of cell death in more depth.

To further characterise the interactions of MYXT2, VARG4R and MPVJ2R with human cellular TNFRs, it was anticipated to next obtain structural information about each vTNFR. Currently no CRM-B family member or T2 molecule family member structures has been solved. To date the only known full length vTNFR homologue structure of cellular TNFRs is CRM-E, from Vaccinia virus (Graham et al. 2007). This structure, although a homologue of TNFRs, is a truncated version of CRM-B and T2 molecules lacking a 4^{th} CRD and C-terminal SECRET domain (Graham et al. 2007). The structure of CRM-E contains the same highly conserved folds as TNFR1 and conforms to the A1-B2, A1-B2 and A2-B1 modules found in CRDs 1-3 respectively (Graham et al. 2007). This is interesting as vTNFRs share a higher amino acid sequence identity to TNFR2 (TNFR1 27.5% vs TNFR2 31.1%)(Saraiva & Alcami 2001). Considering that T2 and CRM-B vTNFRs also share a higher amino acid sequence identity to TNFR2 (Gileva et al. 2006) and an even higher sequence identity to CRM-E, it is likely that MYXT2, VARG4R and MPVJ2R proteins would adopt a similar conformation (Table 5-1). While a structure for each MYXT2, VAR G4R and MPVJ2R would be a first for CRM-B and T2 vTNFRs, an even more fascinating structure would be that of the vTNFRs in complex with cellular TNFRS. Thus it was attempted to obtain crystal structures of the vTNFRs individually and also in complex with human TNFR1 and TNFR2. A structure of vTNFRs with TNFR1 or TNFR2 in complex would provide strong evidence for the interaction but also show the regions of the vTNFR molecules important to the association. Using this information it could be then possibly used to design specific inhibitors based on the vTNFR interactions.

Unfortunately for unknown reasons, bacterial expression of the vTNFR and human TNFR proteins was unsuccessful, despite numerous optimisation attempts. As a result this prevented obtaining any of the crystal structures for MYXT2, VARG4R and MPVJ2R individually and in complex with human TNFRs.

The discovery of the PLAD in TNFR1 and TNFR2 led to the hypothesis that soluble PLAD proteins could be used as potential therapeutics (Deng et al. 2005). Using proteins consisting of the PLAD from TNFR1 or TNFR2 in a mouse model of arthritis, it was shown that TNFR1 PLAD proteins had a protective effect, reducing inflammation (Deng et al. 2005). Furthermore the PLAD proteins do not interact with TNF, suggesting that PLAD proteins reduce inflammation via interrupting TNFR association or complex formation (Deng 2007). Whether vTNFRs may function in the same manner is unknown, however although the efficacy of the PLAD proteins was shown *in vivo*, it is not clearly defined. By using the vTNFRs as a model for anti-TNFR therapeutics, a more specific inhibitor of TNFR1 or TNFR2 could be designed based on further characterisation of the vTNFR-cellular TNFR interaction.

Although the attempts in generating crystal structures were unsuccessful, additional structural information was obtained through the use of FRET. For this a method was developed and optimised on the LSRII flow cytometer that resulted in a highly sensitive and high-throughput method of detecting TNFR interactions. The FRET method was then used to investigate the interactions of each of the vTNFRs with human TNFR1 and TNFR2 and determine the stoichiometries and orientations of these interactions. Though the FRET method had proven sensitive enough to detect changes induced by single amino acid changes by TRAPS mutations, no FRET emission was detectable between MYXT2,

VARG4R or MPVJ2R with TNFR1 or TNFR2. The absence of FRET detection with cellular TNFRs, despite MYXT2's known association with human TNFR1 and TNFR2 (Sedger et al. 2006), suggested that the orientation of the FRET occurred in a manner positioning the C-terminal regions further than 10nm apart. This may have either been due to differences in protein lengths or orientation of the association. As a further test of the FRET method, because MYXT2 is also known to form dimers (Schreiber, Rajarathnam & McFadden 1996), FRET was expected to occur between homodimers. However again no FRET was detected between any of the vTNFRs. The lack of FRET between vTNFRs and cellular TNFRs or even self-homodimers led to the hypothesis that a number of alternate conformations would be possible preventing FRET occurring. Although the N-N-parallel dimer of cellular TNFRs is often depicted and represented as the most likely conformation, an alternate C-N conformation has also repeatedly been observed in crystal structures of TNFR1 and CRM-E (Graham et al. 2007; Naismith et al. 1996). An antiparallel dimer is not generally believed to be relevant in a native biological system as it is was formed in high pH condition (Naismith et al. 1996), however low pH conditions certainly exist in subcellular compartments such as endosomes and lysosomes. Therefore to provide evidence for each of the possible conformations of the interactions occurring between vTNFRs and cellular TNFRs, comparative homology modelling was used.

Using the previously solved structures for human TNFR1 (Banner et al. 1993; Naismith et al. 1996), TNFR2 (Mukai et al. 2010), Vaccinia virus CRM-E (Graham et al. 2007) and the SECRET domain of Ectromelia CRM-D (Xue et al. 2011), predicted structures for MYXT2, VARG4R and MPVJ2R were generated. Each of the predicted models adopted the canonical TNFR structure in the N-terminal region and the C-terminal region adopted

an almost identical structure to the SECRET domain found in CRM-D. Amongst MYXT2, VARG4R and MPVJ2R however differences were observed, in particular within CRD4. It is uncertain if this variability was due to a lack of structure template within the solved TNFR1 and CRM-E structures, and without a full length vTNFR containing a SECRET domain this could not be confirmed. Regardless statistical validation of the models showed that each of the selected models was reliable and structurally resembled the template structures. As high amino acid sequence similarity usually translates into similar structure homology (Sali & Blundell 1993), it is probable that each of the vTNFR predicted models would closely represent the full length vTNFR molecules of MYXT2, VARG4R and MPVJ2R as each contain high homology in the amino acid sequences to the templates (Antonets, Nepomnyashchikh & Shchelkunov 2010; Gileva et al. 2006; Nepomnyashchikh et al. 2010). These predicted models were then used in docking predictions to analyse potential conformations of the vTNFR-TNFR interactions.

MYXT2, VARG4R and MPVJ2R were each docked against TNFR1, both individually and in complex with LTα. It was predicted that when the vTNFRs were bound to TNFR1 interactions were largely contributed by CRD1 of the vTNFRs that interacted with CRD3 or CRD4 of TNFR1. CRM-B molecules are known to bind LTα (Hu, Smith & Pickup 1994) and the predictive modelling of LTα bound to the receptor complex, predicts that the PLAD of the vTNFRs remains in contact with CRD3 or CRD4 whilst the CRD3 of the vTNFRS makes contacts to LTα. This conformation supports the evidence of the FRET data in chapter 5, as this C-N anti-parallel orientation positions the C-terminal regions such that the CFP and YFP fusion proteins would not be capable of FRET. If the interaction of vTNFRs and cellular TNFRs occurs at the plasma membrane then this orientation would also allow greater access of chemokines to access the SECRET domain. Whether the

function of this domain in MYXT2 serves a similar function to the SECRET domain VARG4R and CRM-B molecules (Antonets, Nepomnyashchikh & Shchelkunov 2010) is unknown, but given the high sequence similarity between them it is quite possible. In support of this orientation it was also predicted that each of the vTNFRs bound TNF similarly in an orientation opposite to TNFR1 or TNFR2 (Eck & Sprang 1989). Each of the vTNFRs were then also docked against human TNFR2. However due to bound state of TNFR2 to TNF, this proved difficult because of the hinge movements and conformational change in the receptor. Regardless all three vTNFRs bound to TNFR2 largely through the PLAD in an anti-parallel N-C conformation, although, in a much more open state resembling that of the vTNFRs when bound to the TNFR1 and LTα From all of the predicted models it strongly suggests that the viral TNFR PLAD domain is in fact an essential component of the viral TNFR-cellular TNFR interaction. However the interactions between vTNFRs and cellular TNFRs is anti-parallel possibly allowing for greater access to the C-terminal chemokine binding domains if the interaction membrane bound. Structural data from crystallography would have been ideal to confirm the preliminary models, but the data does allow interpretations of the structural data from the FRET and other experiments. Further in vitro studies will always be needed to confirm these predictions, however this information allows for more targeted hypothesis and methods to test them. For example knowing that the orientation is possibly anti-parallel, instead of using C-terminal tags on each of the protein pairs, N-terminal tags could possibly be used with linker regions to specifically determine protein orientations. Currently no biological evidence exists to support the anti-parallel conformation, but with further experimentation this may reveal specific targeted pathways for the blockade of TNFR1 or TNFR2. The common observation of TNF-independent signalling amongst TRAPS mutations also suggest that blockade of TNF,

although has proven effective for many diseases, may not be the best drug target, especially due to blockade of all the beneficial effects of TNF (Agnholt, Dahlerup & Kaltoft 2003; Breda et al. 2011). By designing a target specifically involving the PLAD it may also avoid reverse signalling associated with membrane bound TNF and antagonist having a pro-inflammatory effect (Mitoma et al. 2005).

Indeed the work presented in this study demonstrates the importance of the PLAD domain in TNFR interactions as well as vTNFR-TNFR interactions *in vitro*. This work structurally furthers our understanding of the vTNFR-cellular TNFR interaction as well as show its existence in other orthopoxviral proteins for the first time. It is evident that the novel intracellular mechanism of TNFR subversion requires further investigation however in doing so it will also further our understanding of TNFR biology and define a possible new target and design of TNFR antagonists.

Conclusions

The development of novel TNF antagonists paved the way for the use in once difficult to treat diseases such as rheumatoid arthritis (Rahman, Lucas & McFadden 2009b; Sedger & McDermott 2014). Current TNF biologics have proven effective in many inflammatory disease however there has always been a large proportion of patients who still fail to respond to treatment for unknown reasons or suffer compromising side effects such as increased risk to lymphomas and infection (Askling 2010; Toussirot & Bereau 2014). It is clear that the treatment of these disease is much more complex than the blockade of TNF due to the pleiotrophic nature of TNFRs and involvement in a wide array of biological processes. Further to this all current anti-TNF agents are essentially

engineered antibodies except in the case of Etanercept (which is a recombinant human TNFR2 receptor fused the IgG FC region) and are associated with a high cost to treatment (Sedger & McDermott 2014). Thus although effective, there is still a need for the development of a new generation of anti-TNF agents.

The discovery of a novel mechanism from MYXT2 to inhibit TNFR1-induced cell death offers insight into a new route into which the effects of TNF can be subverted, through the TNFRs themselves. This together with the discovery of the PLAD in TNFR family molecules demonstrated that PLAD interactions are required for many of the functions for TNFR biology, independent of the TNF ligand. Therefore using a syndrome defined by missense mutations in the TNFR1 receptor known as TRAPS, together with three vTNFR proteins, MYXT2 from Myxoma virus, VARG4R from Variola virus and MPVJ2R from Monkeypox virus, PLAD interactions and their effect on TNFR biology were investigated further. From the results in this study it was found that single amino acid mutations to TNFR1 have the ability to change TNFR signalling, resulting in reduced sensitivity or capability to induce TNFR1-induced cell death. It was also found that TRAPS mutations in the PLAD domain result in altered trafficking and possibly the formation of higher order complexes. This reinforced the importance of PLAD interactions in TNFR biology and requirement of higher order complexes to competently signal. The intracellular subversion was then further characterised for MYXT2, VARG4r and MPVJ2R and it was found that each is capable of subverting human TNFR1-induced cell death. The question of how the interaction occurs between vTNFRs was then investigated for the remainder of the study largely through FRET and comparative homology modelling. This again highlighted the requirement of the PLAD to subvert TNFRs possibly through an anti-parallel C-N conformation. Combined this evidence suggests new ways of

exploring and testing the association to reveal more about its impact on TNFR biology and ways to hopefully specifically target more specific aspects of TNFR downstream signalling. The work presented in this thesis investigated the impact of PLAD mutations and VTNFR association on TNFR1 induced cell death, yet a number of other TNFR pathways are still needed to be defined such as the effect on NFκB activation, to clearly define the mechanism.

In addition to these discoveries the development of a highly sensitive and high-throughput analysis method of FRET by flow cytometry was developed. In future work this optimised method could be used for investigation of a number of applications. For example small molecule libraries, targeting the PLAD could be used to screen their effect on TNFR molecules via FRET flow cytometry. To date only the initial discovery of the intracellular mechanism of MYXT2 has been published and the evidence presented here furthers our understanding for MYXT2 as well as for orthopoxvirsues VARG4R and MPVJ2R in TNFR subversion. Now that a characterisation of TRAPS biology and vTNFR subversion has been brought forward, the next step would be to investigate how TRAPS mutations may affect the interaction of VTNFRs. How we might gain from viral subversion of TNFRs will require further understanding of vTNFR subversion, and how signalling pathways may be targeted specifically. This study therefore brings us closer to identify a mechanism of TNFR inhibition that may lead to the first of more specific TNFR antagonists. Even though viruses such as Variola and Monkeypox viruses pose as extreme biohazards, there is still much to be benefited by learning how such pathogens have co-evolved with humans to become efficient in subverting host immune responses.

References

Abbruzzese, J.L., Levin, B., Ajani, J.A., Faintuch, J.S., Pazdur, R., Saks, S., Edwards, C. & Gutterman, J.U. 1990, 'A phase II trial of recombinant human interferon-gamma and recombinant tumor necrosis factor in patients with advanced gastrointestinal malignancies: results of a trial terminated by excessive toxicity', *J Biol Response Mod*, vol. 9, no. 5, pp. 522-7.

Abraham, E., Laterre, P.F., Garbino, J., Pingleton, S., Butler, T., Dugernier, T., Margolis, B., Kudsk, K., Zimmerli, W., Anderson, P., Reynaert, M., Lew, D., Lesslauer, W., Passe, S., Cooper, P., Burdeska, A., Modi, M., Leighton, A., Salgo, M. & Van der Auwera, P. 2001, 'Lenercept (p55 tumor necrosis factor receptor fusion protein) in severe sepsis and early septic shock: a randomized, double-blind, placebo-controlled, multicenter phase III trial with 1,342 patients', *Crit Care Med*, vol. 29, no. 3, pp. 503-10.

Afonso, C.L., Delhon, G., Tulman, E.R., Lu, Z., Zsak, A., Becerra, V.M., Zsak, L., Kutish, G.F. & Rock, D.L. 2005, 'Genome of deerpox virus', *J Virol*, vol. 79, no. 2, pp. 966-77.

Aggarwal, B.B. 2000, 'Tumour necrosis factors receptor associated signalling molecules and their role in activation of apoptosis, JNK and NF-kappa B', *Annals of the Rheumatic Diseases*, vol. 59, pp. 6-16.

Aggarwal, B.B. 2003, 'Signalling pathways of the TNF superfamily: a double-edged sword', *Nature Reviews Immunology*, vol. 3, no. 9, pp. 745-56.

Agnholt, J., Dahlerup, J.F. & Kaltoft, K. 2003, 'The effect of etanercept and infliximab on the production of tumour necrosis factor alpha, interferon-gamma and GM-CSF in in vivo activated intestinal T lymphocyte cultures', *Cytokine*, vol. 23, no. 3, pp. 76-85.

Aksentijevich, I. 2014, *Infevers database; TNFRSF1A sequence variants*, http://fmf.igh.cnrs.fr/ISSAID/infevers/, viewed 12/01/2015 2014, <http://fmf.igh.cnrs.fr/ISSAID/infevers/search.php>.

Aksentijevich, I., Galon, J., Soares, M., Mansfield, E., Hull, K., Oh, H.-H., Goldbach-Mansky, R., Dean, J., Athreya, B., Reginato, A.J., Henrickson, M., Pons-Estel, B., O'Shea, J.J. & Kastner, D.L. 2001, 'The Tumor-Necrosis-Factor Receptor-Associated Periodic Syndrome: New Mutations in TNFRSF1A, Ancestral Origins, Genotype-Phenotype Studies, and Evidence for Further Genetic Heterogeneity of Periodic Fevers', *The American Journal of Human Genetics*, vol. 69, no. 2, pp. 301-14.

Al-Lamki, R.S., Wang, J., Skepper, J.N., Thiru, S., Pober, J.S. & Bradley, J.R. 2001, 'Expression of tumor necrosis factor receptors in normal kidney and rejecting renal transplants', *Lab Invest*, vol. 81, no. 11, pp. 1503-15.

Alcami, A. 2003, 'Viral mimicry of cytokines, chemokines and their receptors', *Nature Reviews Immunology*, vol. 3, no. 1, p. 36.

Alcami, A., Khanna, A., Paul, N.L. & Smith, G.L. 1999, 'Vaccinia virus strains Lister, USSR and Evans express soluble and cell-surface tumour necrosis factor receptors', *J Gen Virol*, vol. 80 (Pt 4), pp. 949-59.

Alejo, A., Ruiz-Argüello, M.B., Ho, Y., Smith, V.P., Saraiva, M. & Alcami, A. 2006, 'A chemokine-binding domain in the tumor necrosis factor receptor from variola (smallpox) virus', *Proceedings of the National Academy of Sciences*, vol. 103, no. 15, pp. 5995-6000.

Antonets, D.V., Nepomnyashchikh, T.S. & Shchelkunov, S.N. 2010, 'SECRET domain of variola virus CRM-B protein can be a member of poxviral type II chemokine-binding proteins family', *BMC Res Notes*, vol. 3, p. 271.

Arita, I. & Henderson, D.A. 1968, 'Smallpox and monkeypox in non-human primates', *Bull World Health Organ*, vol. 39, no. 2, pp. 277-83.

Askling, J. 2010, 'The risk of malignancies in RA patients treated with biologics', *Z Rheumatol*, vol. 69, no. 9, pp. 774-9.

Bahl, C.P., Wu, R., Itakura, K., Katagiri, N. & Narang, S.A. 1976, 'Chemical and enzymatic synthesis of lactose operator of Escherichia coli and its binding to lactose repressor', *Proc Natl Acad Sci U S A*, vol. 73, no. 1, pp. 91-4.

Baldi, L., Muller, N., Picasso, S., Jacquet, R., Girard, P., Thanh, H.P., Derow, E. & Wurm, F.M. 2005, 'Transient Gene Expression in Suspension HEK-293 Cells: Application to Large-Scale Protein Production', *Biotechnology Progress*, vol. 21, no. 1, pp. 148-53.

Bandín, I. & Dopazo, C.P. 2011, 'Host range, host specificity and hypothesized host shift events among viruses of lower vertebrates', *Veterinary Research*, vol. 42, no. 1, pp. 67-.

Baneyx, F. & Mujacic, M. 2004, 'Recombinant protein folding and misfolding in Escherichia coli', *Nat Biotech*, vol. 22, no. 11, pp. 1399-408.

Banner, D.W., D'Arcy, A., Janes, W., Gentz, R., Schoenfeld, H.-J., Broger, C., Loetscher, H. & Lesslauer, W. 1993, 'Crystal structure of the soluble human 55 kd TNF receptor-human TNF^2 complex: Implications for TNF receptor activation', *Cell*, vol. 73, no. 3, pp. 431-45.

Barnes, P.J. & Karin, M. 1997, 'Nuclear factor-kappaB: a pivotal transcription factor in chronic inflammatory diseases', *N Engl J Med*, vol. 336, no. 15, pp. 1066-71.

Baseta, J.G. & Stutman, O. 2000, 'TNF Regulates Thymocyte Production by Apoptosis and Proliferation of the Triple Negative (CD3-CD4-CD8-) Subset', *J Immunol*, vol. 165, no. 10, pp. 5621-30.

Baxby, D. 1977, 'Poxvirus hosts and reservoirs', *Archives of Virology*, vol. 55, no. 3, pp. 169-79.

Belge, K.-U., Dayyani, F., Horelt, A., Siedlar, M., Frankenberger, M., Frankenberger, B., Espevik, T. & Ziegler-Heitbrock, L. 2002, 'The Proinflammatory CD14+CD16+DR++ Monocytes Are a Major Source of TNF', *J Immunol*, vol. 168, no. 7, pp. 3536-42.

Belmahi, L., Sefiani, A., Fouveau, C., Feingold, J., Delpech, M., Grateau, G. & Dode, C. 2006, 'Prevalence and distribution of MEFV mutations among Arabs from the Maghreb patients suffering from familial Mediterranean fever', *C R Biol*, vol. 329, no. 2, pp. 71-4.

Bendele, A.M., McComb, J., Gould, T., Frazier, J., Chlipala, E., Seely, J., Kieft, G. & Edwards, C.K., 3rd 1999, 'Effects of PEGylated soluble tumor necrosis factor receptor type I (PEG sTNF-RI) alone and in combination with methotrexate in adjuvant arthritic rats', *Clin Exp Rheumatol*, vol. 17, no. 5, pp. 553-60.

Benedict, C.A., Banks, T.A. & Ware, C.F. 2003, 'Death and survival: viral regulation of TNF signaling pathways', *Current Opinion in Immunology*, vol. 15, no. 1, pp. 59-65.

Berney, C. & Danuser, G. 2003, 'FRET or No FRET: A Quantitative Comparison', *Biophysical Journal*, vol. 84, no. 6, pp. 3992-4010.

Beutler, B., Milsark, I.W. & Cerami, A.C. 1985, 'Passive immunization against cachectin/tumor necrosis factor protects mice from lethal effect of endotoxin', *Science*, vol. 229, no. 4716, pp. 869-71.

Bhol, K.C., Tracey, D.E., Lemos, B.R., Lyng, G.D., Erlich, E.C., Keane, D.M., Quesenberry, M.S., Holdorf, A.D., Schlehuber, L.D., Clark, S.A. & Fox, B.S. 2013, 'AVX-470: a novel oral anti-TNF antibody with therapeutic potential in inflammatory bowel disease', *Inflamm Bowel Dis*, vol. 19, no. 11, pp. 2273-81.

Black, R.A. 2002, 'Tumor necrosis factor-[alpha] converting enzyme', *The International Journal of Biochemistry & Cell Biology*, vol. 34, no. 1, pp. 1-5.

Bodmer, J.-L., Schneider, P. & Tschopp, J. 2002, 'The molecular architecture of the TNF superfamily', *Trends in Biochemical Sciences*, vol. 27, no. 1, pp. 19-26.

Boillot, A., Capellier, G., Racadot, E., Wijdenes, J., Herve, P. & Barale, F. 1995, 'Pilot clinical trial of an anti-TNF alpha monoclonal antibody for the treatment of septic shock', *Clin Intensive Care*, vol. 6, no. 2, pp. 52-6.

Boldin, M.P., Mett, I.L., Varfolomeev, E.E., Chumakov, I., Shemer-Avni, Y., Camonis, J.H. & Wallach, D. 1995, 'Self-association of the Death Domains of the p55 Tumor Necrosis Factor (TNF) Receptor and Fas/APO1 Prompts Signaling for TNF and Fas/APO1 Effects', *Journal of Biological Chemistry*, vol. 270, no. 1, pp. 387-91.

Bonavida, B. 1991, 'Immunomodulatory effect of tumor necrosis factor', *Biotherapy*, vol. 3, no. 2, pp. 127-33.

Boschert, V., Krippner-Heidenreich, A., Branschädel, M., Tepperink, J., Aird, A. & Scheurich, P. 2010, 'Single chain TNF derivatives with individually mutated receptor binding sites reveal differential stoichiometry of ligand receptor complex formation for TNFR1 and TNFR2', *Cellular Signalling*, vol. 22, no. 7, pp. 1088-96.

Branschädel, M., Aird, A., Zappe, A., Tietz, C., Krippner-Heidenreich, A. & Scheurich, P. 2010, 'Dual function of cysteine rich domain (CRD) 1 of TNF receptor type 1: Conformational stabilization of CRD2 and control of receptor responsiveness', *Cellular Signalling*, vol. 22, no. 3, pp. 404-14.

Bratke, K.A., McLysaght, A. & Rothenburg, S. 2013, 'A survey of host range genes in poxvirus genomes', *Infection, Genetics and Evolution*, vol. 14, no. 0, pp. 406-25.

Breda, L., Del Torto, M., De Sanctis, S. & Chiarelli, F. 2011, 'Biologics in children's autoimmune disorders: efficacy and safety', *European Journal of Pediatrics*, vol. 170, no. 2, pp. 157-67.

Brenner, D.A., O'Hara, M., Angel, P., Chojkier, M. & Karin, M. 1989, 'Prolonged activation of jun and collagenase genes by tumour necrosis factor-[alpha]', *Nature*, vol. 337, no. 6208, pp. 661-3.

Brown, L.R. & Harris, D.A. 2003, 'Copper and zinc cause delivery of the prion protein from the plasma membrane to a subset of early endosomes and the Golgi', *J Neurochem*, vol. 87, no. 2, pp. 353-63.

Brunetti, C.R., Paulose-Murphy, M., Singh, R., Qin, J., Barrett, J.W., Tardivel, A., Schneider, P., Essani, K. & McFadden, G. 2003, 'A secreted high-affinity inhibitor of human TNF from Tanapox virus', *Proc Natl Acad Sci U S A*, vol. 100, no. 8, pp. 4831-6.

Buchan, G., Barrett, K., Turner, M., Chantry, D., Maini, R.N. & Feldmann, M. 1988, 'Interleukin-1 and tumour necrosis factor mRNA expression in rheumatoid arthritis: prolonged production of IL-1 alpha', *Clin Exp Immunol*, vol. 73, no. 3, pp. 449-55.

Bujalowski, W.M. & Jezewska, M.J. 2012, 'Using structure-function constraints in FRET studies of large macromolecular complexes', *Methods Mol Biol*, vol. 875, pp. 135-64.

Buller, R.M. & Palumbo, G.J. 1991, 'Poxvirus pathogenesis', *Microbiol. Mol. Biol. Rev.*, vol. 55, no. 1, pp. 80-122.

Bulua, A.C., Simon, A., Maddipati, R., Pelletier, M., Park, H., Kim, K.Y., Sack, M.N., Kastner, D.L. & Siegel, R.M. 2011, 'Mitochondrial reactive oxygen species promote production of proinflammatory cytokines and are elevated in TNFR1-associated periodic syndrome (TRAPS)', *J Exp Med*, vol. 208, no. 3, pp. 519-33.

Cagatay, T., Aydın, M., Sunmez, S., Cagatay, P., Gulbaran, Z., Gul, A., Artım, B. & Kilicaslan, Z. 2010, 'Follow-up results of 702 patients receiving tumor necrosis factor-alpha antagonists and evaluation of risk of tuberculosis', *Rheumatology International*, vol. 30, no. 11, pp. 1459-63.

Carpenter, E.P., Beis, K., Cameron, A.D. & Iwata, S. 2008, 'Overcoming the challenges of membrane protein crystallography', *Current Opinion in Structural Biology*, vol. 18, no. 5, pp. 581-6.

Carswell, E.A., Old, L.J., Kassel, R.L., Green, S., Fiore, N. & Williamson, B. 1975, 'An endotoxin-induced serum factor that causes necrosis of tumors', *Proceedings of the National Academy of Sciences of the United States of America*, vol. 72, no. 9, pp. 3666-70.

Chae, J.J., Komarow, H.D., Cheng, J., Wood, G., Raben, N., Liu, P.P. & Kastner, D.L. 2003, 'Targeted Disruption of Pyrin, the FMF Protein, Causes Heightened Sensitivity to Endotoxin and a Defect in Macrophage Apoptosis', *Molecular Cell*, vol. 11, no. 3, pp. 591-604.

Chan, F.K.-M. 2000, 'The pre-ligand binding assembly domain: a potential target of inhibition of tumour necrosis factor receptor function', *Annals of the Rheumatic Diseases*, vol. 59, no. suppl 1, pp. i50-i3.

Chan, F.K.-M. 2007, 'Three is better than one: Pre-ligand receptor assembly in the regulation of TNF receptor signaling', *Cytokine*, vol. 37, no. 2, pp. 101-7.

Chan, F.K.-M., Chun, H.J., Zheng, L., Siegel, R.M., Bui, K.L. & Lenardo, M.J. 2000a, 'A Domain in TNF Receptors That Mediates Ligand-Independent Receptor Assembly and Signaling', *Science*, vol. 288, no. 5475, pp. 2351-4.

Chan, F.K.-M., Siegel, R.M., Zacharias, D., Swofford, R., Holmes, K.L., Tsien, R.Y. & Lenardo, M.J. 2001, 'Fluorescence resonance energy transfer analysis of cell surface receptor interactions and signaling using spectral variants of the green fluorescent protein', *Cytometry*, vol. 44, no. 4, pp. 361-8.

Chan, F.K., Chun, H.J., Zheng, L., Siegel, R.M., Bui, K.L. & Lenardo, M.J. 2000b, 'A domain in TNF receptors that mediates ligand-independent receptor assembly and signaling', *Science (New York, N.Y.)*, vol. 288, no. 5475, pp. 2351-4.

Chang, V.T., Crispin, M., Aricescu, A.R., Harvey, D.J., Nettleship, J.E., Fennelly, J.A., Yu, C., Boles, K.S., Evans, E.J., Stuart, D.I., Dwek, R.A., Jones, E.Y., Owens, R.J. & Davis, S.J. 2007, 'Glycoprotein Structural Genomics: Solving the Glycosylation Problem', *Structure(London, England:1993)*, vol. 15, no. 3, pp. 267-73.

Chen, N., Buller, R.M.L., Wall, E.M. & Upton, C. 2000, 'Analysis of host response modifier ORFs of ectromelia virus, the causative agent of mousepox', *Virus Research*, vol. 66, no. 2, pp. 155-73.

Chen, N., Li, G., Liszewski, M.K., Atkinson, J.P., Jahrling, P.B., Feng, Z., Schriewer, J., Buck, C., Wang, C., Lefkowitz, E.J., Esposito, J.J., Harms, T., Damon, I.K., Roper, R.L., Upton, C. & Buller, R.M.L. 2005, 'Virulence differences between

monkeypox virus isolates from West Africa and the Congo basin', *Virology*, vol. 340, no. 1, pp. 46-63.
Chen, X., Fischel-Ghodsian, N., Cercek, A., Hamon, M., Ogur, G., Lotan, R., Danon, Y. & Shohat, M. 1998, 'Assessment of pyrin gene mutations in Turks with familial Mediterranean fever (FMF)', *Human Mutation*, vol. 11, no. 6, pp. 456-60.
Chinnaiyan, A.M., Tepper, C.G., Seldin, M.F., O'Rourke, K., Kischkel, F.C., Hellbardt, S., Krammer, P.H., Peter, M.E. & Dixit, V.M. 1996, 'FADD/MORT1 Is a Common Mediator of CD95 (Fas/APO-1) and Tumor Necrosis Factor Receptor-induced Apoptosis', *Journal of Biological Chemistry*, vol. 271, no. 9, pp. 4961-5.
Choi, S.J., Lee, K.-H., Park, H.S., Kim, S.-K., Koh, C.-M. & Park, J.Y. 2005, 'Differential Expression, Shedding, Cytokine Regulation and Function of TNFR1 and TNFR2 in Human Fetal Astrocytes', *Yonsei Medical Journal*, vol. 46, no. 6, pp. 818-26.
Choy, E.H., Hazleman, B., Smith, M., Moss, K., Lisi, L., Scott, D.G., Patel, J., Sopwith, M. & Isenberg, D.A. 2002, 'Efficacy of a novel PEGylated humanized anti-TNF fragment (CDP870) in patients with rheumatoid arthritis: a phase II double-blinded, randomized, dose-escalating trial', *Rheumatology (Oxford)*, vol. 41, no. 10, pp. 1133-7.
Churchman, S.M., Church, L.D., Savic, S., Coulthard, L.R., Hayward, B., Nedjai, B., Turner, M.D., Mathews, R.J., Baguley, E., Hitman, G.A., Gooi, H.C., Wood, P.M.D., Emery, P. & McDermott, M.F. 2008, 'A novel TNFRSF1A splice mutation associated with increased nuclear factor κappaB (NF-κB) transcription factor activation in patients with tumour necrosis factor receptor associated periodic syndrome (TRAPS)', *Annals of the Rheumatic Diseases*, vol. 67, no. 11, pp. 1589-95.
Comeau, S.R., Gatchell, D.W., Vajda, S. & Camacho, C.J. 2004a, 'ClusPro: a fully automated algorithm for protein-protein docking', *Nucleic Acids Res*, vol. 32, no. Web Server issue, pp. W96-9.
Comeau, S.R., Gatchell, D.W., Vajda, S. & Camacho, C.J. 2004b, 'ClusPro: an automated docking and discrimination method for the prediction of protein complexes', *Bioinformatics*, vol. 20, no. 1, pp. 45-50.
Creaven, P.J., Plager, J.E., Dupere, S., Huben, R.P., Takita, H., Mittelman, A. & Proefrock, A. 1987, 'Phase I clinical trial of recombinant human tumor necrosis factor', *Cancer Chemother Pharmacol*, vol. 20, no. 2, pp. 137-44.
Crompton, T., Peitsch, M.C., MacDonald, H.R. & Tschopp, J. 1992, 'Propidium iodide staining correlates with the extent of DNA degradation in isolated nuclei', *Biochem Biophys Res Commun*, vol. 183, no. 2, pp. 532-7.
D'Osualdo, A., Ferlito, F., Prigione, I., Obici, L., Meini, A., Zulian, F., Pontillo, A., Corona, F., Barcellona, R., Duca, M.D., Santamaria, G., Traverso, F., Picco, P., Baldi, M., Plebani, A., Ravazzolo, R., Ceccherini, I., Martini, A. & Gattorno, M. 2006, 'Neutrophils from patients with TNFRSF1A mutations display resistance to tumor necrosis factor–induced apoptosis: Pathogenetic and clinical implications', *Arthritis & Rheumatism*, vol. 54, no. 3, pp. 998-1008.
Dandona, P., Aljada, A. & Bandyopadhyay, A. 2004, 'Inflammation: the link between insulin resistance, obesity and diabetes', *Trends in Immunology*, vol. 25, no. 1, pp. 4-7.
Das, R., Qian, B., Raman, S., Vernon, R., Thompson, J., Bradley, P., Khare, S., Tyka, M.D., Bhat, D., Chivian, D., Kim, D.E., Sheffler, W.H., Malmstrom, L., Wollacott, A.M., Wang, C., Andre, I. & Baker, D. 2007, 'Structure prediction for CASP7 targets

using extensive all-atom refinement with Rosetta@home', *Proteins*, vol. 69 Suppl 8, pp. 118-28.
Delhase, M. & Yi, C. 1999, 'Positive and negative regulation of IkappaB kinase activity through IKKbeta subunit phosphorylation', *Science*, vol. 284, no. 5412, p. 309.
Dempsey, P.W., Doyle, S.E., He, J.Q. & Cheng, G. 2003, 'The signaling adaptors and pathways activated by TNF superfamily', *Cytokine & Growth Factor Reviews*, vol. 14, no. 3-4, pp. 193-209.
Deng, G.M. 2007, 'Tumor necrosis factor receptor pre-ligand assembly domain is an important therapeutic target in inflammatory arthritis', *BioDrugs*, vol. 21, no. 1, pp. 23-9.
Deng, G.M., Zheng, L., Chan, F.K. & Lenardo, M. 2005, 'Amelioration of inflammatory arthritis by targeting the pre-ligand assembly domain of tumor necrosis factor receptors', *Nat Med*, vol. 11, no. 10, pp. 1066-72.
Deng, Y., Ren, X., Yang, L., Lin, Y. & Wu, X. 2003, 'A JNK-Dependent Pathway Is Required for TNF[alpha]-Induced Apoptosis', *Cell*, vol. 115, no. 1, pp. 61-70.
Deria, A., Jezek, Z., Markvart, K., Carrasco, P. & Weisfeld, J. 1980, 'The world's last endemic case of smallpox: surveillance and containment measures', *Bull World Health Organ*, vol. 58, no. 2, pp. 279-83.
Dodé, C., André, M., Bienvenu, T., Hausfater, P., Pêcheux, C., Bienvenu, J., Lecron, J.C., Reinert, P., Cattan, D., Piette, J.C., Szajnert, M.F., Delpech, M. & Grateau, G. 2002, 'The enlarging clinical, genetic, and population spectrum of tumor necrosis factor receptor–associated periodic syndrome', *Arthritis & Rheumatism*, vol. 46, no. 8, pp. 2181-8.
Dumbell, K.R., Bedson, H.S. & Rossier, E. 1961, 'Laboratory differentiation between variola major and variola minor', *Bulletin of the World Health Organization*, vol. 25, no. 1, pp. 73-8.
Dumbell, K.R. & Huq, F. 1986, 'The virology of variola minor correlation of laboratory tests with the geographic distribution and human virulence of variola isolates', *American Journal of Epidemiology*, vol. 123, no. 3, pp. 403-15.
Dumon-Seignovert, L., Cariot, G. & Vuillard, L. 2004, 'The toxicity of recombinant proteins in Escherichia coli: a comparison of overexpression in BL21(DE3), C41(DE3), and C43(DE3)', *Protein Expression and Purification*, vol. 37, no. 1, pp. 203-6.
Dunlop, K.V., Irvin, R.T. & Hazes, B. 2005, 'Pros and cons of cryocrystallography: should we also collect a room-temperature data set?', *Acta Crystallogr D Biol Crystallogr*, vol. 61, no. Pt 1, pp. 80-7.
Dunn, K.W., Kamocka, M.M. & McDonald, J.H. 2011, 'A practical guide to evaluating colocalization in biological microscopy', *American Journal of Physiology - Cell Physiology*, vol. 300, no. 4, pp. C723-C42.
Dye, B.T. 2005, 'Flow cytometric analysis of CFP–YFP FRET as a marker for in vivo protein–protein interaction', *Clinical and Applied Immunology Reviews*, vol. 5, no. 5, pp. 307-24.
Ea, C.-K., Deng, L., Xia, Z.-P., Pineda, G. & Chen, Z.J. 2006, 'Activation of IKK by TNF[alpha] Requires Site-Specific Ubiquitination of RIP1 and Polyubiquitin Binding by NEMO', *Molecular Cell*, vol. 22, no. 2, pp. 245-57.
Eck, M.J. & Sprang, S.R. 1989, 'The structure of tumor necrosis factor-alpha at 2.6 A resolution. Implications for receptor binding', *Journal of Biological Chemistry*, vol. 264, no. 29, pp. 17595-605.

Eichholtz-Wirth, H., Fritz, E. & Wolz, L. 2003, 'Overexpression of the 'silencer of death domain', SODD/BAG-4, modulates both TNFR1- and CD95-dependent cell death pathways', *Cancer Letters*, vol. 194, no. 1, pp. 81-9.

El-Shanti, H., Majeed, H.A. & El-Khateeb, M. 2006, 'Familial mediterranean fever in Arabs', *Lancet*, vol. 367, no. 9515, pp. 1016-24.

El Mortaji, L., Terrasse, R., Dessen, A., Vernet, T. & Di Guilmi, A.M. 2010, 'Stability and Assembly of Pilus Subunits of Streptococcus pneumoniae', *The Journal of Biological Chemistry*, vol. 285, no. 16, pp. 12405-15.

Elliott, M.J., Maini, R.N., Feldmann, M., Kalden, J.R., Antoni, C., Smolen, J.S., Leeb, B., Breedveld, F.C., Macfarlane, J.D., Bijl, H. & et al. 1994, 'Randomised double-blind comparison of chimeric monoclonal antibody to tumour necrosis factor alpha (cA2) versus placebo in rheumatoid arthritis', *Lancet*, vol. 344, no. 8930, pp. 1105-10.

Elliott, M.J., Maini, R.N., Feldmann, M., Long-Fox, A., Charles, P., Katsikis, P., Brennan, F.M., Walker, J., Bijl, H., Ghrayeb, J. & et al. 1993, 'Treatment of rheumatoid arthritis with chimeric monoclonal antibodies to tumor necrosis factor alpha', *Arthritis Rheum*, vol. 36, no. 12, pp. 1681-90.

Ellner, P.D. 1998, 'Smallpox: Gone but not forgotten', *Infection*, vol. 26, no. 5, pp. 263-9.

Enari, M., Sakahira, H., Yokoyama, H., Okawa, K., Iwamatsu, A. & Nagata, S. 1998, 'A caspase-activated DNase that degrades DNA during apoptosis, and its inhibitor ICAD', *Nature*, vol. 391, no. 6662, pp. 43-50.

Epperson, M.L., Lee, C.A. & Fremont, D.H. 2012, 'Subversion of cytokine networks by virally encoded decoy receptors', *Immunological Reviews*, vol. 250, no. 1, pp. 199-215.

Eramian, D., Eswar, N., Shen, M.Y. & Sali, A. 2008, 'How well can the accuracy of comparative protein structure models be predicted?', *Protein Sci*, vol. 17, no. 11, pp. 1881-93.

Esposito, J.J., Sammons, S.A., Frace, A.M., Osborne, J.D., Olsen-Rasmussen, M., Zhang, M., Govil, D., Damon, I.K., Kline, R., Laker, M., Li, Y., Smith, G.L., Meyer, H., LeDuc, J.W. & Wohlhueter, R.M. 2006, 'Genome Sequence Diversity and Clues to the Evolution of Variola (Smallpox) Virus', *Science*, vol. 313, no. 5788, pp. 807-12.

Essbauer, S., Pfeffer, M. & Meyer, H. 2010, 'Zoonotic poxviruses', *Veterinary Microbiology*, vol. 140, no. 3-4, pp. 229-36.

Eyler, J.M. 2003, 'Smallpox in history: the birth, death, and impact of a dread disease', *Journal of Laboratory and Clinical Medicine*, vol. 142, no. 4, pp. 216-20.

Feinberg, B., Kurzrock, R., Talpaz, M., Blick, M., Saks, S. & Gutterman, J.U. 1988, 'A phase I trial of intravenously-administered recombinant tumor necrosis factor-alpha in cancer patients', *J Clin Oncol*, vol. 6, no. 8, pp. 1328-34.

Feinstein, E., Kimchi, A., Wallach, D., Boldin, M. & Varfolomeev, E. 1995, 'The death domain - a module shared by proteins with diverse cellular functions', *Trends in Biochemical Sciences*, vol. 20, no. 9, pp. 342-4.

Fenner, F. 1959, 'Myxomatosis', *Br Med Bull*, vol. 15, pp. 240-5.

Fenner, F. 1988, *Smallpox and its eradication*, World Health Organization.

Fenner, F. 1993, 'Smallpox: emergence, global spread, and eradication', *Hist Philos Life Sci*, vol. 15, no. 3, pp. 397-420.

Fenner, F., Wittek, R. & Dumbell, K.R. 1989, *The orthopoxviruses*, Academic Press.

Fernandez-Castane, A., Vine, C.E., Caminal, G. & Lopez-Santin, J. 2012, 'Evidencing the role of lactose permease in IPTG uptake by Escherichia coli in fed-batch high cell density cultures', *J Biotechnol*, vol. 157, no. 3, pp. 391-8.

Fernández de Marco, M.d.M., Alejo, A., Hudson, P., Damon, I.K. & Alcami, A. 2010, 'The highly virulent variola and monkeypox viruses express secreted inhibitors of type I interferon', *The FASEB Journal*, vol. 24, no. 5, pp. 1479-88.

Fields, B.N., Knipe, D.M. & Howley, P.M. 2007, *Fields' Virology*, Wolters Kluwer Health/Lippincott Williams & Wilkins.

Fotin-Mleczek, M., Henkler, F., Samel, D., Reichwein, M., Hausser, A., Parmryd, I., Scheurich, P., Schmid, J.A. & Wajant, H. 2002, 'Apoptotic crosstalk of TNF receptors: TNF-R2-induces depletion of TRAF2 and IAP proteins and accelerates TNF-R1-dependent activation of caspase-8', *J Cell Sci*, vol. 115, no. 13, pp. 2757-70.

Fu, Z.-Q., Harrison, R.W., Reed, C., Wu, J., Xue, Y.-N., Chen, M.-J. & Weber, I.T. 1995, 'Model complexes of tumor necrosis factor-α with receptors Rl and R2', *Protein Engineering*, vol. 8, no. 12, pp. 1233-41.

Ganesan, S., Ameer-beg, S.M., Ng, T.T.C., Vojnovic, B. & Wouters, F.S. 2006, 'A dark yellow fluorescent protein (YFP)-based Resonance Energy-Accepting Chromoprotein (REACh) for Förster resonance energy transfer with GFP', *Proceedings of the National Academy of Sciences of the United States of America*, vol. 103, no. 11, pp. 4089-94.

Gileva, I.P., Nepomnyashchikh, T.S., Antonets, D.V., Lebedev, L.R., Kochneva, G.V., Grazhdantseva, A.V. & Shchelkunov, S.N. 2006, 'Properties of the recombinant TNF-binding proteins from variola, monkeypox, and cowpox viruses are different', *Biochimica et Biophysica Acta (BBA) - Proteins and Proteomics*, vol. 1764, no. 11, pp. 1710-8.

Gileva, I.P., Ryazankin, I.A., Nepomnyashchikh, T.S., Totmenin, A.V., Maxutov, Z.A., Lebedev, L.R., Afinogenova, G.N., Pustoshilova, N.M. & Shchelkunov, S.N. 2005, 'Expression of genes for orthopoxviral TNF-binding proteins in insect cells and investigation of the recombinant TNF-binding proteins', *Molecular Biology*, vol. 39, no. 2, pp. 218-25.

Giroir, B.P. 1993, 'Mediators of septic shock: new approaches for interrupting the endogenous inflammatory cascade', *Crit Care Med*, vol. 21, no. 5, pp. 780-9.

Gosselin, J., Menezes, J., D'Addario, M., Hiscott, J., Flamand, L., Lamoureux, G. & Oth, D. 1991, 'Inhibition of tumor necrosis factor-alpha transcription by Epstein-Barr virus', *Eur J Immunol*, vol. 21, no. 1, pp. 203-8.

Graham, F.L., Smiley, J., Russell, W.C. & Nairn, R. 1977, 'Characteristics of a human cell line transformed by DNA from human adenovirus type 5', *J Gen Virol*, vol. 36, no. 1, pp. 59-74.

Graham, S.C., Bahar, M.W., Abrescia, N.G.A., Smith, G.L., Stuart, D.I. & Grimes, J.M. 2007, 'Structure of CRM-E, a Virus-encoded Tumour Necrosis Factor Receptor', *Journal of Molecular Biology*, vol. 372, no. 3, pp. 660-71.

Granel, B., Serratrice, J., Dode, C., Grateau, G., Disdier, P. & Weiller, P.J. 2007, 'Overlap syndrome between FMF and TRAPS in a patient carrying MEFV and TNFRSF1A mutations', *Clin Exp Rheumatol*, vol. 25, no. 4 Suppl 45, pp. S93-5.

Gravestein, L.A., Nieland, J.D., Kruisbeek, A.M. & Borst, J. 1995, 'Novel mAbs reveal potent co-stimulatory activity of murine CD27', *International Immunology*, vol. 7, no. 4, pp. 551-7.

Gray, P.W., Barrett, K., Chantry, D., Turner, M. & Feldmann, M. 1990, 'Cloning of human tumor necrosis factor (TNF) receptor cDNA and expression of recombinant soluble TNF-binding protein', *Proceedings of the National Academy of Sciences of the United States of America*, vol. 87, no. 19, pp. 7380-4.

Grell, M., Zimmermann, G., Hulser, D., Pfizenmaier, K. & Scheurich, P. 1994, 'TNF receptors TR60 and TR80 can mediate apoptosis via induction of distinct signal pathways', *J Immunol*, vol. 153, no. 5, pp. 1963-72.

Haas, T.L., Emmerich, C.H., Gerlach, B., Schmukle, A.C., Cordier, S.M., Rieser, E., Feltham, R., Vince, J., Warnken, U., Wenger, T., Koschny, R., Komander, D., Silke, J. & Walczak, H. 2009, 'Recruitment of the Linear Ubiquitin Chain Assembly Complex Stabilizes the TNF-R1 Signaling Complex and Is Required for TNF-Mediated Gene Induction', *Molecular Cell*, vol. 36, no. 5, pp. 831-44.

Haridas, V., Darnay, B.G., Natarajan, K., Heller, R. & Aggarwal, B.B. 1998, 'Overexpression of the p80 TNF Receptor Leads to TNF-Dependent Apoptosis, Nuclear Factor-{kappa}B Activation, and c-Jun Kinase Activation', *J Immunol*, vol. 160, no. 7, pp. 3152-62.

Havla, J., Lohse, P., Gerdes, L.A., Hohlfeld, R. & Kumpfel, T. 2013, 'Symptoms related to tumor necrosis factor receptor 1-associated periodic syndrome, multiple sclerosis, and severe rheumatoid arthritis in patients carrying the TNF receptor superfamily 1A D12E/p.Asp41Glu mutation', *J Rheumatol*, vol. 40, no. 3, pp. 261-4.

Hawari, F.I., Rouhani, F.N., Cui, X., Yu, Z.-X., Buckley, C., Kaler, M. & Levine, S.J. 2004, 'Release of full-length 55-kDa TNF receptor 1 in exosome-like vesicles: A mechanism for generation of soluble cytokine receptors', *Proceedings of the National Academy of Sciences of the United States of America*, vol. 101, no. 5, pp. 1297-302.

He, L., Bradrick, T.D., Karpova, T.S., Wu, X., Fox, M.H., Fischer, R., McNally, J.G., Knutson, J.R., Grammer, A.C. & Lipsky, P.E. 2003, 'Flow cytometric measurement of fluorescence (Forster) resonance energy transfer from cyan fluorescent protein to yellow fluorescent protein using single-laser excitation at 458 nm', *Cytometry A*, vol. 53, no. 1, pp. 39-54.

He, L., Wu, X., Simone, J., Hewgill, D. & Lipsky, P.E. 2005, 'Determination of tumor necrosis factor receptor-associated factor trimerization in living cells by CFP->YFP->mRFP FRET detected by flow cytometry', *Nucleic Acids Res*, vol. 33, no. 6, p. e61.

Heim, M.E., Siegmund, R., Illiger, H.J., Klee, M., Rieche, K., Berdel, W.E. & Edler, L. 1990, 'Tumor necrosis factor in advanced colorectal cancer: a phase II study. A trial of the phase I/II study group of the Association for Medical Oncology of the German Cancer Society', *Onkologie*, vol. 13, no. 6, pp. 444-7.

Heinrich, K., Matthew, C., Riminton, D.S., Frances, A.L., Robert, M.H., Birgit, L., Frank, K., Barbara Fazekas de St, G. & Jonathon, D.S. 1997, 'Distinct roles for lymphotoxin-alpha and tumor necrosis factor in organogenesis and spatial organization of lymphoid tissue', *European Journal of Immunology*, vol. 27, no. 10, pp. 2600-9.

Heinrich, M., Neumeyer, J., Jakob, M., Hallas, C., Tchikov, V., Winoto-Morbach, S., Wickel, M., Schneider-Brachert, W., Trauzold, A., Hethke, A. & Schutze, S. 2004, 'Cathepsin D links TNF-induced acid sphingomyelinase to Bid-mediated caspase-9 and -3 activation', *Cell Death Differ*, vol. 11, no. 5, pp. 550-63.

Helenius, A. & Aebi, M. 2004, 'Roles of N-linked glycans in the endoplasmic reticulum', *Annu Rev Biochem*, vol. 73, pp. 1019-49.
Henderson, D.A. 2011, 'The eradication of smallpox – An overview of the past, present, and future', *Vaccine*, vol. 29, Supplement 4, no. 0, pp. D7-D9.
Herbein, G. & O'Brien, W.A. 2000, 'Tumor necrosis factor (TNF)-alpha and TNF receptors in viral pathogenesis', *Proc Soc Exp Biol Med*, vol. 223, no. 3, pp. 241-57.
Herrlich, A., Mayr, A., Mahnel, H. & Munz, E. 1963, 'Experimental studies on transformation of the variola virus into the vaccinia virus', *Archiv für die gesamte Virusforschung*, vol. 12, no. 5, pp. 579-99.
Hoffmann, F., Lohse, P., Stojanov, S., Shin, Y.S., Renner, E.D., KÃ©ry, A., Zellerer, S. & Belohradsky, B.H. 2005, 'Identification of a novel mevalonate kinase gene mutation in combination with the common MVK V377I substitution and the low-penetrance TNFRSF1A R92Q mutation', *European Journal of Human Genetics*, vol. 13, no. 4, pp. 510-2.
Hongxiu, L. & Xin, L. 2008, 'Positive and negative signaling components involved in TNF[alpha]-induced NF-[kappa]B activation', *Cytokine*, vol. 41, no. 1, pp. 1-8.
Hsu, H., Huang, J., Shu, H.-B., Baichwal, V. & Goeddel, D.V. 1996, 'TNF-Dependent Recruitment of the Protein Kinase RIP to the TNF Receptor-1 Signaling Complex', *Immunity*, vol. 4, no. 4, pp. 387-96.
Hsu, H., Shu, H.-B., Pan, M.-G. & Goeddel, D.V. 1996, 'TRADD-TRAF2 and TRADD-FADD Interactions Define Two Distinct TNF Receptor 1 Signal Transduction Pathways', *Cell*, vol. 84, no. 2, pp. 299-308.
Hsu, H., Xiong, J. & Goeddel, D.V. 1995, 'The TNF receptor 1-associated protein TRADD signals cell death and NF-[kappa]B activation', *Cell*, vol. 81, no. 4, pp. 495-504.
Hu, F.-Q., Smith, C.A. & Pickup, D.J. 1994, 'Cowpox Virus Contains Two Copies of an Early Gene Encoding a Soluble Secreted Form of the Type II TNF Receptor', *Virology*, vol. 204, no. 1, pp. 343-56.
Huggins, M.L., Radford, P.M., McIntosh, R.S., Bainbridge, S.E., Dickinson, P., Draper-Morgan, K.-A., Tighe, P.J., Powell, R.J. & Todd, I. 2004, 'Shedding of mutant tumor necrosis factor receptor superfamily 1A associated with tumor necrosis factor receptor-associated periodic syndrome: Differences between cell types', *Arthritis & Rheumatism*, vol. 50, no. 8, pp. 2651-9.
Hull, K.M., Drewe, E., Aksentijevich, I., Singh, H.K., Wong, K., McDermott, E.M., Dean, J., Powell, R.J. & Kastner, D.L. 2002, 'The TNF Receptor-Associated Periodic Syndrome (TRAPS): Emerging Concepts of an Autoinflammatory Disorder', *Medicine (Baltimore)*, vol. 81, no. 5, pp. 349-68.
Inoué, S., Shimomura, O., Goda, M., Shribak, M. & Tran, P.T. 2002, 'Fluorescence polarization of green fluorescence protein', *Proceedings of the National Academy of Sciences*, vol. 99, no. 7, pp. 4272-7.
Jacobs, Z. & Ciaccio, C.E. 2010, 'Periodic Fever syndromes', *Curr Allergy Asthma Rep*, vol. 10, no. 6, pp. 398-404.
Janssen Biotech Inc 2014, *Remicade, Infliximab*, <http://www.remicade.com/>.
Jesus, A.A., Oliveira, J.B., Aksentijevich, I., Fujihira, E., Carneiro-Sampaio, M.M.S., Duarte, A.J.S. & Silva, C.A.A. 2008, 'TNF receptor-associated periodic syndrome (TRAPS): Description of a novel TNFRSF1A mutation and response to etanercept', *European Journal of Pediatrics*, vol. 167, no. 12, pp. 1421-5.

Jezek, Z., Grab, B., Szczeniowski, M.V., Paluku, K.M. & Mutombo, M. 1988, 'Human monkeypox: secondary attack rates', *Bull World Health Organ*, vol. 66, no. 4, pp. 465-70.

Johnston, J.B. & McFadden, G. 2003, 'Poxvirus Immunomodulatory Strategies: Current Perspectives', *J. Virol.*, vol. 77, no. 11, pp. 6093-100.

Jones, S.J., Ledgerwood, E.C., Prins, J.B., Galbraith, J., Johnson, D.R., Pober, J.S. & Bradley, J.R. 1999, 'TNF Recruits TRADD to the Plasma Membrane But Not the trans-Golgi Network, the Principal Subcellular Location of TNF-R1', *J Immunol*, vol. 162, no. 2, pp. 1042-8.

Jonkman, J. & Brown, C.M. 2015, 'Any Way You Slice It—A Comparison of Confocal Microscopy Techniques', *Journal of Biomolecular Techniques : JBT*, vol. 26, no. 2, pp. 54-65.

Jordan, M., Köhne, C. & Wurm, F. 1998, 'Calcium-phosphate mediated DNA transfer into HEK-293 cells in suspension: control of physicochemical parameters allows transfection in stirred media. Transfection and protein expression in mammalian cells', *Cytotechnology*, vol. 26, no. 1, pp. 39-47.

Ka-Ming Chan, F. & Lenardo, M.J. 2000, 'A crucial role for p80 TNF-R2 in amplifying p60 TNF-R1 apoptosis signals in T lymphocytes', *European Journal of Immunology*, vol. 30, no. 2, pp. 652-60.

Kanazawa, T., Takematsu, H., Yamamoto, A., Yamamoto, H. & Kozutsumi, Y. 2008, 'Wheat germ agglutinin stains dispersed post-golgi vesicles after treatment with the cytokinesis inhibitor psychosine', *J Cell Physiol*, vol. 215, no. 2, pp. 517-25.

Kandiel, A., Fraser, A.G., Korelitz, B.I., Brensinger, C. & Lewis, J.D. 2005, 'Increased risk of lymphoma among inflammatory bowel disease patients treated with azathioprine and 6-mercaptopurine', *Gut*, vol. 54, no. 8, pp. 1121-5.

Karin, M., Liu, Z.-g. & Zandi, E. 1997, 'AP-1 function and regulation', *Current Opinion in Cell Biology*, vol. 9, no. 2, pp. 240-6.

Kim, K.-J., Kim, H.-E., Lee, K.-H., Han, W., Yi, M.-J., Jeong, J. & Oh, B.-H. 2004, 'Two-promoter vector is highly efficient for overproduction of protein complexes', *Protein Science : A Publication of the Protein Society*, vol. 13, no. 6, pp. 1698-703.

Kimberley, F., Lobito, A., Siegel, R. & Screaton, G. 2007, 'Falling into TRAPS - receptor misfolding in the TNF receptor 1-associated periodic fever syndrome', *Arthritis Research & Therapy*, vol. 9, no. 4, p. 217.

Korpimaki, T., Kurittu, J. & Karp, M. 2003, 'Surprisingly fast disappearance of beta-lactam selection pressure in cultivation as detected with novel biosensing approaches', *J Microbiol Methods*, vol. 53, no. 1, pp. 37-42.

Kramer, J.M., Hanel, W., Shen, F., Isik, N., Malone, J.P., Maitra, A., Sigurdson, W., Swart, D., Tocker, J., Jin, T. & Gaffen, S.L. 2007, '78 Dissecting the IL-17 Receptor: Identification of a Pre-ligand Assembly Domain (PLAD) and Ligand Binding Site in IL-17RA', *Cytokine*, vol. 39, no. 1, pp. 22-.

Kriegel, M.A., Huffmeier, U., Scherb, E., Scheidig, C., Geiler, T., Kalden, J.R., Reis, A. & Lorenz, H.M. 2003, 'Tumor necrosis factor receptor-associated periodic syndrome characterized by a mutation affecting the cleavage site of the receptor: implications for pathogenesis', *Arthritis Rheum*, vol. 48, no. 8, pp. 2386-8.

Kriegler, M., Perez, C., DeFay, K., Albert, I. & Lu, S.D. 1988, 'A novel form of TNF/cachectin is a cell surface cytotoxic transmembrane protein: ramifications for the complex physiology of TNF', *Cell*, vol. 53, no. 1, pp. 45-53.

Kristensen, M., Chu, C.Q., Eedy, D.J., Feldmann, M., Brennan, F.M. & Breathnach, S.M. 1993, 'Localization of tumour necrosis factor-alpha (TNF-alpha) and its receptors in normal and psoriatic skin: epidermal cells express the 55-kD but not the 75-kD TNF receptor', *Clin Exp Immunol*, vol. 94, no. 2, pp. 354-62.

Kroeger, K.M., Carville, K.S. & Abraham, L.J. 1997, 'The -308 tumor necrosis factor-[alpha] promoter polymorphism effects transcription', *Molecular Immunology*, vol. 34, no. 5, pp. 391-9.

Lachmann, H.J. 2011, 'Clinical Immunology Review Series: An approach to the patient with a periodic fever syndrome', *Clinical & Experimental Immunology*, vol. 165, no. 3, pp. 301-9.

Lachmann, H.J., Papa, R., Gerhold, K., Obici, L., Touitou, I., Cantarini, L., Frenkel, J., Anton, J., Kone-Paut, I., Cattalini, M., Bader-Meunier, B., Insalaco, A., Hentgen, V., Merino, R., Modesto, C., Toplak, N., Berendes, R., Ozen, S., Cimaz, R., Jansson, A., Brogan, P.A., Hawkins, P.N., Ruperto, N., Martini, A., Woo, P., Gattorno, M., for the Paediatric Rheumatology International Trials Organisation , t.E. & Project, t.E. 2013, 'The phenotype of TNF receptor-associated autoinflammatory syndrome (TRAPS) at presentation: a series of 158 cases from the Eurofever/EUROTRAPS international registry', *Annals of the Rheumatic Diseases*.

Laemmli, U.K. 1970, 'Cleavage of structural proteins during the assembly of the head of bacteriophage T4', *Nature*, vol. 227, no. 5259, pp. 680-5.

Lahaxe, L., Josse, S., Grateau, G., Levesque, H. & Marie, I. 2010, 'TRAPS: Clinical significance of genotype. A report of two cases', *La Revue de Médecine Interne*, vol. 31, no. 9, pp. 637-9.

Lainka, E., Neudorf, U., Lohse, P., Timmann, C., Stojanov, S., Huss, K., von Kries, R. & Niehues, T. 2009, 'Incidence of TNFRSF1A mutations in German children: epidemiological, clinical and genetic characteristics', *Rheumatology*, vol. 48, no. 8, pp. 987-91.

Lawrance, I.C., Radford-Smith, G.L., Bampton, P.A., Andrews, J.M., Tan, P.-K., Croft, A., Gearry, R.B. & Florin, T.H.J. 2010, 'Serious infections in patients with inflammatory bowel disease receiving anti-tumor-necrosis-factor-alpha therapy: An Australian and New Zealand experience', *Journal of Gastroenterology and Hepatology*, vol. 25, no. 11, pp. 1732-8.

Legler, D.F., Micheau, O., Doucey, M.-A., Tschopp, J. & Bron, C. 2003, 'Recruitment of TNF Receptor 1 to Lipid Rafts Is Essential for TNF[alpha]-Mediated NF-[kappa]B Activation', *Immunity*, vol. 18, no. 5, pp. 655-64.

Lesk, A.M. & Chothia, C. 1980, 'How different amino acid sequences determine similar protein structures: the structure and evolutionary dynamics of the globins', *J Mol Biol*, vol. 136, no. 3, pp. 225-70.

Lewis, A.K., Valley, C.C. & Sachs, J.N. 2012, 'TNFR1 Signaling Is Associated with Backbone Conformational Changes of Receptor Dimers Consistent with Overactivation in the R92Q TRAPS Mutant', *Biochemistry*, vol. 51, no. 33, pp. 6545-55.

Li, Y., Carroll, D.S., Gardner, S.N., Walsh, M.C., Vitalis, E.A. & Damon, I.K. 2007, 'On the origin of smallpox: correlating variola phylogenics with historical smallpox records', *Proc Natl Acad Sci U S A*, vol. 104, no. 40, pp. 15787-92.

Likos, A.M., Sammons, S.A., Olson, V.A., Frace, A.M., Li, Y., Olsen-Rasmussen, M., Davidson, W., Galloway, R., Khristova, M.L., Reynolds, M.G., Zhao, H., Carroll, D.S., Curns, A., Formenty, P., Esposito, J.J., Regnery, R.L. & Damon, I.K. 2005a, 'A tale of two clades: monkeypox viruses', *J Gen Virol*, vol. 86, no. Pt 10, pp. 2661-72.

Likos, A.M., Sammons, S.A., Olson, V.A., Frace, A.M., Li, Y., Olsen-Rasmussen, M., Davidson, W., Galloway, R., Khristova, M.L., Reynolds, M.G., Zhao, H., Carroll, D.S., Curns, A., Formenty, P., Esposito, J.J., Regnery, R.L. & Damon, I.K. 2005b, 'A tale of two clades: monkeypox viruses', *Journal of General Virology*, vol. 86, no. 10, pp. 2661-72.

Liszewski, M.K., Leung, M.K., Hauhart, R., Fang, C.J., Bertram, P. & Atkinson, J.P. 2009, 'Smallpox inhibitor of complement enzymes (SPICE): dissecting functional sites and abrogating activity', *J Immunol*, vol. 183, no. 5, pp. 3150-9.

Liu, Z.-g., Hsu, H., Goeddel, D.V. & Karin, M. 1996, 'Dissection of TNF Receptor 1 Effector Functions: JNK Activation Is Not Linked to Apoptosis While NF-[kappa]B Activation Prevents Cell Death', *Cell*, vol. 87, no. 3, pp. 565-76.

Lobito, A.A., Gabriel, T.L., Medema, J.P. & Kimberley, F.C. 2011, 'Disease causing mutations in the TNF and TNFR superfamilies: Focus on molecular mechanisms driving disease', *Trends in Molecular Medicine*, vol. 17, no. 9, pp. 494-505.

Lobito, A.A., Kimberley, F.C., Muppidi, J.R., Komarow, H., Jackson, A.J., Hull, K.M., Kastner, D.L., Screaton, G.R. & Siegel, R.M. 2006, 'Abnormal disulfide-linked oligomerization results in ER retention and altered signaling by TNFR1 mutants in TNFR1-associated periodic fever syndrome (TRAPS)', *Blood*, vol. 108, no. 4, pp. 1320-7.

Loetscher, H., Gentz, R., Zulauf, M., Lustig, A., Tabuchi, H., Schlaeger, E.J., Brockhaus, M., Gallati, H., Manneberg, M. & Lesslauer, W. 1991, 'Recombinant 55-kDa tumor necrosis factor (TNF) receptor. Stoichiometry of binding to TNF alpha and TNF beta and inhibition of TNF activity', *Journal of Biological Chemistry*, vol. 266, no. 27, pp. 18324-9.

Loetscher, H., Pan, Y.-C.E., Lahm, H.-W., Gentz, R., Brockhaus, M., Tabuchi, H. & Lesslauer, W. 1990, 'Molecular cloning and expression of the human 55 kd tumor necrosis factor receptor', *Cell*, vol. 61, no. 2, pp. 351-9.

Loetscher, H., Schlaeger, E.J., Lahm, H.W., Pan, Y.C., Lesslauer, W. & Brockhaus, M. 1990, 'Purification and partial amino acid sequence analysis of two distinct tumor necrosis factor receptors from HL60 cells', *Journal of Biological Chemistry*, vol. 265, no. 33, pp. 20131-8.

Lofquist, J.M., Weimert, N.A. & Hayney, M.S. 2003, 'Smallpox: a review of clinical disease and vaccination', *Am J Health Syst Pharm*, vol. 60, no. 8, pp. 749-56; quiz 57-8.

Loparev, V.N., Massung, R.F., Esposito, J.J. & Meyer, H. 2001, 'Detection and Differentiation of Old World Orthopoxviruses: Restriction Fragment Length Polymorphism of the CRM-B Gene Region', *J. Clin. Microbiol.*, vol. 39, no. 1, pp. 94-100.

Loparev, V.N., Parsons, J.M., Knight, J.C., Panus, J.F., Ray, C.A., Buller, R.M., Pickup, D.J. & Esposito, J.J. 1998, 'A third distinct tumor necrosis factor receptor of orthopoxviruses', *Proc Natl Acad Sci U S A*, vol. 95, no. 7, pp. 3786-91.

Lopez-Olivo, M.A., Tayar, J.H., Martinez-Lopez, J.A., Pollono, E.N., Cueto, J.P., Gonzales-Crespo, M.R., Fulton, S. & Suarez-Almazor, M.E. 2012, 'Risk of malignancies in

patients with rheumatoid arthritis treated with biologic therapy: a meta-analysis', *JAMA*, vol. 308, no. 9, pp. 898-908.
Lourie, B., Bingham, P.G., Evans, H.H., Foster, S.O., Nakano, J.H. & Herrmann, K.L. 1972, 'Human infection with monkeypox virus: laboratory investigation of six cases in West Africa', *Bull World Health Organ*, vol. 46, no. 5, pp. 633-9.
Lourie, B., Nakano, J.H., Kemp, G.E. & Setzer, H.W. 1975, 'Isolation of Poxvirus from an African Rodent', *Journal of Infectious Diseases*, vol. 132, no. 6, pp. 677-81.
Macaulay, C., Upton, C. & McFadden, G. 1987, 'Tumorigenic poxviruses: Transcriptional mapping of the terminal inverted repeats of shope fibroma virus', *Virology*, vol. 158, no. 2, pp. 381-93.
Macdonald, T.T., Hutchings, P., Choy, M.Y., Murch, S. & Cooke, A. 1990, 'Tumour necrosis factor-alpha and interferon-gamma production measured at the single cell level in normal and inflamed human intestine', *Clinical & Experimental Immunology*, vol. 81, no. 2, pp. 301-5.
MacEwan, D.J. 2002, 'TNF receptor subtype signalling: Differences and cellular consequences', *Cellular Signalling*, vol. 14, no. 6, pp. 477-92.
Maini, R., St Clair, E.W., Breedveld, F., Furst, D., Kalden, J., Weisman, M., Smolen, J., Emery, P., Harriman, G., Feldmann, M. & Lipsky, P. 1999, 'Infliximab (chimeric anti-tumour necrosis factor alpha monoclonal antibody) versus placebo in rheumatoid arthritis patients receiving concomitant methotrexate: a randomised phase III trial. ATTRACT Study Group', *Lancet*, vol. 354, no. 9194, pp. 1932-9.
Marennikova, S.S. 1979, 'Field and experimental studies of poxvirus infections in rodents', *Bull World Health Organ*, vol. 57, no. 3, pp. 461-4.
Marennikova, S.S., Shelukhina, E.M. & Efremova, E.V. 1984, 'New outlook on the biology of cowpox virus', *Acta Virol*, vol. 28, no. 5, pp. 437-44.
Marshall, I.D. & Fenner, F. 1960, 'Studies in the epidemiology of infectious myxomatosis of rabbits: VII. The virulence of strains of myxoma virus recovered from Australian wild rabbits between 1951 and 1959', *The Journal of Hygiene*, vol. 58, no. 4, pp. 485-8.
Marsters, S.A., Frutkin, A.D., Simpson, N.J., Fendly, B.M. & Ashkenazi, A. 1992, 'Identification of cysteine-rich domains of the type 1 tumor necrosis factor receptor involved in ligand binding', *Journal of Biological Chemistry*, vol. 267, no. 9, pp. 5747-50.
Marth, J.D. & Grewal, P.K. 2008, 'Mammalian glycosylation in immunity', *Nature reviews. Immunology*, vol. 8, no. 11, pp. 874-87.
Mascarenhas, N.M. & Kastner, J. 2012, 'Are different stoichiometries feasible for complexes between lymphotoxin-alpha and tumor necrosis factor receptor 1?', *BMC Struct Biol*, vol. 12, p. 8.
Masson, C., Simon, V., Hoppé, E., Insalaco, P., Cissé, I. & Audran, M. 2004, 'Tumor necrosis factor receptor-associated periodic syndrome (TRAPS): definition, semiology, prognosis, pathogenesis, treatment, and place relative to other periodic joint diseases', *Joint Bone Spine*, vol. 71, no. 4, pp. 284-90.
Massung, R.F., Esposito, J.J., Liu, L.I., Qi, J., Utterback, T.R., Knight, J.C., Aubin, L., Yuran, T.E., Parsons, J.M., Loparev, V.N. & et al. 1993, 'Potential virulence determinants in terminal regions of variola smallpox virus genome', *Nature*, vol. 366, no. 6457, pp. 748-51.
Massung, R.F., Liu, L.-I., Qi, J., Knight, J.C., Yuran, T.E., Kerlavage, A.R., Parsons, J.M., Venter, J.C. & Esposito, J.J. 1994, 'Analysis of the Complete Genome of

Smallpox Variola Major Virus Strain Bangladesh-1975', *Virology*, vol. 201, no. 2, pp. 215-40.
Masters, S.C. 2004, 'Co-immunoprecipitation from transfected cells', *Methods Mol Biol*, vol. 261, pp. 337-50.
Masters, S.L., Simon, A., Aksentijevich, I. & Kastner, D.L. 2009, 'Horror Autoinflammaticus: The Molecular Pathophysiology of Autoinflammatory Disease', *Annual review of immunology*, vol. 27, pp. 621-68.
Mathew, S.J., Haubert, D., Kronke, M. & Leptin, M. 2009, 'Looking beyond death: a morphogenetic role for the TNF signalling pathway', *J Cell Sci*, vol. 122, no. 12, pp. 1939-46.
Maury, C.P. & Teppo, A.M. 1989, 'Tumor necrosis factor in the serum of patients with systemic lupus erythematosus', *Arthritis Rheum*, vol. 32, no. 2, pp. 146-50.
McDermott, E.M., Smillie, D.M. & Powell, R.J. 1997, 'Clinical spectrum of familial Hibernian fever: A 14-year follow-up study of the index case and extended family', *Mayo Clinic Proceedings*, vol. 72, no. 9, p. 806.
McDermott, M.F., Aksentijevich, I., Galon, J., McDermott, E.M., Ogunkolade, B.W., Centola, M., Mansfield, E., Gadina, M., Karenko, L., Pettersson, T., McCarthy, J., Frucht, D.M., Aringer, M., Torosyan, Y., Teppo, A.-M., Wilson, M., Karaarslan, H.M., Wan, Y., Todd, I., Wood, G., Schlimgen, R., Kumarajeewa, T.R., Cooper, S.M., Vella, J.P., Amos, C.I., Mulley, J., Quane, K.A., Molloy, M.G., Ranki, A., Powell, R.J., Hitman, G.A., O'Shea, J.J. & Kastner, D.L. 1999, 'Germline Mutations in the Extracellular Domains of the 55 kDa TNF Receptor, TNFR1, Define a Family of Dominantly Inherited Autoinflammatory Syndromes', *Cell*, vol. 97, no. 1, pp. 133-44.
McDermott, M.F., Ogunkolade, B.W., McDermott, E.M., Jones, L.C., Wan, Y., Quane, K.A., McCarthy, J., Phelan, M., Molloy, M.G., Powell, R.J., Amos, C.I. & Hitman, G.A. 1998, 'Linkage of Familial Hibernian Fever to Chromosome 12p13', *The American Journal of Human Genetics*, vol. 62, no. 6, pp. 1446-51.
McFadden, G. 2005, 'Poxvirus tropism', *Nature Reviews Microbiology*, vol. 3, no. 3, pp. 201-13.
Melo, F., Sanchez, R. & Sali, A. 2002, 'Statistical potentials for fold assessment', *Protein Sci*, vol. 11, no. 2, pp. 430-48.
Menu, P., Mayor, A., Zhou, R., Tardivel, A., Ichijo, H., Mori, K. & Tschopp, J. 2012, 'ER stress activates the NLRP3 inflammasome via an UPR-independent pathway', *Cell Death & Disease*, vol. 3, no. 1, p. e261.
Meredith, A.L. 2013, 'Viral skin diseases of the rabbit', *Vet Clin North Am Exot Anim Pract*, vol. 16, no. 3, pp. 705-14.
Micheau, O. & Tschopp, J. 2003, 'Induction of TNF Receptor I-Mediated Apoptosis via Two Sequential Signaling Complexes', *Cell*, vol. 114, no. 2, pp. 181-90.
Miki, K. & Eddy, E.M. 2002, 'Tumor Necrosis Factor Receptor 1 Is an ATPase Regulated by Silencer of Death Domain', *Mol. Cell. Biol.*, vol. 22, no. 8, pp. 2536-43.
Miroux, B. & Walker, J.E. 1996, 'Over-production of proteins in Escherichia coli: mutant hosts that allow synthesis of some membrane proteins and globular proteins at high levels', *J Mol Biol*, vol. 260, no. 3, pp. 289-98.
Mitoma, H., Horiuchi, T., Hatta, N., Tsukamoto, H., Harashima, S., Kikuchi, Y., Otsuka, J., Okamura, S., Fujita, S. & Harada, M. 2005, 'Infliximab induces potent anti-inflammatory responses by outside-to-inside signals through transmembrane TNF-alpha', *Gastroenterology*, vol. 128, no. 2, pp. 376-92.

Morrison, T.E., Mauser, A., Klingelhutz, A. & Kenney, S.C. 2004, 'Epstein-Barr Virus Immediate-Early Protein BZLF1 Inhibits Tumor Necrosis Factor Alpha-Induced Signaling and Apoptosis by Downregulating Tumor Necrosis Factor Receptor 1', *Journal of Virology*, vol. 78, no. 1, pp. 544-9.

Mukai, Y., Nakamura, T., Yoshikawa, M., Yoshioka, Y., Tsunoda, S., Nakagawa, S., Yamagata, Y. & Tsutsumi, Y. 2010, 'Solution of the structure of the TNF-TNFR2 complex', *Sci Signal*, vol. 3, no. 148, p. ra83.

Mukai, Y., Shibata, H., Nakamura, T., Yoshioka, Y., Abe, Y., Nomura, T., Taniai, M., Ohta, T., Ikemizu, S., Nakagawa, S., Tsunoda, S., Kamada, H., Yamagata, Y. & Tsutsumi, Y. 2009, 'Structure-function relationship of tumor necrosis factor (TNF) and its receptor interaction based on 3D structural analysis of a fully active TNFR1-selective TNF mutant', *J Mol Biol*, vol. 385, no. 4, pp. 1221-9.

Müller, S.M., Galliardt, H., Schneider, J., Barisas, B.G. & Seidel, T. 2013, 'Quantification of Förster resonance energy transfer by monitoring sensitized emission in living plant cells', *Frontiers in Plant Science*, vol. 4, p. 413.

Murali, R., Cheng, X., Berezov, A., Du, X., Schön, A., Freire, E., Xu, X., Chen, Y.H. & Greene, M.I. 2005, 'Disabling TNF receptor signaling by induced conformational perturbation of tryptophan-107', *Proceedings of the National Academy of Sciences of the United States of America*, vol. 102, no. 31, pp. 10970-5.

Nagy, P., Vamosi, G., Bodnar, A., Lockett, S.J. & Szollosi, J. 1998, 'Intensity-based energy transfer measurements in digital imaging microscopy', *Eur Biophys J*, vol. 27, no. 4, pp. 377-89.

Naismith, J.H., Devine, T.Q., Kohno, T. & Sprang, S.R. 1996, 'Structures of the extracellular domain of the type I tumor necrosis factor receptor', *Structure*, vol. 4, no. 11, pp. 1251-62.

Naismith, J.H. & Sprang, S.R. 1998, 'Modularity in the TNF-receptor family', *Trends in Biochemical Sciences*, vol. 23, no. 2, pp. 74-9.

Nedjai, B., Hitman, G.A., Church, L.D., Minden, K., Whiteford, M.L., McKee, S., Stjernberg, S., Pettersson, T., Ranki, A., Hawkins, P.N., Arkwright, P.D., McDermott, M.F. & Turner, M.D. 2011, 'Differential cytokine secretion results from p65 and c-Rel NF-[kappa]B subunit signaling in peripheral blood mononuclear cells of TNF receptor-associated periodic syndrome patients', *Cellular Immunology*, vol. 268, no. 2, pp. 55-9.

Nedjai, B., Hitman, G.A., Quillinan, N., Coughlan, R.J., Church, L., McDermott, M.F. & Turner, M.D. 2009, 'Proinflammatory action of the antiinflammatory drug infliximab in tumor necrosis factor receptor–associated periodic syndrome', *Arthritis & Rheumatism*, vol. 60, no. 2, pp. 619-25.

Nedjai, B., Hitman, G.A., Yousaf, N., Chernajovsky, Y., Stjernberg-Salmela, S., Pettersson, T., Ranki, A., Hawkins, P.N., Arkwright, P.D., McDermott, M.F. & Turner, M.D. 2008, 'Abnormal tumor necrosis factor receptor I cell surface expression and NF-kappaB activation in tumor necrosis factor receptor-associated periodic syndrome', *Arthritis & Rheumatism*, vol. 58, no. 1, pp. 273-83.

Nedjai, B., Quillinan, N., Coughlan, R.J., Church, L., McDermott, M.F., Hitman, G.A. & Turner, M.D. 2011, 'Lessons from anti-TNF biologics: infliximab failure in a TRAPS family with the T50M mutation in TNFRSF1A', *Adv Exp Med Biol*, vol. 691, pp. 409-19.

Negrier, M.S., Pourreau, C.N., Palmer, P.A., Ranchere, J.Y., Mercatello, A., Viens, P., Blaise, D., Jasmin, C., Misset, J.L., Franks, C.R. & et al. 1992, 'Phase I trial of

recombinant interleukin-2 followed by recombinant tumor necrosis factor in patients with metastatic cancer', *J Immunother (1991)*, vol. 11, no. 2, pp. 93-102.

Nepomnyashchikh, T.S., Antonets, D.V., Lebedev, L.R., Gileva, I.P. & Shchelkunov, S.N. 2010, '3D structure modeling of complexes formed by CRM-B TNF-binding proteins of Variola and cowpox viruses with murine and human TNFs', *Molecular Biology*, vol. 44, no. 6, pp. 939-47.

Niforou, K.N., Anagnostopoulos, A.K., Vougas, K., Kittas, C., Gorgoulis, V.G. & Tsangaris, G.T. 2008, 'The Proteome Profile of the Human Osteosarcoma U2OS Cell Line', *Cancer Genomics - Proteomics*, vol. 5, no. 1, pp. 63-77.

Nowlan, M.L., Drewe, E., Bulsara, H., Esposito, N., Robins, R.A., Tighe, P.J., Powell, R.J. & Todd, I. 2006, 'Systemic cytokine levels and the effects of etanercept in TNF receptor-associated periodic syndrome (TRAPS) involving a C33Y mutation in TNFRSF1A', *Rheumatology (Oxford)*, vol. 45, no. 1, pp. 31-7.

Offerman, K., Carulei, O., van der Walt, A.P., Douglass, N. & Williamson, A.-L. 2014, 'The complete genome sequences of poxviruses isolated from a penguin and a pigeon in South Africa and comparison to other sequenced avipoxviruses', *BMC Genomics*, vol. 15, pp. 463-.

Oie, K.L. & Pickup, D.J. 2001, 'Cowpox Virus and Other Members of the Orthopoxvirus Genus Interfere with the Regulation of NF-κB Activation', *Virology*, vol. 288, no. 1, pp. 175-87.

Pahl, H.L. & Baeuerle, P.A. 1997, 'The ER-overload response: activation of NF-[kappa]B', *Trends in Biochemical Sciences*, vol. 22, no. 2, pp. 63-7.

Pahl, H.L., Sester, M., Burgert, H.G. & Baeuerle, P.A. 1996, 'Activation of transcription factor NF-kappaB by the adenovirus E3/19K protein requires its ER retention', *The Journal of Cell Biology*, vol. 132, no. 4, pp. 511-22.

Parker, S. & Buller, R.M. 2013, 'A review of experimental and natural infections of animals with monkeypox virus between 1958 and 2012', *Future Virol*, vol. 8, no. 2, pp. 129-57.

Parker, S., Nuara, A., Buller, R.M. & Schultz, D.A. 2007, 'Human monkeypox: an emerging zoonotic disease', *Future Microbiol*, vol. 2, no. 1, pp. 17-34.

PARODI, A.J. 2000, 'Role of N-oligosaccharide endoplasmic reticulum processing reactions in glycoprotein folding and degradation', *Biochemical Journal*, vol. 348, no. 1, pp. 1-13.

Pfeffer, K. 2003, 'Biological functions of tumor necrosis factor cytokines and their receptors', *Cytokine & Growth Factor Reviews*, vol. 14, no. 3-4, pp. 185-91.

Poddubnyy, D. & Rudwaleit, M. 2011, 'Efficacy and safety of adalimumab treatment in patients with rheumatoid arthritis, ankylosing spondylitis and psoriatic arthritis', *Expert Opin Drug Saf*, vol. 10, no. 4, pp. 655-73.

Ponten, J. & Saksela, E. 1967, 'Two established in vitro cell lines from human mesenchymal tumours', *Int J Cancer*, vol. 2, no. 5, pp. 434-47.

Quillinan, N., Mohammad, A., Mannion, G., O'Keeffe, D., Bergin, D., Coughlan, R., McDermott, M.F. & McGonagle, D. 2010, 'Imaging evidence for persistent subclinical fasciitis and arthritis in tumour necrosis factor receptor-associated periodic syndrome (TRAPS) between febrile attacks', *Annals of the Rheumatic Diseases*, vol. 69, no. 7, pp. 1408-9.

Rahman, M.M., Barrett, J.W., Brouckaert, P. & McFadden, G. 2006, 'Variation in ligand binding specificities of a novel class of poxvirus-encoded tumor necrosis factor-binding protein', *J Biol Chem*, vol. 281, no. 32, pp. 22517-26.

Rahman, M.M., Lucas, A.R. & McFadden, G. 2009a, 'Viral TNF inhibitors as potential therapeutics', *Adv Exp Med Biol*, vol. 666, pp. 64-77.
Rahman, M.M., Lucas, A.R. & McFadden, G. 2009b, 'Viral TNF Inhibitors as Potential Therapeutics

Pathogen-Derived Immunomodulatory Molecules', in P.G. Fallon (ed.)vol. 666, Springer New York, pp. 64-77.
Raicu, V. & Singh, D.R. 2013, 'FRET spectrometry: a new tool for the determination of protein quaternary structure in living cells', *Biophys J*, vol. 105, no. 9, pp. 1937-45.
Raitano, A.B., Scuderi, P. & Korc, M. 1991, 'Upregulation of interferon-gamma binding by tumor necrosis factor and lymphotoxin: disparate potencies of the cytokines and modulation of their effects by phorbol ester', *J Interferon Res*, vol. 11, no. 1, pp. 61-7.
Ranzinger, J., Krippner-Heidenreich, A., Haraszti, T., Bock, E., Tepperink, J., Spatz, J.P. & Scheurich, P. 2009, 'Nanoscale arrangement of apoptotic ligands reveals a demand for a minimal lateral distance for efficient death receptor activation', *Nano Lett*, vol. 9, no. 12, pp. 4240-5.
Rath, P.C. & Aggarwal, B.B. 1999, 'TNF-induced signaling in apoptosis', *J Clin Immunol*, vol. 19, no. 6, pp. 350-64.
Rauert, H., Wicovsky, A., Müller, N., Siegmund, D., Spindler, V., Waschke, J., Kneitz, C. & Wajant, H. 2010, 'Membrane Tumor Necrosis Factor (TNF) Induces p100 Processing via TNF Receptor-2 (TNFR2)', *Journal of Biological Chemistry*, vol. 285, no. 10, pp. 7394-404.
Ravet, N., Rouaghe, S., Dodé, C., Bienvenu, J., Stirnemann, J., Lévy, P., Delpech, M. & Grateau, G. 2006, 'Clinical significance of P46L and R92Q substitutions in the tumour necrosis factor superfamily 1A gene', *Annals of the Rheumatic Diseases*, vol. 65, no. 9, pp. 1158-62.
Reading, P.C., Khanna, A. & Smith, G.L. 2002, 'Vaccinia virus CRM-E encodes a soluble and cell surface tumor necrosis factor receptor that contributes to virus virulence', *Virology*, vol. 292, no. 2, pp. 285-98.
Rebelo, S.L., Bainbridge, S.E., Amel-Kashipaz, M.R., Radford, P.M., Powell, R.J., Todd, I. & Tighe, P.J. 2006, 'Modeling of tumor necrosis factor receptor superfamily 1A mutants associated with tumor necrosis factor receptor-associated periodic syndrome indicates misfolding consistent with abnormal function', *Arthritis & Rheumatism*, vol. 54, no. 8, pp. 2674-87.
Reimund, J.M., Wittersheim, C., Dumont, S., Muller, C.D., Baumann, R., Poindron, P. & Duclos, B. 1996, 'Mucosal inflammatory cytokine production by intestinal biopsies in patients with ulcerative colitis and Crohn's disease', *Journal of Clinical Immunology*, vol. 16, no. 3, pp. 144-50.
Ribas, E. 1911, 'Alastrim, amaas, or milk-pox', *Transactions of The Royal Society of Tropical Medicine and Hygiene*, vol. 4, no. 8, pp. 224-32.
Riccardi, C. & Nicoletti, I. 2006, 'Analysis of apoptosis by propidium iodide staining and flow cytometry', *Nat Protoc*, vol. 1, no. 3, pp. 1458-61.
Rivers, T.M. 1930, 'INFECTIOUS MYXOMATOSIS OF RABBITS : OBSERVATIONS ON THE PATHOLOGICAL CHANGES INDUCED BY VIRUS MYXOMATOSUM (SANARELLI)', *The Journal of Experimental Medicine*, vol. 51, no. 6, pp. 965-76.
Rodríguez, M., Cabal-Hierro, L., Carcedo, M.T., Iglesias, J.M., Artime, N., Darnay, B.G. & Lazo, P.S. 2011, 'NF-κB Signal Triggering and Termination by Tumor Necrosis

Factor Receptor 2', *Journal of Biological Chemistry*, vol. 286, no. 26, pp. 22814-24.
Rose, J. & Eisenmenger, F. 1991, 'A fast unbiased comparison of protein structures by means of the Needleman-Wunsch algorithm', *J Mol Evol*, vol. 32, no. 4, pp. 340-54.
Rosell, F.I. & Boxer, S.G. 2003, 'Polarized absorption spectra of green fluorescent protein single crystals: transition dipole moment directions', *Biochemistry*, vol. 42, no. 1, pp. 177-83.
Rösen-Wolff, A., Kreth, H.-W., Hofmann, S., Höhne, K., Heubner, G., Möbius, D., Zintl, F., Gahr, M. & Roesler, J. 2001, 'Periodic fever (TRAPS) caused by mutations in the TNF alpha; receptor 1 (TNFRSF1A) gene of three German patients', *European Journal Of Haematology*, vol. 67, no. 2, pp. 105-9.
Ross, J.J. 2007, 'Goats, germs, and fever: Are the pyrin mutations responsible for familial Mediterranean fever protective against Brucellosis?', *Medical Hypotheses*, vol. 68, no. 3, pp. 499-501.
Rothe, M., Sarma, V., Dixit, V. & Goeddel, D. 1995, 'TRAF2-mediated activation of NF-kappa B by TNF receptor 2 and CD40', *Science*, vol. 269, no. 5229, pp. 1424-7.
Rothe, M., Wong, S.C., Henzel, W.J. & Goeddel, D.V. 1994, 'A novel family of putative signal transducers associated with the cytoplasmic domain of the 75 kDa tumor necrosis factor receptor', *Cell*, vol. 78, no. 4, pp. 681-92.
Ruffer, M.A. & Ferguson, A.R. 1911, 'Note on an eruption resembling that of variola in the skin of a mummy of the twentieth dynasty (1200–1100 B.C.)', *The Journal of Pathology and Bacteriology*, vol. 15, no. 1, pp. 1-3.
Rydén, M., Arvidsson, E., Blomqvist, L., Perbeck, L., Dicker, A. & Arner, P. 2004, 'Targets for TNF-[alpha]-induced lipolysis in human adipocytes', *Biochemical and Biophysical Research Communications*, vol. 318, no. 1, pp. 168-75.
Saida, F., Uzan, M., Odaert, B. & Bontems, F. 2006, 'Expression of Highly Toxic Genes in E. coli: Special Strategies and Genetic Tools', *Current Protein & Peptide Science*, vol. 7, no. 1, pp. 47-56.
Sali, A. & Blundell, T.L. 1993, 'Comparative protein modelling by satisfaction of spatial restraints', *J Mol Biol*, vol. 234, no. 3, pp. 779-815.
Salvana, E.M.T. & Salata, R.A. 2009, 'Infectious Complications Associated with Monoclonal Antibodies and Related Small Molecules', *Clinical Microbiology Reviews*, vol. 22, no. 2, pp. 274-90.
Salvesen, G.S. & Dixit, V.M. 1999, 'Caspase activation: The induced-proximity model', *Proceedings of the National Academy of Sciences*, vol. 96, no. 20, pp. 10964-7.
Saraiva, M. & Alcami, A. 2001, 'CRM-E, a Novel Soluble Tumor Necrosis Factor Receptor Encoded by Poxviruses', *J. Virol.*, vol. 75, no. 1, pp. 226-33.
Sarrauste de Menthia re, C., Terria re, S., Pugna re, D., Ruiz, M., Demaille, J. & Touitou, I. 2003, 'INFEVERS: the Registry for FMF and hereditary inflammatory disorders mutations', *Nucleic Acids Research*, vol. 31, no. 1, pp. 282-5.
Scallon, B., Cai, A., Solowski, N., Rosenberg, A., Song, X.-Y., Shealy, D. & Wagner, C. 2002, 'Binding and Functional Comparisons of Two Types of Tumor Necrosis Factor Antagonists', *Journal of Pharmacology and Experimental Therapeutics*, vol. 301, no. 2, pp. 418-26.
Scallon, B.J., Moore, M.A., Trinh, H., Knight, D.M. & Ghrayeb, J. 1995, 'Chimeric anti-TNF-alpha monoclonal antibody cA2 binds recombinant transmembrane TNF-alpha and activates immune effector functions', *Cytokine*, vol. 7, no. 3, pp. 251-9.

Schall, T.J., Lewis, M., Koller, K.J., Lee, A., Rice, G.C., Wong, G.H.W., Gatanaga, T., Granger, G.A., Lentz, R., Raab, H., Kohr, W.J. & Goeddel, D.V. 1990, 'Molecular cloning and expression of a receptor for human tumor necrosis factor', *Cell*, vol. 61, no. 2, pp. 361-70.

Schneider-Brachert, W., Tchikov, V., Neumeyer, J., Jakob, M., Winoto-Morbach, S., Held-Feindt, J., Heinrich, M., Merkel, O., Ehrenschwander, M., Adam, D., Mentlein, R., Kabelitz, D. & Schutze, S. 2004, 'Compartmentalization of TNF receptor 1 signaling: Internalized TNF receptosomes as death signaling vesicles', *Immunity*, vol. 21, no. 3, pp. 415-28.

Schreiber, M. & McFadden, G. 1994, 'The Myxoma Virus TNF-Receptor Homologue (T2) Inhibits Tumor Necrosis Factor-α in a Species-Specific Fashion', *Virology*, vol. 204, no. 2, pp. 692-705.

Schreiber, M. & McFadden, G. 1996, 'Mutational analysis of the ligand-binding domain of MYXT2 protein, the tumor necrosis factor receptor homologue of myxoma virus', *Journal of Immunology*, vol. 157, no. 10, pp. 4486-95.

Schreiber, M., Rajarathnam, K. & McFadden, G. 1996, 'Myxoma Virus T2 Protein, a Tumor Necrosis Factor (TNF) Receptor Homolog, Is Secreted as a Monomer and Dimer That Each Bind Rabbit TNFα, but the Dimer Is a More Potent TNF Inhibitor', *Journal of Biological Chemistry*, vol. 271, no. 23, pp. 13333-41.

Schreiber, M., Sedger, L. & McFadden, G. 1997, 'Distinct domains of MYXT2, the myxoma virus tumor necrosis factor (TNF) receptor homolog, mediate extracellular TNF binding and intracellular apoptosis inhibition', *J Virol*, vol. 71, no. 3, pp. 2171-81.

Schreiber, S., Rutgeerts, P., Fedorak, R.N., Khaliq-Kareemi, M., Kamm, M.A., Boivin, M., Bernstein, C.N., Staun, M., Thomsen, O.O. & Innes, A. 2005, 'A randomized, placebo-controlled trial of certolizumab pegol (CDP870) for treatment of Crohn's disease', *Gastroenterology*, vol. 129, no. 3, pp. 807-18.

Schutze, S., Tchikov, V. & Schneider-Brachert, W. 2008, 'Regulation of TNFR1 and CD95 signalling by receptor compartmentalization', *Nat Rev Mol Cell Biol*, vol. 9, no. 8, pp. 655-62.

Schwarz, M., Taubitz, A., Eltrich, N., Mulay, S.R., Allam, R. & Vielhauer, V. 2013, 'Analysis of TNF-mediated recruitment and activation of glomerular dendritic cells in mouse kidneys by compartment-specific flow cytometry', *Kidney Int*, vol. 84, no. 1, pp. 116-29.

Sedger, L. 2005, 'Viral Inhibition of Tumour Necrosis Factor α (TNFα) and TNF-Receptor Induced Apoptosis and Inflammation', *Curr. Med. Chem. – Anti-Inflammatory & Anti-Allergy Agents*, vol. 4, pp. 597-615.

Sedger, L.M. & McDermott, M.F. 2014, 'TNF and TNF-receptors: From mediators of cell death and inflammation to therapeutic giants – past, present and future', *Cytokine & Growth Factor Reviews*, vol. 25, no. 4, pp. 453-72.

Sedger, L.M., Osvath, S.R., Xu, X.-M., Li, G., Chan, F.K.M., Barrett, J.W. & McFadden, G. 2006, 'Poxvirus Tumor Necrosis Factor Receptor (TNFR)-Like T2 Proteins Contain a Conserved Preligand Assembly Domain That Inhibits Cellular TNFR1-Induced Cell Death', *J. Virol.*, vol. 80, no. 18, pp. 9300-9.

Sekar, R.B. & Periasamy, A. 2003, 'Fluorescence resonance energy transfer (FRET) microscopy imaging of live cell protein localizations', *The Journal of Cell Biology*, vol. 160, no. 5, pp. 629-33.

Selmaj, K., Raine, C.S., Cannella, B. & Brosnan, C.F. 1991, 'Identification of lymphotoxin and tumor necrosis factor in multiple sclerosis lesions', *J Clin Invest*, vol. 87, no. 3, pp. 949-54.

Shambharkar, P.B., Blonska, M., Pappu, B.P., Li, H., You, Y., Sakurai, H., Darnay, B.G., Hara, H., Penninger, J. & Lin, X. 2007, 'Phosphorylation and ubiquitination of the IkappaB kinase complex by two distinct signaling pathways', *The EMBO journal*, vol. 26, no. 7, pp. 1794-805.

Shchelkunov, S.N. 2003, 'Immunomodulatory Proteins of Orthopoxviruses', *Molecular Biology*, vol. 37, no. 1, pp. 37-48.

Shchelkunov, S.N. 2011, 'Emergence and reemergence of smallpox: The need for development of a new generation smallpox vaccine', *Vaccine*, vol. 29, Supplement 4, no. 0, pp. D49-D53.

Shchelkunov, S.N., Blinov, V.M. & Sandakhchiev, L.S. 1993, 'Genes of variola and vaccinia viruses necessary to overcome the host protective mechanisms', *FEBS Letters*, vol. 319, no. 1–2, pp. 80-3.

Shchelkunov, S.N., Marennikova, S.S. & Moyer, R.W. 2006, *Orthopoxviruses Pathogenic for Humans*, Springer.

Shchelkunov, S.N., Totmenin, A.V., Babkin, I.V., Safronov, P.F., Ryazankina, O.I., Petrov, N.A., Gutorov, V.V., Uvarova, E.A., Mikheev, M.V., Sisler, J.R., Esposito, J.J., Jahrling, P.B., Moss, B. & Sandakhchiev, L.S. 2001, 'Human monkeypox and smallpox viruses: genomic comparison', *FEBS Letters*, vol. 509, no. 1, pp. 66-70.

Shen, M.Y. & Sali, A. 2006, 'Statistical potential for assessment and prediction of protein structures', *Protein Sci*, vol. 15, no. 11, pp. 2507-24.

Shih, V.F.-S., Tsui, R., Caldwell, A. & Hoffmann, A. 2011, 'A single NF[kappa]B system for both canonical and non-canonical signaling', *Cell Res*, vol. 21, no. 1, pp. 86-102.

Shinawi, M., Brik, R., Berant, M., Kasinetz, L. & Gershoni-Baruch, R. 2000, 'Familial Mediterranean fever: high gene frequency and heterogeneous disease among an Israeli-Arab population', *J Rheumatol*, vol. 27, no. 6, pp. 1492-5.

Siebert, S., Amos, N., Fielding, C.A., Wang, E.C.Y., Aksentijevich, I., Williams, B.D. & Brennan, P. 2005, 'Reduced tumor necrosis factor signaling in primary human fibroblasts containing a tumor necrosis factor receptor superfamily 1A mutant', *Arthritis & Rheumatism*, vol. 52, no. 4, pp. 1287-92.

Siebert, S., Fielding, C.A., Williams, B.D. & Brennan, P. 2005, 'Mutation of the extracellular domain of tumour necrosis factor receptor 1 causes reduced NF-[kappa]B activation due to decreased surface expression', *FEBS Letters*, vol. 579, no. 23, pp. 5193-8.

Siegel, R.M., Frederiksen, J.K., Zacharias, D.A., Chan, F.K.-M., Johnson, M., Lynch, D., Tsien, R.Y. & Lenardo, M.J. 2000, 'Fas Preassociation Required for Apoptosis Signaling and Dominant Inhibition by Pathogenic Mutations', *Science*, vol. 288, no. 5475, pp. 2354-7.

Sievers, F., Wilm, A., Dineen, D., Gibson, T.J., Karplus, K., Li, W., Lopez, R., McWilliam, H., Remmert, M., Soding, J., Thompson, J.D. & Higgins, D.G. 2011, 'Fast, scalable generation of high-quality protein multiple sequence alignments using Clustal Omega', *Mol Syst Biol*, vol. 7, p. 539.

Silva, J., Dasgupta, S., Wang, G., Krishnamurthy, K., Ritter, E. & Bieberich, E. 2006, 'Lipids isolated from bone induce the migration of human breast cancer cells', *J Lipid Res*, vol. 47, no. 4, pp. 724-33.

Simon, A., Park, H., Maddipati, R., Lobito, A.A., Bulua, A.C., Jackson, A.J., Chae, J.J., Ettinger, R., de Koning, H.D., Cruz, A.C., Kastner, D.L., Komarow, H. & Siegel, R.M. 2010, 'Concerted action of wild-type and mutant TNF receptors enhances inflammation in TNF receptor 1-associated periodic fever syndrome', *Proceedings of the National Academy of Sciences of the United States of America*, vol. 107, no. 21, pp. 9801-6.

Singh, S., Kumar, N., Loftus, E.V., Jr. & Kane, S.V. 2013, 'Neurologic complications in patients with inflammatory bowel disease: increasing relevance in the era of biologics', *Inflamm Bowel Dis*, vol. 19, no. 4, pp. 864-72.

Smith, C.A., Davis, T., Anderson, D.M., Solam, L., Beckmann, M.P., Jerzy, R., Dower, S.K., Cosman, D. & Goodwin, R.G. 1990, 'A Receptor of Tumour Necrosis Factor Defines an Unusual Family of Cellular and Viral Proteins', *Science*, vol. 248, no. 4958, pp. 1019-24.

Smith, C.A., Davis, T., Wignall, J.M., Din, W.S., Farrah, T., Upton, C., McFadden, G. & Goodwin, R.G. 1991a, 'T2 open reading frame from the Shope fibroma virus encodes a soluble form of the TNF receptor', *Biochem Biophys Res Commun*, vol. 176, no. 1, pp. 335-42.

Smith, C.A., Davis, T., Wignall, J.M., Din, W.S., Farrah, T., Upton, C., McFadden, G. & Goodwin, R.G. 1991b, 'T2 open reading frame from the shope fibroma virus encodes a soluble form of the TNF receptor', *Biochemical and Biophysical Research Communications*, vol. 176, no. 1, pp. 335-42.

Smith, C.A., Hu, F.-Q., Smith, T.D., Richards, C.L., Smolak, P., Goodwin, R.G. & Pickup, D.J. 1996a, 'Cowpox Virus Genome Encodes a Second Soluble Homologue of Cellular TNF Receptors, Distinct from CRM-B, That Binds TNF but Not LTα', *Virology*, vol. 223, no. 1, pp. 132-47.

Smith, C.A., Hu, F.Q., Smith, T.D., Richards, C.L., Smolak, P., Goodwin, R.G. & Pickup, D.J. 1996b, 'Cowpox virus genome encodes a second soluble homologue of cellular TNF receptors, distinct from CRM-B, that binds TNF but not LT alpha', *Virology*, vol. 223, no. 1, pp. 132-47.

Smyth, M.S. & Martin, J.H.J. 2000, 'X-Ray crystallography', *Molecular Pathology*, vol. 53, no. 1, pp. 8-14.

Snapp, E. 2005, 'Design and Use of Fluorescent Fusion Proteins in Cell Biology', *Current protocols in cell biology / editorial board, Juan S. Bonifacino ... [et al.]*, vol. CHAPTER, pp. Unit-21.4.

Storey, H., Stewart, A., Vandenabeele, P. & Luzio, J.P. 2002, 'The p55 tumour necrosis factor receptor TNFR1 contains a trans-Golgi network localization signal in the C-terminal region of its cytoplasmic tail', *Biochem. J.*, vol. 366, no. 1, pp. 15-22.

Strieter, R.M., Kunkel, S.L. & Bone, R.C. 1993, 'Role of tumour necrosis factor alpha in disease states and inflammation', *Critical Care Medicine*, vol. 21, no. 10, pp. S447-S63.

Sukits, S.F., Lin, L.-L., Hsu, S., Malakian, K., Powers, R. & Xu, G.-Y. 2001, 'Solution structure of the tumor necrosis factor receptor-1 death domain1', *Journal of Molecular Biology*, vol. 310, no. 4, pp. 895-906.

Sun, S.-C. & Ley, S.C. 2008, 'New insights into NF-[kappa]B regulation and function', *Trends in Immunology*, vol. 29, no. 10, pp. 469-78.

Takada, H., Chen, N.-J., Mirtsos, C., Suzuki, S., Suzuki, N., Wakeham, A., Mak, T.W. & Yeh, W.-C. 2003, 'Role of SODD in Regulation of Tumor Necrosis Factor Responses', *Molecular and Cellular Biology*, vol. 23, no. 11, pp. 4026-33.

Tang, E.D., Wang, C.-Y., Xiong, Y. & Guan, K.-L. 2003, 'A Role for NFκB Essential Modifier/IκB Kinase-γ (NEMO/IKKγ) Ubiquitination in the Activation of the IκB Kinase Complex by Tumor Necrosis Factor-α', *Journal of Biological Chemistry*, vol. 278, no. 39, pp. 37297-305.

Tang, P., Hung, M.C. & Klostergaard, J. 1996, 'Human pro-tumor necrosis factor is a homotrimer', *Biochemistry*, vol. 35, no. 25, pp. 8216-25.

Tartaglia, L., Goeddel, D., Reynolds, C., Figari, I., Weber, R., Fendly, B. & Palladino, M. 1993, 'Stimulation of human T-cell proliferation by specific activation of the 75-kDa tumor necrosis factor receptor', *The Journal of Immunology*, vol. 151, no. 9, pp. 4637-41.

Tchernitchko, D., Goossens, M. & Wajcman, H. 2004, 'In Silico Prediction of the Deleterious Effect of a Mutation: Proceed with Caution in Clinical Genetics', *Clinical Chemistry*, vol. 50, no. 11, pp. 1974-8.

Terasaki, M., Henson, J., Begg, D., Kaminer, B. & Sardet, C. 1991, 'Characterization of sea urchin egg endoplasmic reticulum in cortical preparations', *Developmental Biology*, vol. 148, no. 1, pp. 398-401.

Terasaki, M., Song, J., Wong, J.R., Weiss, M.J. & Chen, L.B. 1984, 'Localization of endoplasmic reticulum in living and glutaraldehyde-fixed cells with fluorescent dyes', *Cell*, vol. 38, no. 1, pp. 101-8.

Tewari, M., Telford, W.G., Miller, R.A. & Dixit, V.M. 1995, 'CRM-A, a Poxvirus-encoded Serpin, Inhibits Cytotoxic T-lymphocyte-mediated Apoptosis', *Journal of Biological Chemistry*, vol. 270, no. 39, pp. 22705-8.

Todd, I., Radford, P.M., Daffa, N., Bainbridge, S.E., Powell, R.J. & Tighe, P.J. 2007, 'Mutant tumor necrosis factor receptor associated with tumor necrosis factor receptor-associated periodic syndrome is altered antigenically and is retained within patients' leukocytes', *Arthritis & Rheumatism*, vol. 56, no. 8, pp. 2765-73.

Todd, I., Radford, P.M., Draper-Morgan, K.-A., McIntosh, R., Bainbridge, S., Dickinson, P., Jamhawi, L., Sansaridis, M., Huggins, M.L., Tighe, P.J. & Powell, R.J. 2004, 'Mutant forms of tumour necrosis factor receptor I that occur in TNF-receptor-associated periodic syndrome retain signalling functions but show abnormal behaviour', *Immunology*, vol. 113, no. 1, pp. 65-79.

Todd, I., Radford, P.M., Ziegler-Heitbrock, L., Ghaemmaghami, A.M., Powell, R.J. & Tighe, P.J. 2007, 'Elevated CD16 expression by monocytes from patients with tumor necrosis factor receptor-associated periodic syndrome', *Arthritis & Rheumatism*, vol. 56, no. 12, pp. 4182-8.

Todd, I., Tighe, P.J. & Powell, R.J. 2005, 'TNF and TNF Receptors in TRAPS', *Current Medicinal Chemistry - Anti-Inflammatory & Anti-Allergy Agents*, vol. 4, no. 6, pp. 577-85.

Toussirot, E. & Bereau, M. 2014, 'The risk of progressive multifocal leukoencephalopathy under biological agents used in the treatment of chronic inflammatory diseases', *Inflamm Allergy Drug Targets*, vol. 13, no. 2, pp. 121-7.

Tresch, S., Trüeb, R.M., Kamarachev, J., French, L.E. & Hofbauer, G.F.L. 2009, 'Disseminated Herpes Zoster Mimicking Rheumatoid Vasculitis in a Rheumatoid Arthritis Patient on Etanercept', *Dermatology*, vol. 219, no. 4, pp. 347-9.

Trón, L., Szöllősi, J., Damjanovich, S., Helliwell, S.H., Arndt-Jovin, D.J. & Jovin, T.M. 1984, 'Flow cytometric measurement of fluorescence resonance energy transfer on cell surfaces. Quantitative evaluation of the transfer efficiency on a cell-by-cell basis', *Biophysical Journal*, vol. 45, no. 5, pp. 939-46.

Tsimberidou, A.-M., Waddelow, T., Kantarjian, H.M., Albitar, M. & Giles, F.J. 2003, 'Pilot study of recombinant human soluble tumor necrosis factor (TNF) receptor (p75) fusion protein (TNFR:Fc; Enbrel) in patients with refractory multiple myeloma: increase in plasma TNFα levels during treatment', *Leukemia Research*, vol. 27, no. 5, pp. 375-80.

Tulman, E.R., Afonso, C.L., Lu, Z., Zsak, L., Kutish, G.F. & Rock, D.L. 2004, 'The Genome of Canarypox Virus', *Journal of Virology*, vol. 78, no. 1, pp. 353-66.

Turner, M.D., Chaudhry, A. & Nedjai, B. 2012, 'Tumour necrosis factor receptor trafficking dysfunction opens the TRAPS door to pro-inflammatory cytokine secretion', *Biosci Rep*, vol. 32, no. 2, pp. 105-12.

Upton, C., DeLange, A.M. & McFadden, G. 1987, 'Tumorigenic poxviruses: Genomic organization and dna sequence of the telomeric region of the shope fibroma virus genome', *Virology*, vol. 160, no. 1, pp. 20-30.

Upton, C., Macen, J.L., Schreiber, M. & McFaddeni, G. 1991, 'Myxoma virus expresses a secreted protein with homology to the tumor necrosis factor receptor gene family that contributes to viral virulence', *Virology*, vol. 184, no. 1, pp. 370-82.

Vaday, G.G., Hershkoviz, R., Rahat, M.A., Lahat, N., Cahalon, L. & Lider, O. 2000, 'Fibronectin-bound TNF-{alpha} stimulates monocyte matrix metalloproteinase-9 expression and regulates chemotaxis', *J Leukoc Biol*, vol. 68, no. 5, pp. 737-47.

van Aken, J. & Hammond, E. 2003, 'Genetic engineering and biological weapons', *EMBO Rep*, vol. 4, no. Supp1, pp. S57-S60.

van Schouwenburg, P.A., Rispens, T. & Wolbink, G.J. 2013a, 'Immunogenicity of anti-TNF biologic therapies for rheumatoid arthritis', *Nat Rev Rheumatol*, vol. 9, no. 3, pp. 164-72.

van Schouwenburg, P.A., Rispens, T. & Wolbink, G.J. 2013b, 'Immunogenicity of anti-TNF biologic therapies for rheumatoid arthritis', *Nat Rev Rheumatol*, vol. 9, no. 3, pp. 164-72.

Wang, J., Al-Lamki, R.S., Zhang, H., Kirkiles-Smith, N., Gaeta, M.L., Thiru, S., Pober, J.S. & Bradley, J.R. 2003, 'Histamine Antagonizes Tumor Necrosis Factor (TNF) Signaling by Stimulating TNF Receptor Shedding from the Cell Surface and Golgi Storage Pool', *Journal of Biological Chemistry*, vol. 278, no. 24, pp. 21751-60.

Wang, T., Ma, X., Du, G. & Chen, J. 2012, 'Overview of regulatory strategies and molecular elements in metabolic engineering of bacteria', *Mol Biotechnol*, vol. 52, no. 3, pp. 300-8.

Warzocha, K. 1998, 'The Tumor Necrosis Factor Signaling Complex: Choosing a Path Toward Cell Death or Cell', *Leukemia & Lymphoma*, vol. 29, no. 1/2, p. 81.

Weaver, J.R. & Isaacs, S.N. 2008, 'Monkeypox virus and insights into its immunomodulatory proteins', *Immunological Reviews*, vol. 225, no. 1, pp. 96-113.

Weinblatt, M.E., Keystone, E.C., Furst, D.E., Moreland, L.W., Weisman, M.H., Birbara, C.A., Teoh, L.A., Fischkoff, S.A. & Chartash, E.K. 2003, 'Adalimumab, a fully human anti-tumor necrosis factor alpha monoclonal antibody, for the treatment of rheumatoid arthritis in patients taking concomitant methotrexate: the ARMADA trial', *Arthritis Rheum*, vol. 48, no. 1, pp. 35-45.

Whitehead, R.P., Fleming, T., Macdonald, J.S., Goodman, P.J., Neefe, J., Braun, T.J., Swinnen, L.J. & Hersh, E.M. 1990, 'A phase II trial of recombinant tumor necrosis factor in patients with metastatic colorectal adenocarcinoma: a Southwest Oncology Group study', *J Biol Response Mod*, vol. 9, no. 6, pp. 588-91.

Wilkinson, G.W.G. & Akrigg, A. 1992, 'Constitutive and enhanced expression from the CMV major IE promoter in a defective adenovirus vector', *Nucleic Acids Research*, vol. 20, no. 9, pp. 2233-9.

Williams, R.O., Feldmann, M. & Maini, R.N. 1992, 'Anti-tumor necrosis factor ameliorates joint disease in murine collagen-induced arthritis', *Proceedings of the National Academy of Sciences of the United States of America*, vol. 89, no. 20, pp. 9784-8.

Williams, R.O., Ghrayeb, J., Feldmann, M. & Maini, R.N. 1995, 'Successful therapy of collagen-induced arthritis with TNF receptor-IgG fusion protein and combination with anti-CD4', *Immunology*, vol. 84, no. 3, pp. 433-9.

Williamson, L.M., Hull, D., Mehta, R., Reeves, W.G., Robinson, B.H.B. & Toghill, P.J. 1982, 'Familial Hibernian Fever', *QJM*, vol. 51, no. 4, pp. 469-80.

Woclawek-Potocka, I., Kowalczyk-Zieba, I., Tylingo, M., Boruszewska, D., Sinderewicz, E. & Skarzynski, D.J. 2013, 'Effects of lysophopatidic acid on tumor necrosis factor alpha and interferon gamma action in the bovine corpus luteum', *Mol Cell Endocrinol*, vol. 377, no. 1-2, pp. 103-11.

Xanthoulea, S., Pasparakis, M., Kousteni, S., Brakebusch, C., Wallach, D., Bauer, J., Lassmann, H. & Kollias, G. 2004, 'Tumor Necrosis Factor (TNF) Receptor Shedding Controls Thresholds of Innate Immune Activation That Balance Opposing TNF Functions in Infectious and Inflammatory Diseases', *J. Exp. Med.*, vol. 200, no. 3, pp. 367-76.

Xiao, G., Harhaj, E.W. & Sun, S.-C. 2001, 'NF-kB-Inducing Kinase Regulates the Processing of NF-kB2 p100', *Molecular Cell*, vol. 7, no. 2, pp. 401-9.

Xue, X., Lu, Q., Wei, H., Wang, D., Chen, D., He, G., Huang, L., Wang, H. & Wang, X. 2011, 'Structural basis of chemokine sequestration by CRM-D, a poxvirus-encoded tumor necrosis factor receptor', *PLoS Pathog*, vol. 7, no. 7, p. e1002162.

Yang, Z., West, A.P. & Bjorkman, P.J. 2009, 'Crystal structure of TNFα complexed with a poxvirus MHC-related TNF binding protein', *Nat Struct Mol Biol*, vol. 16, no. 11, p. 1189.

Yousaf, N., Gould, D.J., Aganna, E., Hammond, L., Mirakian, R.M., Turner, M.D., Hitman, G.A., McDermott, M.F. & Chernajovsky, Y. 2005, 'Tumor necrosis factor receptor I from patients with tumor necrosis factor receptor-associated periodic syndrome interacts with wild-type tumor necrosis factor receptor I and induces ligand-independent NF-kappaB activation', *Arthritis & Rheumatism*, vol. 52, no. 9, pp. 2906-16.

Zeigerer, A., Gilleron, J., Bogorad, R.L., Marsico, G., Nonaka, H., Seifert, S., Epstein-Barash, H., Kuchimanchi, S., Peng, C.G., Ruda, V.M., Del Conte-Zerial, P., Hengstler, J.G., Kalaidzidis, Y., Koteliansky, V. & Zerial, M. 2012, 'Rab5 is necessary for the biogenesis of the endolysosomal system in vivo', *Nature*, vol. 485, no. 7399, pp. 465-70.

Zhang, Y. 2007, 'Template-based modeling and free modeling by I-TASSER in CASP7', *Proteins*, vol. 69 Suppl 8, pp. 108-17.

Zhou, H., Jang, H., Fleischmann, R.M., Bouman-Thio, E., Xu, Z., Marini, J.C., Pendley, C., Jiao, Q., Shankar, G., Marciniak, S.J., Cohen, S.B., Rahman, M.U., Baker, D., Mascelli, M.A., Davis, H.M. & Everitt, D.E. 2007, 'Pharmacokinetics and safety of golimumab, a fully human anti-TNF-alpha monoclonal antibody, in subjects with rheumatoid arthritis', *J Clin Pharmacol*, vol. 47, no. 3, pp. 383-96.

Ziegler-Heitbrock, H.W.L., Möller, A., Linke, R.P., Haas, J.G., Rieber, E.P. & Riethmüller, G. 1986, 'Tumor Necrosis Factor as Effector Molecule in Monocyte Mediated Cytotoxicity', *Cancer Research*, vol. 46, no. 11, pp. 5947-52.

Zillner, K., Jerabek-Willemsen, M., Duhr, S., Braun, D., Langst, G. & Baaske, P. 2012, 'Microscale thermophoresis as a sensitive method to quantify protein: nucleic acid interactions in solution', *Methods Mol Biol*, vol. 815, pp. 241-52.

Appendix 1

9.1 Supplementary Figures

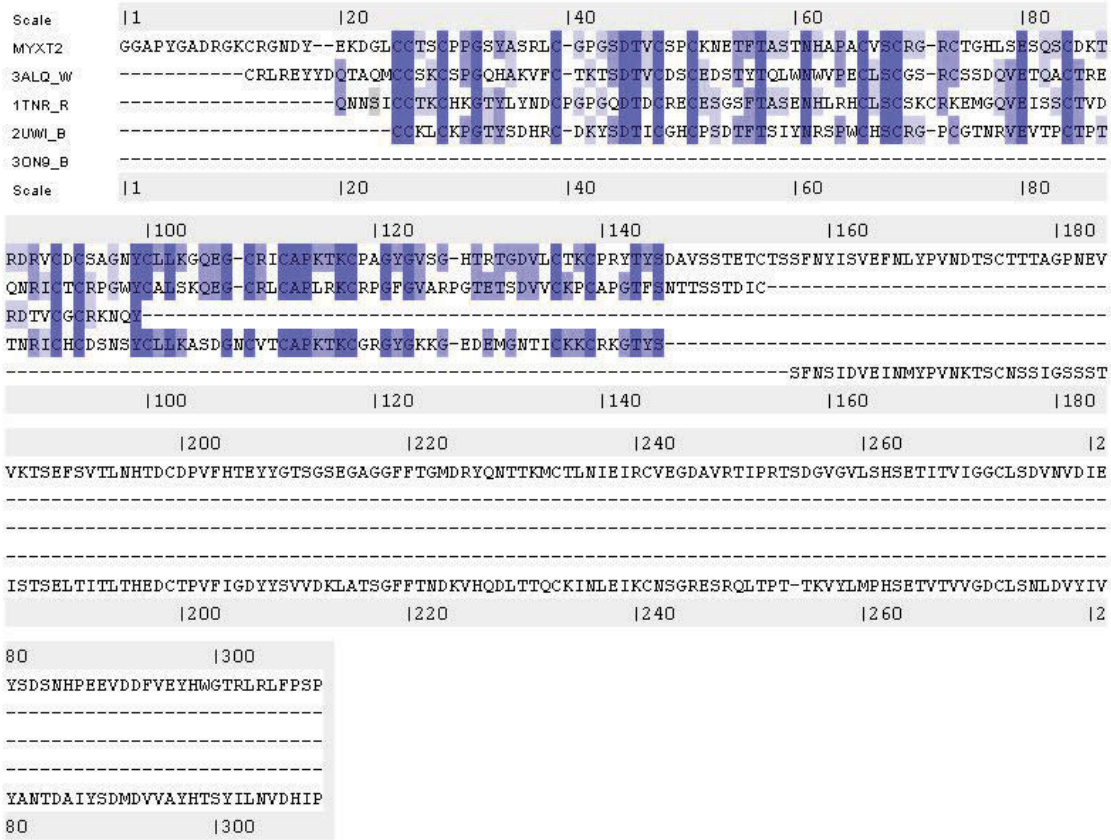

Figure 9.1 Multiple alignments for the comparative homology modelling of MYXT2

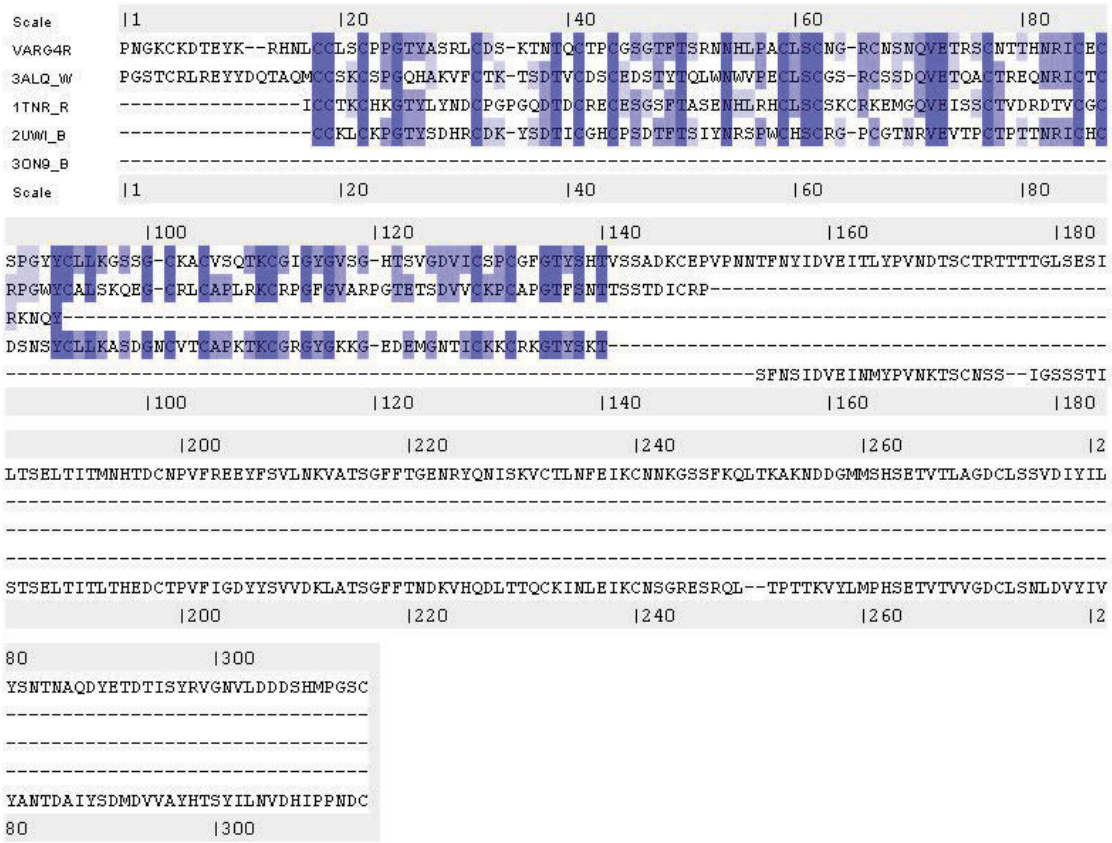

Figure 9.2 Multiple alignments for the comparative homology modelling of VARG4R

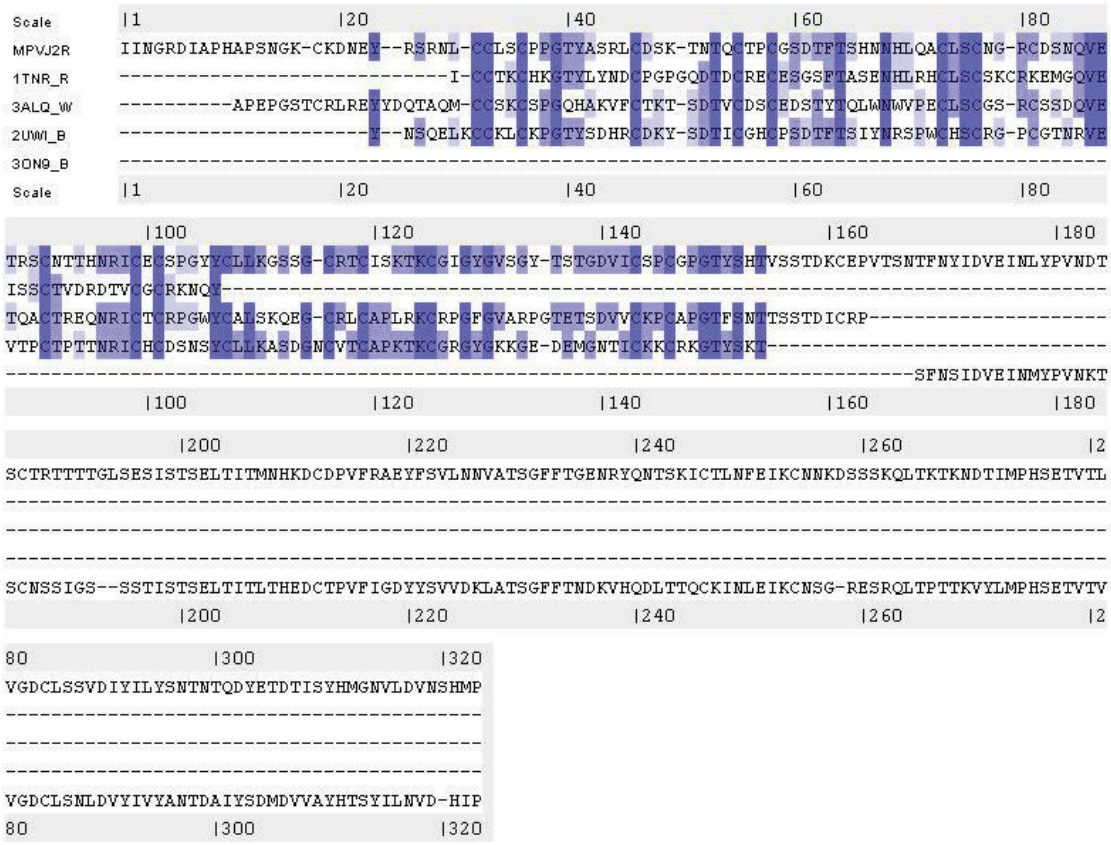

Figure 9.3 Multiple alignments for the comparative homology modelling of MPVJ2R

A

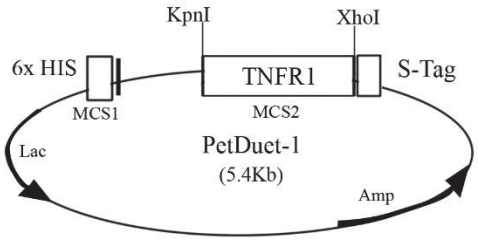
KpnI
XhoI
6x HIS
TNFR1
S-Tag
MCS1
MCS2
PetDuet-1
(5.4Kb)
Lac
Amp

B

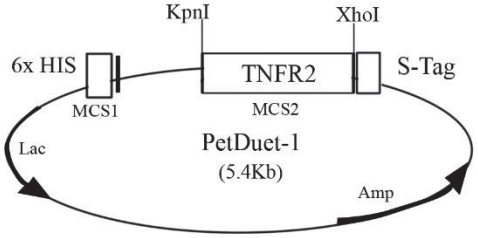
KpnI
XhoI
6x HIS
TNFR2
S-Tag
MCS1
MCS2
PetDuet-1
(5.4Kb)
Lac
Amp

C

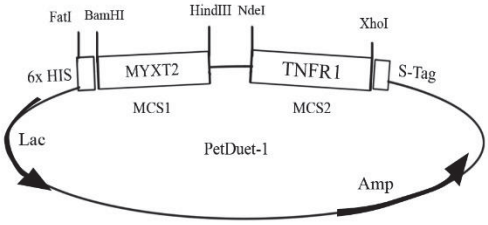
FatI
BamHI
HindIII
NdeI
XhoI
6x HIS
MYXT2
TNFR1
S-Tag
MCS1
MCS2
Lac
PetDuet-1
Amp

D

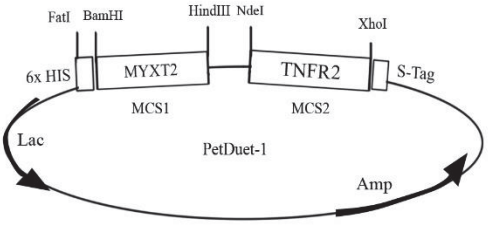
FatI
BamHI
HindIII
NdeI
XhoI
6x HIS
MYXT2
TNFR2
S-Tag
MCS1
MCS2
Lac
PetDuet-1
Amp

E

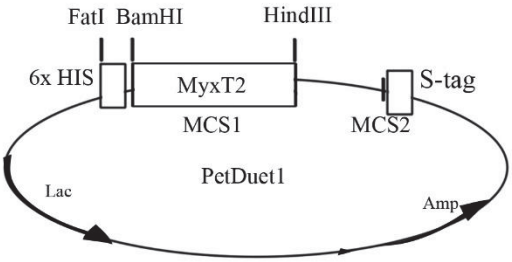
FatI
BamHI
HindIII
6x HIS
MyxT2
S-tag
MCS1
MCS2
PetDuet1
Lac
Amp

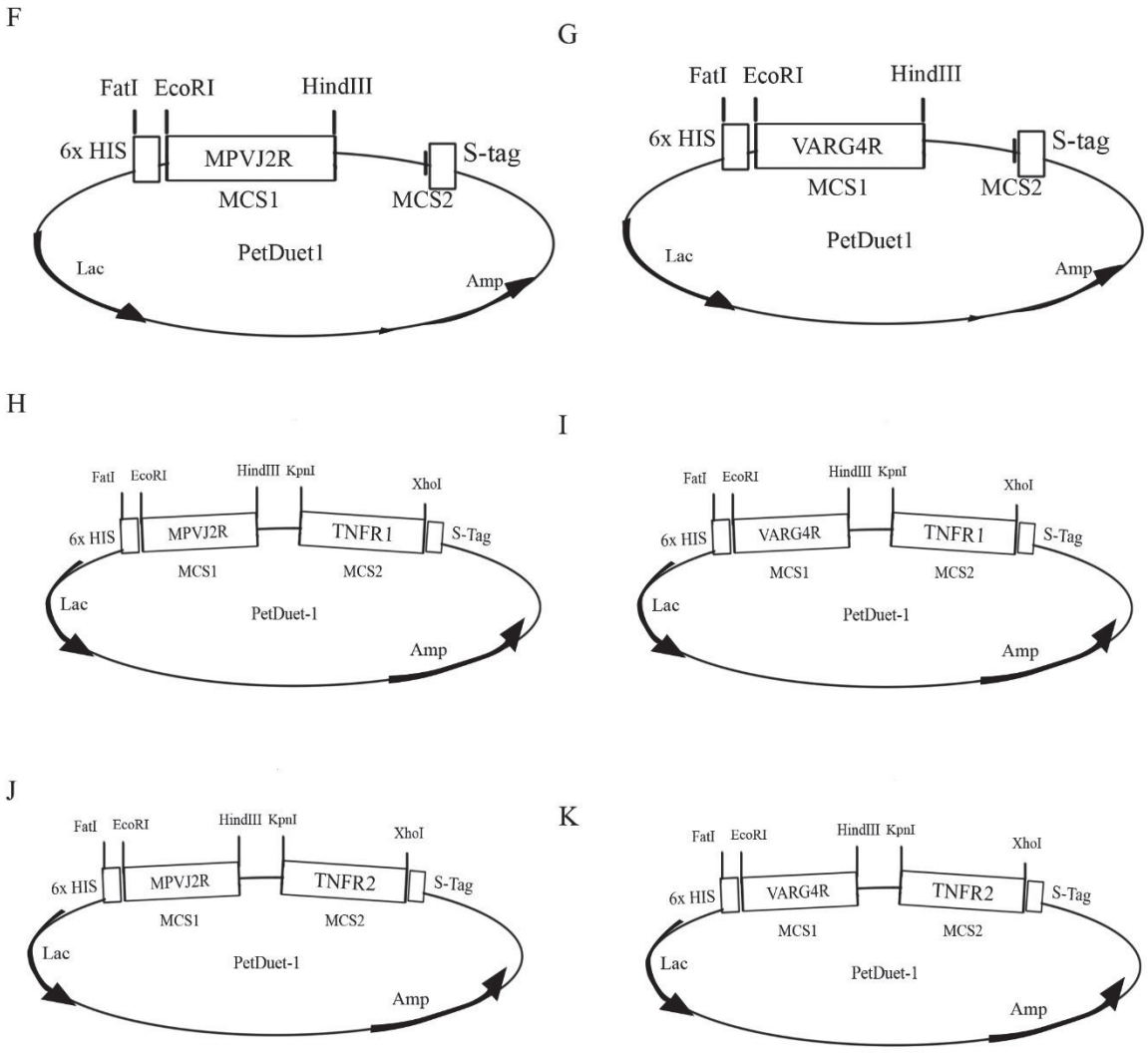

Figure 9.4 Plasmid maps of pET-Duet-1 plasmids

A) pETDuet.TNFR1B) pETDuet.TNFR2 C) pETDuet.MYXT2.TNFR1 D) pETDuet.MYXT2.TNFR1 E) pETDuet.MYXT2 F) pETDuet.MPVJ2R G) pETDuet.VARG4R H) pETDuet.MPVJ2R.TNFR1 I) pETDuet.VARG4R.TNFR1 J) pETDuet.MPVJ2R.TNFR2 K) pETDuet.VARG4R.TNFR2